AERATION OF ROBERTS SPLITTERS THROUGH AN INTERNAL GALLERY OF A DAM

by

Gerard Calitz

Thesis submitted to the University of Stellenbosch in partial fulfilment of the requirements for the degree of

Master of Engineering

Department of Civil Engineering
University of Stellenbosch
Private Bag X1, Matieland, 7602
Stellenbosch, South Africa

Supervisor: Prof. G.R. Basson

December 2016

DECLARATION

By submitting this document, I declare that the entirety of the work contained therein is my own, original work, that I am the sole author thereof (save to the extent explicitly otherwise stated), that reproduction and publication thereof by Stellenbosch University will not infringe any third party rights and that I have not previously in its entirety or in part submitted it for obtaining any qualification.

Signed ……..

Date ……..

SUMMARY

Roberts splitters have effectively been used for more than 75 years to dissipate the flood discharge energy of more than 30 dam spillways in South Africa and abroad. Roberts' (1943) standard, unaerated splitter design procedure is, however, limited to a spillway head (H) of 3.0 m, equivalent to a unit discharge (q) of 12 m²/s.

In order to avoid cavitation at higher design spillway heads, the flow is aerated by local air vents positioned on the splitters. On current dams, these air vents are individually fed by intake pipes placed in the step directly below the splitters. However, problems emerge when these pipes need to drain water entering the air vents. To avoid drowning the intake pipes, aeration through an internal gallery that is open to the atmosphere is proposed, with the end goal of increasing the unit discharge limit of Roberts splitters.

A 1:20 scale hydraulic model of an ogee spillway equipped with Roberts splitters was constructed. Two aerated models, with different sized air vents, were compared to an unaerated control model in order to determine the effect that the proposed aeration system has on the cavitation risk of the splitters at prototype unit discharges (q) of up to 50 m²/s.

At the maximum tested spillway head of 7.6 m (q = 50 m²/s), the minimum pressures and air concentration around the splitters of both aerated models increased considerably. This indicated that the proposed aeration system completely alleviates the high cavitation risk of unaerated splitters. It was further observed that the unaerated splitters were prone to drowning at high spillway heads, leading to unfavourable hydraulic conditions that should be avoided at all cost.

To summarise, the addition of aeration through an internal aeration gallery can increase the unit discharge capacity of Roberts splitters to at least 50 m²/s (up by 43%, from the unaerated limit of 35 m²/s, as tested during this study) while the proposed aeration gallery provides a solution to the problem of draining the inflow water of the air vents, without jeopardising the effective aeration of the splitters.

OPSOMMING

Roberts stroombrekers word al vir langer as 75 jaar op meer as 30 damoorlope in Suid-Afrika en oorsee gebruik om die energie van vloede te dissipeer. Die oorspronklike ontwerpriglyne vir onbelugte stroombrekers is beperk tot oorloophoogtes (H) van hoogstens 3.0 m, gelykstaande aan 'n eenheidsdeurstroming (q) van 12 m²/s.

By hoër oorloophoogtes word kavitasie verhoed deur die vloei te belug deur middel van luggate in die stroombrekers. Tipies word lug aan die luggate voorsien deur individuele inlaatpype in die trap direk onder die stroombrekers. Dit veroorsaak egter probleme omdat die inlaatpype water moet dreineer wat by die luggate ingeloop het. Die belugting van Roberts stroombrekers deur middel van 'n interne gallery wat oop is na buite, word voorgestel om te verhoed dat die inlaatpype versuip sal word, met die einddoel om Roberts stroombrekers se eenheidsdeurtromingskapasiteit van te verhoog

Vir hierdie studie is 'n 1:20 skaalmodel van 'n ogee-oorloop met Roberts stroombrekers gebou. Twee belugte modelle met verskillende luggatgroottes is met 'n onbelugte kontrole model vergelyk om die uitwerking te bepaal wat die voorgestelde belugtingsisteem gehad het op die kavitasierisiko van die stroombrekers. Dit is gedoen vir eenhiedsdeurstromings (q) tot en met 50 m²/s.

By die maksimum toetsoorloophoogte van 7.6 m (q = 50 m²/s), het die minimum drukke en luginhoud rondom die stroombrekers van beide belugte modelle aansienlik verhoog. Dit het veroorsaak dat die hoë kavitasierisiko van onbelugte stroombrekers heeltemal verhoed word deur die voorgestelde belugtingsisteem. Daar is verder waargeneem dat onbelugte stroombrekers geneig is om versuip te word by hoë oorloophoogtes. Dit veroorsaak ongunstige hidrouliese toestande wat te alle tye verhoed moet word.

Ter opsomming is dit duidelik dat die eenheidsdeurstromingskapasiteit van Roberts stroombrekers tot ten minste 50 m²/s verhoog kan word deur belugting te verskaf (verhoog met 43%, vanaf 35 m²/s vir onbelugte stroombrekers). Verder het die voorgestelde belugtingsgallery 'n oplossing gebied aan die probleem om invloeiwater

vanaf die luggate te dreineer, sonder om doeltreffende belugting van die stroombrekers in gedrang te bring.

ACKNOWLEDGEMENTS

I would like to extend my deepest gratitude toward the following persons for their advice, guidance and support in making this thesis a reality:

- My study leader, Prof. Gerrit Basson, for his all-round support, mentorship, confidence and patience;
- The University of Stellenbosch and the Wilhelm Frank Trust for the financial support in making this study possible;
- Mr. Christiaan Visser for his help in the construction of the model, and assistance with the necessary software to allow brisk and accurate model testing;
- Mr. Johan Nieuwoudt, Mr. Iliyaaz Williams and Mr. Marvin Lindoor at the University of Stellenbosch's Hydraulic Laboratory, for their assistance, patience and hard work during the construction and testing of the model;
- Mr. Gert Isaks of the DWS at the Gariep Dam Office, for the insightful tour of the Gariep Dam and its galleries;
- My father, Johan Calitz, for his unmatched support during my studies, and my mother, Fransa Calitz, for her immense belief and motivation in realising my potential;
- All my friends and loved ones for their contribution to these two unforgettable years.

TABLE OF CONTENTS

LIST OF FIGURES

LIST OF TABLES

ACRONYMS AND ABBREVIATIONS

2D	Two dimensional
A	Ampère
AFR	Asphalt faced rockfill (embankment dam)
Approx.	Approximately
Avg.	Average
bar	Unit of pressure, equivalent to 100 000 Pa
BC	Before Christ
BN	Beaufort number
CCR	Clay core rockfill (embankment dam)
CFD	Computational fluid dynamics
CFR	Concrete faced rockfill (embankment dam)
DN	Nominal diameter of a pipe, usually followed by a dimension in millimetres
DWS	Department of Water & Sanitation (South Africa)
Eq.	Equation
ft	Foot
GUI	Graphical user interface
h	Hour
hp	Horsepower
Hz	Hertz

ICOLD	International Commission on Large Dams
k	Kilo (10^3)
kHz	Kilohertz
kPa	Kilopascal
l	Litre
m	Metre
M	Mega (10^6)
m^3	Cubic metres
mA	Milliampère
masl	Metres above mean sea level
Max.	Maximum
mbar	Millibar
Min.	Minimum
min	Minute
mm	Millimetre
MPa	Megapascal
ms	Milliseconds
N	Newton
N.A.	Not applicable
No. / no.	Number
Nos. / nos.	Numbers
Pa	Pascal
Prob. Min.	Probable minimum
RCC	Roller compacted concrete

RMF	Regional Maximum Flood
s	Second
SANCOLD	South African National Committee on Large Dams
SI	International System (of Units)(Abbreviated from French)
Std dev	Standard deviation of a population
TE	Traditional earthfill (embankment dam)
UK	United Kingdom
USA	United States of America
USBR	United States Bureau of Reclamation
Ω	Ohm

NOMENCLATURE

a	Acceleration (m/s^2)
A	Cross-sectional area of flow (m^2)
A_{duct}	Cross-sectional area of aeration duct (m^2)
$(A_{duct})_{min}$	Minimum cross-sectional-area of aeration duct, including safety factor (m^2)
a_m	Acceleration in the model (m/s^2)
A_m	Area in the model (m^2)
A_{main}	Cross-sectional area of main air vents (m^2)
a_p	Acceleration in the prototype (m/s^2)
A_p	Area in the prototype (m^2)
A_{proj}	Projected area of a body (m^2)
A_{shaft}	Cross-sectional area of the aeration shaft (m^2)
A_{side}	Cross-sectional area of side air vents (m^2)
A_{vents}	Sum of the area of all air vents per splitter (m^2)
$\sum A_{vents}$	Sum of A_{vents} off all splitters (m^2)
$Air\%$	Air concentration as a percentage of volume of two phase flow (%)
$Air\%_{min}$	Minimum air concentration (%)
b	Width of channel (m)
c_d	Drag coefficient (dimensionless)
C_e	Ogee final discharge coefficient (dimensionless)
C_0	Ogee design discharge coefficient (dimensionless)
d	General flow depth (m); *and* Depth of flow approaching Roberts splitters (m)
d_C	Depth of flow approaching the splitters associated with the splitter critical head H_C (m)
d_D	Design depth of flow approaching the splitters (m)

d_I	Depth of flow at the point of inception (m)
Eu	Euler number (dimensionless)
$f[\,]$	Denotes a function
F^*	Froude number defined in terms of roughness – relevant to point of inception (dimensionless)
F_d	Drag force (N)
F_m	Force in the model (N)
F_p	Force in the prototype (N)
Fr	Froude number (dimensionless)
g	Gravitational acceleration constant (taken as 9.81 m/s^2)
h	Pressure as metres of water depth (m)
H	Spillway head – the damming height above the spillway crest (m)
H_0	Design head of ogee spillway (m)
h_a	Velocity head for ogee spillway (m)
H_C	Critical spillway head at which Roberts splitter become drowned (m)
H_D	Design spillway head of Roberts splitters (m)
H_e	Energy head of ogee spillway (m)
H_m	Model spillway head (mm)
H_{max}	Maximum pressure range of pressure transmitter in metres of water (m)
h_{min}	Minimum pressure (m)
H_{min}	Minimum pressure range of pressure transmitter in metres of water (m)
H_{out}	Output pressure head from pressure transmitter (m)
h_p	Prototype pressure as metres of water depth (m)
H_p	Prototype spillway head (m)
h_{prob}	Probable minimum pressure (m)
I_{max}	Maximum current output of the pressure transmitters (A)
I_{min}	Minimum current output of the pressure transmitters (A)
K	Ogee spillway downstream profile constant (dimensionless); *and* Constant in Mason' (1983) splitter design procedure (dimensionless)
K'	Constant in Mason' (1983) splitter design procedure (dimensionless)

k_s	Hydraulic roughness coefficient (m)
L	Length of splitter (m); *and* Length of homologous sections in the model and prototype (m)
L_{eff}	Effective spillway length (m)
L_I	Distance between the point of inception and the spillway crest (m)
L_m	Length in model (m)
L_p	Length in prototype (m)
L_{proj}	Projected splitter height in the direction of the oncoming flow (m)
L_s	Width of step in splitter design procedure (m)
$[\ ]_m$	(subscript) Denotes that the parameter is related to the model
n	Ogee spillway downstream profile constant (dimensionless)
$[\ ]_p$	(subscript) Denotes that the parameter is related to the prototype
p	Pressure (Pa)
P	Dam height in ogee spillway design procedure (m); *and* Height of splitters below spillway crest in splitter design procedure (m)
p_0	Dynamic fluid pressure at point 0 (Pa) – see Section 2.4.2
p_1	Dynamic fluid pressure at point 1 (Pa) – see Section 2.4.2
p_M	Dynamic fluid pressure at point M (Pa) – see Section 2.4.2
p_v	Vapour pressure of fluid (Pa)
q	Unit flow rate (m²/s)
Q	Flow rate (m³/s)
Q_{air}	Air discharge through air vents, per splitter (m³/s)
Q_{drain}	Drainage discharge from aeration duct (m³/s)
Q_{inflow}	Water inflow discharge through air vents, per splitter (m³/s)
Q_{intake}	Intake air discharge of aeration duct (m³/s)
q_m	Unit discharge in model (m²/s)
Q_m	Model discharge (l/s)
q_p	Unit discharge in prototype (m²/s)
Q_p	Prototype discharge (m²/s)
R	Resistance of the pressure transmitters (Ω)

R_1	Ogee upstream dimension (m)
R_2	Ogee upstream dimension (m)
Re	Reynolds number (dimensionless)
R_{max}	Horizontal distance between the inside of nappe to the toe of the dam at tailwater height (m)
R_{min}	Horizontal distance between the outside of nappe to the toe of the dam at tailwater height (m)
S	Spacing between splitters (m); *and* Scale factor
t	Time (s)
T	Height of splitters above step (m)
t_m	Time in model (s)
t_n	Time step of air concentration analysis (s)
t_p	Time in prototype (s)
t_{void}	Time it takes a void to travel over the air probe needle (s)
v	Flow velocity (m/s)
V	Volume of water (m^3)
v_0	Mean flow velocity at point 0 (m/s) – see Section 2.4.2
$(v_{air})_{avg}$	Average air velocity in aeration duct (m/s)
$(v_{air})_{max}$	Maximum air velocity in aeration duct (m/s)
V_{atm}	Voltage output of pressure transmitter at atmospheric pressure (V)
v_m	Velocity in model (m/s)
v_M	Local flow velocity at point M (m/s) – see Section 2.4.2
V_m	Volume in model (m^3)
v_p	Velocity in prototype (m/s)
V_p	Volume in prototype (m^3)
v_{wind}	Wind speed (m/s)
W	Width of splitters (m)
We	Weber number (dimensionless)
x	Distance (m)
$\boldsymbol{x}$	Output voltage reading from pressure transmitter (V)

X_1	Ogee upstream dimension (m)
X_c	Ogee upstream dimension (m)
y	Flow depth normal to flow lines (m)
Y_c	Ogee upstream dimension (m)
Z_0	Elevation of point 0 (masl) – see Section 2.4.2
Z_M	Elevation of point M (masl) – see Section 2.4.2
δ^*	Boundary layer depth (m)
Δp	Pressure difference (Pa)
Δp_m	Pressure difference in the model (Pa)
Δp_p	Pressure difference in the prototype (Pa)
$\emptyset$	Diameter (m)
$\emptyset_{main}$	Inside diameter of circular main air vent (m)
$\emptyset_{side}$	Inside diameter of circular side air vent (m)
γ	Specific weight of a fluid (N/m^3)
μ	Mean of a random variable population given a sample
ν	Kinematic viscosity (m^2/s)
ν_m	Kinematic viscosity of the model (m^2/s)
ν_p	Kinematic viscosity of the prototype (m^2/s)
ρ	Density of fluid (kg/m^3)
ρ_{air}	Density of air (taken as 1.225 kg/m^3)
ρ_m	Fluid density in model (kg/m^3)
ρ_p	Fluid density in prototype (kg/m^3)
σ	Cavitation index (dimensionless); *and* Standard deviation of a random variable population given a sample
σ_C	Critical cavitation number (dimensionless)
σ_i	Cavitation index at condition of incipient cavitation (dimensionless)
τ	Surface tension of a fluid (N/m)
τ_m	Model fluid surface tension (N/m)
τ_p	Prototype fluid surface tension (N/m)
θ	Spillway downstream face angle with the horizontal (degrees)

PART I – MAIN REPORT

CHAPTER 1

INTRODUCTION

Dams consist of two main features: the reservoir and the dam (i.e. the dam wall) (Chadwick *et al.*, 2013). By nature, the inflow of the impounded reservoir is variable and there will be times where the reservoir is full and the inflow will surpass the demand of the reservoir. The excess flow must therefore be safely discharged in order to prevent catastrophic failure of the dam through overtopping by using carefully designed overflow passages or channels – known as spillways (Chadwick *et al.*, 2013). The main design variable in spillways is an extreme flood of the catchment area that the dam's spillway needs to accommodate, such as the regional maximum flood (RMF) or the Probable Maximum Flood (PMF). This is the flood that can be expected from the most severe combination of critical meteorological and hydrological conditions that are reasonably possible in the region (Khatsuria, 2005). The RMF of a spillway can be quite large (16 700 m^3/s in the case of the Gariep Dam (Back *et al.*, 1973)) and very high velocities can be attained on spillways resulting in flow containing high amounts of energy. Because of this, a form of energy-dissipating measure is usually present to prevent failure of the structure through scouring and undermining (Wright, 2006).

Roberts splitters is a type of energy-dissipating measure located near the top of dam spillways, see Figure 1-1. They are normally used on high dams where the spillway flow velocities are too fast for a stilling basin, or the unit discharge (q, in m^2/s) too high for a stepped spillway. The main aim of Roberts splitters is to deflect the flow away from the toe of the dam while creating enough turbulence in the flow to enhance the dispersion of the jet that plunges to the river valley below (see Figure 1-2 of the Gariep Dam spillway in operation).

During operation, the intended goal of the splitters is to split the sheet of water flowing down the spillway. By doing this, the direction of the flow is rapidly changed and flow separation may exist around the splitters, leading to sub-atmospheric pressures. If the pressure in the fluid becomes too low (approaches vapour pressure), cavitation may

occur resulting in serious damage (see Section 2.4 for a detailed description of cavitation).

Figure 1-1: Example of Roberts splitters on the Vanderkloof Dam spillway (vanderkloofdam.com, 2014)

Figure 1-2: Roberts splitters in operation on the Gariep Dam spillway, very similar to that of the Vanderkloof Dam (Calitz & Basson, 2015)

Cavitation in general, can be mitigated in two ways: firstly, by ensuring the fluid pressure remains high enough (Chadwick *et al.*, 2013), and secondly, by introducing air into the flow (Chanson, 1992). On a dam spillway with Roberts splitters, air can be introduced to the water flow at atmospheric pressure via air vents connected to an atmospheric air source. This is called aeration. It is important to note that although Roberts splitters aerate the flow naturally downstream of the system, internal aeration is quite different and relies on some sort of opening or supply to provide air into the flow in a way other than natural air inception through the boundary layer of the flow. This air flow to the air vents need not be pumped or pressurised if properly designed as sub-atmospheric pressures within the nappe created by the separated flow over splitters will naturally suck air out of the vents. This is true provided that the pressure of the air in the cavity of the aforementioned nappe is lower than the air in air vent (which should be atmospheric or higher).

Although aeration has previously been provided for the Roberts splitters on the spillways of the Gariep and Vanderkloof Dams (both on the Orange River in South Africa), 'the need or effectiveness of aeration by internal ducts has, however, not been proved conclusively' (Jordaan, 1989, p 319).

The subject of this thesis is to determine the effect of aeration by an internal aeration gallery, and proving its necessity, in alleviating cavitation risks of Roberts splitters. To this end, an internal aeration gallery that is open to the atmosphere was proposed. As part of this project, hydraulic model tests were conducted in the hydraulic laboratory of the Civil Engineering Department of the University of Stellenbosch.

The hydraulic model methodology is described in Chapter 3, and consisted of three separate set-ups:

1. A 1:20 scale control model of unaerated Roberts splitters on an ogee spillway, intended to measure the pressure and air concentration around a splitter and justify the ideal positioning of air vents on the splitters;
2. A 1st aerated model of Roberts splitters, containing small air vents, intended to alleviate cavitation risks of the splitters and analyse the performance of the proposed aeration gallery (see Figure 1-3);
3. A 2nd aerated model of Roberts splitters, containing larger air vents, intended to further improve the flow conditions as stated above, and compare aeration performance with that of the 1st aerated model.

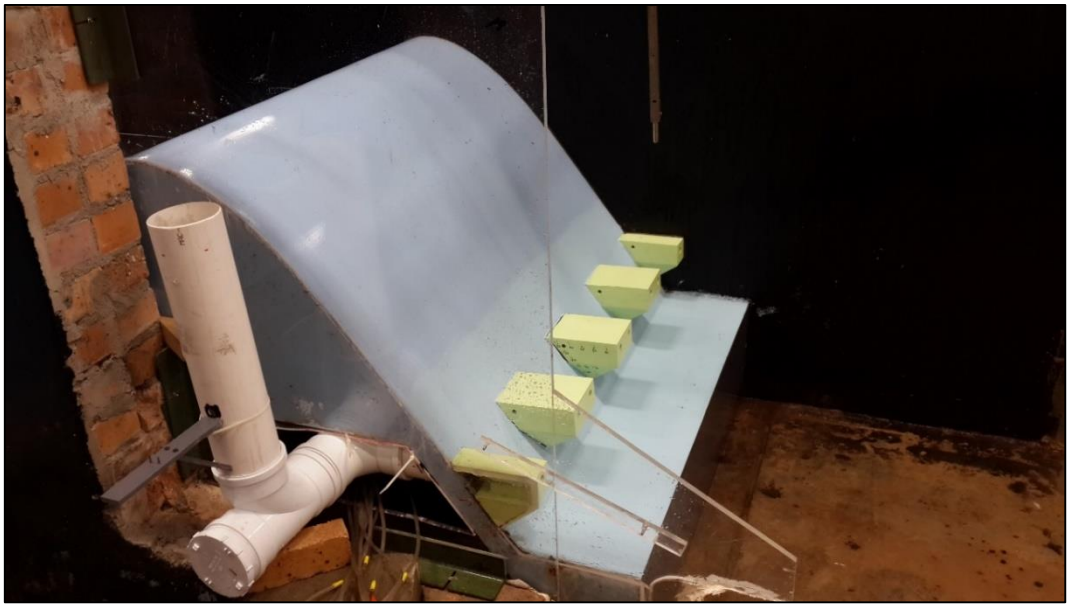

Figure 1-3: The model, showing the splitters and aeration supply

1.1. Objectives of the Proposed Study

The main objective of this study is:

- To determine the effect that the aeration of Roberts splitters, through an internal gallery, has on the local negative pressures around the splitters, with the goal of alleviating cavitation risks at prototype unit discharges of up to 50 m^2/s.

The secondary objective of this study is:

- To determine the effectiveness of the proposed aeration system, and provide practical recommendations on the application thereof.

1.2. Motivation for the Thesis

The primary motivation for this study is to determine the effect that the aeration of Roberts splitters, through an internal gallery, has on alleviating the cavitation risks associated with this energy-dissipating structure. If the spillway capacity (H_0) can be increased without jeopardising the safety of the system, the size of the spillway can be decreased.

It makes economic sense to fine tune the existing Roberts splitters design procedure as material and building costs can be lowered by eliminating uncertainty and avoiding unnecessary model studies. Roberts splitters is quite a complex and detailed structure to build in practice compared to other dam spillway types, for example a stepped spillway

or free overfall spillway (note the intricate splitter teeth in Figure 1-1). With many dams reaching the end of their design life, requiring rehabilitation or possible heightening, increasing the spillway capacity can be advantageous and save money by minimising the requirement of intensely detailed and specific structures.

Safety is of paramount importance in dam engineering. It is advantageous to push the limits of a design in model studies to gain expertise and experience to employ such knowledge on a prototype scale. This study aims to extend the design limit of the conventional Roberts splitters design procedure.

1.3. Thesis Structure

The thesis consists of six chapters including this introductory chapter, as well as the appendices relevant to the research. This takes the reader from the motivation for the study (Chapter 1), through the literature that reflects the current status of knowledge (Chapter 2) and on to the set-up of the hydraulic model tests (Chapter 3). The results and analysis of these tests (Chapter 4) lead to the conclusions and recommendations for the effective use of Roberts splitters in practice and the aeration thereof (Chapter 5 and Chapter 6). Figure 1-4 shows the logical interaction of the various phases and sub-phases of the research methodology, in the context of the entire structure of the thesis.

Appendix A to Appendix C include further background literature, assumed to be common knowledge to the advanced reader, while Appendix D includes the USBR (1987) ogee design procedure. The complete model design and design drawings are contained within Appendix E and Appendix F. The complete hydraulic model testing schedule is tabulated in Appendix G. All data resulting from the model tests are included in Appendix H, Appendix I and Appendix J. Finally, the document concludes with the photographs of the separate tests in Appendix K.

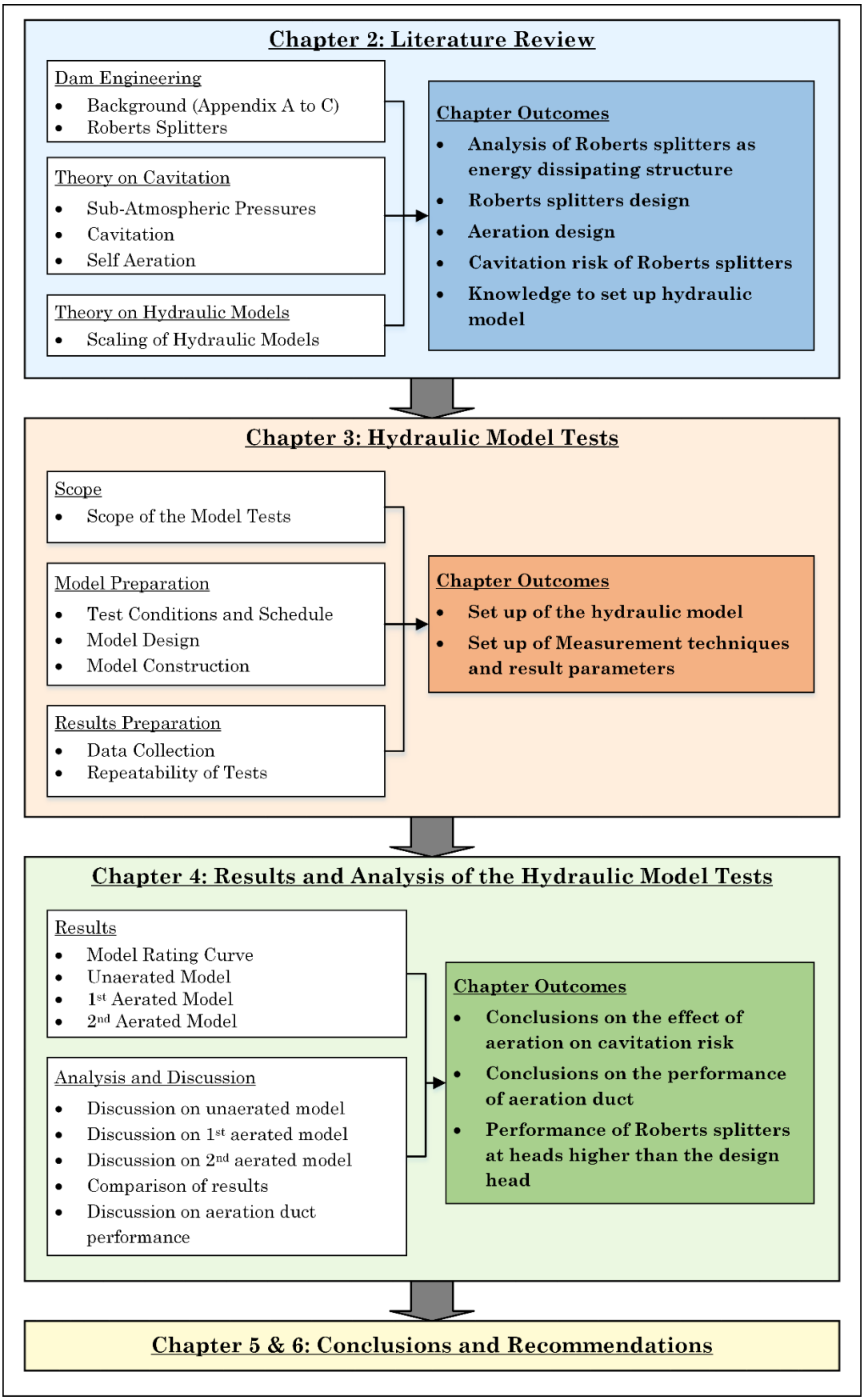

Figure 1-4: Thesis structure and research methodology

CHAPTER 2

LITERATURE REVIEW

The aim of the literature review is twofold. Firstly, pronounced knowledge of the subject was needed in order to accurately perform the necessary hydraulic model study for this thesis. Secondly, it provides the reader with an opportunity to understanding the theory behind the study of Roberts splitters and the aeration thereof, as well as the risks associated with safely handling severe flood events on dam spillways.

The literature review is set out to initially provide a brief background on dams, dam spillways and energy dissipators. This is mainly contained in Appendix A, Appendix B and Appendix C. Thereafter follows an extensive, in depth review of spillway crest splitters as envisaged as far back as 1936 by Lt. Col. D.F. Roberts (Van Vuuren, 2008), including the complete history thereof and the application thereof, that have subsequently been referred to as 'Roberts splitters'. All instances where Roberts splitters have previously been artificially aerated were studied and the characteristics of each case shown and explained in order to explore new problems and possibilities through the hydraulic model tests. Known limits of the usage of Roberts splitters as an energy-dissipating structure are listed and explained and Roberts' (1943) original design procedure is thoroughly examined and described. Mason's (1983) findings and improved design procedure relevant to high arch dams are discussed and explained in conclusion to a detailed review of spillway crest splitters.

The study of sub-atmospheric pressures that might occur around Roberts splitters is a major objective of this thesis. As such, other cases of known sub-atmospheric pressure on dam spillways and hydraulic structures were studied and the findings included aiming to predict the nature of the pressure distribution of the hydraulic model.

The process of cavitation is very complex and is considered a serious risk when designing hydraulic structures and energy dissipators, including Roberts splitters. The concept of cavitation is described in detail, and known mitigation measures included. The phenomenon of self-aeration and the relevance of the point of inception, as well as the theory behind the scaling of hydraulic models are mentioned briefly.

The literature review concludes with a summary of key findings and conclusions that aid in the hydraulic model study.

2.1. Background

The goal of the background information is to provide the general reader with the necessary knowledge on dams, spillways and energy-dissipating structures to fully understand the context of what is to follow. For the advanced reader this information might be common knowledge and is therefore excluded from the main report. It is, however, included in Appendix A, Appendix B and Appendix C. This section provides a short synopsis of the background information included in the appendices.

In its simplest form, a dam is a structure constructed to store water from a stream. Dams have been built by humans since ancient times, and the history of dam construction is briefly discussed. Shah & Kumar (2008) report that the earliest evidence of hydraulic engineering is found in Mesopotamia, dating back over 8000 years. ICOLD (2016) currently classifies 58 402 large dams according to their specified criteria.

Dams can be built from a variety of materials, for a multitude of reasons, the most common material being earthfill and rockfill (Hagen, 2015). The main reason for the construction of dams is to provide water for domestic and irrigation purposes (Schnitter, 1994, Geringer, 2015).

Most dams are required to have a spillway, a chute specifically and deliberately designed to safely discharge the design flood of the stream impounded by the dam. A multitude of spillway types exists, ranging from the original ogee spillway, to modern labyrinth and piano key spillways.

Spillways should generally include some sort of energy-dissipating measure, to dissipate the high amount of energy accompanying a given design flood. This can be as simple as allowing the spilled discharge to freely fall into a deep plunge pool, or generating a controlled hydraulic jump in a stilling basin to allow subcritical flow back into the watercourse.

Roberts splitters is an energy-dissipating structure almost exclusively found on standard ogee spillways. The Wadi Dayqah Dam in Oman being an example where Roberts splitters have been used in conjunction with a stepped spillway (Mason, 2016).

2.2. Roberts Splitters

2.2.1. History of Roberts Splitters

The Loskop Dam, situated in the area north of the town of Middelburg in the Mpumalanga province of South Africa, was planned in 1936 to provide irrigation supply to local farmers in the Olifants River valley (Van Vuuren, 2008). It is of interest as it was the first ever dam where crest splitters were used as an effective means of energy dissipation (Jordaan, 1989). The man who developed these crest splitters was Lt. Col. D.F. Roberts, the resident engineer to South Africa's Department of Irrigation's first hydraulic laboratory (Van Vuuren, 2008, Roberts, 1943), and subsequently, the crest splitter system was named after him.

Roberts' model studies to develop the design principles of his splitters were done in conjunction with the construction of the dam wall. His 1 in 10 scale model consisted of steel and timber to allow for fast alterations if required and was built outdoors relying on a nearby irrigation canal for water supply (Roberts, 1943). Figure 2-1 and Figure 2-2 show the general layout of the model built and used by Roberts to develop the design principles of his crest splitters. As stated by Roberts (1943), the main reason for the geometry of the energy dissipation system was a 6 ft. wide step on the downstream side of the dam wall to "provide for future raising". Elevatorski (1959, p. 154) also mentions the 6 ft. wide step on the spillway of the Loskop Dam, further stating that the energy generated at the toe of the dam totals around 1 000 000 hp. Furthermore, Roberts (1943) noted that a stilling basin at the toe of spillway, as was the norm at the time, was deemed too expensive as a subsidiary weir would be needed. These factors drove Roberts to develop his system as a continuous step with a series of protruding splitters or "teeth" immediately above the step.

After the success of the Roberts splitters on the spillway of the Loskop Dam (having a spillway head of 3.2 m prior to being raised by 9 m in 1979 (Roberts, 1977)), the system has been adopted on several South African dams. The application of Roberts splitters gained international recognition when it was used for the Gariep, Vanderkloof (both South Africa) and Victoria (Sri Lanka) Dams by Sir Alexander Gibb and Partners (Jordaan, 1989). Apart from the Victoria Dam, international examples of Roberts splitters include the Palawan Dam in Zimbabwe and the Madupatty Dam in India (Mason, 1983). As mentioned in earlier, Roberts splitters have been used on more than 30 dams in South Africa and abroad (Jordaan, 1989). Table 2-1 includes statistics and

characteristics of 23 South African dams equipped with Roberts splitters (Roberts, 1977).

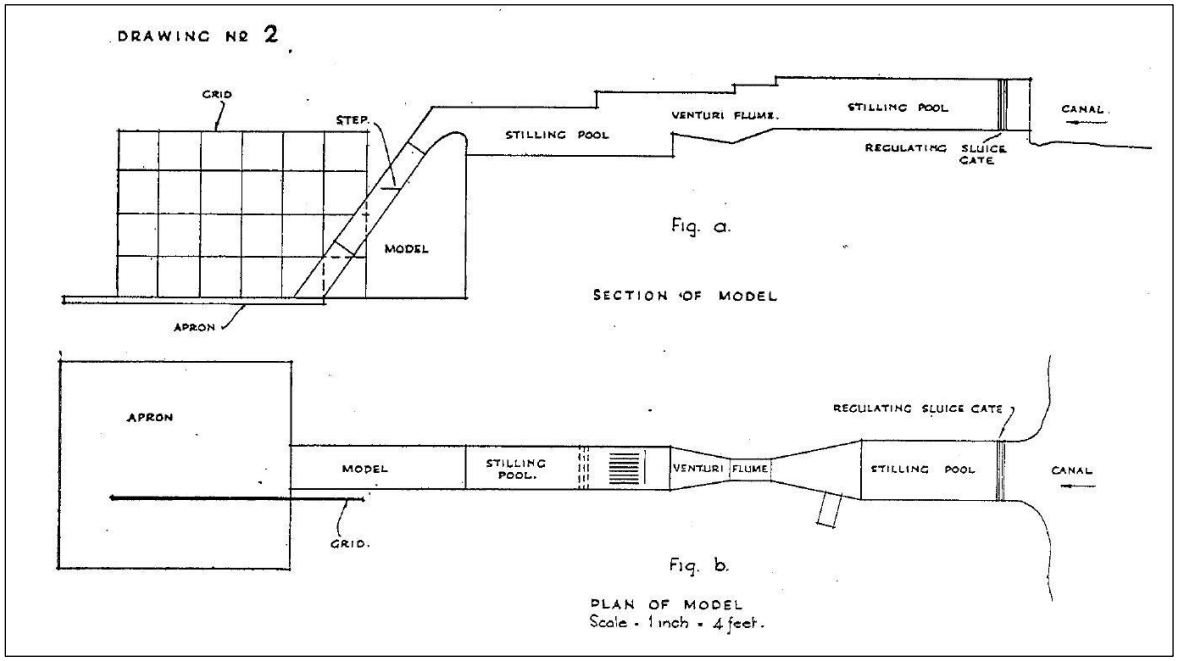

Figure 2-1: Original layout of Lt. Col. Roberts' model, circa 1936 (Roberts, 1943)

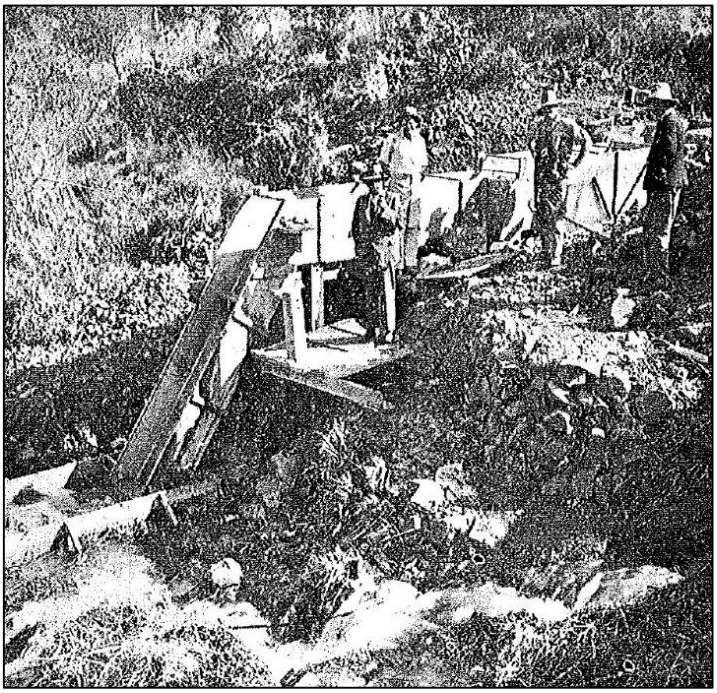

Figure 2-2: Old photograph showing Lt. Col. Roberts' model, circa 1936 (Roberts, 1943)

Table 2-1: Characteristics of South African dams equipped with Roberts splitters prior to 1977 (Roberts, 1977)

Name of Dam	Completion Year	Dam Height (m)	Spillway Characteristics						Remarks
			Discharge Capacity (m^3/s)	Spillway Length (m)	Spillway Head (m)	Unit Discharge (m^2/s)	Concrete Apron[1]	Energy Dissipated[2] (MW/m)	
Vaal	1938	57	4 500	493.8	3.0	9.1	A	5.1	
Loskop	1939	45	2 830	243.8	3.2	11.6	A	5.1	
Nagle	1950	50	640	120.6	1.8	5.3		2.6	
Albasini	1952	35	150	85.2	3.8	15.8		5.4	
Roodeplaat	1959	59	970	143.4	2.1	6.8		3.9	Splitters first used on arch dam
Erfenis	1960	46	2 070	182.9	3.0	11.3		5.1	
Allemanskraal	1960	38	2 260	211.8	3.0	10.7		4.0	
Alice Dale	1960	22	850	149.4	2.0	5.7	A	1.2	
Clanwilliam	1969	43	1 530	101.0	3.8	15.1	A	6.4	
Primkop	1970	27	870	118.9	1.5	7.3		1.9	
Klipvoor	1970	30	2 830	158.5	4.6	17.8		5.3	
Buffelskloof	1971	39	650	91.4	2.2	7.1		2.7	
Da Gama	1971	35	370	45.7	2.4	8.1		2.7	
Vaalkop	1972	32	2 830	213.4	2.6	13.3		4.2	
Gariep	1972	88	15 580	233.4	9.1	66.8	A	57.6	Aeration provided for first time
Spioenkop	1973	55	3 820	158.5	3.9	24.1	A	13.0	
Lakenvalley	1974	56	540	45.8	3.1	11.8	A	6.5	
Blyderivierspoort	1974	66	2 350	90.0	5.0	26.1	A	16.9	
Elandskloof	1975	67	420	30.0	3.0	14	A	9.2	
Albert Falls	1976	34	1 570	100.0	3.8	15.7	A	5.2	
Miertjeskraal	1977	24	510	75.0	2.1	6.8		1.6	
Hazelmere	1977	50	3 800	91.0	8.0	41.8	A	20.5	Aeration provided
Vanderkloof	1977	107	13 000	212.0	9.0	61.3	A	64.3	Aeration provided

Notes: 1. A = Concrete apron constructed. Blank indicates unlined river section downstream of dam

2. Energy dissipated per unit length of spillway = $9.81 \times dam\ height \times unit\ discharge\ (in\ kW/m)$

2.2.2. Application of Roberts Splitters

As mentioned earlier, the Roberts splitters system consists of a series of projecting teeth or splitters immediately upstream of a continuous lip or step (Mason, 1983). The sheet of water flowing down the spillway will hit the splitters first and be projected forward as a set of jets from each individual splitter. The water flowing in between the splitters will in turn hit the step, also being projected forward as a separate set of jets. Through this interaction, a large amount of air gets entrained into flow by the turbulence created. If designed correctly the two sets of jets will collide in mid-air, breaking up into spray, and dissipate the energy through air resistance (Roberts, 1980). This will also spread the plunging jet over a large area on the apron of the dam, or plunge pool, and by doing so, decrease the impact loadings on the foundation.

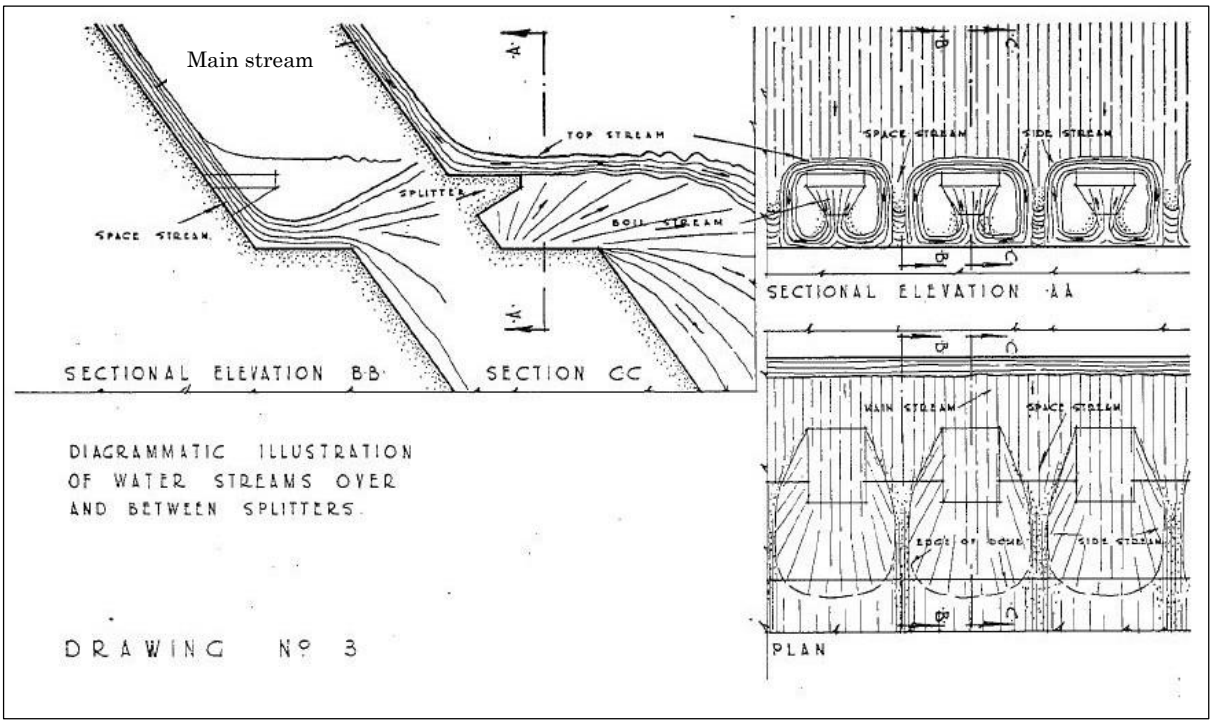

Figure 2-3: Roberts' (1943) original illustration of stream lines over and between splitters

Roberts' (1943) initial observations and findings on the detailed functioning of his splitters were summarised by Roberts (1980) (referring to Figure 2-3) as follows:

i. As the main stream over the spillway meets the splitters, it is divided into:
   a. The top and side streams flowing over the top of the splitters, and,
   b. The space stream flowing between the splitters.

ii. As the space stream passes across the step, it converges. Its velocity stays more or less constant and thus its depth increases. With the correct spacing of splitters, the space stream leaves the step as a very narrow and deep sheet.

iii. The side streams strike the step close to the space stream and forms a dome together with the top stream. Upon striking the step, the two side streams turn in towards each other to meet underneath and on the centreline of the splitter. The side streams then combine to form the boil stream, which travels upwards underneath the splitter and eventually outwards, meeting the top stream to form a boil.

iv. The dome expands laterally with increasing spillway head eventually touching mingling with the domes of the adjacent splitters. The thinned out, deep space stream in between the domes is very stable and breaks up completely as it leaves the step.

v. At low heads, the domes are not formed completely, but as the flow is small, the streams breaks up naturally.

vi. At a certain critical head, a stage is reached where the splitters are drowned, limiting the dispersing action of the system and inducing large amounts of vibration.

As with deflector bucket type spillways, the toe of the spillway and the apron must be designed to accommodate even low flow in the case of Roberts splitters. This is to avoid erosion and potential undermining damage from continuous spilling short of the intended landing area.

2.2.3. Aeration of Roberts Splitters

When referring to 'aeration of Roberts splitters', it is important to differentiate between artificial aeration and self-aeration. Self-aeration occurs when the boundary layer of a certain flow reaches the surface and naturally mingles with the air above. This phenomenon is explained in more detail in Section 2.5. When referring to 'aeration of hydraulic structures' or 'aeration of Roberts splitters', the author is referring to artificial aeration.

The aeration of Roberts splitters, or any hydraulic structure in general, relies on an opening that supplies unpressurised air to a cavity or nappe within the flow. Figure 2-4 shows a simple type of aeration device in a simple chute explaining this principle (Chanson, 1992). Referring to Figure 2-4: as the flow passes over the deflector at a

reasonable velocity, a zone of sub-atmospheric pressure will exist immediately downstream of the deflector. This zone of sub-atmospheric pressure will suck air from the atmosphere, through the duct, and aerate the flow. The aeration of the flow happens similarly as with self-aeration and can be done if a high risk of cavitation is present to alleviate some of the severe pressure induced by the collapse of bubbles (further explained in Section 2.4).

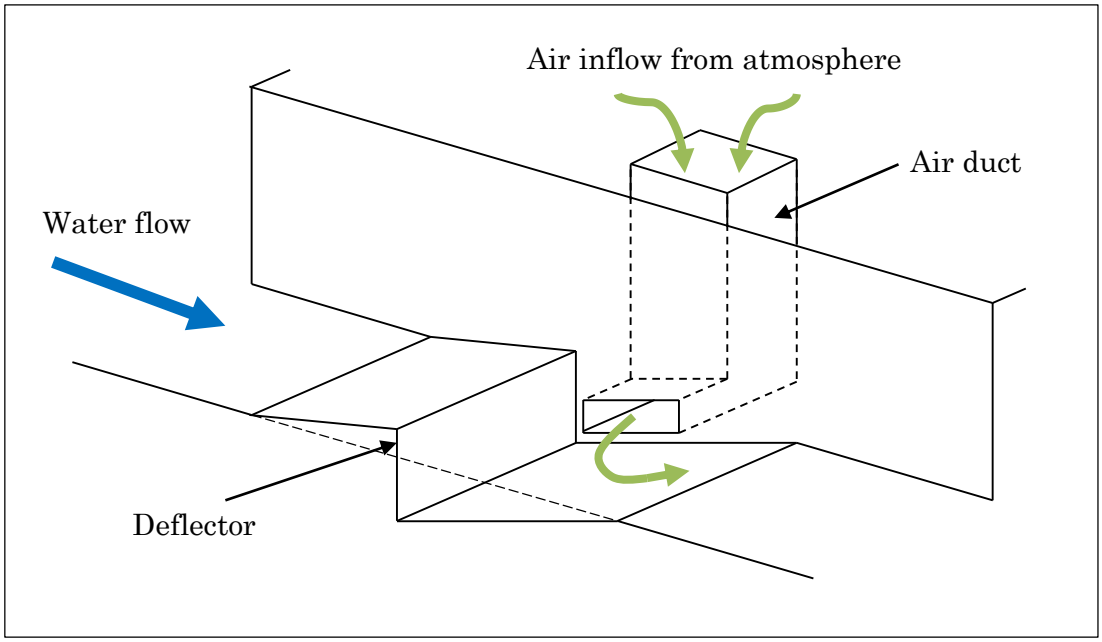

Figure 2-4: Simple flow aerator

This philosophy is similarly used on Roberts splitters to increase the sub-atmospheric presssures present around the system. The first prototype where aeration was provided for Roberts splitters was the spillway of the Gariep Dam in 1972 and then later at the downstream Vanderkloof Dam in 1977 and the Hazelmere Dam in KwaZulu-Natal, also in 1977 (Roberts, 1977). The succesfull application of aeration then migrated internationally to Sri Lanka at the Victoria Dam, completed in 1985, and also the Wadi Dayqah Dam in Oman, completed in 2009.

2.2.3.1. The Gariep and Vanderkloof Dams

The splitters and aeration of the Gariep and Vanderkloof Dams were similarly and simultaneously designed and tested by the Société Grenobloise d'Etudes et d'Applications Hydrauliques (Sogreah, now Artelia) in Grenoble, France (Mason, 2016). It consists of two 0.6 m diameter air vents at the end of each splitter along with a single 0.3 m diameter lateral air vent on both sides of each splitter. A series of larger 0.9 m diameter vents are placed below the continuous step downstream of the splitters (see

Figure 2-6 and Figure 2-8). According to Mason (2016), the splitter air vents are fed by the larger intake vents set in the step below, hence circulating air locally for each splitter (Figure 2-5). The aeration gallery is not open to the atmosphere, hence the air needed to aerate the flow only comes from the intake vents in the step. The aeration gallery rather serves to connect the step's large air vents with the smaller vents of the splitter, and for inspection and access to the splitters. Figure 2-7 shows the aeration gallery of the Gariep Dam as well as the two 0.6 m vents as seen from inside this gallery. Note the safety screen to prohibit direct access to the area connecting the large step vents below to the four splitter vents. The aeration gallery is relatively small compared to the main galleries of the dam being only 1.8 m high and 0.75 m wide.

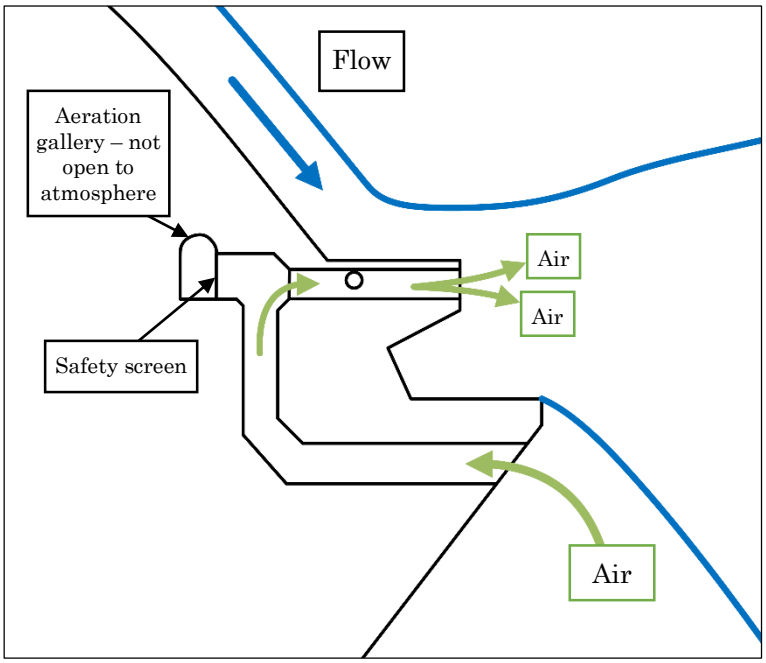

Figure 2-5: Working of Gariep Dam splitter aeration system

Figure 2-6: The Roberts splitters of the Gariep Dam showing aeration vents (Photo courtesy Gert Isaks, DWS)

Figure 2-7: Splitter air vents and aeration gallery of the Gariep Dam

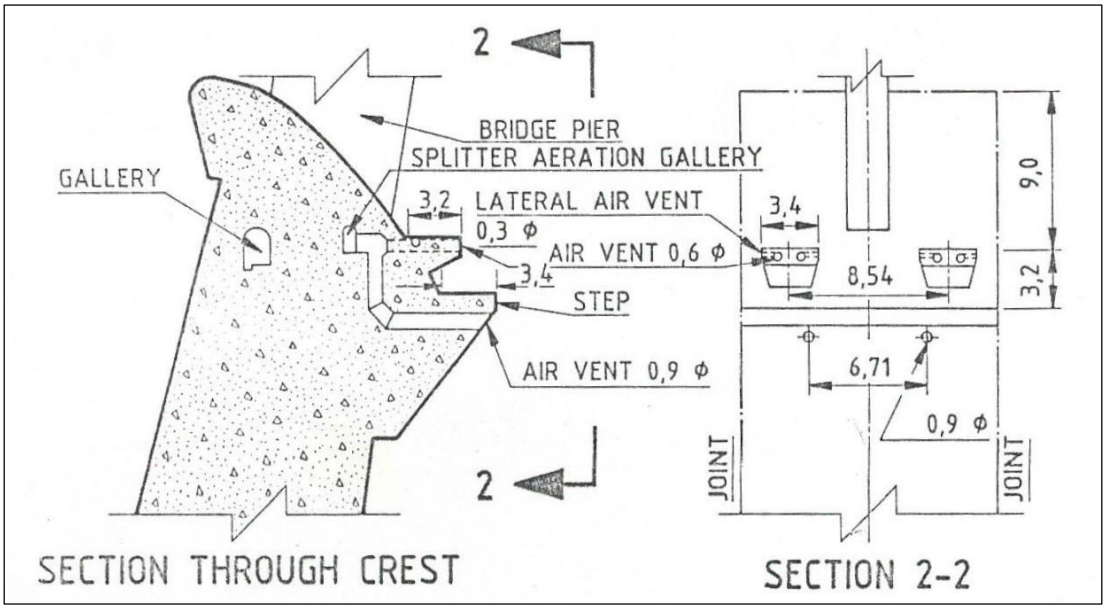

Figure 2-8: Typical detail of Gariep Dam splitter aeration (Roberts, 1977)

2.2.3.2. The Victoria Dam

The aeration ducts were slightly altered with the design of the Victoria Dam compared to the previous designs at the Gariep, Vanderkloof and Hazelmere Dams. The two main aeration vents at the end of each splitter were replaced by a short gallery to allow access to the step for inspection purposes, but still providing aeration (Figure 2-9). In effect the splitters were constructed as a roof and sides only structure (Mason, 2016). The splitters still contain the two minor side vents and the larger vents on the step.

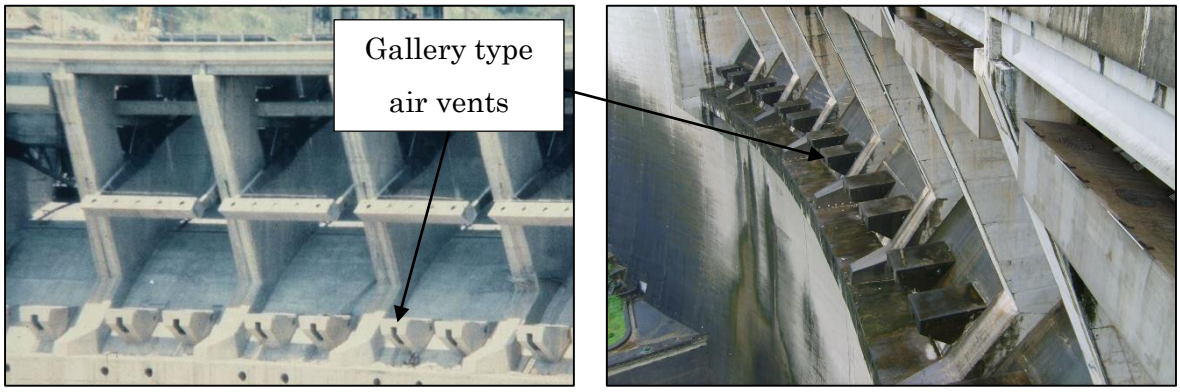

Figure 2-9: The Roberts splitters on the Victoria Dam showing gallery type air vents (Mason, 2004)

2.2.3.3. The Wadi Dayqah Dam

The splitters of the Wadi Dayqah Dam each have one larger vent at their ends instead of the two side by side vents as is the case on the three previously mentioned dams. It further incorporated the ideas of the Victoria Dam by allowing access to the step, but only through the two end splitters by using the same short gallery type vents. The rest of the splitters in between the two side splitters have more conventional round vents. Once again, the two minor side vents were kept on all splitters (Mason, 2016). A further alteration to the aeration design was the inclusion of "window vents" on the downstream face of the dam at either end and beyond the limits of the spillway, visible on the furthest wing wall of the spillway on the photograph of Figure 2-10. During model testing of the dam, it was found that the system performed better if the aeration gallery was open to the atmosphere via these "window vents" (Mason, 2016). Air would now be supplied by air vents in the step, along with the aeration gallery.

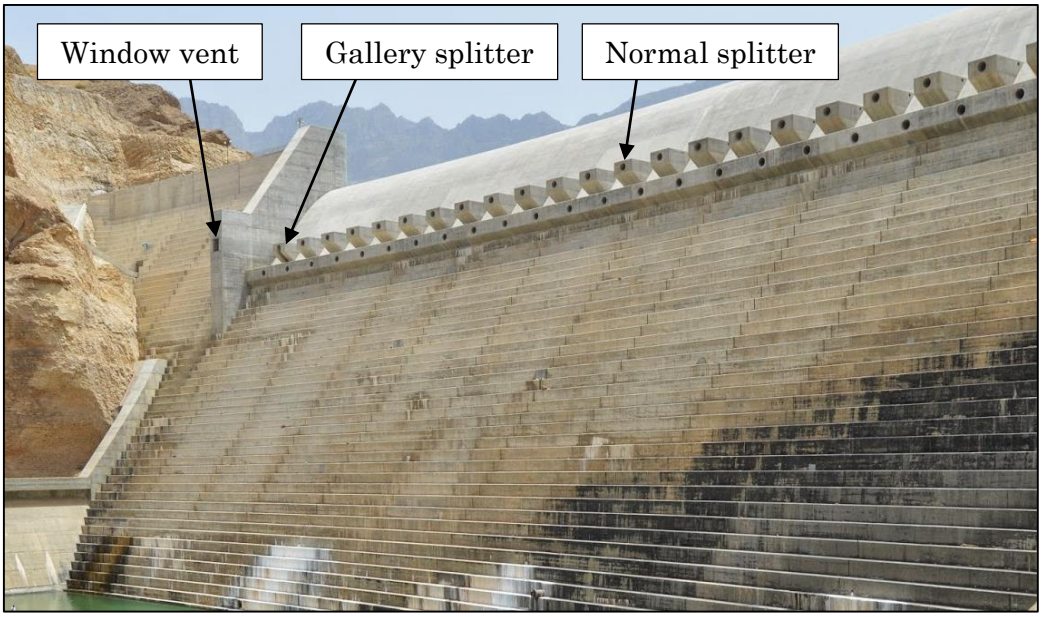

Figure 2-10: The spillway of the Wadi Dayqah Dam in Oman, equipped with Roberts splitters (Acharjya, 2014)

Figure 2-11: The Roberts splitters of the Wadi Dayqah Dam, showing the scale of the single main air vents (Mason, 2012)

2.2.3.4. Safety of Aeration Gallery

The operating staff at the Gariep Dam prohibits anyone from entering the aeration gallery during spilling to ensure their safety as wind speeds can get quite high in such a case (Isaks, 2016). The air velocities in Victoria Dam's aeration gallery also gets dangerously high. In previous spilling events, persons had to totally withdraw from the gallery as a result of the high wind speeds (Mason, 2016).

To fulfil the objective of implementing a safe aeration gallery for a dam equipped with Roberts splitters, the effect of air velocity on humans should be considered. Safety must be guaranteed to allow access to the aeration gallery during a flood. Air velocity, or wind speed, can be generalised using the Beaufort scale, thus giving a qualitative description of its effects, shown Table 2-2.

Table 2-2: Beaufort scale of wind speeds (Da Silva *et al.*, 1995, Lee, 1999)

Beaufort Number	Wind	Wind Speed Interval		Description
		m/s	km/h	
0	Calm	0.0 – 0.2	0.0 - 0.7	Calm, smoke rises vertically
1	Light air	0.2 – 1.8	0.7 - 6.5	Direction of wind shown by smoke, but not by wind vanes
2	Light breeze	1.8 – 3.3	6.5 - 11.9	Wind felt on face; leaves rustle; ordinary vane moved by wind
3	Gentle breeze	3.3 – 5.4	11.9 - 19.4	Leaves and small twigs in constant motion; wind extends light flag
4	Moderate breeze	5.4 – 8.5	19.4 - 30.6	Raises dust and loose paper; small branches are moved
5	Fresh breeze	8.5 – 11.0	30.6 - 39.6	Small trees in leaf begin to sway; crest wavelets form on inland waters
6	Strong breeze	11.0 – 14.1	39.6 - 50.8	Large braches in motion; telegraph wires whistle; umbrellas used with difficulty
7	Near gale	14.1 – 17.2	50.8 - 61.9	Whole trees in motion; inconvenience in walking against wind
8	Gale	17.2 – 20.8	61.9 - 74.9	Breaks twigs of trees; generally impedes progress
9	Strong gale	20.8 – 24.4	74.9 - 87.8	slight structural damage occurs; chimney pots and slates removed
10	Storm	24.4 – 28.6	87.8 - 103.0	Trees uprooted; considerable structural damage occurs
11	Violent storm	28.6 – 32.7	103.0 - 117.7	Very rarely experienced; accompanied by widespread damage
12	Hurricane	>32.7	>117.7	Devastation occurs

If a person stands or moves in a wind, a drag force would act on them directly proportional to their projected area according to Eq. (2-1):

$$F_d = \frac{1}{2} \cdot c_d \cdot \rho_{air} \cdot (v_{wind})^2 \cdot A_{proj} \qquad (2\text{-}1)$$

where F_d is the force acting on them, c_d is their drag coefficient, ρ_{air} is the density of air, v_{wind} is the relative wind speed and A_{proj} is the person's projected area in the wind's direction. Table 2-3 shows the acting drag force on an average person standing in wind.

Table 2-3: Wind force acting on a person at various Beaufort numbers (Lee, 1999)

	BN = 4	BN = 5	BN = 6	BN = 7
Force on standing person with frontal wind exposure[1] (N)	33	60	99	148

Note: 1: Based on a projected area of 0.73 m^2 and a drag coefficient of 1.15

Lee (1999) argues that a person would be uncomfortable and inconvenienced in wind with a Beaufort number of 7. This led to the conclusion that a to permit persons to enter a proposed aeration gallery during flood events, the velocity in the duct must be kept below 14.1 m/s. This can be done by increasing the size of the aeration gallery.

2.2.4. Limitations of Roberts Splitters

The Roberts splitters system has a few limitations as described below:

2.2.4.1. Spillway Head Limit

Roberts (1943) first introduced the limit of 3.0 m of spillway head. He stated that individual model tests were required in order to validate his design if the design head of a given prototype was greater than 3.0 m. If using a conventional ogee spillway, this typically equates to a unit discharge of 12 m^2/s. This rule was followed for all subsequent dam designs until that of the Gariep and Vanderkloof Dams. With the introduction of aeration and the dam type being a double curvature arch dam, the distance the jet had to travel away from the toe of the dam decreased considerably, and the allowable spillway heads (considering future raising) were tripled to 9.1 m and 9.0 m respectively (Jordaan, 1989). The splitters were however dimensioned for a spillway head of 7.3 m and while it was discovered that sub-atmospheric pressures existed on the spillway just downstream of the crest at heads greater than 6.0 m, the cavitation co-efficient of $\sigma = 0.3$ was considered acceptable (Back *et al.*, 1973). The highest allowed head for Roberts splitters is that of the Victoria Dam at 10.0 m (Jordaan, 1989).

This study aimed to investigate in detail the pressures specifically around the splitters as the spillway head increases and exceeds the design head.

2.2.4.2. Critical Head Limit

Roberts (1943) further stated that a critical head exists at which the splitters become drowned. He designated this as 1.2 times the design head. Further tests at the Rhenosterkop Dam in Mpumalanga, South Africa confirmed Roberts' initial suggestions (Jordaan, 1989).

2.2.4.3. Dam Height Limit

The highest dam where Roberts splitters were successfully used is the Victoria Dam at a height of 122 m. Years later it was considered as one of three options for the spillway of the 180 m high Katse Dam in Lesotho, along with a slightly dentated ogee and a

serrated bucket ogee. The option of the dentated ogee was discarded prima facie and after model tests it was found that the Roberts splitters performed unsatisfactory and the serrated ogee bucket was chosen as the final design (Jordaan, 1989). The trajectories of the different jets caused by the splitter and step arrangement drew closer together again after the maximum spread had occurred at about 90 m below the crest. This phenomenon, along with increased impact velocities from the high plunge, substantially increased the pressures on the apron of the dam and the scour risk (Jordaan, 1989). According to Jordaan (1989) the upper limit for dam height for Roberts splitters appears to be 120 m. This study did not look into this limit, as later described with the design and scale of the hydraulic model.

2.2.4.4. Cavitation Limit

The cavitation limit is not necessarily applicable to only Roberts splitters, but to hydraulic structures in general. Chadwick *et al.* (2013) states that a general limit of -7 m of pressure head (gauge), equivalent to 3 m absolute, will be sufficient to avoid cavitation. An alleviating factor is however air concentration within the flow. Summarising Chanson's (1992) recommendations, an air concentration of between 4% and 8% within the flow will prevent cavitation erosion on spillways for velocities of up to 45 m/s. The concept of cavitation is, however, much more complex than this and is described in more detail in Section 2.4. For the purpose of this study, it was accepted that if a gauge pressure of less than -7 m existed anywhere on the hydraulic model, cavitation could occur if the air concentration of the fluid is less than 8%.

2.2.4.5. Spray Generated from Plunging Jet

Roberts (1977) reported that the only drawback of Roberts splitters is the spray that is generated from the plunging jet of water. This must be considered in the presence of nearby electrical control rooms and hydro-electric power stations.

2.2.5. Roberts Splitters Design Procedure

Roberts' (1943) original procedure for the design of crest splitters were summarised by Roberts (1980) at a course presented at the University of Pretoria on the design of dams. The procedure as set out below follows the summary of Roberts (1980). Table 2-4 provides the symbols used in the design along with a description. Figure 2-12 shows the general profile of Roberts splitters, as depicted on a concrete gravity dam much like that of the Loskop Dam (Roberts, 1980).

Table 2-4: Symbols referred to in the design of Roberts splitters

Symbol	Meaning
H_D	Design head
H_C	Maximum head before drowning of dispersing action
H_a	Minimum head for efficient operation
x	Vertical distance from reservoir water level (top of design head) to the top of the water flow on the step
y	Vertical distance from the top of the flow on the step to the top of the tailwater
N	Number of splitters per bay
B	Bay width
P	Vertical distance from apex of crest to top of splitter
C	Vertical distance from apex of crest to top of step
T	Vertical distance from top of splitter to top of step
W	Width of splitter
S	Gap width between splitters
L	Length of splitter
L_S	Length of step
R_{min}	Horizontal distance between the inside of nappe to the toe of the dam at tailwater height
R_{max}	Horizontal distance between the outside of nappe to the toe of the dam at tailwater height
θ	Angle of downstream face with the horizontal

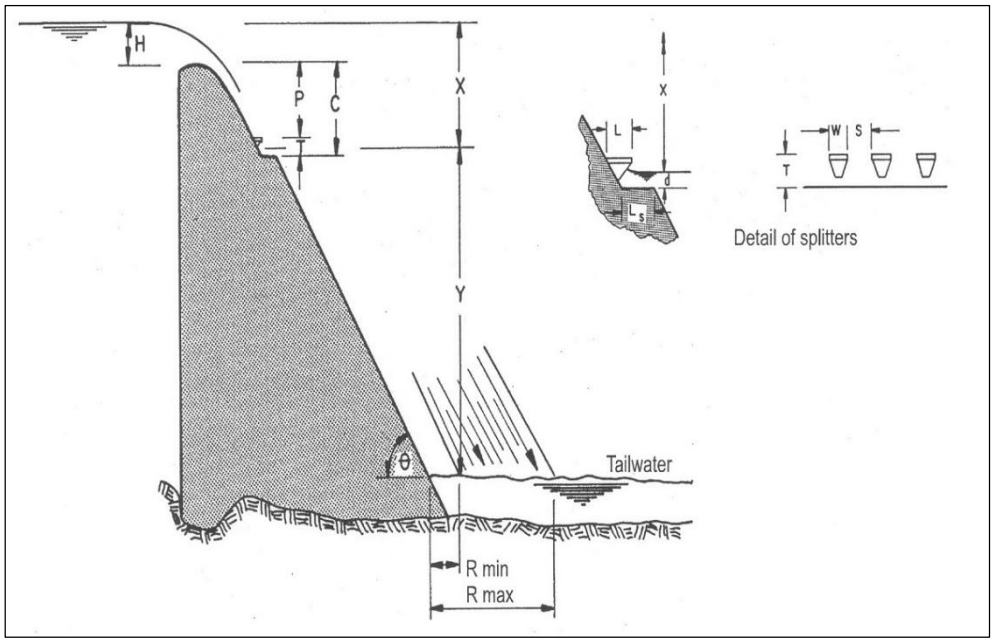

Figure 2-12: General profile of Roberts splitters (Roberts, 1980)

2.2.5.1. Important Considerations Regarding the Design Procedure:

i. The method is empirical and relies on the ingenuity of the designer. There can thus be different designs for the same spillway and design head.

ii. The design relies on the designer to choose the dimension P, the height of the splitters below the crest, as well as the number of splitters N.

iii. A series of iterations should be made in order to match up the dimensions of the splitters, calculated in two different ways.

iv. The values of R_{min} and R_{max} indicates the profile of the plunging jet as determined by Roberts (1943). It can be used by the designer to ensure that the jet falls where he/she wants it to.

v. Careful consideration must be made in choosing the number and position of the splitters, as more and smaller splitters requires a larger distance P to allow the same dispersing action of less and larger splitters. The spillway length may however, allow only a certain amount of splitters.

2.2.5.2. Roberts' (1943) Procedure

The procedure is set out in a series of numbered steps and reference to step are made within block brackets, e.g. [step 1].

Step 1: Determine H_C and H_a as follows:

$$H_C = 1.2H_D \tag{2-2}$$

$$H_a = \frac{H_C}{4.4} \tag{2-3}$$

where H_C is the critical head where the splitters become drowned, H_a is the minimum operating head where dispersive action commences and H_D is the design head of the splitters.

Step 2: For the splitters to function effectively, check:

$$x + y > 4H_D \tag{2-4}$$

where x is the vertical distance from reservoir water level (top of design head) to the top of the water flow on the step and y is the vertical distance from the top of the flow on the step to the top of the tailwater.

Step 3: Choose number of splitters per bay as N

a. Therefore

$$(S + W) = \frac{B}{N} \tag{2-5}$$

b. as

$$S = T = L = 1.33W \tag{2-6}$$

c. therefore

$$W = \frac{(B/N)}{2.33} \tag{2-7}$$

d. and

$$S = T = L = \frac{4}{7} \times \frac{B}{N} \tag{2-8}$$

where S, T, L and W are splitter dimensions (refer to Table 2-4 and Figure 2-12) and B is the spillway width

Step 4: Select L_s so that:

$$1.25 \leq \frac{L_s}{L} \leq 1.5 \tag{2-9}$$

where L_s is the length of the step.

Step 5: Assume a value for the vertical distance from apex of crest to top of splitter P, and:

a. Determine (W/P) using (H_C/P) from Figure 2-13;
b. Calculate

$$W = P \times (W/P) \tag{2-10}$$

c. Check that $W\ from\ eq.(2\text{-}10) \approx W\ determined\ from\ eq.(2\text{-}7)$

Step 6: Determine

$$x \approx H_D + P \tag{2-11}$$

$$y = (Dam\ height + H_D - Tailwater\ depth) - x \tag{2-12}$$

Step 7: Determine f from Figure 2-14 using $\frac{C}{H_D}$, where f is a correction factor based on the height of the splitters and step below the crest of the dam.

Step 8: Calculate R_{min} and R_{max} using:

$$R_{min} = f \times \sqrt{xy} - y \cdot cot\theta \tag{2-13}$$

$$R_{max} = 2f \times \sqrt{xy} - y \cdot cot\theta \tag{2-14}$$

Where R_{min} is the horizontal distance between the inside of nappe to the toe of the dam at tailwater height, and R_{max} is horizontal distance between the outside of nappe to the toe of the dam at tailwater height.

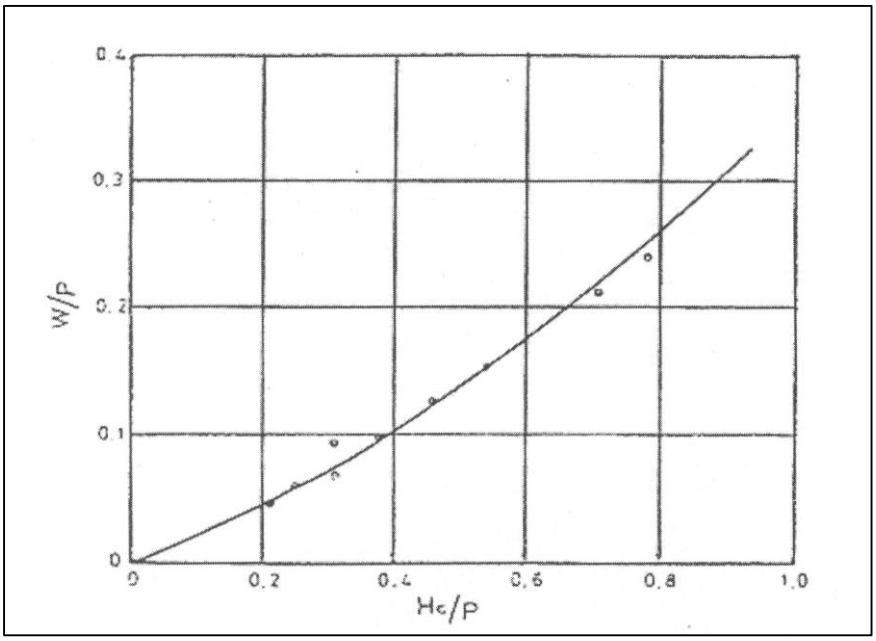

Figure 2-13: Dimensions of splitters (Roberts, 1980)

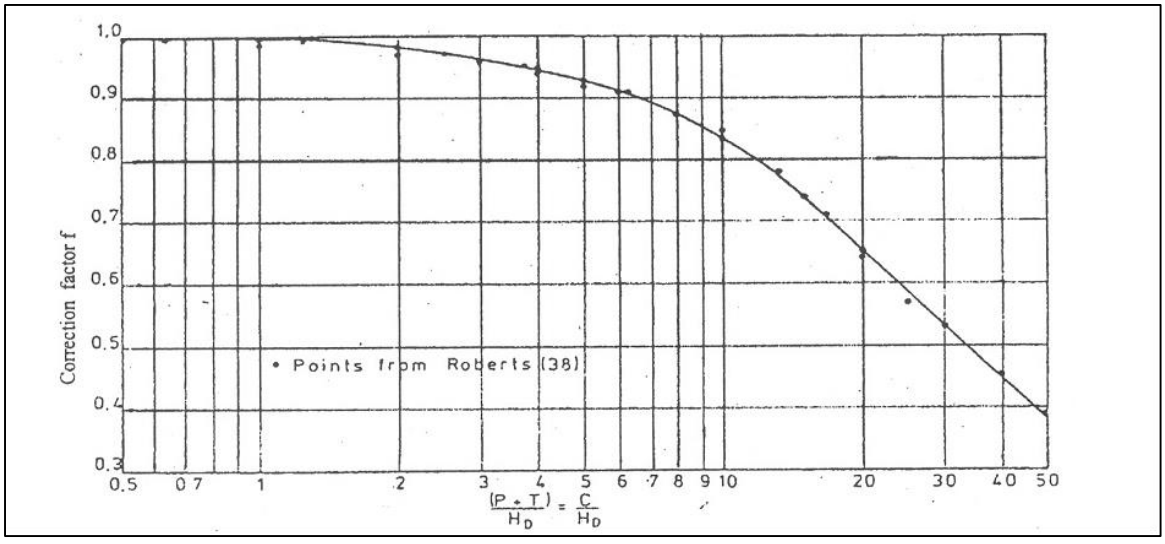

Figure 2-14: Correction factor *f* as a function of step below the crest and design head (Roberts, 1980)

The design is sufficient subject to the following criteria:

i. All considerations were met as put out in Section 2.2.5.1;
ii. The value for W from Eq. (2-10) must coincide reasonably with that from Eq. (2-7);
iii. The value of dimension L_S must come from [step 4];
iv. The value of dimension P must come from [step 5];

All other final dimensions of the splitters should, unless impossible, come from [step 3].

2.2.6. Variances to Roberts Splitters

After the original Roberts (1943) design procedure had successfully been used on several South African concrete gravity dams, Jordaan (1989) stated that with concrete gravity dams like the Loskop Dam, the constant downstream face aided the rotational energy imparted on the dispersing jet, increasing the natural aeration as the jet falls freely to the plunge pool below. With high, thin arch dams however, this phenomenon was not present and the impact conditions differ to those of concrete gravity dams as the jets had much higher impact velocities, hence creating more severe pressures on concrete aprons or natural scour holes. Mason (1983) found that adjustments were made to the splitter dimensions for each of the major dams where aeration was provided (see Section 2.2.3) to optimise the pressures on the aprons of these dams – three of these being high arch dams. He concluded from his findings that improvements could be made to Roberts' (1943) original procedure.

2.2.6.1. Mason's (1983) Procedure

Mason (1983) related the dimensions of the optimised system to the depth of the flow reaching the splitters, similar to the approach used to proportion the dimensions of baffle blocks in stilling basins. The meaning of symbols are shown in Figure 2-15 and relate closely to those of Roberts' (1943) procedure.

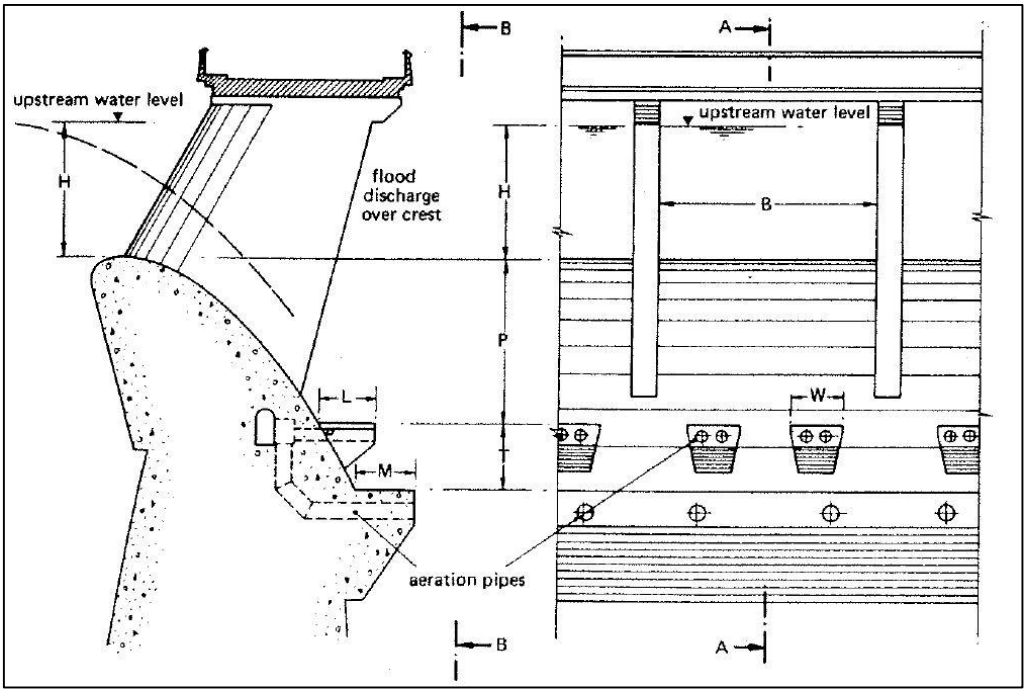

Figure 2-15: Typical splitter arrangement for Mason's (1983) procedure

Mason (1983) showed that, from basic energy equations:

$$P + H = d + v^2/2g \tag{2-15}$$

where d is the depth of flow approaching the splitters, while for a free overspill crest:

$$q = KH^{3/2}$$

$$\text{thus } v = \frac{KH^{\frac{3}{2}}}{d} \tag{2-16}$$

where K is a constant. Substituting Eq. (2-16) into Eq. (2-15), and using a second constant K', gives:

$$P + H = d + K' \cdot \frac{H^3}{d^2}$$

$$\text{where } K' = K^2/2g$$

Hence:

$$(P + H) \cdot d^2 = d^3 + K' \cdot H^3$$

$$d^2 \cdot (P + H - d) = K' \cdot H^3$$

$$d = \sqrt{\frac{K' \cdot H^3}{P + H - d}} \tag{2-17}$$

Assuming d is small in relation to $P + H$, from Eq. (2-17):

$$d \propto \sqrt{\frac{H^3}{P+H}}$$

so that:

$$\frac{d}{(P+H)} \propto \left[\frac{H}{(P+H)}\right]^{3/2}$$

$$\frac{d}{(P+H)} = f\left[\frac{H}{(P+H)}\right] \quad (2\text{-}18)$$

Eq. (2-18) is dimensionless and relates the parameter $d/(P+H)$ to the parameter $H/(P+H)$. He argued that if the dimensions of the splitter arrangement (T, L and W) were proportional to the flow depth d approaching the splitters, then any one of them divided by $(P+H)$ should also be proportional to $H/(P+H)$.

He tested his hypothesis against the hydraulic model test results from the four major dams with aerated Roberts splitters at the time, being the Gariep, the Vanderkloof, the Hazelmere and Victoria Dams (henceforth referred to as the prototype cases) to determine the best relationships of the splitter dimensions to the parameter $(H+P)$. Figure 2-16 shows these plots. The following relationships were deduced by Mason (1983):

- $T = 0.15\ to\ 0.25(H+P)$
- $L = 0.15\ to\ 0.25(H+P)$
- $W = 0.1\ to\ 0.25(H+P)$

From Figure 2-16 it can further be seen that for all four prototype cases the selected value for P was chosen so that:

$$H_{max}/(H_{max}+P) \approx 0.5 \quad (2\text{-}19)$$

Eq. (2-19) becomes:

$$P \approx H_{max} \quad (2\text{-}20)$$

From Eq. (2-20) and Figure 2-16, Mason (1983) suggested the following relationships:

- $T = 0.4 \cdot P$
- $L = 0.4 \cdot P$
- $W = 0.3 \cdot P$

The value of M was determined by again referring back to the four prototype case and relating M to L. The value of M/L for the four cases are 1.12, 1.00, 1.05 and 1.03. He assumed it reasonable to deduct that:

$$M = L$$

This is significantly less than between $1.25L$ and $1.5L$ recommended by Roberts (1943), probably because three of the prototype cases are very high arch dams, not needing the extra step length to project the flow away from the toe of the dams.

Mason (1983) noted that the space between splitters, S, was not as simple to relate to W as Roberts (1943) proposed. This was because all prototype cases included crest piers on their spillways. However, if N is taken as the number of splitters per width B, the width of an opening between piers, the relationships $(N \cdot W)/B$ for the prototype cases were 0.43, 0.48, 0.52 and 0.48. He argued that it can safely be assumed that over the width of any one opening:

$$\sum S \approx \sum W \tag{2-21}$$

In the absence of crest piers, Eq. (2-21) would become:

$$S = W$$

According to Mason (1983), Roberts' (1943) relationship of $S = 1.33W$ was also acceptable.

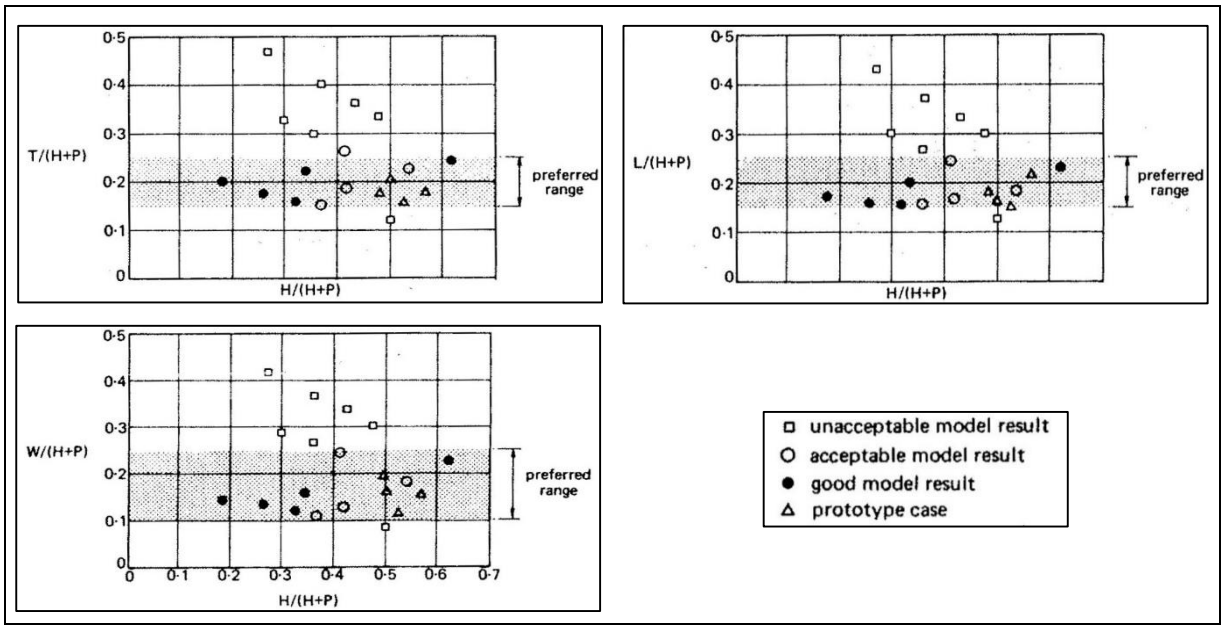

Figure 2-16: Dimensionless plots for parameters *T, L* and *W* from prototype and model results (Mason, 1983)

The effectiveness of Mason's (1983) proposals were confirmed when Back and Mee (1991) reported that the impact pressures of the jet on the downstream apron of the Victoria Dam was reduced from 30 m to 18 m by modifying Roberts' (1943) relationships (Khatsuria, 2005). These results are shown in Figure 2-17.

It is important to note that these improvements are still subject to model studies if different types of dams are required. Mason's (1983) splitter configuration produced best results on the spillways of high arch dams. In an email from Mason (Mason, 2016), it was stated that the Roberts splitters designed for the Wadi Dayqah Dam was done according to this procedure. During model studies of the spillway, it was found that the height *P* had to be increased to allow for sufficient flow velocity to project the jet further. The Wadi Dayqah Dam is an RCC gravity dam, and not a high arch dam.

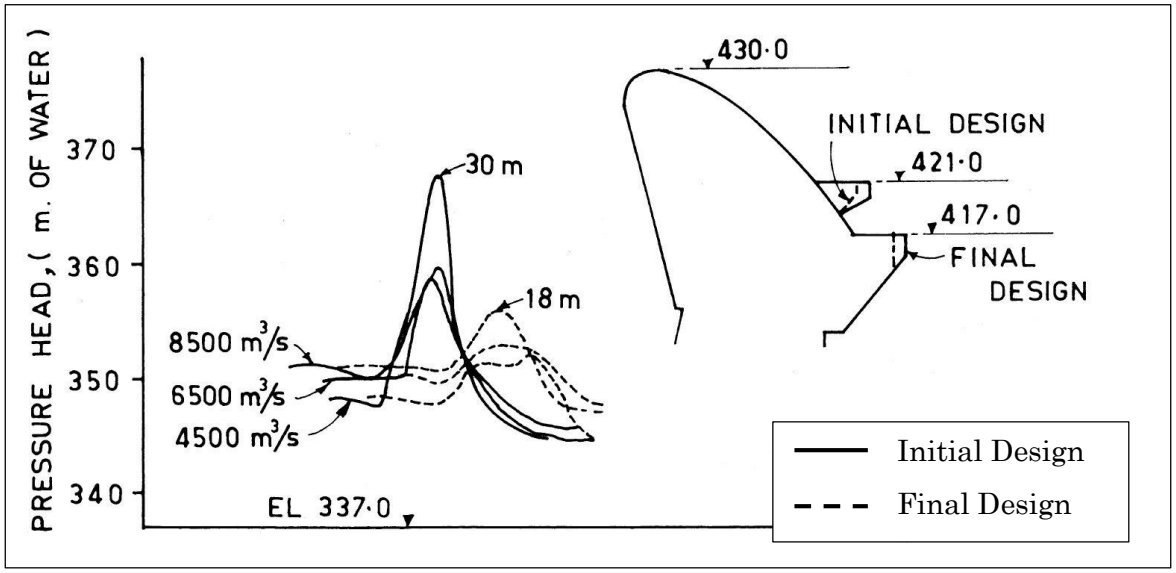

Figure 2-17: The effect of Mason's (1983) splitters on apron impact pressures (Back & Mee, 1991)

2.3. Sub-Atmospheric Pressures on Spillways

Sub-atmospheric pressures can occur on spillways when high velocity flows tend to leave the surface upon which it flows. This is called flow separation. This can happen when an ogee spillway is under designed, or when hydraulic structures like steps, baffles, or teeth i.e. Roberts splitters, deflect high velocity flow. Unaerated flow separation can lead to sub-atmospheric pressures and cavitation. This section focusses on when and where sub-atmospheric pressures can be expected on dam spillways, in order to predict such pressures on Roberts splitters. The first instance is on the crest of the ogee spillway, and the second instance is on the splitters.

2.3.1. On the Crest of a Spillway

The complete design of an ogee spillway according to the USBR (1987) method is explained in Appendix D.

An important factor concerning the design of an ogee spillway is sub-atmospheric pressures existing on the crest. An ogee spillway resembles the nappe formed by a design head H_0 discharging over a sharp crested weir. If the spillway head, H_e, of the ogee is exactly equal to the design head, a state of equilibrium will exist on the crest resulting in zero nett pressure, or atmospheric pressure. If H_e is less than H_0, the pressure on the crest will be nett positive, or more than atmospheric. And if H_e is greater than H_0, the pressure on the crest will be nett negative, or sub-atmospheric.

Ogee spillways are however designed for less than maximum head, i.e. H_0 is less than H_{max}, with H_{max} being the spillway head of the design flood, for economic reasons (USBR, 1987). Tests have shown that the sub-atmospheric pressures found on the crest of an ogee will be less than $0.5H_0$ and will extend down the crest a horizontal distance of H_0 if:

$$H_0 = 0.75 \cdot H_e$$

This will greatly reduce the width of the spillway, as the ogee follows a smaller nappe. The sub-atmospheric crest pressures are shown in Figure 2-18. The sub-atmospheric crest pressures can be expected to vary linearly when ratios of design head to spillway head other than 0.75 occur.

However, care must be taken during construction in ensuring the surface of the crest be finished as smooth as possible and that the shape of the ogee be built as precise as possible. Any unevenness, depressions, projections or abrupt offsets such as construction joints will amplify the pressures and intensify the risk of cavitation (USBR, 1987).

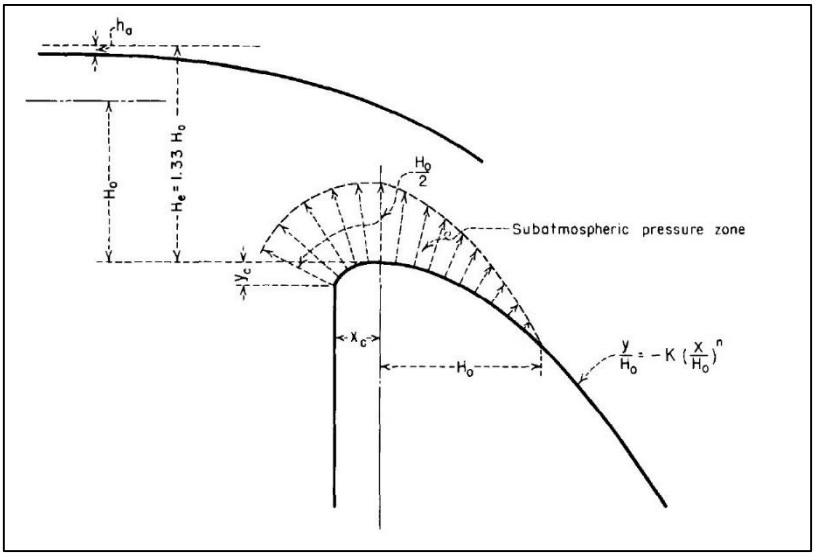

Figure 2-18: Sub-atmospheric crest pressures for $H_0 = 0.75H_e$ (USBR, 1987)

2.3.2. On Steps on a Spillway

The occurrence of sub-atmospheric pressures on stepped spillways has been widely studied and numerous publications exist on the subject. It is relevant to the study of sub-atmospheric pressures on Roberts splitters, as it gives an initial indication of where to expect these pressures on the hydraulic model.

Chen *et al.* (2002) conducted experiments on a stepped spillway model, positioning ten piezometers per step as shown in Figure 2-19. The results were compared with those obtained from CFD modelling, and were found to be similar. The comparison is shown in Figure 2-20. The only sub-atmospheric pressures occurred on the vertical face of each of the steps during high discharges, producing a skimming flow regime.

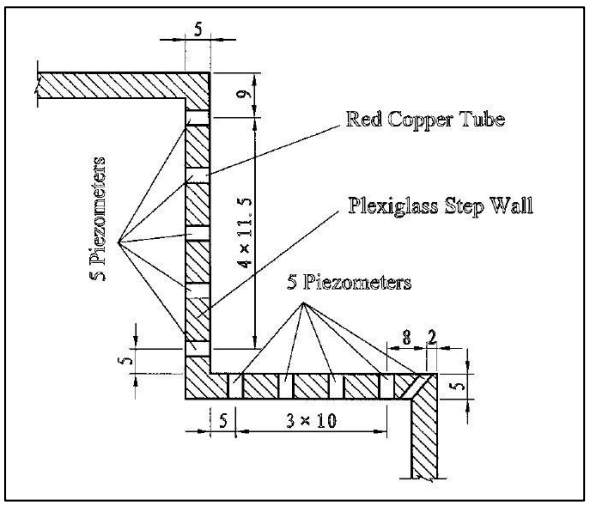

Figure 2-19: Set-up of piezometers (dimensions in mm) (Chen *et al.*, 2002)

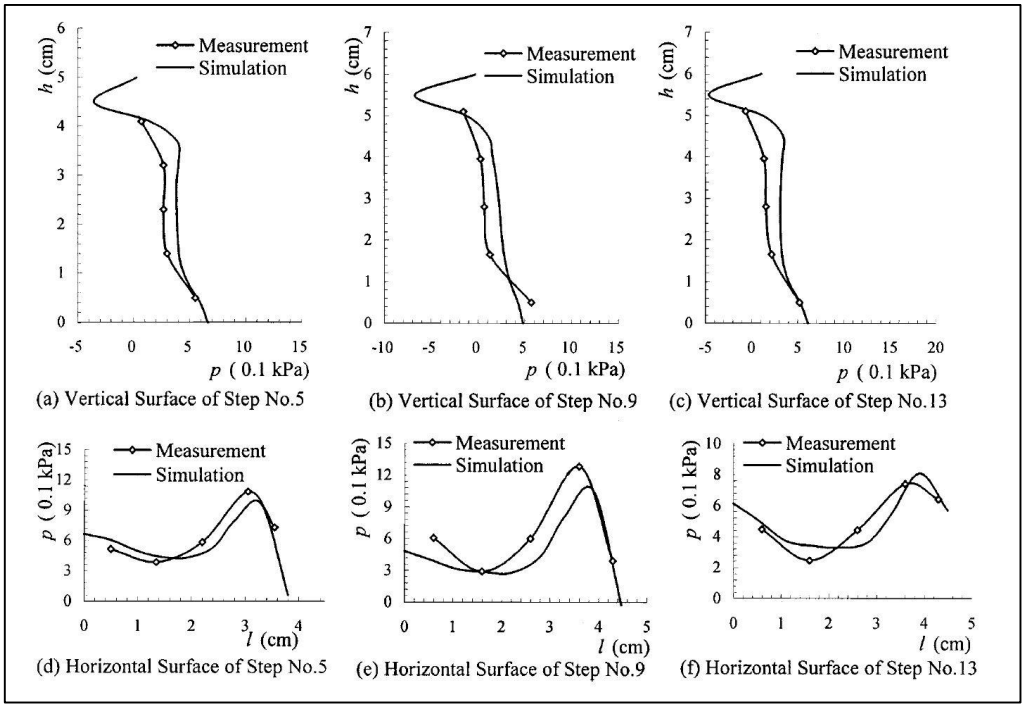

Figure 2-20: Pressure profiles on steps of stepped spillway (Chen *et al.*, 2002)

Nikseresht *et al*. (2013) conducted similar CFD modelling, revealing similar results. Once again the only sub-atmospheric pressures occurred on the vertical face of each of the steps, and concentrated towards the top edge. The findings are shown on Figure 2-21.

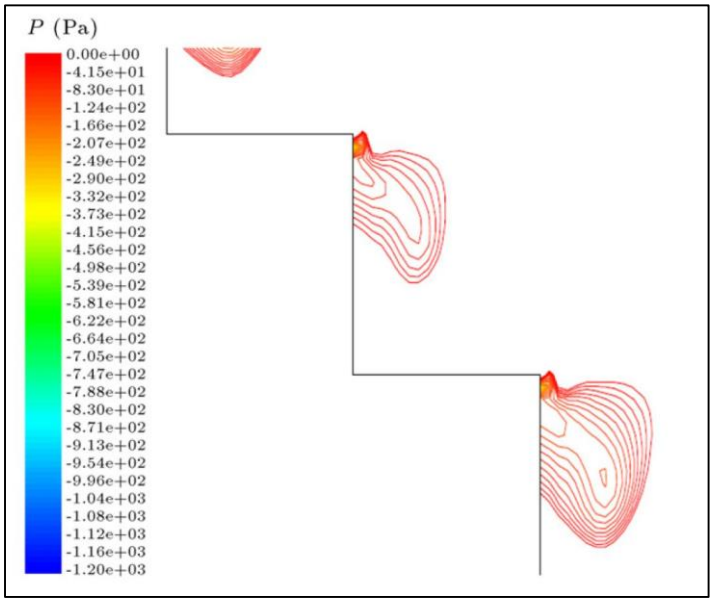

Figure 2-21: The local negative pressure on steps in a two-phase flow model (Nikseresht *et al.*, 2013)

The conclusion from these findings is that sub-atmospheric pressures can be expected where high velocity flow leaves a step or edge of a structure. According to Wright (2006),

the presence of vortices will further induce sub-atmospheric spikes, even though it might be highly aerated.

2.4. Cavitation

2.4.1. Mechanism of Cavitation

The simplest form of cavitation occurring on a day to day basis is the boiling of water. As the water is heated, its vapour pressure increases, until it reaches the pressure of the fluid and begins to boil (Khatsuria, 2005). Essentially, cavitation (or boiling) commences when either the vapour pressure of a fluid is increased and reaches the pressure of the fluid, or, more commonly in hydraulic structures, the fluid pressure is reduced and reaches its vapour pressure.

The vapour pressure of water at room temperature is 3.17 kPa (absolute) (Lide, 2005), or equal to ~0.3 m of pressure head. As the pressure of atmosphere is 101.3 kPa, equal to a pressure head of 10.3 m, theoretically and following the above description, cavitation will commence when the fluid pressure drops to 0.3 m (absolute), or -10 m atmospheric. However, it is inadvisable operate hydraulic structures at pressure heads less than 3 m absolute (-7 m atmospheric) as small solid particles in suspension or the presence of dissolved gases causes cavitation to commence at higher pressures (Chadwick *et al.*, 2013).

Fundamentally in hydraulic structures, cavitation is characterised by the severe and explosive growth and collapse of vapour bubbles. Either a drop in dynamic fluid pressure, or a rise in temperature, or a combination of both may cause these vapour bubbles to form (Chanson, 1988).

The three main types of cavitation are (Chanson, 1988):

i. Vaporous cavitation – the appearance and growth of bubbles due to dynamic pressure reduction;
ii. Gaseous cavitation – diffusion of dissolved gas out of the solution, causing the growth of gas bubbles;
iii. Boiling – continuously growing vapour bubbles as the vapour pressure is constantly higher than the dynamic fluid pressure.

When the fluid pressure again increases to higher than its vapour pressure, the growth of bubbles will be reversed. Chanson (1988) states that the bubbles will disappear either

by gas solution and vapour condensation (in the case of the boiling process), by collapse (vaporous cavitation) or a by a combination of both (gaseous cavitation). In hydraulic structures and spillways, vaporous cavitation is generally regarded as the most important type of cavitation (Khatsuria, 2005), as fluctuating sub-atmospheric pressures can easily occur (see Section 2.3).

Chanson (1988) indicated that weak spots or the presence of a nucleus in the liquid was necessary for cavities to form and thus, for cavitation to commence. Nuclei-free liquids are rare in practice and have very high tensile strengths. The presence of nuclei is generally associated with undissolved gas or suspended solids with the liquid.

2.4.2. Cavitation Index

The cavitation index is used in hydraulics to estimate the likelihood of cavitation to commence with a certain flow system. Khatsuria (2005) summarised the concept as follows, with point M being the location where the cavitation index was to be calculated:

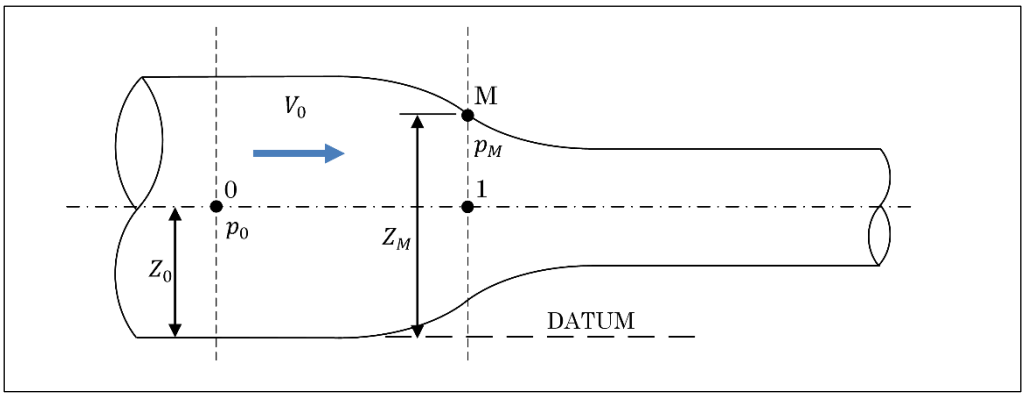

Figure 2-22: Concept of cavitation index (Khatsuria, 2005)

Referring to Figure 2-22, the static fluid pressure at point 0 is defined as p_0. At point 1 it is calculated with reference to point M as:

$$p_1 = p_M + \gamma \cdot (Z_M - Z_0) \tag{2-22}$$

where:

p_M = Static pressure at point M

γ = Specific weight of fluid

Z_M and Z_0 are the elevations at points M and 0

As the fluid moves along a stream line from point 0 to point 1, the pressure drop is now:

$$\Delta p = p_0 - [p_M + \gamma \cdot (Z_M - Z_0)] \tag{2-23}$$

Khatsuria (2005) stated that the cavitation index σ normalised this pressure drop to the dynamic pressure $\frac{1}{2}\rho V_0^2$, where ρ was the mass density of the fluid and V_0 was the velocity at point 0. Thus:

$$\sigma = \frac{p_0 - [p_M + \gamma \cdot (Z_M - Z_0)]}{\frac{1}{2}\rho V_0^2} \tag{2-24}$$

Now, if cavitation has just started commencing at point M, and a growing bubble would appear, by definition the pressure of the fluid adjacent to the bubble is equal to the pressure inside the bubble, i.e. the vapour pressure, p_v, of the fluid. Hence:

$$p_M = p_v$$

Therefore, from Eq. (2-23), the pressure drop along the streamline from point 0 to point 1 required for cavitation to commence at point M is:

$$\Delta p = p_0 - [p_v + \gamma \cdot (Z_M - Z_0)] \tag{2-25}$$

and the cavitation index at the condition of incipient cavitation is:

$$\sigma_i = \frac{p_0 - [p_v + \gamma \cdot (Z_M - Z_0)]}{\frac{1}{2}\rho V_0^2} \tag{2-26}$$

Khatsuria (2005) argued that the elevation terms could be ignored for large velocities, and therefore the cavitation index became:

$$\sigma_i = \frac{p_0 - p_v}{\frac{1}{2}\rho V_0^2} \tag{2-27}$$

Chanson (1988) explained that to avoid cavitation at any point M where cavitation could be expected within a system, the cavitation index σ should be greater than a critical number referred to as σ_C such that:

$$\sigma_i > \sigma_C \tag{2-28}$$

where the critical cavitation number is calculated as:

$$\sigma_C = \left(\frac{V_M}{V_0}\right)^2 - 1 \tag{2-29}$$

with V_M being the local velocity outside of the boundary layer at point M. The lower the value for σ_i below that of σ_C, the worse the cavitation action will be (Chanson, 1988).

He further mentioned that for simple bodies, such as a sphere, the local velocity V_M could be relatively easily calculated at each position M, but for more complex systems, σ_C must be obtained by model studies or CFD analysis.

2.4.3. Damage due to Cavitation

Consider the situation where vaporous cavitation occurs at a certain position of a hydraulic structure due to very low local fluid pressure and the presence of several nuclei or weak spots within the liquid. The growing bubbles caused by the cavitation will travel along with the fluid, reaching a part of the structure where the pressure again increases to more normal conditions. These bubbles will then collapse, sending out severe shock waves with high pressure on an infinitely small area for only fractions of a second (Khatsuria, 2005). The peak pressure of such a shock wave can be as high as 400 MPa (Chadwick *et al.*, 2013). Although such a single local shock wave may not draw much attention, if the process is prolonged for long enough, even a few minutes, the continuous blows can leave devastating damage and the irregularities of the damaged area will in turn cause more cavitation (Chadwick *et al.*, 2013). Figure 2-23 shows some typical locations where cavitation can occur on hydraulic structures and where to expect the resulting damage.

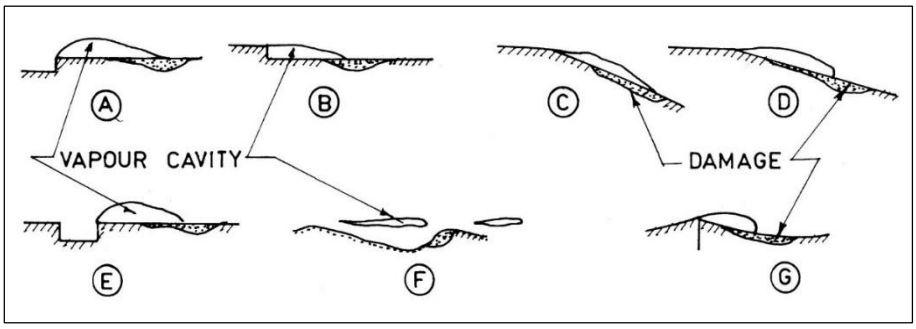

(A) Offset into flow
(B) Offset away from flow
(C) & (D) Abrupt curvature away from flow
(E) Void or transverse groove
(F) Irregular surface
(G) Protruding joint

Figure 2-23: Typical locations where cavitation can be expected (Roberts, 1980, Khatsuria, 2005)

Figure 2-24 shows the different processes of an imploding bubble and the shock waves resulting from the implosion. Three mechanisms exist where a surface can be severely damaged by the process of bubble collapse, all referred to in general as cavitation pitting (May, 1987). The first entails small micro-jets forming and bisecting a collapsing bubble (Figure 2-24 (iii)). As the dynamic fluid pressure increases around a bubble, a weak part

of the bubble gives in first, projecting through the rest of the bubble as a micro-jet, reaching velocities of up to 130 m/s, resulting in pressures of up to 150 MPa (May, 1987). Secondly, the shock waves (Figure 2-24 (v) & (vi)) generated by the collapse and reform of a bubble can produce pressures of up to 20 MPa (Chanson, 1988). The third, and much more damaging mechanism, is the formation of micro-jets. These jets are formed when the shock waves of a collapsing bubble cause an asymmetric collapse of a nearby smaller cavity, similar to the first mechanism (Tomita & Shima, 1986). Dissimilar to the first mechanism of micro-jets, May (1987) reported that the much smaller ultra-jets reached velocities of up to 370 m/s during Tomita & Shima's (1986) experiments, resulting in pressures exceeding 300 MPa (Chanson, 1988).

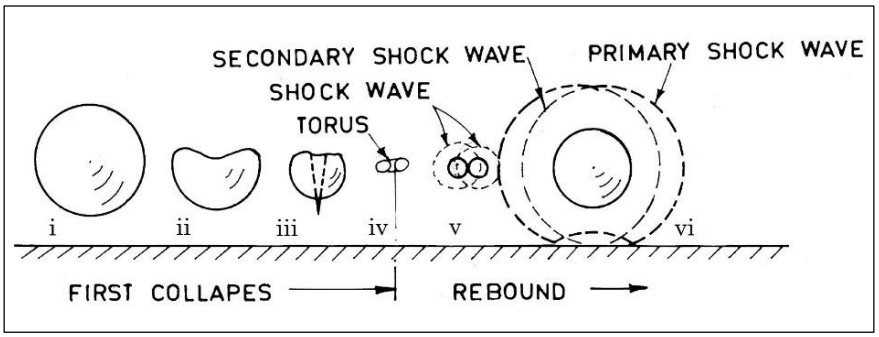

Figure 2-24: Stages of the collapse of a bubble, creating shock waves (Khatsuria, 2005)

Due to interaction between the mortar and coarse aggregates and the presence of micro fractures, cavitation's damage mechanism of concrete is much more complex than that of steel. The high pressure spikes related to cavitation pitting causes compression waves to enter these fissures and produce uplifting forces, loosening pieces of the concrete (Khatsuria, 2005). This phenomenon is similar to the processes developing scour holes downstream of plunging jets.

Several severe cases of cavitation damage have been reported on dam spillways and outlets. A few examples are listed below in Table 2-5. Figure 2-25 and Figure 2-26 show the massive cavitation damage of the Hoover Dam in 1941 and the Glen Canyon Dam in 1983.

Table 2-5: Prototype cases of severe cavitation damage (Chanson, 1988)

Date	Place	Description	Remedy
1983	Glen Canyon Dam, Colorado, USA	Tunnel spillway. Large erosion induced by initial cavitation.	Aeration slots.
1983 & 1941	Hoover Dam, Arizona, USA	Spillway tunnel. Initially damaged in 1941, repaired and again damaged in 1983.	Aeration slots (1983).
1982	Stampede Dam, Nevada, USA	Concrete damage in outlet works.	Aeration slot.
1977	Karun Dam, Iran	Cavitation erosion on open channel spillway induced by surface irregularities.	Fibre concrete and epoxy. Repair not satisfactory.
1974	Tarbela Dam, Pakistan	Cavitation erosion due to surface irregularities.	Fibre concrete and epoxy. Aeration slot.
1972	Libby Dam, Montana, USA	Cavitation erosion of the outlets.	Steel fibre concrete and aeration sluice.
1970	Clear Creek Dam, Colorado, USA	Cavitation erosion of the concrete on outlet conduit.	Installation of air vents.
1967	Turtle Creek Dam, Kansas, USA	Cavitation in the concrete floor downstream of the seal plate.	Steel plate.
1967	Yellowtail Dam, Montana, USA	Tunnel spillway. Cavitation through the lining into the foundation rock.	Aeration slots and epoxy bounded concrete.
1966	Aldea-Davilla Dam, Portugal	Cavitation erosion in the auxiliary tunnel spillway	Aeration
1964	Palisades Dam, Idaho, USA	Cavitation damage downstream of the gates	Aeration
1960	Grand Coulee Dam, USA	Cavitation in the outlets due to abrupt change of direction	Aeration

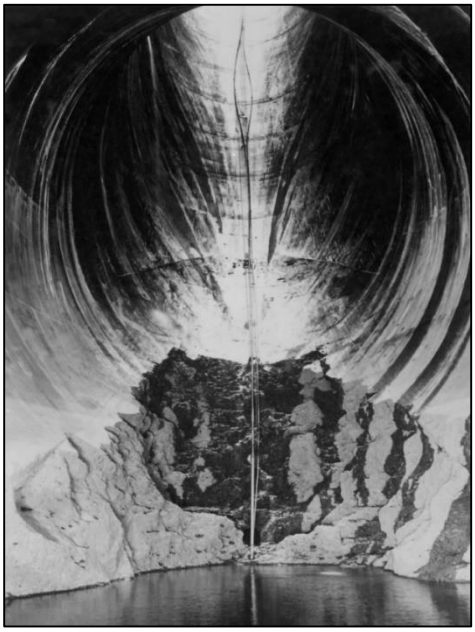

Figure 2-25: Hoover Dam cavitation damage (Rogers, 2010, Morris, 2012)

Figure 2-26: Glen Canyon Dam cavitation damage (Morris, 2012)

Cavitation damage is mostly due to very high velocities coupled with structural or geometric features such as misalignment, surface roughness and inadequate design (Khatsuria, 2005). Chadwick *et al.* (2013) warned that cavitation may occur if flow velocities exceed 30 m/s. However, Roberts (1980) stated that in practice velocities as low as 10 m/s can initiate cavitation. The results of a survey done on 35 dams where cavitation occurred are shown in Table 2-6 and shows that serious damage is likely to occur if flow velocities of more than 30 m/s are observed, but damage might still occur at low velocities.

Table 2-6: Degree of cavitation damage with velocity (Roberts, 1980)

	Percentage of total number with:		
Velocity (m/s)	Serious damage[1]	Damage	No erosion
> 40	50	50	0
30 – 40	33	17	50
20 – 30	0	17	83
< 20	6	12	82

Note: 1: Serious damage denotes erosion greater than 100 mm

Although no serious cavitation damage to Roberts splitters have been reported, there is enough literature and theory to support that given extreme flow or elevated flood conditions, cavitation may transpire. Figure 2-27 shows serious cavitation damage to the splitter teeth of the Pit No. 7 Dam in California, USA. Although not Roberts splitters, the damage occurred to a similar structure as a result of underestimation of spillway head.

Figure 2-27: Pit No. 7 Dam, USA – cavitation damage to splitter teeth (Mason, 2012)

2.4.4. Mitigation of Cavitation

2.4.4.1. Decreasing the Critical Cavitation Number

The most effective method of mitigating cavitation is by reducing the critical cavitation number, σ_C (see Section 2.4.2). This is however not that simple, as this can only be done by decreasing the local flow velocity at an obstruction (i.e. splitter) in relation to the average flow velocity approaching the obstruction. As most hydraulic structures are based on fixed design principles and theory, changing the geometry of these structures in order to reduce local velocities is generally impossible.

2.4.4.2. Avoiding Severe Pressure Conditions

If the critical cavitation number cannot be decreased, the next logical step is to increase the cavitation index σ_i of the flow. This can be done by increasing the dynamic fluid pressure. Increasing the dynamic fluid pressure enough to ensure the cavitation index is more than the critical cavitation number is theoretically enough, but as explained in Section 2.4.1, Chadwick *et al.* (2013) recommends never operating hydraulic structures at a dynamic fluid pressure less than 3 m absolute (or -7 m atmospheric).

2.4.4.3. Improving Construction and Concrete Quality

As stated above, most cases of serious cavitation damage are a result of sloppy construction work or unsatisfactory concrete quality. Offsets, protruding joints and irregularities on the surface of the spillway or energy dissipators can cause flow separation resulting in very low pressures and subsequently a reduced cavitation index. Roberts (1980) refers to certain design criteria for allowable surface finishes. For instance, for a flow depth of 1 m and a velocity of 15 m/s, an irregularity should not exceed 2 mm. Chanson (1988) gives examples of special cavitation resistant materials. These are however expensive and are generally reserved for areas where cavitation cannot be avoided. These include fibre reinforced and polymerised concrete, steel plates and epoxy resin.

2.4.4.4. Flow Aeration

At high flow velocities, the tolerances that must be applied to the spillway surface is too small. As an example, an offset of just 3 mm will induce cavitation at flow velocities approaching 25 m/s (Falvey, 1982). For this reason, and the high costs of cavitation resistant materials, the most efficient method to mitigate cavitation if severe negative

pressures are expected to occur, is to introduce air into the flow at the material surface (Chanson, 1992). The presence of air in the bubbles that forms as a result of cavitation will cushion cavity collapse and reduce the water hammer as a result and the celerity and magnitude of the shock waves will be decreased by air (Chanson, 1992).

Chanson (1992) referred to several hydraulic experiments that were performed to determine the effects of air entrainment on cavitation erosive damage. He found that although cavitation was not necessarily avoided, erosive damage as a result of cavitation was completely mitigated for flow velocities of up to 45 m/s if the entrained air concentration within the flow varied between at least 4% and 8%.

2.5. Self-aeration and the Point of Inception

As mentioned earlier, there is a difference between the artificial aeration of hydraulic structures in general and self-aeration. All aeration is defined as the process of air mixing with the water flow and will occur naturally after the point of inception, and in this instance called self-aeration (Wright, 2006). This section aims to clearly define self-aeration and explains why it is different to artificial aeration.

Self-aeration is common on ogee spillways that have sufficient distance for the point of inception to form. Observations of aeration have shown that it starts when the boundary layer that forms after the crest of a spillway reaches the free surface of the water. This point is called the point of inception (Chadwick *et al.*, 2013). Figure 2-28 shows a general growing boundary layer on an ogee spillway.

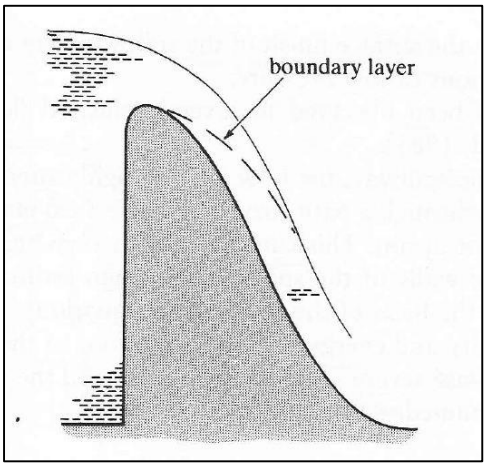

Figure 2-28: Growing boundary layer on a spillway (Chadwick *et al.*, 2013)

This boundary layer growth commences at the leading edge of the crest and its depth, δ^*, will increase with the distance downstream from the crest (Chadwick *et al.*, 2013).

On smooth spillways, the location and characteristics of the point of inception is mainly a function of the discharge and the spillway roughness (Chanson, 1993). Chanson (1993) suggested the following functions to determine firstly, the location of the point of inception, and secondly, the depth at the point of inception:

$$\frac{L_I}{k_s} = f_2(F^*; sin\alpha) \tag{2-30}$$

$$\frac{d_I}{k_s} = f_3(F^*; sin\alpha) \tag{2-31}$$

where L_I is the distance from the start of the boundary layer to the point of inception, and d_I is the water depth at the point of inception. The depth is measured normal to the surface of the spillway (Chanson, 1993). The angle of the downstream face of the spillway with the horizontal is α, while F^* is a Froude number defined in terms of roughness (Chanson, 1993).

Wood *et al*. (1983) suggested that F^* be calculated as follows:

$$F^* = \frac{q_w}{\sqrt{g \cdot sin\alpha \cdot k_s^3}} \tag{2-32}$$

and he estimated the functions f_2 and f_3 to be:

$$\frac{L_I}{k_s} = 13.6 \times (sin\alpha)^{0.0796} \times (F^*)^{0.713} \tag{2-33}$$

$$\frac{d_I}{k_s} = \frac{0.223}{(sin\alpha)^{0.04}} \times (F^*)^{0.643} \tag{2-34}$$

From Eq. (2-33) it can be seen that the point of inception will move downstream as the flow increases. This entails that at lower flows, the point of inception will be higher on the downstream face of the spillway. On smooth spillways, self-aeration will occur after the point of inception and progress through specific aerated regions (Wright, 2006).

2.6. Scaling of Hydraulic Models

2.6.1. Introduction

To design a sufficient hydraulic model to perform the proposed hydraulic analysis, a model scale had to be selected. For true dynamic similarity, all dimensionless parameters of the prototype and model must be equal (Chanson, 2009). According to Chanson (2009) it is impossible to produce true dynamic similarity in hydraulic experiments because the number of dimensionless parameters is too great. Very good dynamic similarity can however be achieved if gravitational and inertial forces are

dominant and the Reynolds number of the prototype and model flows can be kept similar by using highly turbulent flows. Then the Froude number of the model and prototype can be used to determine scale factors for other parameters. The effects of surface tension and viscous forces are two hydraulic phenomena that limit the scale that can be used in experiments as it becomes impossible to keep these effects equal at the same time as keeping the Froude numbers equal and the Reynolds number similar (Chanson, 2009).

2.6.1. Hydraulic Similarity

2.6.1.1. Geometric Similarity

Simply put, geometric similarity refers to all geometry of the model with regards to that of the prototype. Dynamic similarity exists if the ratio of any two dimensions of the model is equal to the ratio of the corresponding dimensions of the prototype as expressed in Eq. (2-35) (Bosman & Basson, 2012):

$$\frac{(L_1)_m}{(L_2)_m} = \frac{(L_1)_p}{(L_2)_p} \tag{2-35}$$

where L_m and L_p are the linear dimensions of the hydraulic model and prototype respectively.

2.6.1.2. Kinematic Similarity

The requirements of kinematic similarity refer to motion of the fluid. Kinematic similarity between the model and the prototype is achieved if the velocities and acceleration at corresponding positions and time frames in both systems have equal ratios (Bosman & Basson, 2012). Eq. (2-36) expresses this relationship:

$$\frac{(v_1)_m}{(v_2)_m} = \frac{(v_1)_p}{(v_2)_p} \textbf{ and } \frac{(a_1)_m}{(a_2)_m} = \frac{(a_1)_p}{(a_2)_p} \tag{2-36}$$

where v_m and v_p are the velocities and a_m and a_p are the accelerations of the hydraulic model and prototype respectively.

2.6.1.3. Dynamic Similarity

To achieve dynamic similarity between the model and prototype, the forces that influence the motion of the fluid must adhere to the same ratios as stated above (Bosman & Basson, 2012). Once again, forces at any two points on the model must have

the same ratio to the forces on the prototype at corresponding points, as expressed in Eq. (2-37):

$$\frac{(F_1)_m}{(F_2)_m} = \frac{(F_1)_p}{(F_2)_p} \tag{2-37}$$

where F_m and F_p are the linear dimensions of the hydraulic model and prototype respectively.

2.6.2. Laws of Hydraulic Similarity

The four main forces acting on the fluid in both the prototype and model systems are gravity, fluid viscosity, surface tension and elasticity (Bosman & Basson, 2012). The regime of the flow due to the influence of these forces can be defined by the dimensionless numbers of the following hydraulic laws:

- Gravity: Froude's Law
- Fluid viscosity: Reynolds' Law
- Surface tension: Weber's Law
- Elasticity: Euler's Law

Bosman and Basson (2012) summarised these laws in order to apply them on the scaling of hydraulic models.

2.6.2.1. Froude's Law

According to Bosman and Basson (2012), gravity and inertial forces are dominant in hydraulic systems such as open channels, spillways, weirs and rivers. In these cases, dynamic similitude is often achieved by designing models according to Froude's Law. This is true if the Froude numbers of the model and prototype systems are equal. The Froude number is defined as follows (Chadwick *et al.*, 2013):

$$Fr = \frac{v}{\sqrt{gL}} \tag{2-38}$$

where Fr is the dimensionless Froude number, v is flow velocity, g is the gravitational acceleration constant (taken as 9.81 m/s^2) and L is a characteristic linear dimension (typically taken as the depth of flow, y, in metres).

From the Froude Law, the corresponding model velocity can be obtained from the prototype velocity by defining a scale factor S so that:

$$S = \frac{L_p}{L_m} \tag{2-39}$$

Taking $L_m = 1$ results in $L_p = S$ so that:

$$\frac{v_p}{\sqrt{gL_p}} = \frac{v_m}{\sqrt{gL_m}}$$

$$\frac{v_p}{S^{0.5}} = v_m$$

$$\frac{v_p}{v_m} = S^{0.5} \tag{2-40}$$

These scale factors are universal in hydraulics when scaling models according to the Froude Law. The time ratio between the model and prototype can now be obtained by combining the length and velocity scale factors in Eq. (2-39) and Eq. (2-40) respectively, and knowing that $t = L/v$, where t is time in seconds:

$$\frac{t_p}{t_m} = \frac{L_p/v_p}{L_m/v_m} \tag{2-41}$$

Re-arranging Eq. (2-41) gives and incorporating Eq. (2-39) and Eq. (2-40) gives:

$$\frac{t_p}{t_m} = \frac{L_p}{L_m} \times \frac{v_m}{v_p} = S \times \frac{1}{S^{0.5}} = S^{0.5} \tag{2-42}$$

Eq. (2-40) indicates that the velocities that occur in hydraulic models are less than those in the prototype case. According to Bosman and Basson (2012), this is beneficial due to improved measuring accuracy at these lower velocities. The same fact is true for time as is evident from Eq. (2-42).

2.6.2.2. Reynolds' Law

The dimensionless Reynolds number, Re, is defined as (Chadwick *et al.*, 2013):

$$Re = \frac{vL}{\nu} \tag{2-43}$$

where v is the fluid velocity, L is the length of homologous sections in the model and prototype and ν is the kinematic viscosity of the fluid (taken as 1.13×10^{-6} m²/s for water). According to the Reynolds Law, corresponding velocities in the prototype and model systems must be related according to Eq. (2-44) (Bosman & Basson, 2012):

$$\frac{v_p}{v_m} = \frac{\nu_p \cdot L_m}{\nu_m \cdot L_p} = \frac{\nu_p}{\nu_m} \times \frac{1}{S} \tag{2-44}$$

Generally, viscous forces are secondary in the prototype case due to water's low viscosity but are however important when considering the onset of turbulence due to boundary frictions (Bosman & Basson, 2012). It is clear from Eq. (2-40) and Eq. (2-44) that both

Froude' and Reynolds' laws cannot be satisfied if the same fluid is used in the prototype and the model systems. However, Bosman and Basson (2012) states that any variation in the Reynolds numbers are negligible when both systems have high Reynolds numbers (> 100 000). Typically, under full-scale conditions, the Reynolds number will be smaller in the model than in the prototype system, and the overall friction factor will in turn be greater than in the prototype (Bosman & Basson, 2012).

2.6.2.3. Weber's Law

According to Bosman and Basson (2012), the surface tension of water is typically ignored during model analysis, unless very low heads, air entrainment, spray or splash exist. The dimensionless Weber number, We, was developed by German naval architect M. Weber and can be used to indicate the significance of a given fluid's surface tension (Chadwick *et al.*, 2013). The Weber number can be calculated using Eq. (2-45):

$$We = v \times \sqrt{\rho L/\tau} \tag{2-45}$$

where v is the flow velocity, ρ is the density of the fluid, L is the length of homologous sections in the model and prototype and τ is the surface tension of the fluid (measured in N/m (Chadwick *et al.*, 2013)).

As with Froude and Reynolds' laws, the corresponding velocities of the model and prototype systems can be related using Weber's Law. This relation is given in Eq. (2-46):

$$\frac{v_p}{v_m} = \left(\frac{\tau_p \cdot \rho_m \cdot L_m}{\tau_m \cdot \rho_p \cdot L_p}\right)^{0.5} = \left(\frac{\tau_p \rho_m}{\tau_m \rho_p}\right)^{0.5} \times \frac{1}{S^{0.5}} \tag{2-46}$$

It can be seen that in terms of scaled velocity, the Froude and Weber laws cannot be satisfied simultaneously, but as mentioned, surface tension forces are generally minor compared to gravitational and inertia forces.

2.6.2.4. Euler's Law

The Euler equation in Eq. (2-47) depicts the relationship between fluid pressure drop (Δp) and fluid velocity (v), where ρ represents the fluid density.

$$Eu = v \times \sqrt{\rho/2 \cdot \Delta p} \tag{2-47}$$

The dimensionless Euler number (Eu) is particularly significant when the viscous forces are negligible compared to the inertia forces of the fluid. Typically this occurs where the turbulence of the fluid is fully developed in enclosed model systems (Bosman & Basson, 2012). From Eq. (2-47) it is evident that gravity and surface tension effects are absent as

pressure is the only controlling factor and thus the independent variable. According to Bosman and Basson (2012), this is contrary to most fluid phenomena, as the fluid pressure is usually a result of the motion of the fluid and thus the dependent variable.

Eq. (2-48) gives the relationship between corresponding model and prototype velocities if scaled according to the Euler Law:

$$\frac{v_p}{v_m} = \left(\frac{\Delta p_p \cdot \rho_m}{\Delta p_m \cdot \rho_p}\right)^{0.5} \tag{2-48}$$

It is evident that the scale factor, S, does not influence the velocities, as the pressure in the system is the only independent variable if the same fluid is used in the model as in the prototype. According to Bosman and Basson (2012), this non-linear relationship between pressure and velocity is universally applicable where inertia forces are dominant and gravity is ignored. If the model is large enough, the Euler Law can be used to relate velocity with the controlling system pressure.

2.6.3. Summary of the Scaling of Hydraulic Models

In the case of the proposed study of Roberts splitters on a dam spillway, gravity and inertia were the dominant forces that influenced the fluid's motion, and therefore Froude's Law is the selected criterion for the scaling of the model. Houston (1983) provided relationships (based on the Froude similarity law) between the prototype and the model of a hydraulic test in Table 2-7 where S is the specific scale factor relating the model to the prototype:

Table 2-7: Scale relationships using the Froude similarity law (Houston, 1983)

Parameter	SI Unit	Ratio
Distance	m	$S = \frac{L_p}{L_m}$
Time	s	$S^{1/2} = \frac{t_p}{t_m}$
Velocity	m/s	$S^{1/2} = \frac{v_p}{v_m}$
Area	m^2	$S^2 = \frac{A_p}{A_m}$
Volume	m^3	$S^3 = \frac{V_p}{V_m}$
Unit Discharge	m^2/s	$S^{3/2} = \frac{q_p}{q_m}$
Discharge	m^3/s	$S^{5/2} = \frac{Q_p}{Q_m}$

The following reasons dictate the choice of scale for hydraulic models, but more specifically, the hydraulic model used in this study:

- To achieve the largest possible prototype discharge, the largest possible scale is needed;
- Scale effects limit the scale of hydraulic models. The maximum scale to be used where scale effects are kept negligible is 1:20 (Robertson, 2014);
- The model should be constructed from hydraulically similar and suitable materials, as far as practically possible.

2.7. Outcomes and Conclusions of the Literature Review

The outcomes and conclusions from the literature review can be summarised as follows:

- ICOLD (2016) included more than 58 000 large dams in their register, each having to safely discharge a certain flood. These floods were safely discharged back into a watercourse by a spillway, generally with some type of energy dissipator.
- Roberts splitters is an effective means of dissipating energy and was designed by South African engineer, Lt. Col. D.F. Roberts (Van Vuuren, 2008). Roberts splitters were used on several South African and international dams, containing aeration vents in at least five cases. Mason (1983) studied these five cases and made recommendations on improving Roberts' (1943) original procedure.
- At the Wadi Dayqah Dam, aeration via the gallery was deemed beneficial to the working of the Roberts splitters and was thus incorporated into the design.
- The air velocity inside an aeration gallery must be limited to 14.1 m/s if a person is allowed to enter it during spilling events;
- Sub-atmospheric pressures exist on the vertical faces of steps on spillways, indicating that such pressures occur where flow projects away from a sudden edge of a hydraulic structure. It can be expected that similar sub-atmospheric pressures should exist at the edges of Roberts splitters.
- Cavitation is a major risk for Roberts splitters. Cavitation commences when the dynamic fluid pressure is less than or equal to the vapour pressure of the fluid. It is however inadvisable to operate any hydraulic structure at dynamic fluid pressure heads less than 3 m absolute (Chadwick *et al.*, 2013). Thus, for the

hydraulic model study, the cavitation pressure threshold was adopted as 3 m absolute (-7 m atmospheric).

- For flow velocities up to 45 m/s, cavitation damage can be mitigated by entraining an air concentration of at least 4 – 8% (Chanson, 1992). For the hydraulic model study, to safely assume that cavitation damage would be completely mitigated, the air concentration threshold was set at 8%.
- Self-aeration is the process whereby air gets entrained into the flow on a spillway when the growing boundary layer reaches the free surface. Artificial aeration (referred to simply as 'aeration') is different as air gets entrained into the flow at the surface of the material through air vents or slots.
- The Froude Law was used to scale the hydraulic model from the prototype and the scale was chosen as 1:20. This was the largest possible scale to maximise the prototype discharge, while safely neglecting scale effects. The model was still practically constructible.
- It was found that an absence of data exists on the risk of cavitation of unaerated Roberts splitters at high unit discharges. This study aimed to contribute model test results of this risk;
- Further shortages of information on the aeration of Roberts splitters through an internal aeration gallery indicated that there is a need for greater knowledge in this regard. This study aimed to formulate practical recommendations on the effective usage of Roberts splitters and the aeration thereof at prototype unit discharges greater than 35 m^2/s.

CHAPTER 3

HYDRAULIC MODEL DESIGN AND TESTS

In order to fulfil the objectives of the study, a 1:20 scale hydraulic model of an ogee spillway equipped with Roberts splitters was designed and built in the Hydraulic Laboratory of the University of Stellenbosch in South Africa. The tests on this model were split up into three parts:

1. A control model consisting of unaerated Roberts splitters, designed according to the original Roberts (1943) procedure – Figure 3-1 (a);
2. The 1st aerated model, designed according to the existing theory and dependant on the results of the 1st model. The aeration was provided by an internal duct or aeration gallery – Figure 3-1 (b);
3. The 2nd aerated model, altering the design of the 1st aerated model by increasing the size of the aeration vents – Figure 3-1 (c).

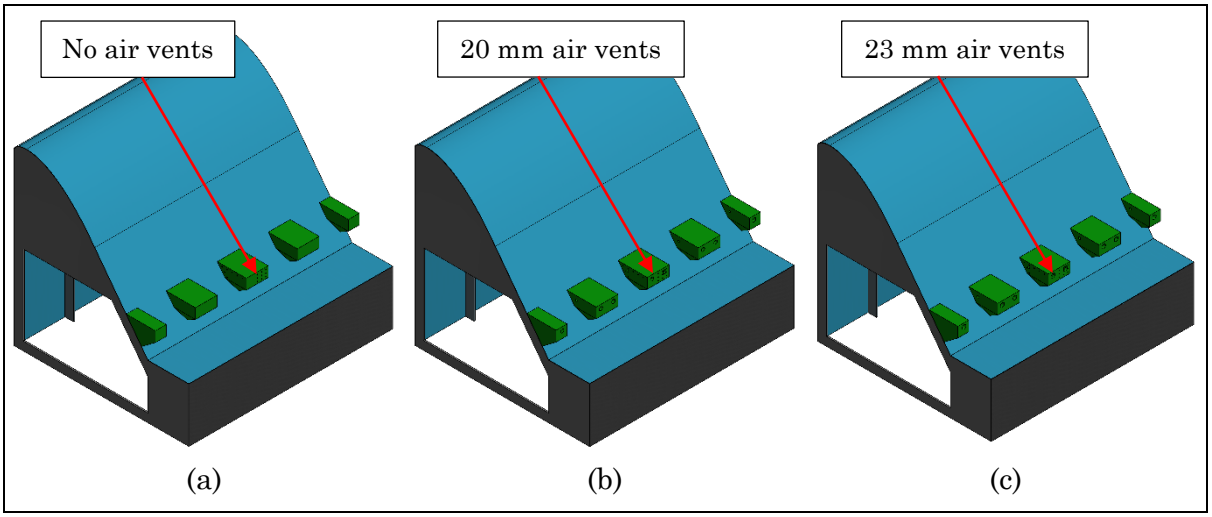

Figure 3-1: The three model setups

During both sets of aerated tests, the effectiveness of the proposed aeration strategy was observed by comparing pressure and air concentration readings, and by measuring the air velocity in the aeration shaft and the water drainage from the aeration duct. This

information was used to formulate valid recommendations of aeration of Roberts splitters through an internal aeration duct.

3.1. Scope of The Hydraulic Model Tests

3.1.1. Model Scale

It was originally proposed that the scale of the model be 1:20. This was to allow a prototype design discharge of 40 m^2/s within the limits of the laboratory whilst minimising scale effects due to viscosity and surface tension.

The model was operated in accordance with the Froude Law of similitude (Section 2.6) as only gravitational forces acted on predominantly free surface flow. It followed that the ratio between inertial and gravitational forces on all particles of the fluid would be equal in magnitude in the model and in the prototype, and that the flow geometry would be preserved throughout the model. This would be true provided that (1) flows were introduced into the model in accordance with the Froude Law and (2) there was geometrical similarity between the prototype and the model (CSIR - Division of Earth, Marine and Atmospheric Science and Technology, 1990).

The following scale ratios and relationships were true for the hydraulic model assuming geometric similarity and equal Froude numbers between the model and the prototype:

$$Linear\ ratio = \frac{L_p}{L_m} = S = 20$$

$$Area\ ratio = \frac{L_p^2}{L_m^2} = S^2 = 400$$

$$Volume\ ratio = \frac{L_p^3}{L_m^3} = S^3 = 8000$$

$$Velocity\ ratio = \frac{v_p}{v_m} = S^{0.5} = 4.472$$

$$Discharge\ ratio = (Velocity\ ratio) \times (Area\ ratio)$$

$$= S^{5/2} = 1\,788.854$$

$$Time\ ratio = \frac{Length\ ratio}{Velocity\ ratio} = S^{0.5} = 4.472$$

If the above ratios were applied to the Froude number, it is shown that the Froude Law is satisfied in that the Froude number ratio is equal to 1.

$$Froude\ number = \frac{v}{\sqrt{gL}} \tag{3-1}$$

where $v = characteristic\ velocity$

$L = characteristic\ length$

$g = gravitational\ constant$

$$\therefore Froude\ number\ ratio = \frac{S^{0.5}}{\sqrt{S}} = 1 \tag{3-2}$$

As mentioned in Section 2.6, the chosen scale of 1:20 was sufficient to keep scale effects negligible (Robertson, 2014).

3.1.2. Laboratory Limitations

The design of the hydraulic models was dictated by the limitations of the Hydraulic Laboratory of the University of Stellenbosch. The design attempted to get the maximum possible prototype unit discharge equivalent to the maximum possible spillway head.

The maximum discharge provided by the five pumps of the laboratory was 700 l/s. This discharge could have been achieved provided the total head of the model was not too high. For instance, if the model had been 1 m lower, the discharge could have been increased to around 800 l/s (in the laboratory), but then the model would have been too low to fit the proposed splitter design.

Through a thorough iterative design process, as described in Section 3.3, the design model discharge was selected as 537.0 l/s to allow for underestimation of the prototype design unit discharge by at least 10 m^2/s.

3.1.3. Model Layout

The general layout of the hydraulic model consisted mainly of the ogee spillway at the end of a 24.5 m long by 1.6 m high by 1.2 m wide plastered brick flume. A constant level stilling tank provided the flume with a very constant flow rate via a DN600 steel pipe. The constant level stilling tank was fed by a maximum of five pumps from the storage tanks below ground. The inlet pipe of the flume was set very low with distribution holes cut in to avoid unnecessarily severe wave action (see Figure 3-2: longitudinal section). Downstream of the ogee spillway the discharge flowed away freely into the drainage canal back to the storage tanks. A baffle wall was constructed 1.2 m downstream of the centreline of the inlet pipe to assist in developing the flow, and to reduce the wave action caused by the inlet flow. The length of the flume was calculated to provide fully

developed flow to the spillway. A Perspex pane was constructed next to the spillway to allow viewing of the splitter action. The water level measuring needle was placed 9.1 m upstream of the crest of the spillway to allow for the drawdown.

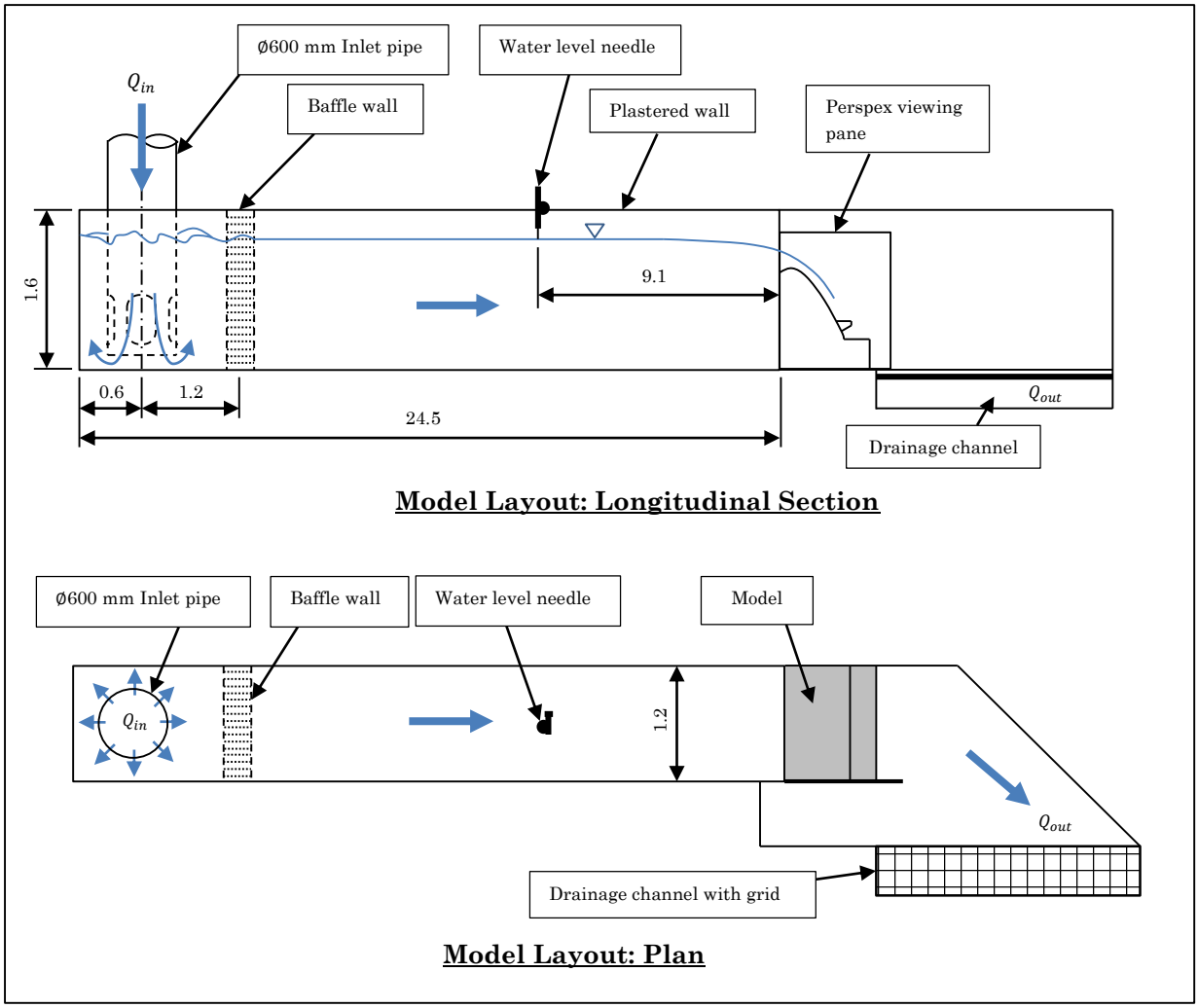

Figure 3-2: General layout of the hydraulic model (illustration not to scale)

3.2. Test Conditions and Schedule

Table 3-1 shows the summarised test conditions of the study. The complete testing schedule is contained within Appendix G.

The tests were divided between two measuring splitters to accommodate the number of pressure sensors within the splitter, as explained in Section 3.4.2. Thus, six rounds of tests were done: one for each measuring splitter per model.

In each round, ten tests were performed starting, at a q_p = 5 m²/s and ending at q_p = 50 m²/s, increasing in steps of 5 m²/s (where q_p is the prototype unit discharge). Four extra independent repeatability tests were done: two each at q_p = 30 m²/s and q_p = 40 m²/s. This gave two sets of three tests to analyse the repeatability of the tests. The repeatability analysis is contained in Section 3.6.

Table 3-1: Summarised test conditions

Test order	q_p (m²/s)	H_p (m)	Q_m (l/s)	H_m (mm)	Comments
1st	5	1.88	67.1	94	
2nd	10	2.90	134.2	145	
3rd	15	3.72	201.2	186	
4th	20	4.44	268.3	222	
5th	25	5.10	335.4	255	
6th	30	5.70	402.5	285	
7th	35	6.26	469.6	313	
8th	40	6.78	536.7	339	
9th	45	7.28	603.7	364	
10th	50	7.76	670.8	388	
11th	30	5.70	402.5	285	Repeatability test
12th	30	5.70	402.5	285	Repeatability test
13th	40	6.78	536.7	339	Repeatability test
14th	40	6.78	536.7	339	Repeatability test

3.3. Model Design

The most important aspects and consideration of the model design are contained in this section. The complete design can however be found in Appendix E. The as-built design drawings of the model are enclosed in Appendix F.

As mentioned previously, the hydraulic model consisted of an ogee spillway, Roberts splitters and an aeration duct, or gallery. The control model's splitters were unaerated, while the 1st and 2nd aerated models contained air vents in the splitters similar to those of the Gariep and Vanderkloof Dams. The design procedures followed are listed in Table 3-2.

Table 3-2: Model design procedures

Design aspect	Procedure
Ogee spillway	USBR (1987) ogee spillway design procedure, described in Appendix D.
Roberts splitters	Original Roberts (1943) crest splitters design procedure, as described in Section 2.2.5.
Splitter air vents	Designed in accordance with the air vents of the Gariep Dam
Aeration duct	Designed so that the splitter air vents was the control for the air velocity and discharge

A simple drawing of the model with model dimensions is shown in Figure 3-3 below and the design input parameters and important values are given in Table 3-3.

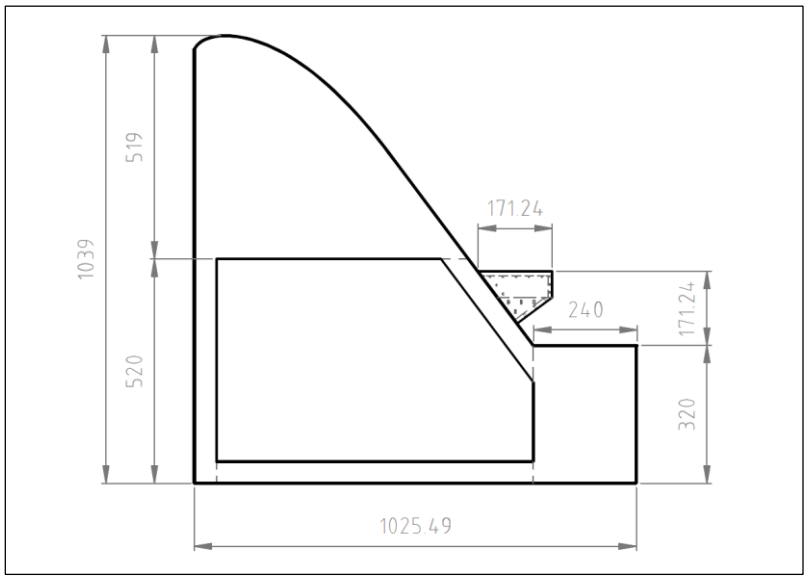

Figure 3-3: The simplified dimensions of the model

Table 3-3: General dimensions and design parameters of the hydraulic model

Parameter	Symbol	Unit	Prototype	Model
Scale				1 : 20
Design discharge	Q	m³/s	960.0	0.537
Design unit discharge	q	m²/s	40.0	0.447
Spillway length	L	m	24.0	1.2
Design head	H_0	m	5.09	0.255
Maximum head	H_e	m	6.79	0.339
Dam height	P	m	20.8	1.039
Flume freeboard		m	11.22	0.561
Downstream slope		(H : V)	0.75 : 1	0.75 : 1

3.3.1. Ogee Design

The design of the ogee spillway was done using the values shown in Table 3-4. The discharge limit of the laboratory dictated the input parameters, resulting in a prototype design unit discharge of 40 m²/s, equivalent to a model discharge of 537 l/s. The design unit discharge was chosen as 40 m²/s in order to test above the design discharge of the prototype.

Table 3-4: Model ogee design input parameters

Input Parameter	Symbol	Unit	Prototype Value	Model Value
Design unit discharge	q	m²/s	40.0	0.447
Flume width	b	m	24.0	1.2
Effective spillway length	L_{eff}	m	24.0	1.2
Design discharge	Q	m³/s	960.0	0.537
Design discharge coefficient	C_0			2.175
Final discharge coefficient	C_e			2.262

The following values were obtained from the ogee design:

Table 3-5: Ogee design output values

Output Parameter	Symbol	Unit	Prototype Value	Model Value
Design head	H_0	m	5.09	0.255
Maximum head	H_e	m	6.79	0.339
Dam height	P	m	20.8	1.039
Design velocity head	h_a	m	0.108	0.005
Ogee shape coefficients	k			0.507
	n			1.855

The calculated shape of the ogee spillway was divided between the upstream crest and the downstream crest and spillway. The dimensions relating to the shape of the upstream crest obtained from the design are shown in Table 3-6.

Table 3-6: Upstream model ogee crest parameters

Parameter (see Figure D-7 and Figure D-8)	Prototype (m)	Model (mm)
R_1	2.545	127.3
R_2	1.018	50.9
Y_c	0.631	31.6
X_1	0.891	44.5
X_c	1.436	71.8

The downstream shape of the ogee was determined using Eq. (3-3). Figure E-1 shows the downstream crest profile of the model ogee.

$$\frac{y}{0.255} = -0.507 \cdot \left(\frac{x}{0.255}\right)^{1.855} \tag{3-3}$$

3.3.2. Roberts Splitters Design

As mentioned, the Roberts splitters system of the hydraulic model was designed according to the Roberts (1943) procedure. Refer to Section 2.2.5 for a full description of the procedure. Following the design of the ogee spillway, the maximum expected head was used as the main parameter in the Roberts splitters design, i.e. $(H_D)_{splitters} = (H_e)_{ogee}$.

Table 3-7: Model Roberts splitters design input parameters

Input Parameter	Symbol	Unit	Prototype Value	Model Value
Design head	H_D	m	6.79	0.339
Spillway length	L	m	24	1.2
Downstream slope	θ	degree	53.1	53.1

Through the iterative design process, it was decided to include 4 cycles of splitters within the spillway width of 1.2 m. The 4 cycles consisted of 3 centrally-located full splitters and 2 half-splitters at the sides of the spillway. Figure 3-4 shows a photograph of the 4 cycles of splitters on the ogee spillway.

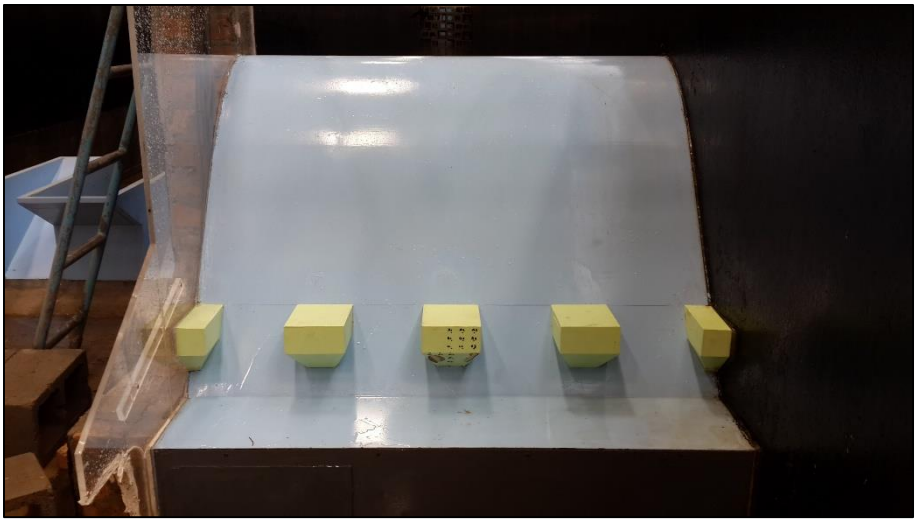

Figure 3-4: Photograph of spillway model with unaerated Roberts splitters

Referring to Table 2-4 and Figure 2-12, the following output design parameters and dimensions were obtained:

Table 3-8: Roberts splitters output parameters and dimensions

Output Parameter	Prototype Value (m)	Model Value (mm)
P	10.964	548.2
W	2.575	128.8
S	3.425	171.2
L	3.425	171.2
L_s	4.800	240.0
T	3.425	171.2
R_{max}	18.483	924.2
R_{min}	5.557	277.9

3.3.3. Splitter Air Vent Design

The design of the air vents was dependent on the results of the control model tests. The vents were placed on the locations where the dynamic fluid pressure would be the overall lowest, meaning that the minimum and average pressure needed to be the lowest. This is explained in more detail during the pressure results analysis of the unaerated model in Section 4.2.1. It was observed that the worst cases of negative pressure existed on the sides of the splitters, close to the spillway surface, with the downstream ends of the splitters also experiencing negative pressures, but less severe. This prompted the placement of air vents on the sides and at the end of each splitter.

This coincides with the air vents found at the Gariep and Vanderkloof Dams. Figure 3-5 shows the relative position of the air vents on the splitters.

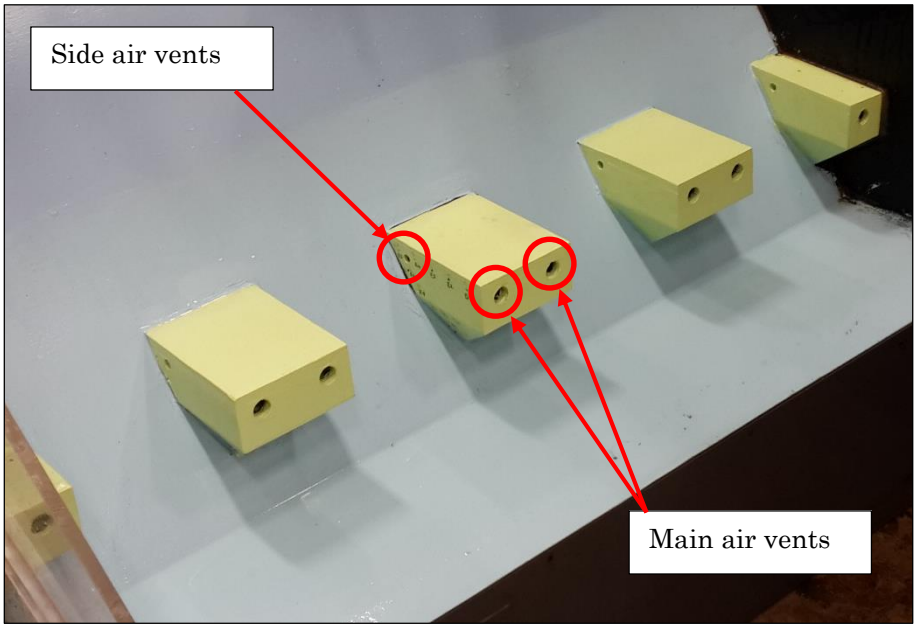

Figure 3-5: Photograph showing relative positions of air vents on splitters

The exact positions of the air vents were also dictated by the existing positions of the pressure sensors. Figure 3-6 shows the exact positions of the model air vents.

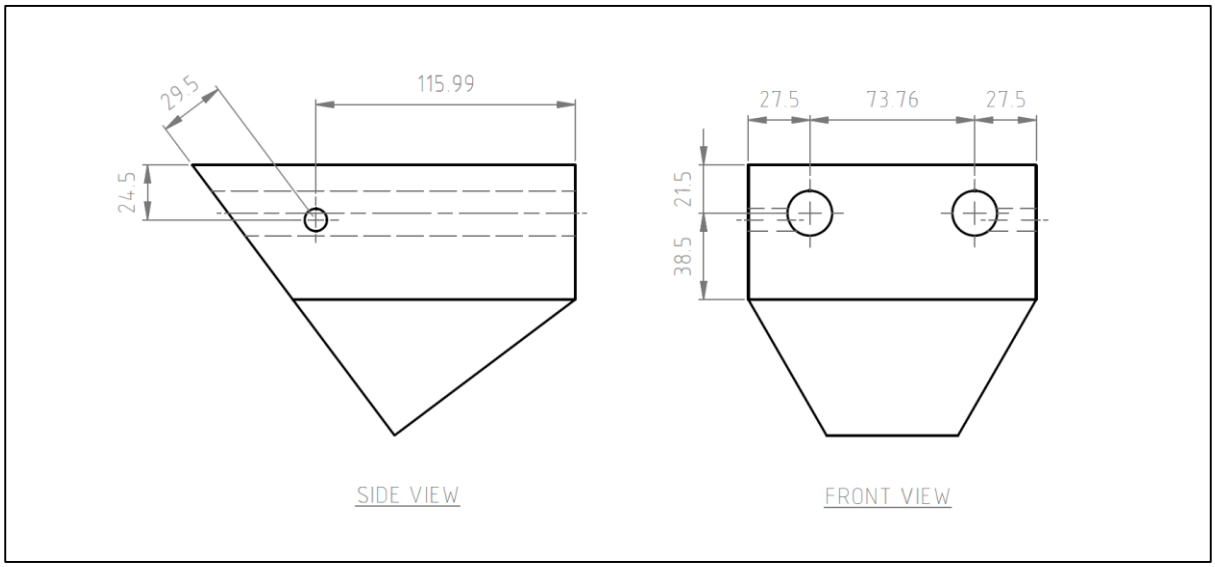

Figure 3-6: Detailed air vent positions (model scale in mm)

The sizing of the vents was based on those at the Gariep Dam, as the air demand discharge of each splitter remained to be measured and was subject to the design of the air vents. The following relationships were obtained of the diameter of the air vents to relative dimensions of the splitters and the design head (Roberts, 1977):

$$\emptyset_{main} = 2 \cdot \emptyset_{side} \quad \text{(3-4 a)}$$

$$\emptyset_{main} = 0.176 \cdot W \quad \text{(3-4 b)}$$

$$\emptyset_{main} = 0.082 \cdot H_0 \quad \text{(3-4 c)}$$

Based on these relationships the following range of model dimensions was obtained for the hydraulic model:

Table 3-9: Proposed model air vent diameter range based on Gariep Dam relationships

Model Parameter	Based on W	Based on H_0
	W_m = 128.8 mm	H_0 = 254.5 mm
$\emptyset_{main}$	22.72 mm	20.92 mm
$\emptyset_{side}$	11.36 mm	10.46 mm

The maximum diameter of the main vents was limited by the pressure sensor positions to 23 mm. From the values in Table 3-9, the following dimensions were chosen for the two aerated models to determine the effect of different air vent size:

Table 3-10: Model air vent diameters

Parameter	1st Aerated Model		2nd Aerated Model	
	Model (mm)	Prototype (m)	Model (mm)	Prototype (m)
$\emptyset_{main}$	20.0	0.4	23.0	0.46
$\emptyset_{side}$	10.0	0.2	11.5	0.23

3.3.4. Aeration Duct Design

The aeration duct was designed to allow the air vents to act as the control of the air flow. This meant that the cross-sectional area of the duct had to be more than the accumulated area of all of the air vents of the 2nd aerated model. The accumulated area of all the prototype air vents was calculated as:

$$\sum A_{vents} = 4 \times (2 \times A_{main} + 2 \times A_{side}) \quad \text{(3-5)}$$

$$\sum A_{vents} = 4 \times [2 \times (\pi \cdot (0.5 \cdot 0.46)^2) + 2 \times (\pi \cdot (0.5 \cdot 0.23)^2)]$$

$$\sum A_{vents} = 1.662\ m^2$$

Adding the safety factor of 2.0, the minimum cross-sectional area of the prototype aeration duct was:

$$(A_{duct})_{min} = 2 \times 1.662 \quad \text{(3-6)}$$

$$(A_{duct})_{min} = 3.324\ m^2$$

3.4. Model Construction

3.4.1. Ogee Spillway

The model ogee spillway and step was constructed by Fabrinox in Paarl, South Africa. The ogee spillway was constructed using a 2 mm thick sheet of mild steel bent over five 8 mm thick mild steel ribs. The ribs were laser cut to a profile 2 mm smaller than that of the ogee profile to allow for the steel sheet on top. The allowable tolerance on the model was ±0.5 mm. The staff at the Hydraulic Laboratory further provided steel strengthening beams for the model and painted it to provide a model surface roughness equivalent to that of prototype concrete. The final as-built drawings are contained in Appendix F.

Figure 3-7: Photographs showing the steel construction of the ogee spillway

3.4.2. Roberts Splitters

The Roberts splitters were constructed from suitable timber by the staff of the laboratory and painted in order to waterproof it. Two central measuring splitters were constructed because the tubes of all the pressure transmitters could not be fitted into a single splitter. The two measuring splitters (with the pressure tubes) were kept completely hollow to allow air to freely pass through in the case of the aerated models. The splitters were fixed and sealed to the painted steel spillway. Large holes were cut in the spillway to provide air to the aerated splitters.

The aerated splitters were constructed from the unaerated ones by drilling the desired aeration vents into them. In each model case, the vents were painted and sealed in order to waterproof the entire splitter.

3.4.3. Aeration Duct

To allow for the minimum allowable air duct cross-sectional area of 3.324 m^2 (prototype value, see Section 3.3.4) a general sewer drainage pipe with a diameter of Ø110 mm was selected to construct the proposed aeration duct system for the model. The cross-sectional area of the selected sewer drainage pipe and its fittings was 9503.3 mm^2, equivalent to a prototype cross-sectional area of 3.801 m^2. This, along with the adaptability of sewer drainage pipes, made it a suitable choice for the aeration duct.

The aeration duct included a drainage port and end cap to allow water entering the system through the air vents to be drained when needed. The system was put together using short sections of the pipe, fitted to a series of T-fittings, with one elbow fitting at the end. This allowed five separate ports to provide air to each splitter as well as the two half-splitters. The whole system was sealed to the back of the steel ogee spillway to allow minimal air leakage. Figure 3-8 shows the aeration duct system.

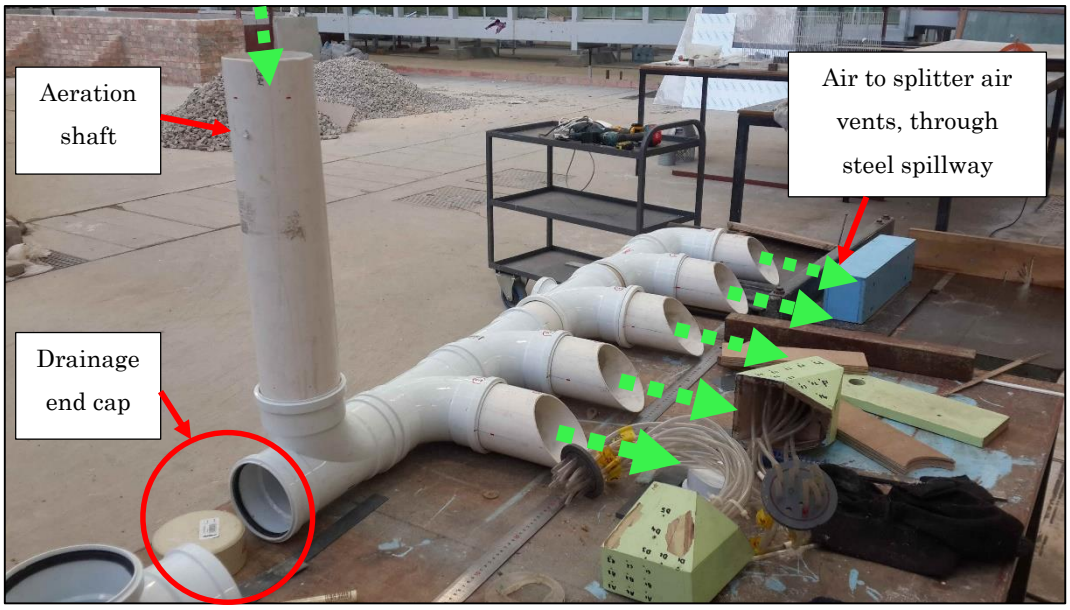

Figure 3-8: The aeration duct system

3.5. Data Collection

The methods used to measure and collect data from the hydraulic model and the analysis and conversion methods to obtain suitable data from these measurements are listed and described in this section. Result parameters were defined subject to necessary statistical analysis of results samples.

3.5.1. Discharge

Each separate model test started by adjusting the flow of the model system to match the predetermined model discharges as dictated by the testing procedure. The testing procedures for each of the hydraulic models are given in Section 3.2.

3.5.1.1. Instrumentation

A Flowmetrix SAFMAG DN600 electromagnetic flow meter, with a ±0.5% accuracy and reading repeatability of ±0.1% was used to measure the discharge. Figure 3-9 shows a typical reading of the flow meter indicating 690.60 l/s flowing over the model spillway.

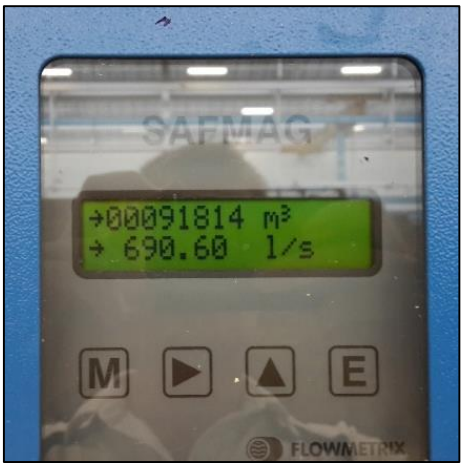

Figure 3-9: Gauge of Flowmetrix SAFMAG DN600 flow meter

3.5.1.2. Duration

The discharge fluctuated for an unspecified amount of time until the pressure head from the constant level tanks stabilised. The discharge was then read off the gauge and manually recorded. The displayed gauge value fluctuated by about ±0.5%.

3.5.1.3. Position

The flow meter was located on the DN600 steel pipe upstream of the test flume. A schematic layout of the laboratory setup is shown in Figure 3-10. The flowmeter was situated on the DN600 steel pipe supplying flow to the model flume a fair distance upstream from the controlling butterfly valve.

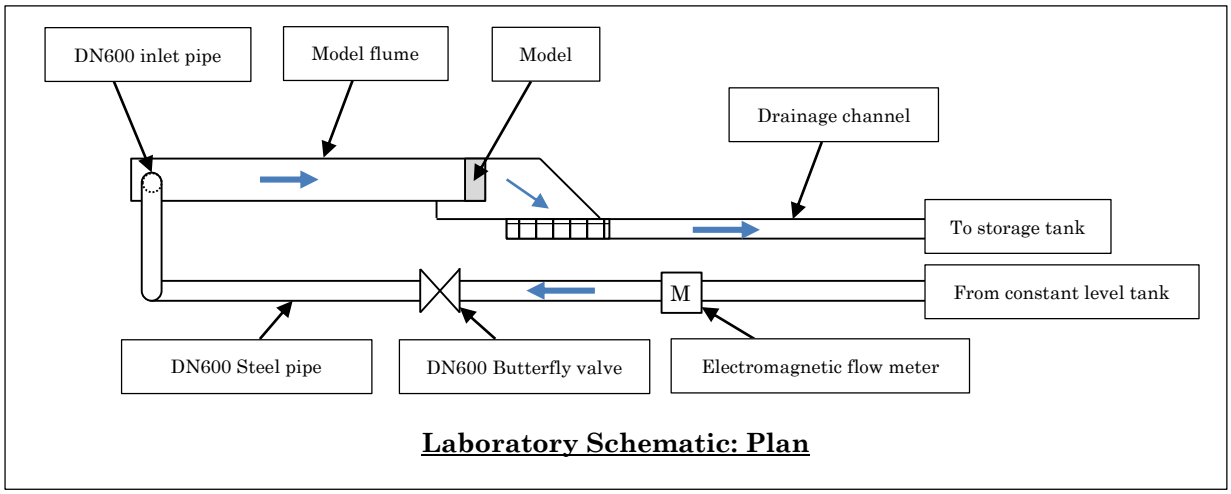

Figure 3-10: Schematic layout of the laboratory setup

3.5.1.4. Definition of Model Discharge

The model discharge was defined as the average discharge of each similar test over the six rounds of testing, as described in Section 3.2.

3.5.2. Water Level

For every test, the water level was measured to find the spillway head of the flow. This was done to verify and calibrate the discharge of each test, and set up the rating curve of the model.

3.5.2.1. Instrumentation, Method and Position

A water level measuring needle, placed 9.1 m upstream of the crest of the spillway, was used to measure the water level. Tests commenced after the correct discharge was measured (see Section 3.5.1), with the water level used to calibrate the accuracy of the measured discharge during the results analysis. This was mainly done to save time during the testing phases of the study. Figure 3-11 shows the water level measuring needle. The accuracy of the measurement was checked before, during and after each test.

Figure 3-11: Water level measurement needle

3.5.2.2. Definition of Model Head

The model spillway head was defined as the average of the measured head for similar tests over the six rounds of testing (the testing conditions were described in Section 3.2).

3.5.3. Pressure on Splitters

The complete pressure profile of all sides of a splitter was determined by measuring the dynamic flow pressure at certain strategic points on this splitter. This was done in order to analyse the cavitation risk of a Roberts splitter. The pressure was measured and presented relative to atmospheric pressure.

3.5.3.1. Instrumentation

Fourteen Wika S-10 high quality pressure transmitters were used to measure the dynamic fluid pressure at several positions on the splitters. These were connected to the two measuring splitters by Ø3 mm outside diameter plastic tubes. The transmitters had a range of ±100 mbar, an accuracy of ±0.2% and a reading repeatability of ±0.1%, as prescribed by the manufacturers, Wika. Figure 3-12 shows one of these transmitters.

Figure 3-12: Wika S-10 high quality pressure transmitter

3.5.3.2. Duration and Frequency

The pressure tests were done for a duration of 3 minutes at a maximum frequency of 100 Hz, giving a total of 18 000 readings per transmitter, per test. Preliminary testing by Calitz (2014) and Langa (2015) indicated that a duration of 3 minutes would be sufficient to provide a statistically variable set of data.

3.5.3.3. Position

The pressure sensors' tubes were symmetrically placed on the central splitter on the spillway, measuring the pressure on four of its faces. This could be mirrored to include all six faces of the splitter. As mentioned in Section 3.4.2, two splitters were constructed. This was done due to the confined space inside the splitter, and to better utilise the 14 pressure sensors. A total of 25 pressure locations were measured: 14 on the first splitter and 11 on the second splitter. Sensors placed on the end face of the splitter were labelled A1 to C3, sensors on the bottom face labelled D1 to D5, sensors on the side face labelled E1 to E7 and the sensors on the side bottom face labelled F1 to F4. Figure 3-13 shows the defined faces of the splitter. Figure 3-14 shows photographs of the two splitters, showing the relative positions of the pressure sensors. Figure 3-15 shows an excerpt from the design drawings showing more detailed locations and the labelling scheme used. For the exact locations, refer to Drawing GC-M01-SPL00 to SPL02 in Appendix F.

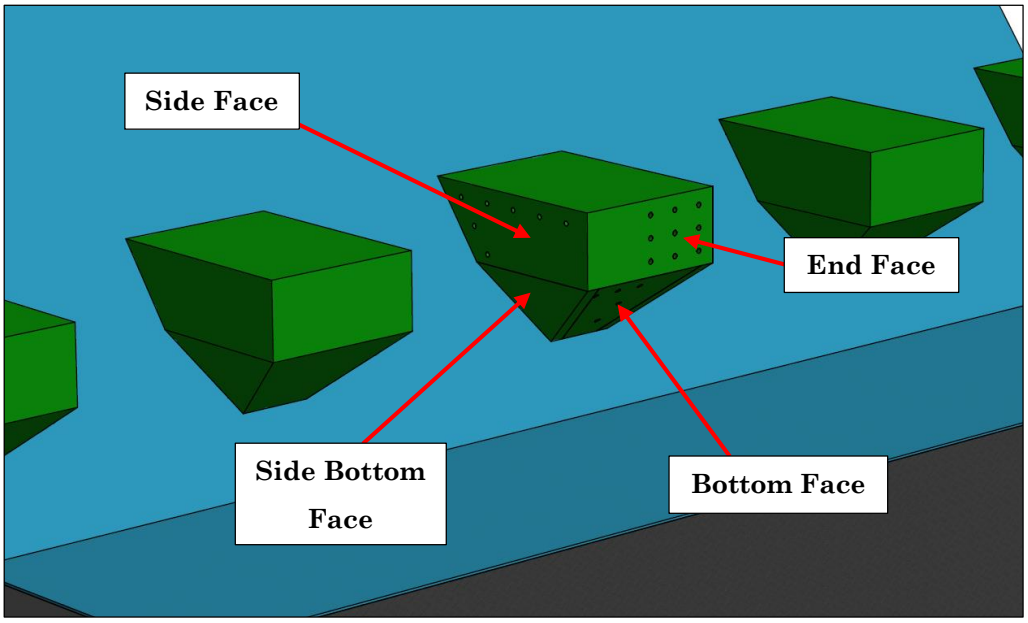

Figure 3-13: Definition of splitter faces

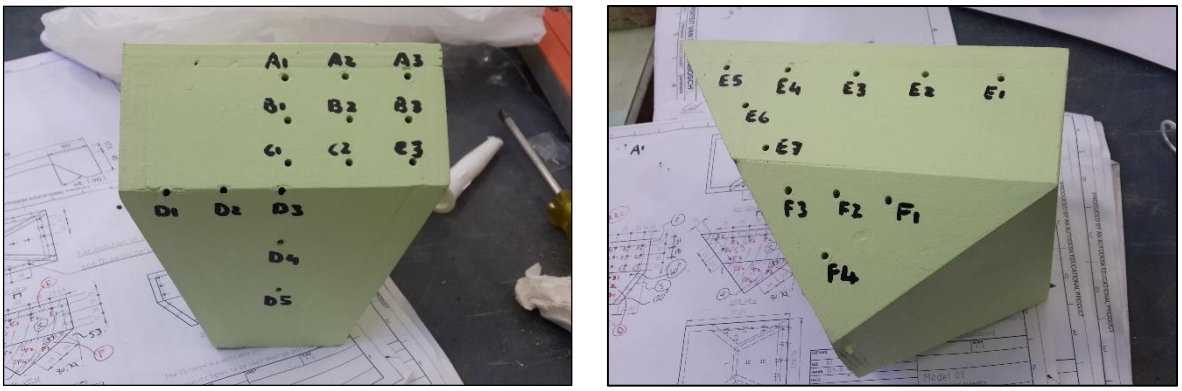

Figure 3-14: Photographs showing relative pressure sensor locations

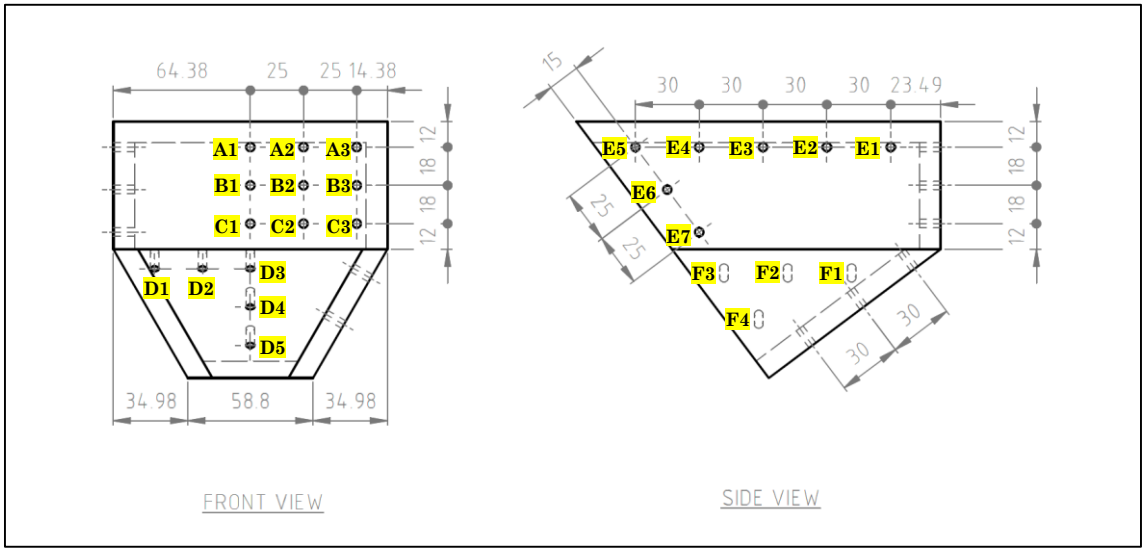

Figure 3-15: Excerpt from design drawings showing detailed pressure sensor locations

3.5.3.4. The Absolute Zero Pressure

As mentioned, all tests were conducted at the Hydraulic Laboratory of the University of Stellenbosch's Civil Engineering Department. This laboratory is located at approximately 120 masl. As such, the pressure of the atmosphere for the tests was calculated using the simplified barometric formula:

$$p_{atm} = p_0(1 - 2.25577 \times 10^{-5} \cdot Z)^{5.25588} \quad (3\text{-}7)$$

$$p_{atm} = 99\,891.7 \text{ Pa}$$

where p_{atm} is the atmospheric pressure used during the tests, p_0 is the atmospheric pressure at sea level (taken as 101 325 Pa) and Z_{lab} is the elevation of the laboratory in metres above sea level (taken as 120 masl).To find the gauge pressure of perfect vacuum, Eq. (3-8) can be used by calculating the pressure in metres of water y, at the absolute zero pressure of perfect vacuum ($p_{ABS} = 0$):

$$p_{ABS} = p_{atm} + \rho g y \quad (3\text{-}8)$$

Thus:

$$\rho g y = -p_{atm}$$

$$y_{zero} = -10.2 \text{ m}$$

Where ρ is the mass density of water (taken as 998 kg/m^3) and g is gravitational acceleration (taken as 9.81 m/s^2). y_{zero} is the absolute zero pressure during the model tests as metres of water, relative to atmospheric pressure.

When the measured pressure was below the absolute zero pressure of -10.2 m, it was assumed that the actual absolute pressure at the sensor was very close to vacuum, as true vacuum cannot be achieved in practice.

3.5.3.5. Statistical Analysis to Determine Minimum Pressure

To determine the risk of cavitation, a reliable representation of the minimum pressure was needed. To avoid outliers a 0.15% confidence limit was chosen according to the central limit theorem. The central limit theorem can be used to determine the probable minimum and maximum values of a population that is normally distributed, given a sample data set and a confidence probability (Montgomery & Runger, 2007).

In order to apply the central limit theorem, the data from four sets of sample readings was tested against a normal distribution. These samples were from pressure sensors A1, D1, E1, and F1, for a prototype unit discharge of 30 m^2/s on an aerated system (refer to

Section 3.5.3.3 for pressure sensor positions). The statistical summary of these four sets is shown in Table 3-11:

Table 3-11: Selected prototype pressure statistics for q = 30 m²/s

Pressure sensor	Sample size	Mean (m)	Std dev (m)	Min. (m)	Max. (m)	Skewness
A1	18 000	-0.144	0.157	-0.666	0.521	0.393
D1	18 000	-0.036	0.449	-1.075	1.425	0.481
E1	18 000	-0.173	0.143	-0.506	0.369	0.345
F1	18 000	-0.188	0.114	-0.468	0.199	0.082

These data sets were then standardised to the normal distribution according to Eq. (3-9):

$$Z = \frac{X - \mu}{\sigma} \tag{3-9}$$

where X is the normal random variable of each sample, μ is the mean of the sample, σ is the standard deviation of the sample and Z is the new dimensionless standardised random variable of the sample with a mean of 0 and a standard deviation of 1. The summary of the standardised data is shown in Table 3-12:

Table 3-12: Selected normally standardised pressure statistics for q = 30 m²/s

Pressure sensor	Sample size	Mean	Std dev	Min.	Max.	Skewness
A1	18 000	0	1	-3.323	4.233	0.393
D1	18 000	0	1	-2.313	3.250	0.481
E1	18 000	0	1	-2.322	3.783	0.345
F1	18 000	0	1	-2.452	3.382	0.082

The standardised sets of data were then each plotted as histograms against a normal distribution representing a data set with a sample size of 18 000 for a range of ±3 standard deviations. These data plots are indicated in Figure 3-16 to Figure 3-19.

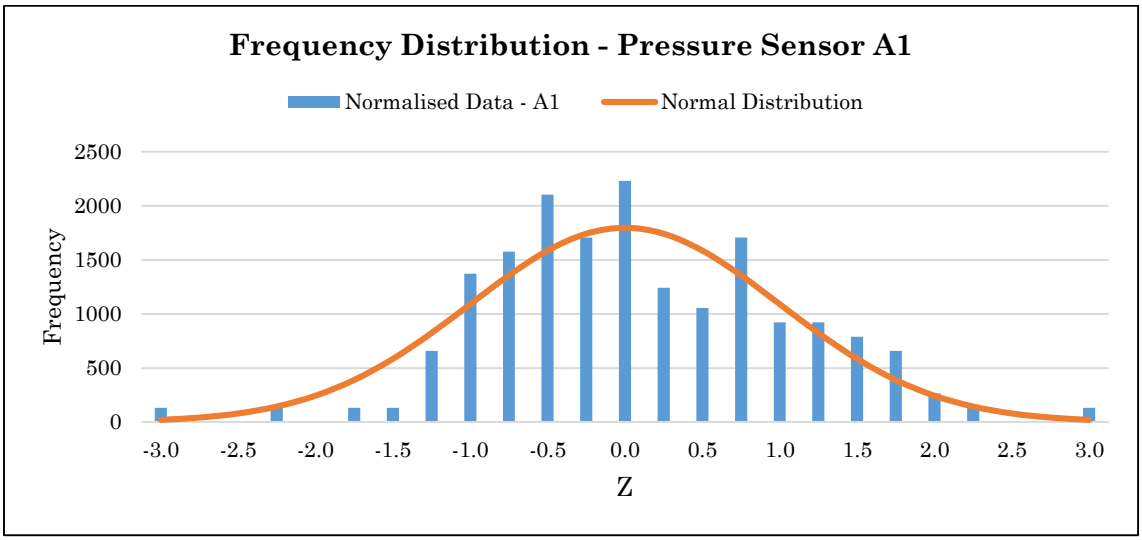

Figure 3-16: Histogram and normal distribution for pressure sensor A1

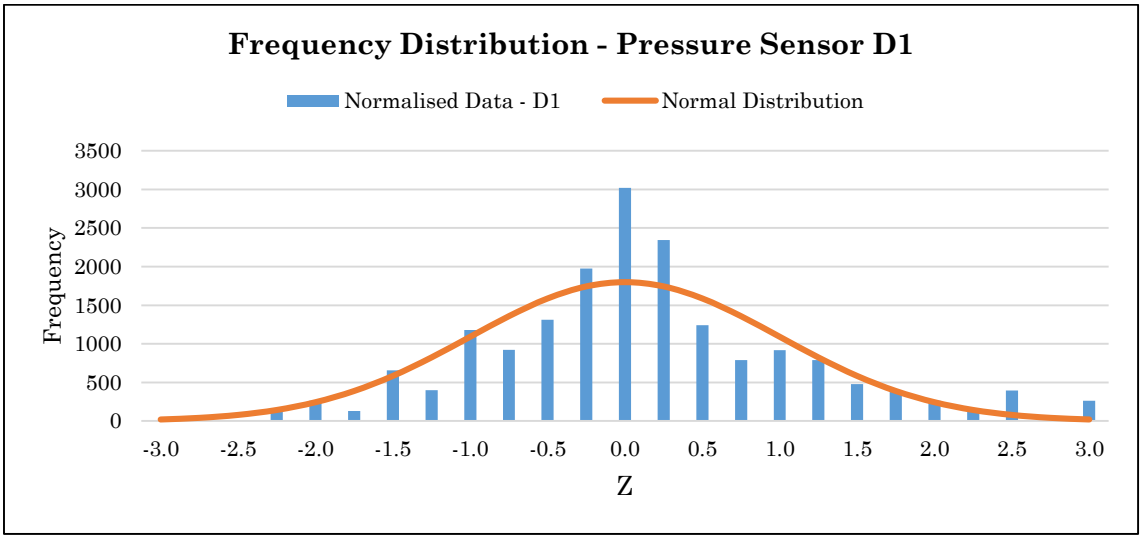

Figure 3-17: Histogram and normal distribution for pressure sensor D1

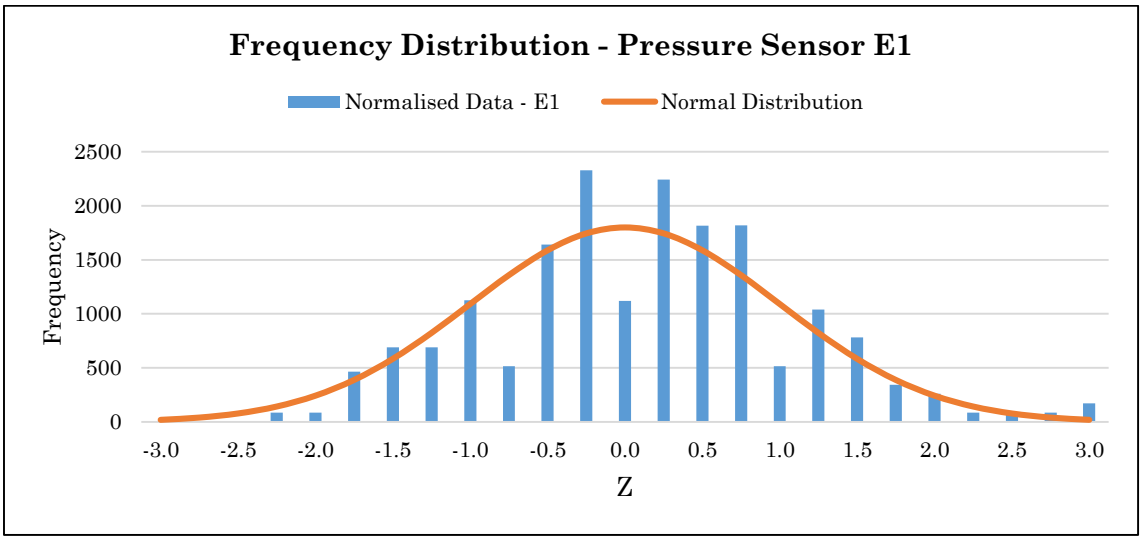

Figure 3-18: Histogram and normal distribution for pressure sensor E1

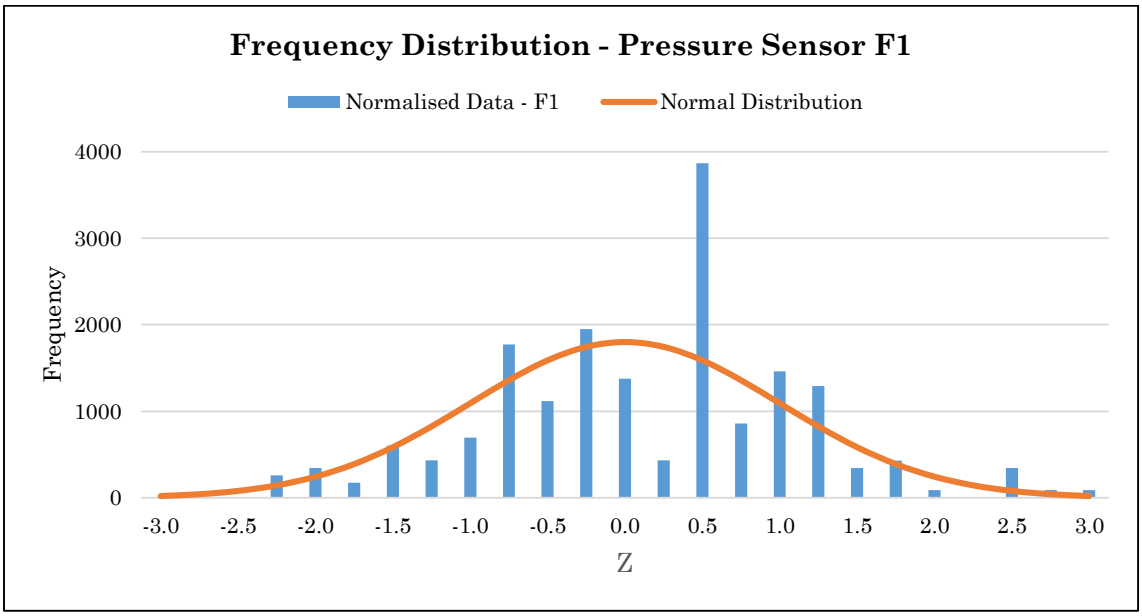

Figure 3-19: Histogram and normal distribution for pressure sensor F1

From the data plots above, the following conclusions were made:

- The data samples fit the normal distribution quite well;
- In all cases, the majority of the readings lie close to the mean, as can be seen by the blue bars towering over the normal distribution at the centre of each graph;
- The data was predominantly skewed to the right, with only sensor A1 (Figure 3-16) producing a measurement at more than 2.5 standard deviations below the mean;

3.5.3.6. Definition of Minimum Pressure for the Study

By assuming a normal distribution of each population, the extreme minimum pressure was defined as the pressure value exceeded 99.85% of the time. Literature showed that an exceedance probability of 0.1% is representative for the extreme minimum pressure in cavitation analysis (Amador *et al.*, 2005). Calitz (2015) suggested an exceedance probability of 0.15% to be representative of the extreme minimum pressure. An exceedance probability of 0.15% was adopted to represent the extreme minimum and maximum pressures of this study.

To account for the evident positive skewness, a probable minimum pressure was also defined as the pressure exceeded 95% of the time. This eliminated the extreme pressure spikes and gave an indication of a tendency of the minimum pressure that can be expected with increasing spillway head. The final pressures obtained from all data sets are defined in Table 3-13:

Table 3-13: Defined pressure parameters for the study

Defined Parameter	Definition
Minimum pressure	The pressure value exceeded 99.85% of the time
Probable minimum pressure	The pressure value exceeded 95% of the time

3.5.3.7. Data Conversion

Table 3-14 indicates the output signals and details of the Wika S-10 pressure transmitters as obtained from the manufacturers. This information was used in converting the measured output signals to usable dynamic fluid pressure heads at the positions of the transmitters.

Table 3-14: Output signals and details of Wika S-10 pressure transmitter

Transmitter Parameter	Symbol	Min. range	Max. Range
Output current	I	4 mA	20 mA
Measurable pressure (atmospheric)	p	-100 mbar	+100 mbar
Measurable pressure as head of water	H	-1 m	+1 m
Power supply	V	DC 10 V	DC 30 V
Resistance	R	120 Ω	

The transmitters function in conjunction with a data logging box, converting the electric current readings to voltage over a 120 Ω resistor according to Ohm's law. Using this knowledge, the pressure head can be related to the measured voltage readings using Eq. (3-10).

$$H_{out} = \frac{H_{max} - H_{\min}}{I_{max} - I_{\min}} \times \frac{\boldsymbol{x}}{R} - V_{atm} \tag{3-10}$$

with the following symbol definitions:

Table 3-15: Symbol description for pressure transmitter conversion equation

Symbol	Unit	Description
H_{out}	m	Measured dynamic pressure head
H_{max}	m	Maximum pressure head limit of transmitter
H_{min}	m	Minimum pressure head limit of transmitter
I_{max}	A	Maximum current output of transmitter
I_{min}	A	Minimum current output of transmitter
$\boldsymbol{x}$	V	Measured voltage reading
R	Ω	Resistance of transmitter
V_{atm}	V	Voltage reading of atmospheric hydrostatic pressure

The transmitter manufacturers recommended using a value of 1.5 V as the reading of atmospheric hydrostatic pressure, but according to Fraser (2015) this would result in a maximum deviation of 5.34% from the actual control reading. Therefore, for all the tests performed, a calibration value for V_{atm} was measured to accurately obtain the dynamic fluid pressure at the position of the pressure transmitters.

For the Wika S-10 transmitters used for the duration of the hydraulic model testing, Eq. (3-10) becomes:

$$H_{out} = \frac{(1)-(-1)}{(0.02)-(0.004)} \times \frac{\boldsymbol{x}}{120} - V_{cal}$$

where V_{cal} was the calibration reading of each transmitter. Simplified this became:

$$H_{out} = \frac{25}{24} \times (\boldsymbol{x} - V_{cal}) \tag{3-11}$$

3.5.4. Air Concentration of Flow

To analyse the cavitation risk of the splitters, the air concentration of the flow was measured at the positions where cavitation was expected.

3.5.4.1. Instrumentation

An intrusive conductive needle probe was used to measure the air concentration of the flow. The diameter of the probe's conductive tip is Ø0.1 mm. The probe operates by measuring the electric conductivity of air and water and returning the acquired voltage to a data logger. The data was logged using Thermo Needle Probe (TNP) software. Both the probe and the software were supplied and calibrated by German based HZDR Innovation. The intrusive conductive needle probe and a close-up of the tip of the probe are shown in Figure 3-20 and Figure 3-21 respectively.

Figure 3-22 is a schematic drawing of bubbles hitting the tip of the probe. The probe measures the conductivity of the air and the water and logs this data using the TNP module. Theoretically the conductivity of water would be one value and the conductivity of the air another, resulting in only two different output values for the air chords and water chords, i.e. a rectangular signal. This was not and will never be the case due to the wetting and drying time of the tip, the measurement response time and the size of the tip (Calitz, 2015).

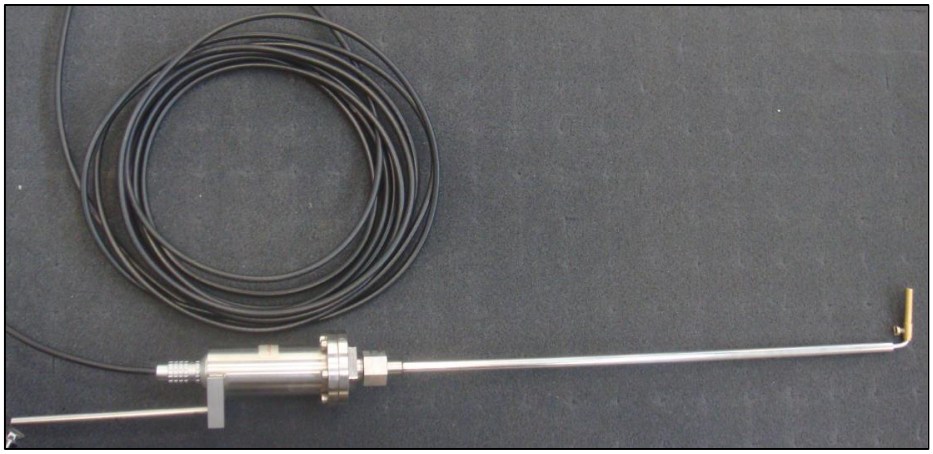

Figure 3-20: Conductive needle probe (Fraser, 2016)

Figure 3-21: Tip of the conductive needle probe (Calitz, 2015)

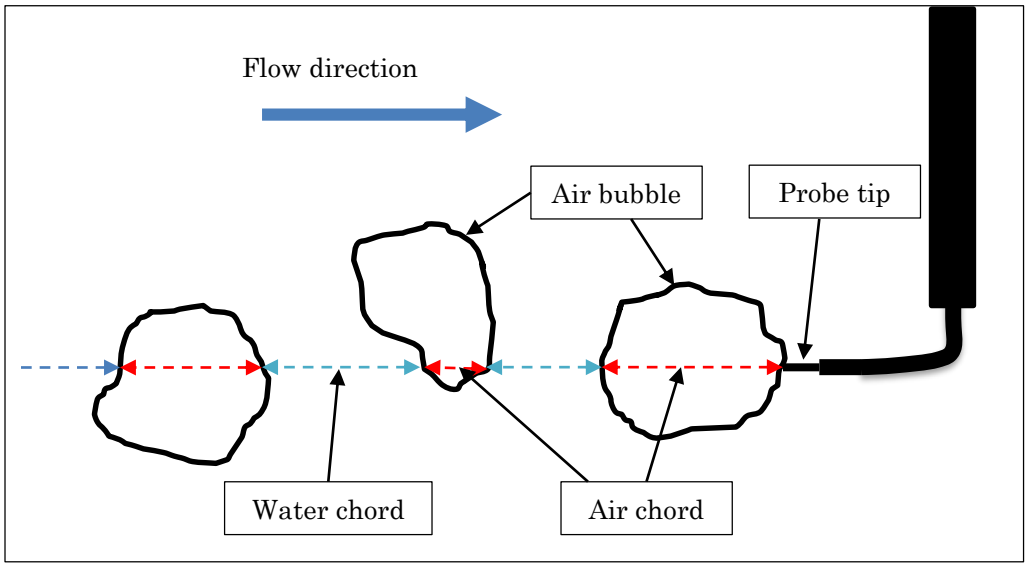

Figure 3-22: Probe needle – phase detection (Chanson, 2013)

The resulting data was then analysed using VoidWizard software, also supplied by HZDR Innovation. The software estimates the phases of the conductivity data and simplifies it to the theoretical binary curve, resulting in either water, or voids. Figure 3-23 shows a typical example of the VoidWizard GUI and the simplified binary data. Note that in this instance the flow was mainly in the air phase, and a conductivity spike occurred any time a water drop or splash hit the tip of the probe. The binarised data was then averaged over a time period of 0.05 s. It was deemed that the data accuracy would not diminish at a time step of 0.05 s. The final air concentration per time step was reported by VoidWizard as the sum of the void periods per time step divided by the time step as per Eq. (3-12):

$$(Air\%)_n = \frac{(\sum t_{void})_n}{t_n} \tag{3-12}$$

where $Air\%$ is the air concentration and t_{void} is the period a void is detected within the n^{th} time step. t_n is the length of the n^{th} time step.

3.5.4.2. Definition of Air Concentration

The air concentration of the flow at a measuring position was defined as the average of all $Air\%$ per sample at that position.

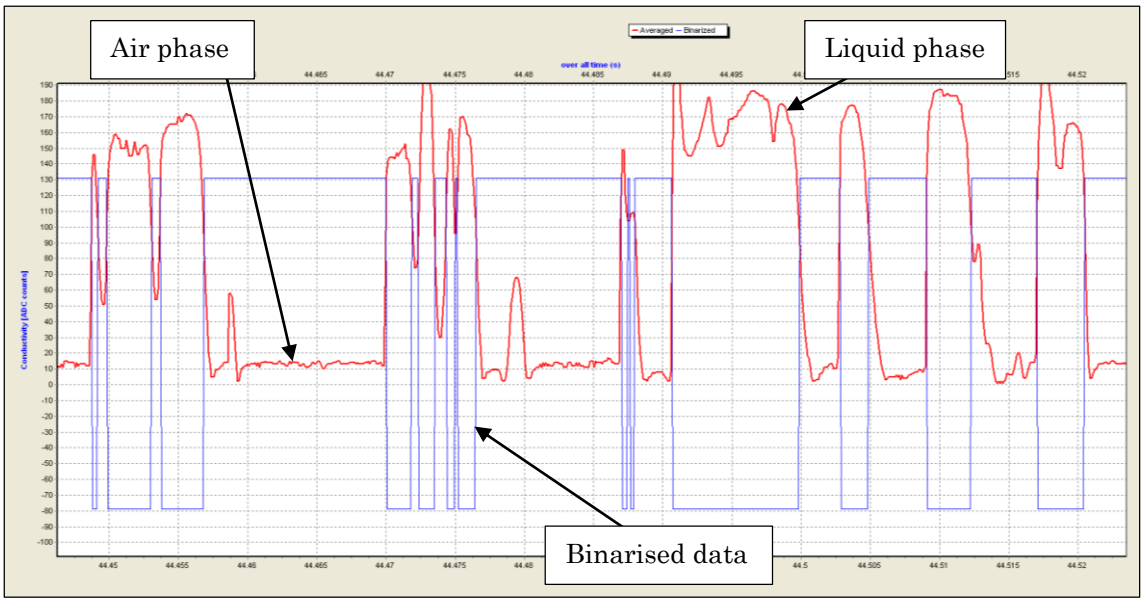

Figure 3-23: Binarised and raw data from the VoidWizard software

3.5.4.3. Duration and Frequency

A sampling duration of 1 minute was selected for the air concentration tests. Literature showed that for the intrusive conductive needle probe used, a sampling time of 15 s is sufficient to obtain a representative set of data, even though a sampling time of 30 s or more should be used (Calitz, 2015). The probe measured and logged samples at a frequency of 10 kHz, supporting the short sampling time chosen to obtain a suitable variable set of data. The final set of data obtained after the VoidWizard analysis had a frequency of 20 Hz as the raw data was averaged over a time step of 0.05 s.

3.5.4.4. Position

The air concentration was measured at three locations around the splitter to complement the pressure readings taken:

- The end of the splitter – the tip of the air probe was positioned 20 mm from the end, in line with the centre of the downstream face;
- The bottom of the splitter – the tip was positioned directly below the end position, 90 mm lower;
- The side of the splitter – the tip was positioned on the same height of the end position, but 100 mm to the side.

Figure 3-24 shows the air measurement positions relative to the model.

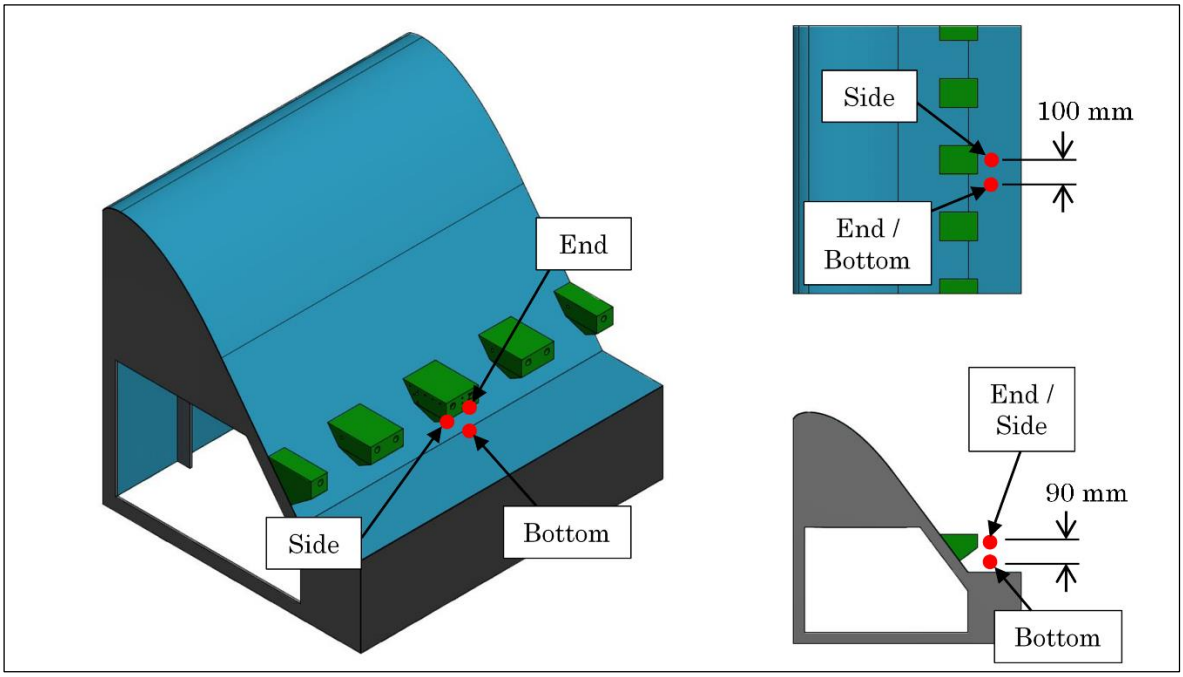

Figure 3-24: Air probe positions

3.5.4.5. Statistical Analysis and Data Conversion

All statistical analysis and data conversion were done automatically using the VoidWizard software provided by HZDR Innovation. The software reported the air concentration as a percentage of voids within the flow. This parameter was defined and explained in Section 3.5.4.1.

3.5.5. Aeration Shaft Air Velocity

The air velocity within the aeration shaft was measured in order to calculate the air discharge within the air duct and the aeration vents of the splitters.

3.5.5.1. Instrumentation

A Lutron hot-wire anemometer was used for data acquisition. The anemometer functioned by heating a thin element and measuring its cooling tempo. This tempo, along with the local air temperature, was used to actively calculate and display the air velocity. The anemometer and the measuring tip of the probe are shown in Figure 3-25 and Figure 3-26 respectively.

Figure 3-25: Hot wire anemometer

Figure 3-26: Tip of telescopic probe

The anemometer had an accuracy of ±1% and was capable of displaying the measured wind velocity in five different measuring units on its three-digit display. The available units and their respective ranges and display resolutions are given in Table 3-16. Although the measurement accuracy of the anemometer was ±1%, data accuracy was lost with the resolution of the three-digit display. It was decided to obtain the data using the unit with the smallest resolution. Thus, all air velocity measurements were taken in ft/min.

Table 3-16: Specification of the hot wire anemometer

Measurement unit	Range	Display Resolution	Resolution as m/s equivalent
m/s	0.2 – 20.0	0.1 m/s	0.1
km/h	0.7 – 72.0	0.1 km/h	0.0278
ft/min	**40 – 3940**	**1.0 ft/min**	**0.0051**
mile/h	0.5 – 44.7	0.1 mile/h	0.0447
knots	0.4 – 38.8	0.1 knots	0.0514

Note: Bold text indicates the measurement unit with the smallest relative display resolution

3.5.5.2. Duration and Frequency

There were no data logging modules available for the anemometer, therefore the air velocity value was written down manually. For consistency and objectivity, the displayed value every 5 s, on the second, for 120 s was noted. This gave a sample size of 24, from which the average was taken as the final value.

3.5.5.3. Position

The air velocity was measured in the centre of the shaft of the aeration duct as this was the straightest, longest part of the aeration system. From here the air discharge could be calculated from the air velocity and proportionally divided per splitter. Through continuity, the air velocity in the internal pipe would be same as in the shaft, providing the diameter is equal and the air had not reached the first splitter yet. The anemometer with the tip of its telescope probe fitted snugly inside the aeration shaft is shown in Figure 3-27.

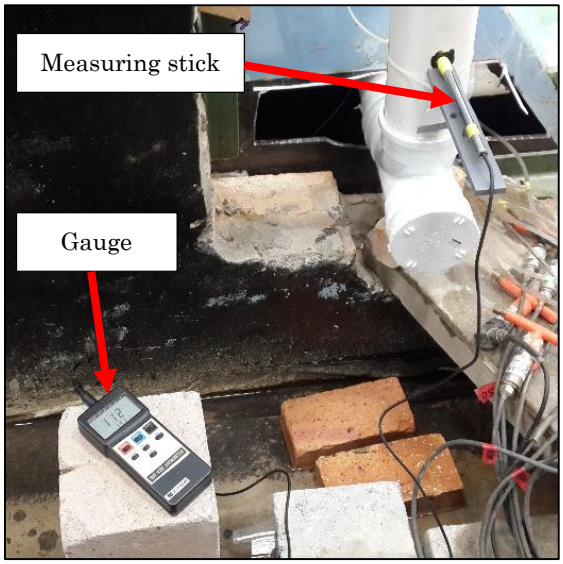

Figure 3-27: Hot wire anemometer positioned during testing

3.5.5.4. Statistical Analysis of Air Velocity

The same statistical approach was followed as with the pressure data (Section 3.5.3.4). The air velocity data was standardised to a normal distribution and plotted as a histogram against a true normal distribution for the sample size. This was done for the air velocity data of two tests on the model splitters with Ø20 mm diameter main air vents. The data frequency distributions are shown in Figure 3-28 and Figure 3-29 for prototype unit discharges of 30 and 40 m²/s respectively, and their statistics provided in Table 3-17 and Table 3-18.

Table 3-17: Selected air velocity data statistics

q_p (m²/s)	Sample size	Mean (ft/min)	Std dev (ft/min)	Min. (ft/min)	Max. (ft/min)	Skewness
30	24	210.167	13.560	182	242	-0.062
40	24	177.625	12.951	155	202	0.061

Table 3-18: Selected normally standardised air velocity statistics

q_p (m²/s)	Sample size	Mean	Std dev	Min.	Max.	Skewness
30	24	0	1	-2.077	2.348	-0.062
40	24	0	1	-1.747	1.882	0.061

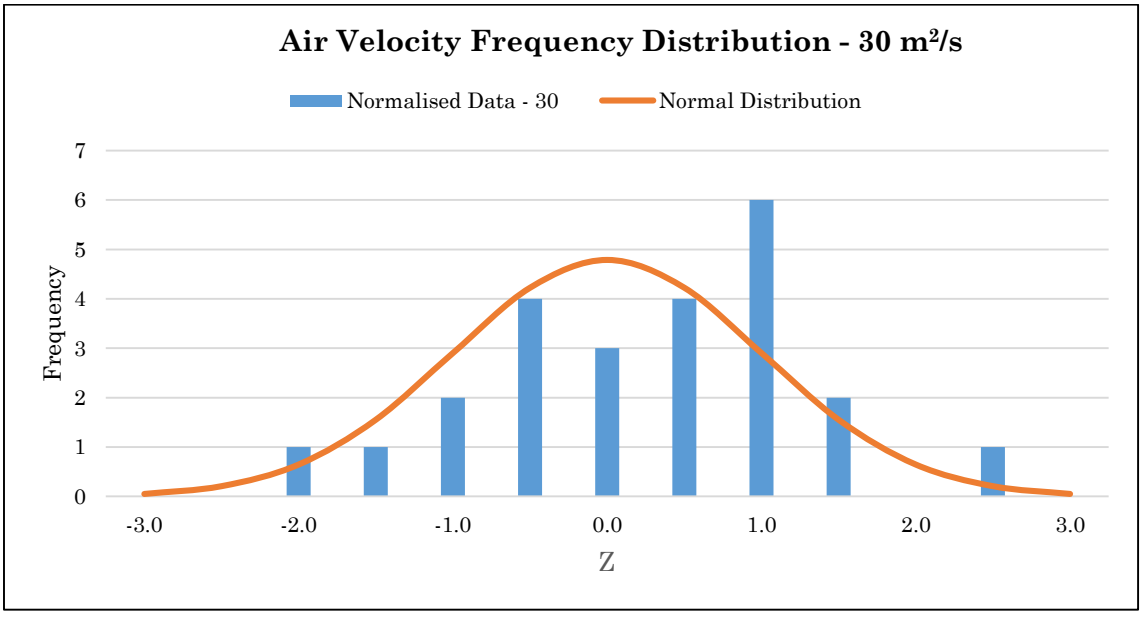

Figure 3-28: Histogram and normal distribution for air velocity – 30 m²/s

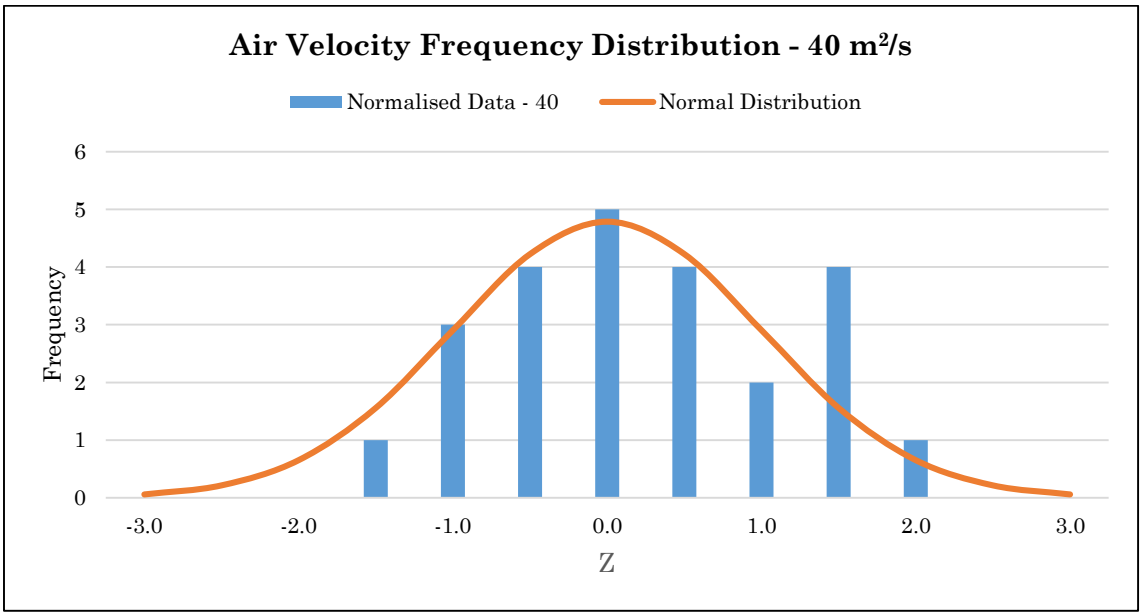

Figure 3-29: Histogram and normal distribution for air velocity – 40 m²/s

The data sets were too small to accurately reflect a normal distribution, but the mean of each set of air velocity measurements was still deemed to be representative of the situation. However, it proved a problem selecting the value for the maximum air velocity. It was deemed conservative to assume that in the instance of a large enough sample, the data would fit a normal distribution and as such, it could be deduced with 99.85% confidence that the maximum value would lie within 3 standard deviations of the mean. This assumption was supported by the very low skewness coefficients of the analysed data sets and the normally standardised maximum values of 2.348 and 1.882, well inside 3 standard deviations. This assumption was further supported by the fact that in every test, the maximum value fell within 3 standard deviations of the mean. This is shown in the results in Chapter 5.

3.5.5.5. Definition of Air Velocity

It was concluded that the air velocity in the aeration shaft would be defined as the average of the measured data and that the maximum air velocity would conservatively be defined as the value 3 standard deviations above the mean.

3.5.5.6. Data Conversion

As mentioned earlier, all model air velocity measurements were taken in ft/min, and was thus converted back to m/s using Eq. (3-13):

$$v_{air_m} = \frac{x}{196.85} \tag{3-13}$$

where v_{air_m} is the model air velocity in the aeration shaft (in m/s) and x is the measured data value (in ft/min).

3.5.6. Air Discharge

The air discharge of the aeration system is directly proportional to the air velocity in the aeration shaft according to Eq. (3-14):

$$Q = v \cdot A \tag{3-14}$$

As the air velocity was measured in a uniform stretch of pipe, the aeration duct's intake air discharge was calculated using the cross-sectional area of the pipe at that point:

$$Q_{intake} = v_{air} \times A_{shaft} \tag{3-15}$$

From continuity, the sum of the air discharge of all splitters equals the intake air discharge of the aeration duct and as all splitters were similar and a uniform sheet of water flowed over them, it was possible to assume that the air discharge per splitter would be equal for all splitters. This meant that in the case of the studied hydraulic model, with four cycles of splitters, the air discharge per splitter was defined as:

$$Q_{air} = \frac{Q_{intake}}{4} \tag{3-16}$$

It was however, impossible to determine or measure the air discharge per air vent of an individual splitter. It could be assumed that the discharge would be symmetrically divided over the width of the splitter.

In summary, the air discharge per splitter was defined as the total air discharge from all four air vents of a single splitter.

3.5.7. Aeration Duct Drainage

Drainage from the aeration duct was not considered a primary measurement objective, but during observations it was found that at certain discharges, water needed to drain from it.

3.5.7.1. Instrumentation, Method and Position

One 9 l bucket was used to capture all drained discharge from the aeration duct during a given time. Figure 3-30 shows the bucket used for the measurement.

Figure 3-30: Captured drainage discharge from aeration duct

The discharge was determined by dividing the volume of the bucket by the time it took to fill up. The position of the bucket was downstream of the drainage end cap provided in the design of the aeration duct, as shown in Figure 3-30. The water inflow rate per splitter was calculated by dividing the total drainage discharge by the number of splitters in the system:

$$Q_{inflow} = \frac{Q_{drain}}{4} \tag{3-17}$$

3.6. Repeatability of Tests

In order to validate the results of the study, the repeatability of the pressure and air concentration tests was determined. This was done by conducting and analysing three independent tests for each model case.

3.6.1. Pressure

Three independent tests were done at a prototype unit discharge of 30 m²/s for all models, and analysed to verify the repeatability of the pressure sensors. Statistics from pressure sensors A2 and E5 for q_p = 30 m²/s are shown in Table 3-19 and Table 3-20 respectively.

Table 3-19: Statistics for pressure sensor A2 at 30 m²/s

	Unaerated Model			1st Aerated Model			2nd Aerated Model		
	Test 1	**Test 2**	**Test 3**	**Test 1**	**Test 2**	**Test 3**	**Test 1**	**Test 2**	**Test 3**
Mean	-0.057	-0.050	-0.070	0.066	0.027	0.105	0.038	-0.030	-0.033
Std dev	0.179	0.154	0.188	0.236	0.228	0.259	0.212	0.188	0.196
Max.	0.665	0.505	0.522	1.315	0.907	1.032	0.979	0.509	0.729
3rd Quartile	0.060	0.047	0.043	0.169	0.157	0.220	0.166	0.071	0.083
Median	-0.065	-0.078	-0.082	0.023	-0.010	0.074	0.041	-0.033	-0.063
1st Quartile	-0.190	-0.140	-0.207	-0.081	-0.114	-0.051	-0.105	-0.137	-0.167
Min.	-0.481	-0.515	-0.478	-0.560	-0.405	-0.385	-0.563	-0.554	-0.542

Table 3-20: Statistics for pressure sensor E5 at 30 m²/s

	Unaerated Model			1st Aerated Model			2nd Aerated Model		
	Test 1	**Test 2**	**Test 3**	**Test 1**	**Test 2**	**Test 3**	**Test 1**	**Test 2**	**Test 3**
Mean	-0.316	-0.340	-0.324	-0.222	-0.242	-0.235	-0.280	-0.263	-0.280
Std dev	0.182	0.192	0.217	0.148	0.112	0.120	0.104	0.111	0.118
Max.	0.188	0.267	0.217	0.127	0.051	0.208	0.063	-0.041	0.022
3rd Quartile	-0.187	-0.212	-0.158	-0.123	-0.157	-0.167	-0.208	-0.187	-0.187
Median	-0.333	-0.337	-0.345	-0.228	-0.240	-0.230	-0.291	-0.249	-0.270
1st Quartile	-0.458	-0.462	-0.449	-0.311	-0.324	-0.313	-0.353	-0.333	-0.353
Min.	-0.854	-0.941	-0.991	-0.603	-0.553	-0.625	-0.603	-0.624	-0.645

Figure 3-31 and Figure 3-32 indicates box and whisker plots of the data from sensors A2 and E5. The box represents the first quartile, the median and the third quartile of each sample. The cross represents the mean of each sample and the whiskers represent the maximum and minimum excluding outliers. Outliers are defined according to Tukey's

(1977) definition as values lying outside 1.5 times the interquartile range from the 1st and 3rd quartile respectively. The dots indicate outliers.

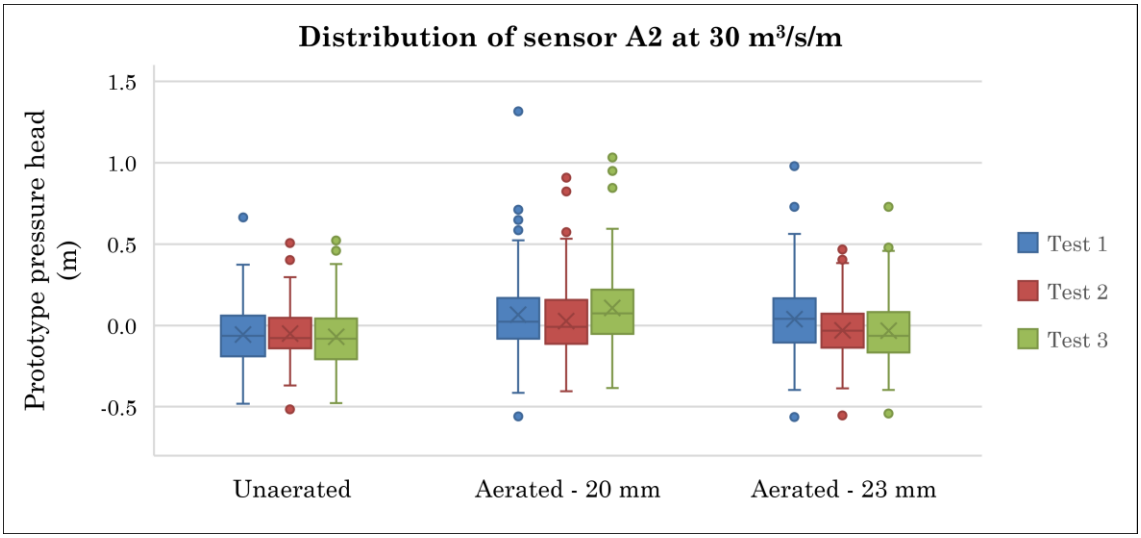

Figure 3-31: Pressure distributions for sensor A2 - 30 m²/s

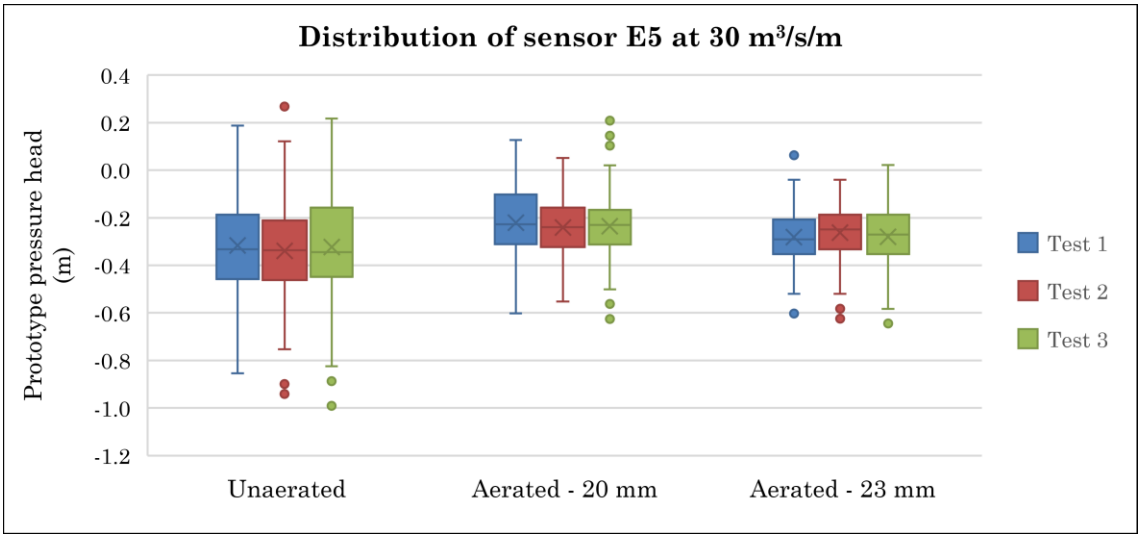

Figure 3-32: Pressure distributions for sensor E5 - 30 m²/s

From these tables and figures, the repeatability of the pressure tests is confirmed by the consistency of the means and medians, as well as the minima and maxima.

3.6.2. Air Concentration

The same approach was followed to determine the repeatability of the air concentration measurements. The air concentration at the end of the splitter was measured on three independent occasions at a prototype discharge of 30 m²/s. The statistics for these tests are shown in Table 3-21 and the distributions as box and whisker plots in Figure 3-33.

Table 3-21: Statistics for air concentration at end of splitter at 30 m²/s

	Unaerated Model			1st Aerated Model			2nd Aerated Model		
	Test 1	Test 2	Test 3	Test 1	Test 2	Test 3	Test 1	Test 2	Test 3
Mean	99.173	99.341	98.663	95.212	97.917	98.066	97.029	92.107	93.893
Std dev	2.111	1.756	3.013	6.904	4.439	3.940	5.147	9.965	8.501
Max.	100.0	100.0	100.0	100.0	100.0	100.0	100.0	100.0	100.0
3rd Quartile	100.0	100.0	100.0	100.0	100.0	100.0	100.0	100.0	100.0
Median	100.0	100.0	100.0	98.0	100.0	100.0	100.0	96.0	97.0
1st Quartile	99.0	100.0	99.0	93.0	98.0	98.0	96.0	88.0	91.0
Min.	75.0	83.0	59.0	34.0	39.0	40.0	59.0	45.0	48.0

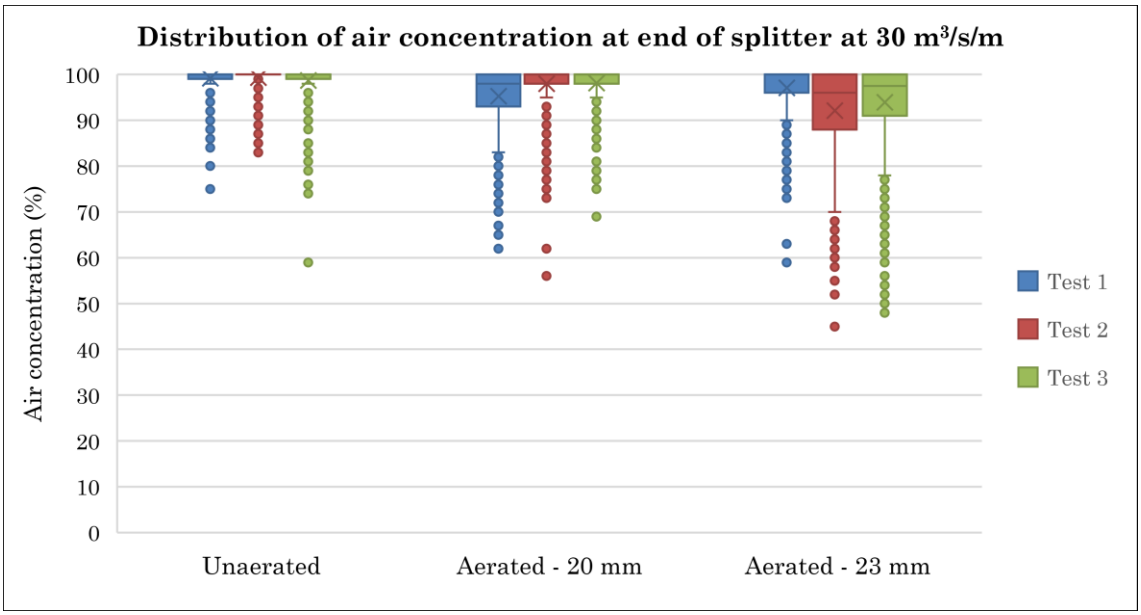

Figure 3-33: Air concentration distribution downstream of the splitter - 30 m²/s

From Table 3-21 and Figure 3-33 it is clear that the majority of data lie close to 100% and that a lot of outliers were measured below the local minimum. The repeatability of the air concentration measurements was however sufficient, and because of the very small variance in data the average of all measurements per position was deemed an accurate representation of the air concentration of the flow at that position.

CHAPTER 4

RESULTS AND ANALYSIS OF THE HYDRAULIC MODEL TESTS

In this chapter, the results obtained from the hydraulic model study are summarised and analysed to determine the performance of the model (as described in Chapter 3) and its aeration improvements. Summarised results are sorted per model. The chapter concludes with a discussion of the results as a whole and how they influenced each other. The complete results are contained within the following sections and appendices:

Table 4-1: Locations of complete results within thesis

Results	Location within thesis
Rating Curve	Section 4.1
Pressure	Appendix H
Air concentration	Appendix I
Air velocity in the aeration duct	Appendix J
Drainage from the aeration duct	Section 4.3 and 4.4

The following definitions are applicable to the results, as defined in Chapter 3:

Table 4-2: Defined measured parameters

Symbol	Parameter	Unit	Definition
Q_m	Model discharge	l/s	Average discharge of similar tests over the six rounds of testing
H_m	Model spillway head	mm	Average spillway head of similar tests over the six rounds of testing
q_p	Prototype unit discharge	m^2/s	Model discharge scaled by a factor of $20^{2.5}$ and divided by the prototype spillway length of 24 m
H_p	Prototype spillway head	m	Model spillway head, scaled up by a factor of 20
h_p	Prototype pressure	m	Prototype dynamic fluid pressure as metres of water
h_{min}	Minimum pressure	m	The pressure exceeded 99.85% of the time
h_{prob}	Probable minimum pressure	m	The pressure exceeded 95% of the time
$Air\%$	Air concentration	%	The average of $(Air\%)_n$ for all time steps

Table 4-2: Defined measured parameters

Symbol	Parameter	Unit	Definition
$(v_{air})_{avg}$	Average air velocity	m/s	Average air velocity
$(v_{air})_{max}$	Maximum air velocity	m/s	Value 3 standard deviations above the mean, i.e. $(v_{air})_{max} = (v_{air})_{avg} + 3 \cdot \sigma$
Q_{air}	Air discharge	m³/s	Total air discharge form the four air vents of a single splitter
Q_{drain}	Drainage discharge	l/s	Average water drainage from aeration duct
Q_{inflow}	Water inflow per splitter	l/s	Average water inflow through all air vents of a single splitter

Note: all following results used the prototype spillway head as the independent variable. As Roberts splitters are dimensioned and studied in terms of the depth of flow approaching the splitters, and the depth of flow is proportional to the spillway head and the spillway unit discharge, the results contained herein are subject to the model spillway's discharge coefficient of 2.262.

4.1. Model Rating Curve

To model rating curve was determined from the model spillway head and the model discharge. The discharge and spillway head was determined through the average of similar tests, and shown in Table 4-3.

Table 4-3: Theoretical and measured model discharge and model spillway head

Test	Theoretical		Measured Discharge				Measured Spillway Head			
q_p (m²/s)	Q_p (m³/s)	H_p (m)	Unaerated	1st Aerated	2nd Aerated	Q_p (m³/s)	Unaerated	1st Aerated	2nd Aerated	H_p (m)
5	**120.0**	**1.9**	121.1	120.0	120.0	**120.4**	1.9	1.9	1.9	**1.9**
10	**240.1**	**2.9**	240.1	240.1	240.1	**240.1**	2.9	2.9	2.9	**2.9**
15	**359.9**	**3.7**	360.1	360.1	360.1	**360.1**	3.7	3.7	3.7	**3.7**
20	**479.9**	**4.4**	480.1	480.1	480.1	**480.1**	4.4	4.4	4.4	**4.4**
25	**600.0**	**5.1**	601.2	601.2	600.3	**600.9**	5.0	5.0	5.0	**5.0**
30	**720.0**	**5.7**	720.4	720.4	720.4	**720.4**	5.6	5.6	5.6	**5.6**
35	**840.0**	**6.3**	841.3	840.4	840.4	**840.8**	6.1	6.1	6.1	**6.1**
40	**960.1**	**6.8**	960.4	960.4	960.4	**960.4**	6.7	6.7	6.6	**6.7**
45	**1079.9**	**7.3**	1080.5	1080.5	1080.5	**1080.5**	7.1	7.1	7.1	**7.1**
50	**1200.0**	**7.8**	1200.5	1200.5	1200.5	**1200.5**	7.6	7.6	7.6	**7.6**

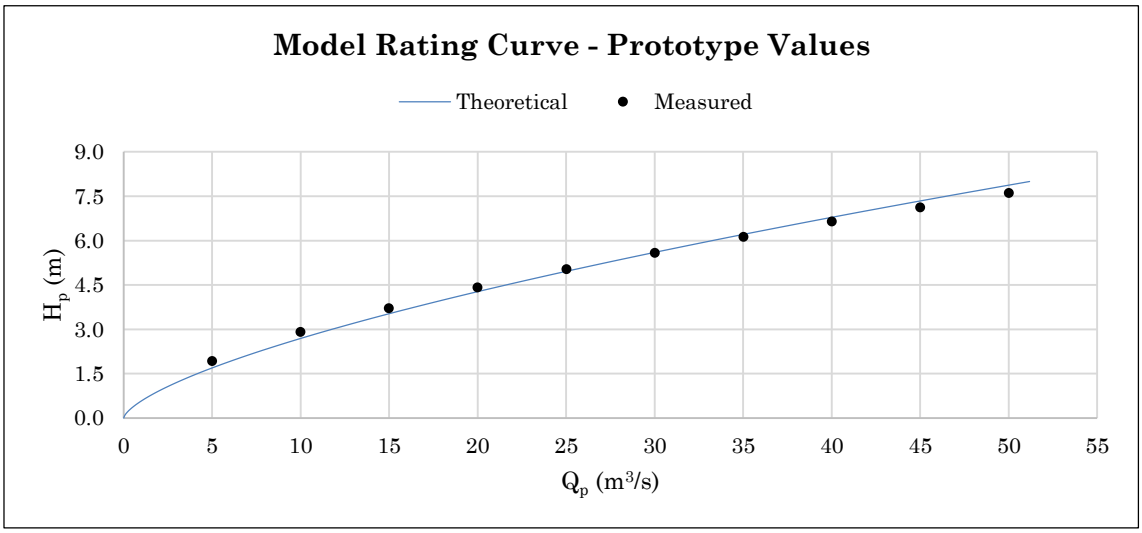

Figure 4-1: Model rating curve - model values

4.1.1. Discussion of Rating Curve

As indicated in Figure 4-1, the measured ratings values deviate slightly from the theoretical curve. At lower discharges, a lower discharge coefficient was observed, while at higher discharges, a higher discharge coefficient was observed. This was due to viscosity and surface tension effects that cannot be scaled down to model specifications. As a result of this deviation, lower spillway heads were measured for the scheduled discharges compared to the theory.

Thus, the measured spillway heads were used as the independent variable for the model study. The theoretical design head of the Roberts splitters, equivalent to the design prototype unit discharge of 40 m^2/s, was 6.8 m. However, the measured prototype design head was 6.7 m.

For the remainder of the chapter, results referring to the design head of the model refer to the measured prototype head of 6.7 m, even though the splitters were dimensioned for 6.8 m.

4.2. Results of the Unaerated Model

The unaerated model served as the control model for pressure and air concentration tests. As mentioned in Chapter 3, the splitters of all models were designed according to the Roberts (1943) procedure, and as such, the unaerated model serves to represent standard Roberts splitters, and what to expect at prototype heads of up to 7.6 m.

4.2.1. Local Pressures

In order to summarise the pressure data according to relevant splitter face, the minimum, probable minimum, average and maximum values were taken for all sensors of each individual face. Refer to Figure 3-13 in Section 3.5.3.3 for splitter face definitions. Table 4-4 contains this summarised data for the prototype design head of 6.7 m and the maximum tested head of 7.6 m. The data for each face is graphically presented in Figure 4-2 to Figure 4-5, also showing the cavitation threshold of -7 m atmospheric as defined in Section 2.7. All pressure readings and results are relative to atmospheric pressure.

Table 4-4: Summarised prototype pressure of each splitter face of the unaerated model

		Prototype pressure (m)			
	H_p	Min.	Prob. Min.	Avg.	Max.
End face	6.7	-14.870	-12.141	-2.694	10.102
	7.6	-16.667	-12.146	-2.728	15.104
Bottom Face	6.7	-18.083	-10.812	-1.361	10.041
	7.6	-22.032	-12.928	-0.519	11.693
Side Face	6.7	-27.916	-21.854	-6.124	10.021
	7.6	-25.358	-20.407	-6.005	16.413
Side Bottom Face	6.7	-6.414	-4.977	-0.898	7.236
	7.6	-5.174	-3.456	0.556	8.144

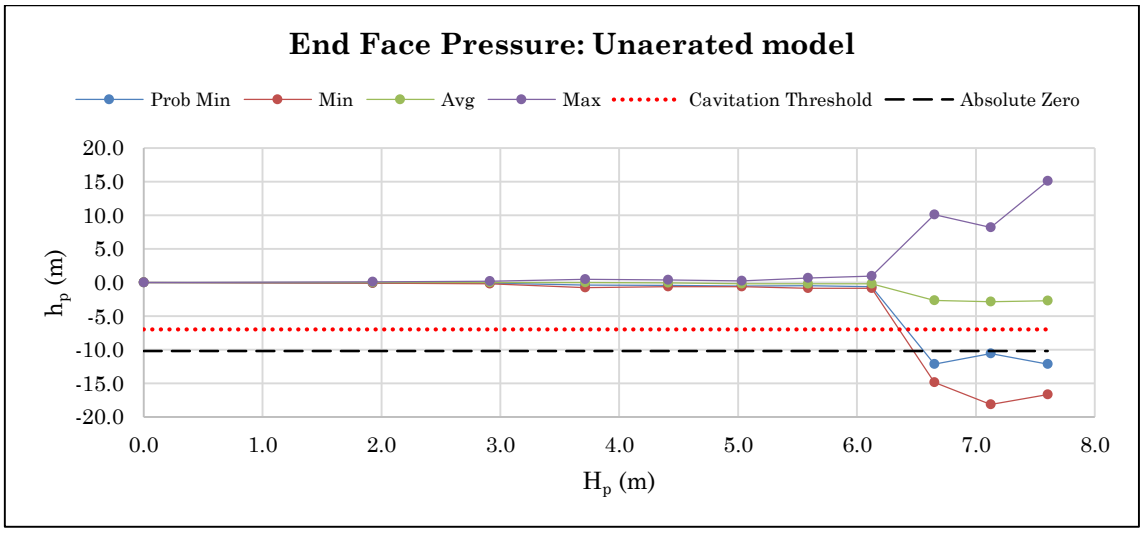

Figure 4-2: Summarised prototype pressure on end face – unaerated model

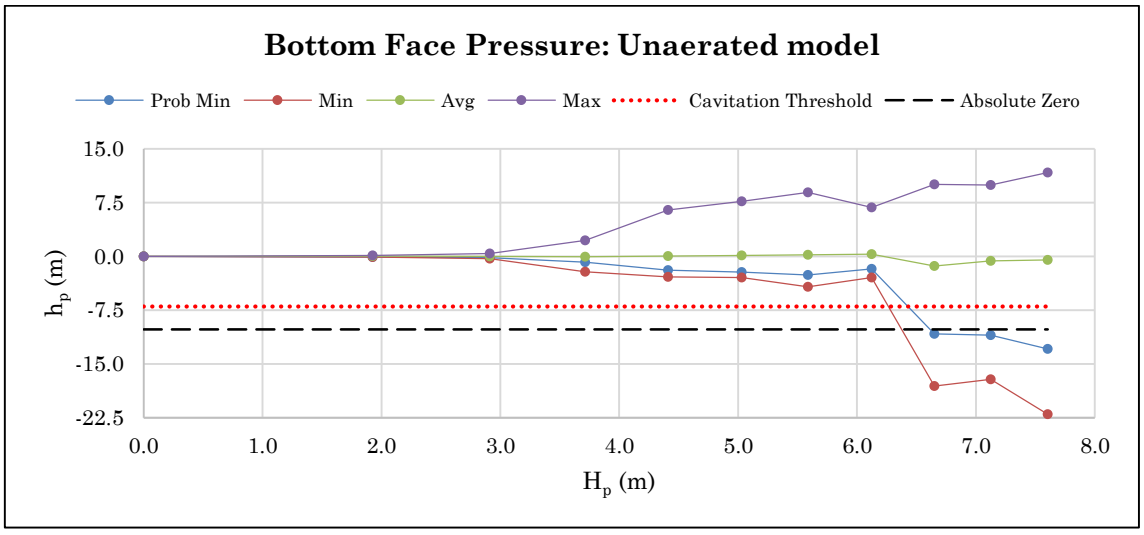

Figure 4-3: Summarised prototype pressure on bottom face – unaerated model

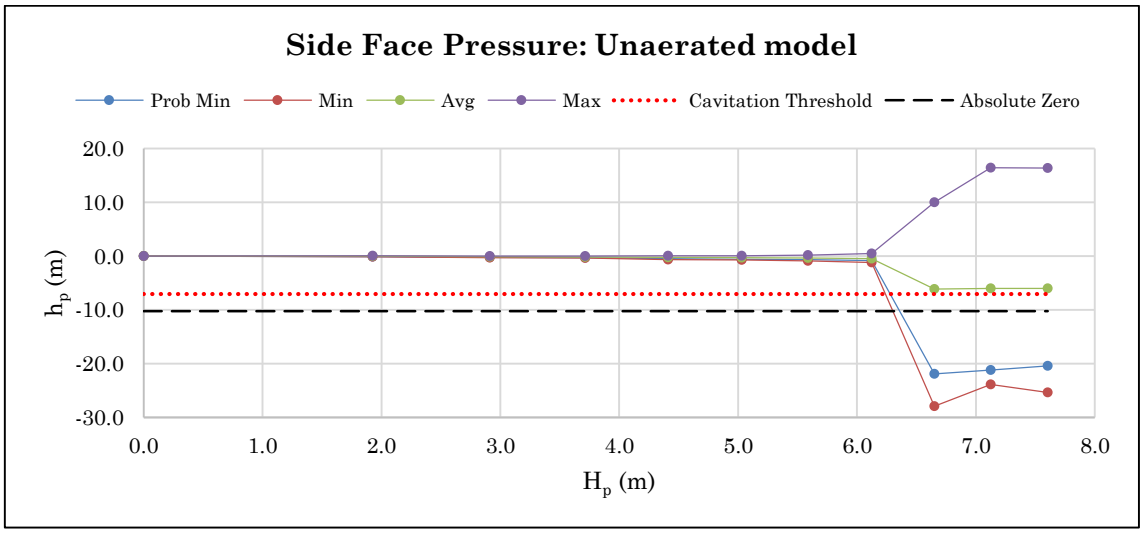

Figure 4-4: Summarised prototype pressure on side face – unaerated model

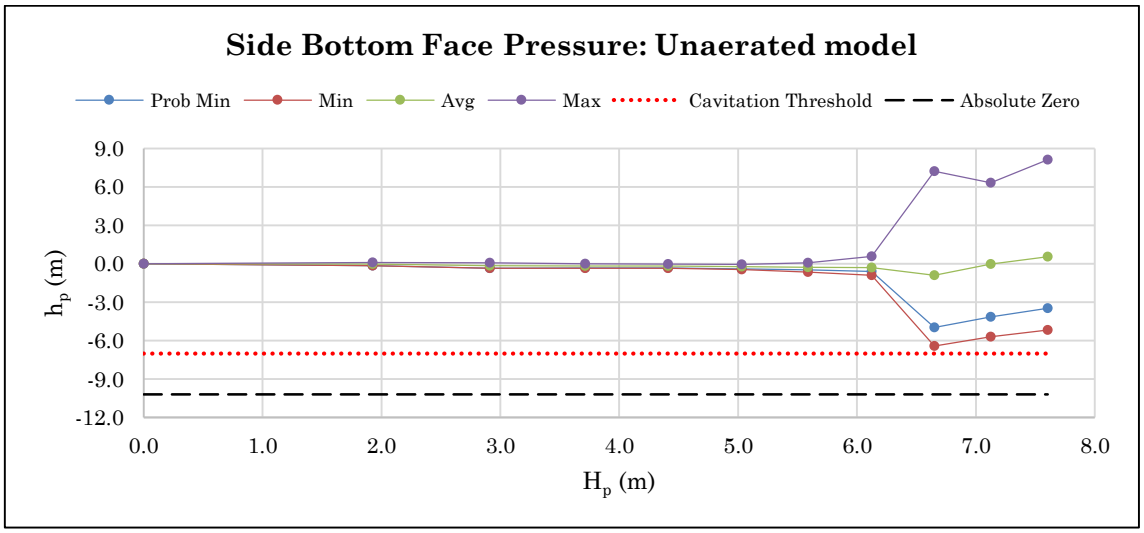

Figure 4-5: Summarised prototype pressure on side bottom face – unaerated model

From Table 4-4 and Figure 4-2 to Figure 4-5, it is clear that the pressures dropped considerably at the design head of 6.7 m and above, and in the cases of the end, side and bottom faces, to well below the 7.0 m cavitation threshold. On the side face of the splitter, the measured pressure dropped to -27.9 m atmospheric. Even though the absolute zero pressure was calculated as -10.2 m, the measured pressure readings from the sensors dropped to well below it. This can be explained by the rapidly fluctuating pressure at the position of the sensors. This moved the water inside the tubes of the sensors resulting in exaggerated measurements. This was only a problem at the most extreme pressure cases. In all cases where the measured pressure was below the absolute zero pressure of -10.2 m, it was assumed that the pressure is in fact very close to absolute zero and cavitation was inevitable in the absence of air within the flow.

Figure 4-6 and Figure 4-7 show two 2D contour plots of the minimum measured prototype pressure on the side face, the end face and the bottom face of the model splitter for the design spillway head of 6.7 m and the maximum tested spillway head of 7.6 m. The side bottom face was excluded from these plots as the four sensors F1 to F4 provided too little data. The white zone to the bottom right of the side face indicates that no sensors were placed in that area, and as such, too little data existed to plot there. The dimensions of the splitter faces in Figure 4-6 and Figure 4-7 are to model scale.

The plots clearly indicate that the locations of the most severe negative pressures are on the side face, near the top and close to the spillway surface. The most severe negative pressure on the end face was measured in the centre, and the most severe negative pressure on the bottom face was measured near the top at the joint with the end face. Table 4-5 summarises the findings of the contour plots of Figure 4-6 and Figure 4-7.

Table 4-5: Splitter face pressure location summary for the unaerated model

Face	Location of most severe negative pressure	Pressure
Side	At the top near the spillway surface	h_p = -27.9 m at H_p = 6.7 m
End	At the centre of the face	h_p = -18.2 m at H_p = 7.1 m
Bottom	At the centre top, near the joint with the end face	h_p = -22.0 m at H_p = 7.6 m

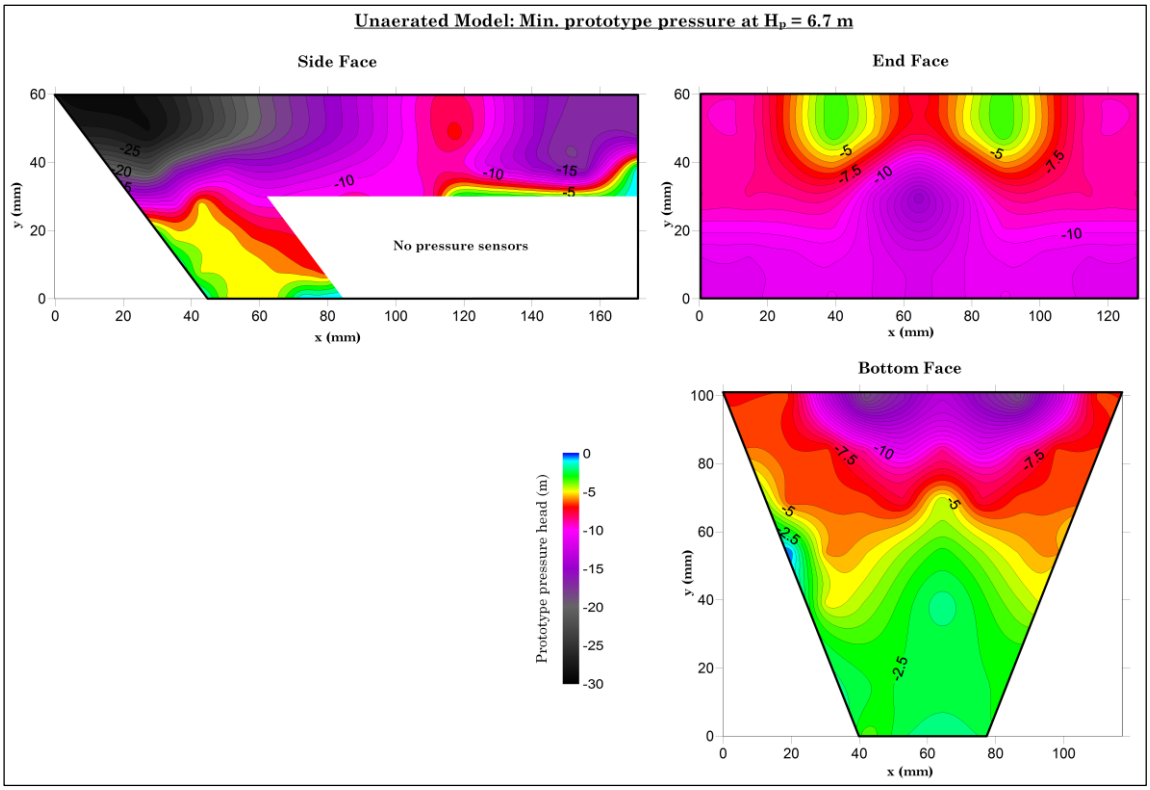

Figure 4-6: Contour plot of minimum prototype pressure on splitter faces of the unaerated model at H_p = 6.7 m

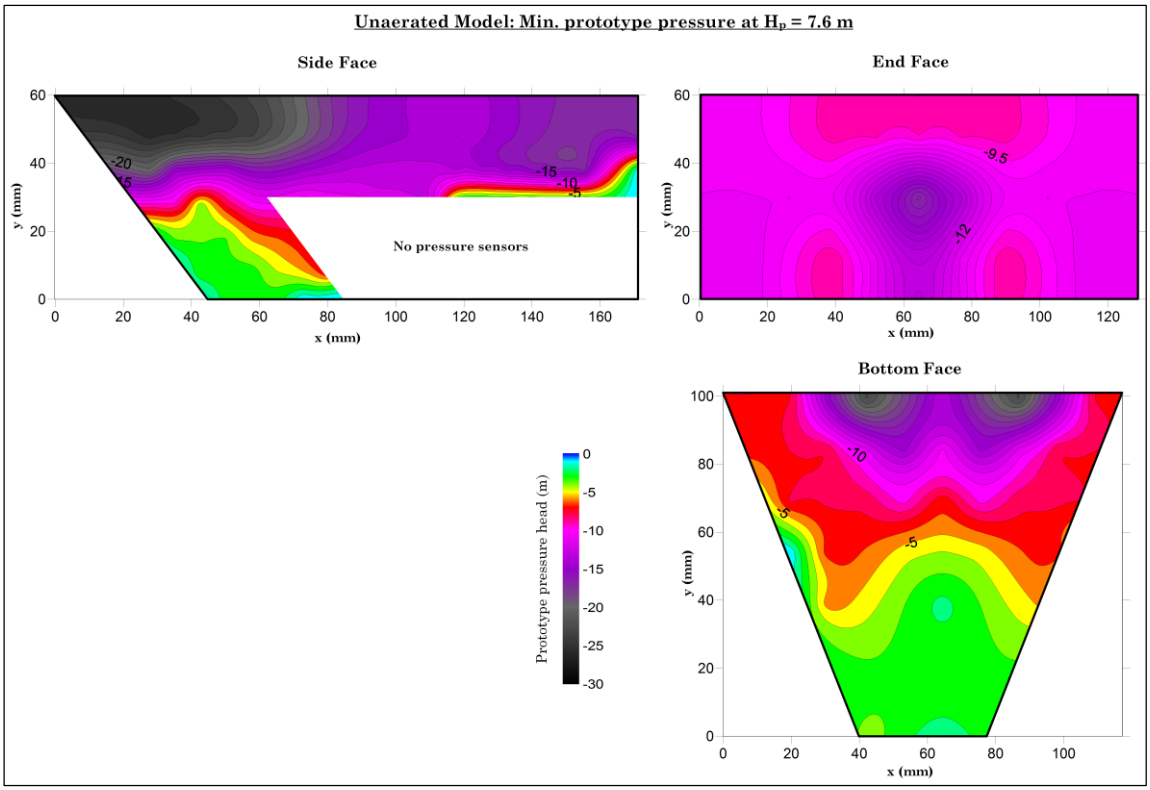

Figure 4-7: Contour plot of minimum prototype pressure on splitter faces of the unaerated model at H_p = 7.6 m

The pressure results of the unaerated model tests indicated where air vents could have been placed on the splitter to alleviate the severe negative pressures. With the placement of air vents, the minimum pressure is not the only parameter that needed to be considered. The average and maximum pressure also played a role. If the average pressure at a given location were to be positive, water would flow into the air vents on a regular basis as the ambient pressure inside the vents is zero metres atmospheric. The maximum pressure also needed to be considered; if the maximum pressure at a location was too high, bursts of water flowed into the air vent, causing the air flow in the duct to fluctuate. Thus the air vents were only placed on the end and side faces as the average pressure on the bottom and side bottom faces was deemed too high.

The 2D contour plots in Figure 4-6 and Figure 4-7, and the location summary in Table 4-5 indicated that the results from the specific sensors at these locations were needed. Figure 4-8 shows the summarised results of sensor E5.

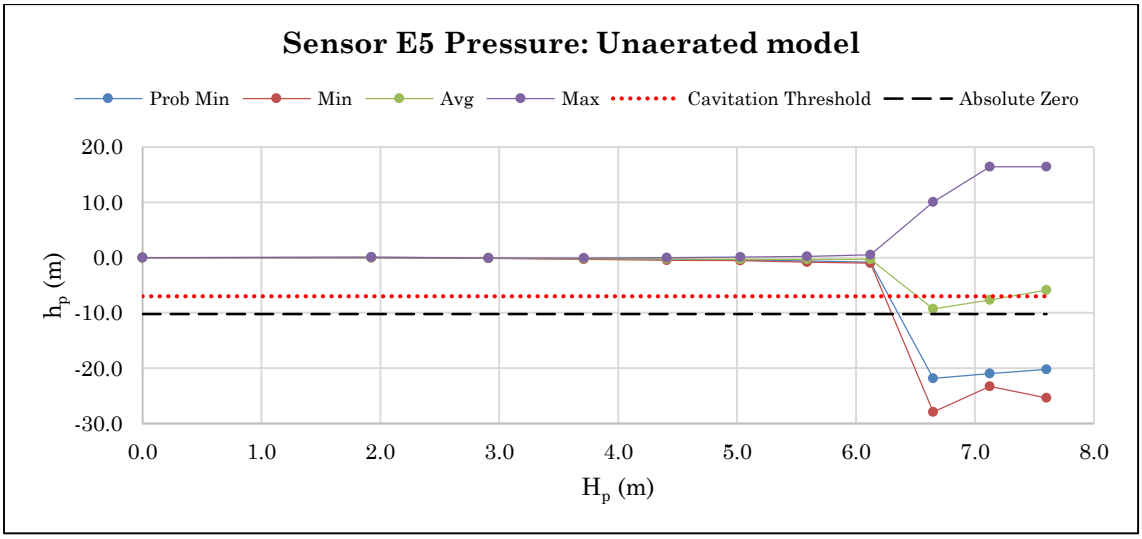

Figure 4-8: Prototype pressure summary of sensor E5

The severe minimum pressure at sensor E5 dictated the conclusion to locate the air vent at that position on the side face, or as close to that position as practically possible. The placement of air vents on the end face were less obvious. Figure 4-9 and Figure 4-10 show the prototype pressure summary of sensors B1 and B2. Sensor B1 was located in the centre of the end face and sensor B2 located 25 mm to the side (refer to Figure 3-15 in Section 3.5.3.3 for exact pressure sensor positions). At the critical point where the splitters became drowned at the design spillway head, the average pressure at both sensors B1 and B2 were quite low at -4.7 m and -3.8 m respectively, indicating that the centre of the face would be ideal for a single large air vent, but the very high maximum

pressures at sensor B1 prompted the decision to rather utilise two air vents placed off centre, closer to sensor B2, as is the case with the Gariep and Vanderkloof Dams (Section 2.2.3.1).

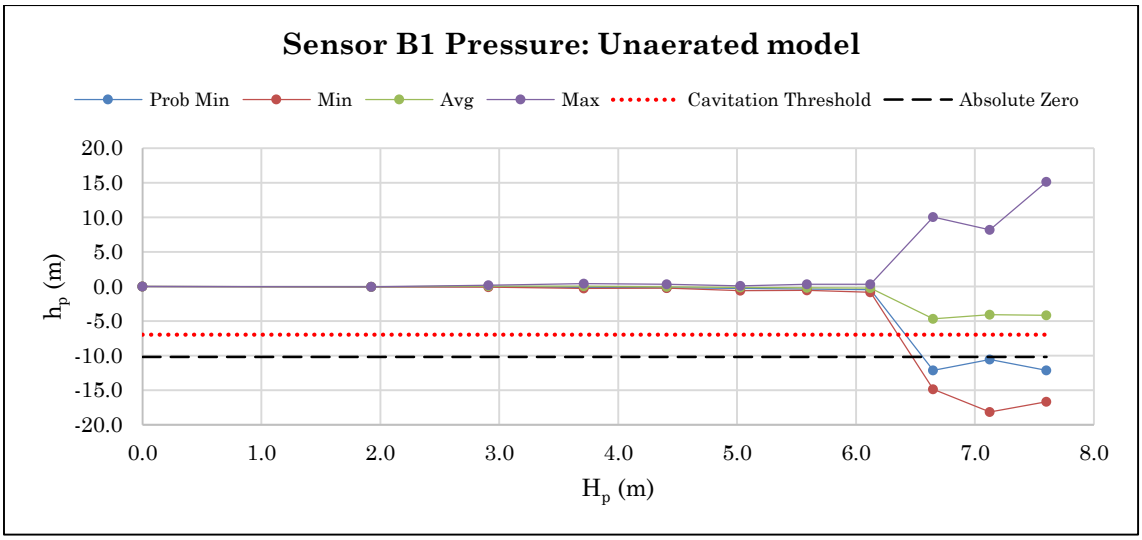

Figure 4-9: Prototype pressure summary of sensor B1

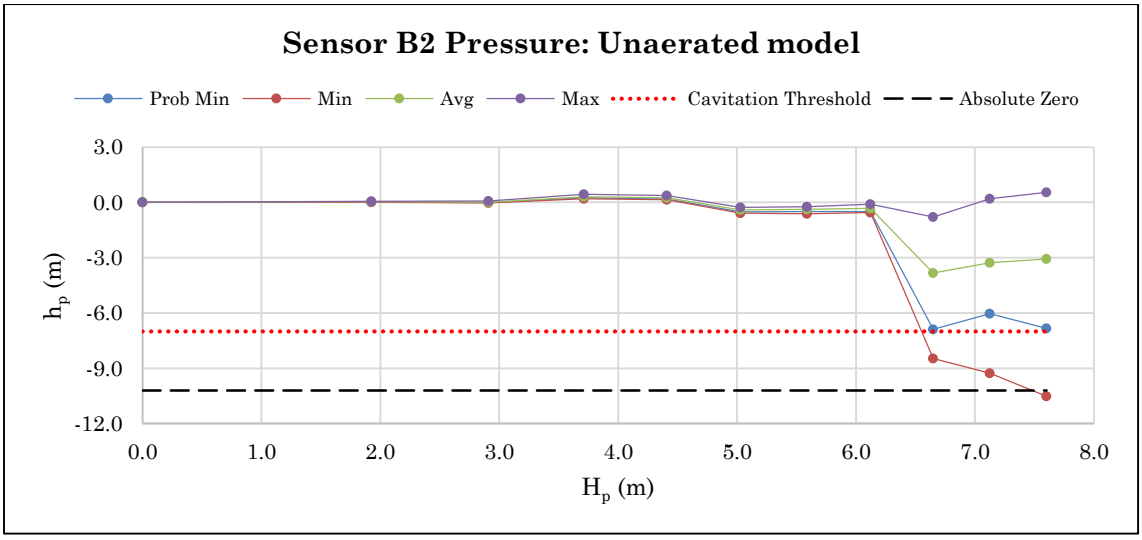

Figure 4-10: Prototype pressure summary of sensor B2

The risk of cavitation arising from the pressure results of the unaerated model is discussed in Section 4.5.1 during the analysis of the results.

4.2.2. Air Concentration

The average air concentrations of the unaerated model are contained in Table 4-6 and graphically presented in Figure 4-11. For the positions of the air concentration measurements, see Figure 3-24 in Section 3.5.4.4.

Table 4-6: Air concentration of the unaerated model

H_p (m)	1.9	2.9	3.7	4.4	5.0	5.6	6.1	6.7	7.1	7.6
Bottom (%)	100	100	100	100	100	100	99	0	0	0
End (%)	100	100	100	99	100	99	92	0	0	0
Side (%)	100	100	100	98	97	94	62	0	0	0

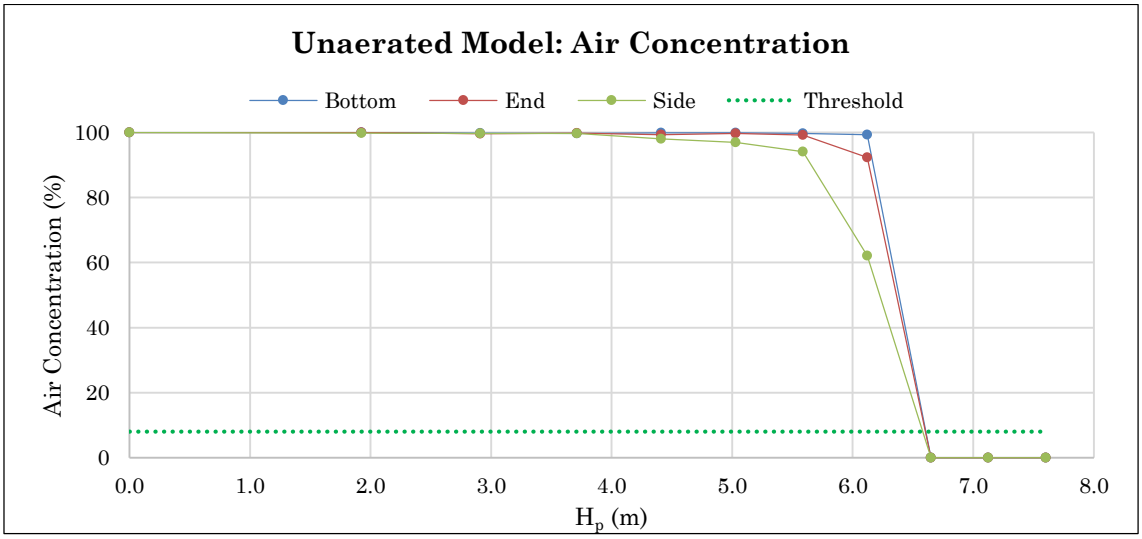

Figure 4-11: Unaerated model air concentration

Results indicate that the air concentrations decreased with increasing prototype spillway head. This was mostly due to the rapid turbulence caused by the splitters at high head. At lower heads (H_p < 4.4 m) the water simply projected over the air probe's needle, meaning that the average air concentration remained close to 100% with the odd droplet of water hitting the needle. At medium heads however (4.4 m < H_p < 7.6 m), the speed of the sheet of water approaching the splitters increased, forcing the top and side streams down rather than out and into the needle. This, along with severe turbulence from the step below increased the water content hitting the needle, hence decreasing the air concentration. At high heads (H_p > 7.6 m) the splitters became drowned, with no air at any part close to the splitters. This, along with the severe negative pressures measured at these heads, indicates a very high cavitation risk. The drowning of the splitters is discussed later in Section 4.5.1.1.

4.3. Results of the 1st Aerated Model

The 1st aerated model had two air vents on the end face and one on each side face, with air provided at atmospheric pressure by an internal aeration duct. The exact locations of the air vents are given and described in Figure 3-6 in Section 3.3.3. The main vents had a model diameter of Ø20 mm and the side vents had a model diameter of Ø10 mm. This represent prototype dimensions of Ø400 mm and Ø200 mm respectively.

In order to compare the results of the 1st aerated model test, the pressure and air concentration was measured in exactly the same manner as before. Additionally, the aeration duct's performance was determined by measuring the air velocity in the aeration shaft and the water discharge from the drainage pipe. These measurements were used to determine air discharge per splitter and water inflow per splitter.

4.3.1. Local Pressures

The same summary of splitter face pressures was done as with the unaerated model. The minimum, probable minimum, average and maximum values for each splitter face at the design head and maximum head are provided in Table 4-7. The results are graphically presented in Figure 4-12 to Figure 4-15.

Table 4-7: Summarised prototype pressure of each splitter face of the 1st aerated model

		Prototype pressure (m)			
	H_p	Min.	Prob. Min.	Avg.	Max.
End face	**6.7**	-2.185	-1.664	-0.413	2.417
	7.6	-8.166	-5.375	-0.746	9.855
Bottom Face	**6.7**	-3.715	-1.652	0.727	10.035
	7.6	-8.938	-5.586	-0.077	10.646
Side Face	**6.7**	-1.726	-1.018	-0.319	0.422
	7.6	-6.667	-3.851	-1.561	0.921
Side Bottom Face	**6.7**	-1.191	-0.734	-0.275	0.518
	7.6	-6.691	-3.878	-1.619	1.522

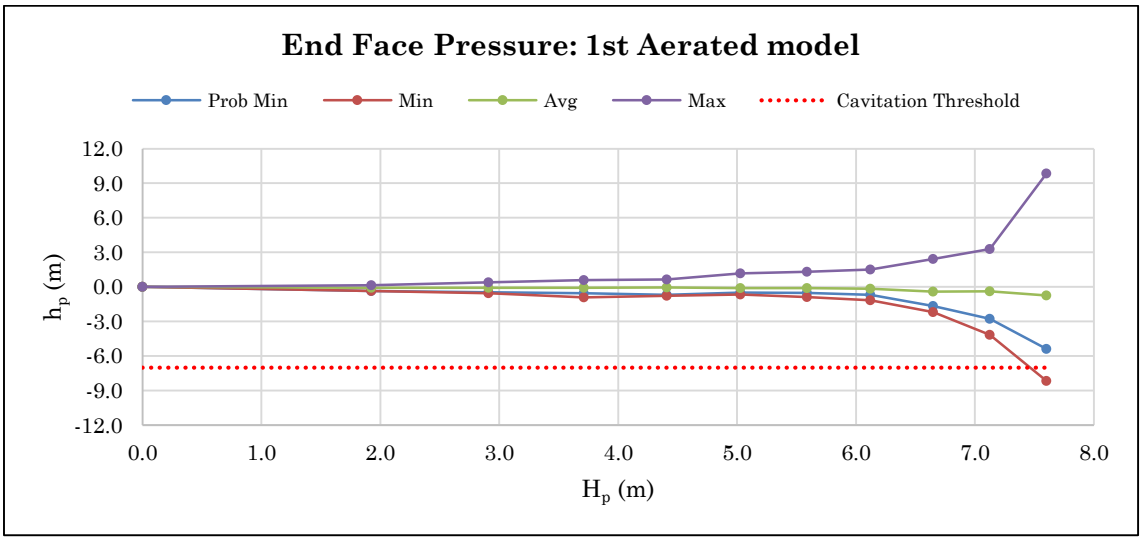

Figure 4-12: Summarised prototype pressure on end face – 1st Aerated model

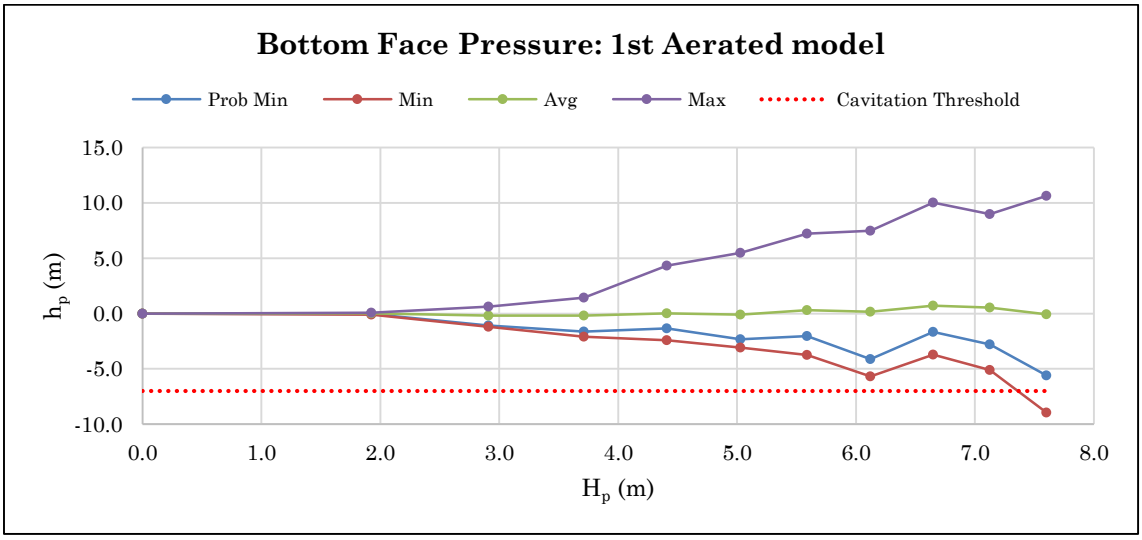

Figure 4-13: Summarised prototype pressure on bottom face – 1st Aerated model

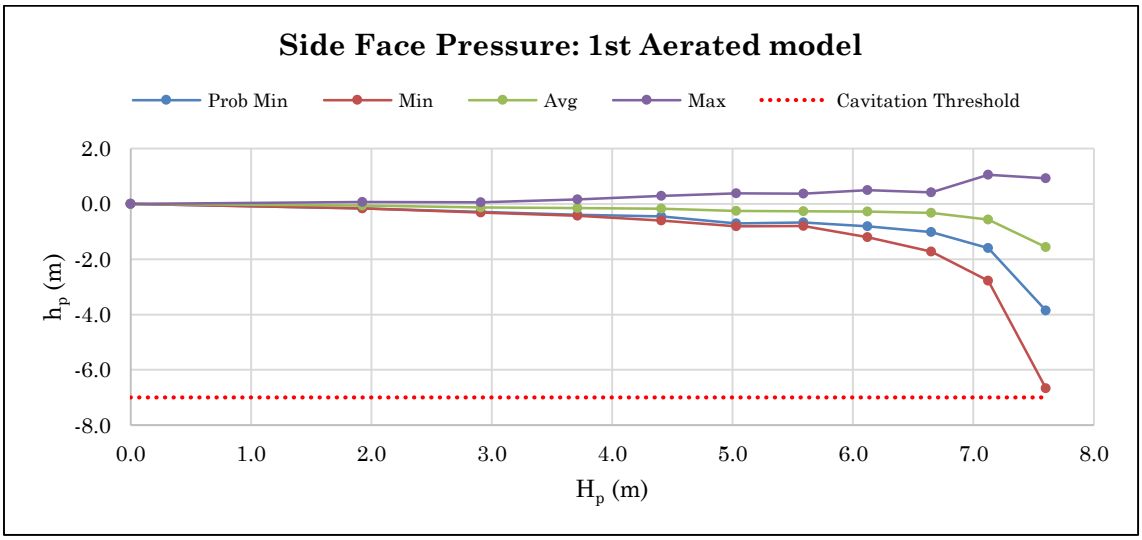

Figure 4-14: Summarised prototype pressure on side face – 1st Aerated model

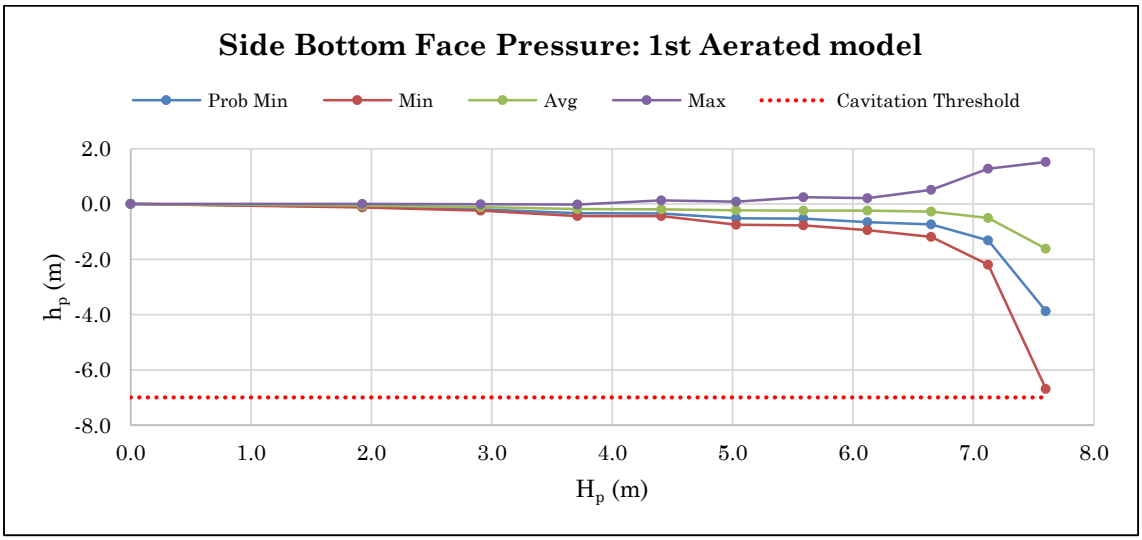

Figure 4-15: Summarised prototype pressure on side bottom face – 1st Aerated model

From the data in Table 4-7 and Figure 4-12 to Figure 4-15, it can be seen that the minimum and probable minimum pressure decreased on all faces of the splitter with increasing spillway head. The variance of all pressure data increased with increasing spillway head. It is important to note that the pressure does not drop below -7 m atmospheric on both the side and side bottom faces of the splitter.

For the positions of any severe pressure states, 2D contour plots were produced for the minimum prototype pressure at spillway heads of 6.7 m and 7.6 m. These plots are shown in Figure 4-16 and Figure 4-17 respectively. Table 4-8 provides a summary of where the most severe negative pressures were measured and the value thereof. Once again the results of the side bottom face was not plotted, as it contained too little data from the four pressure sensors. The white area to the bottom right of the side face contour plot did not contain any pressure sensors, and as such, no contours were plotted.

Table 4-8: Splitter face pressure location summary for the 1st aerated model

Face	Location of most severe negative pressure	Pressure
Side	At the top, midway between the spillway surface and the end of the splitter	h_p = -6.7 m at H_p = 7.6 m
End	At the top of the face, just off-centre on both sides	h_p = -8.2 m at H_p = 7.6 m
Bottom	At the centre bottom, close to the spillway surface	h_p = -8.9 m at H_p = 7.6 m

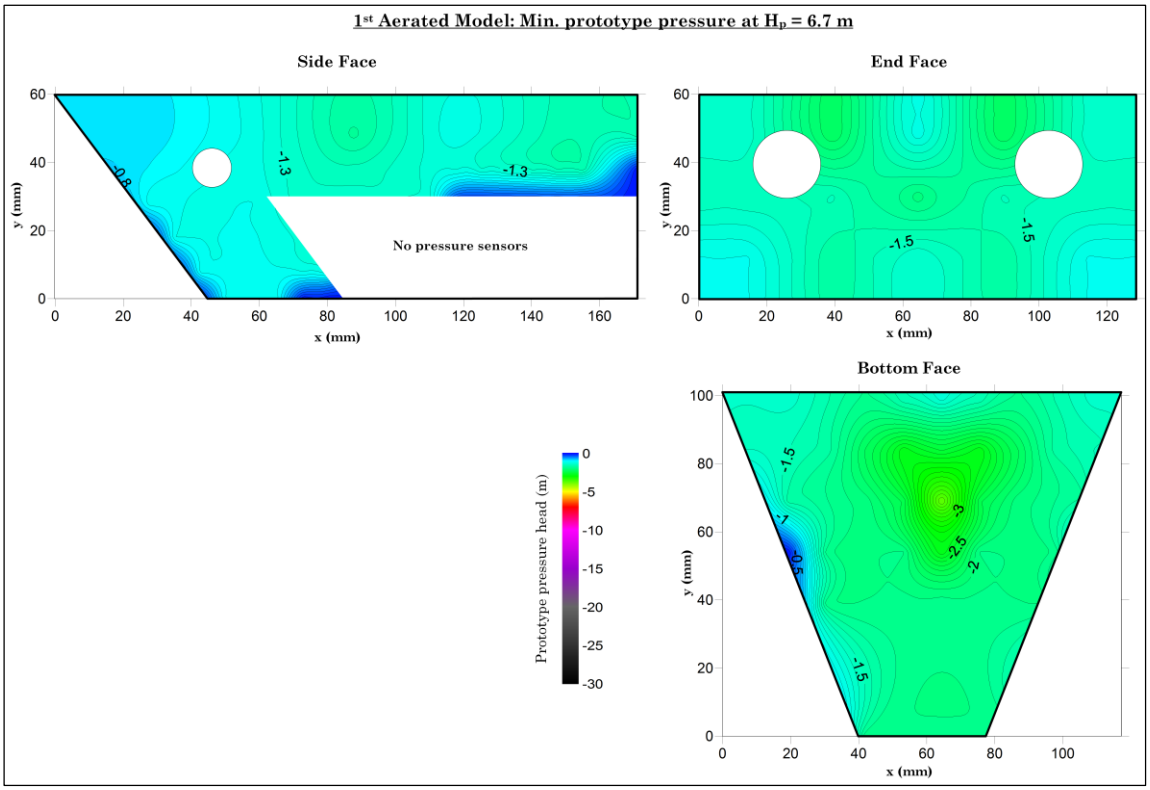

Figure 4-16: Contour plot of minimum prototype pressure on splitter faces of the 1st aerated model at H_p = 6.7 m

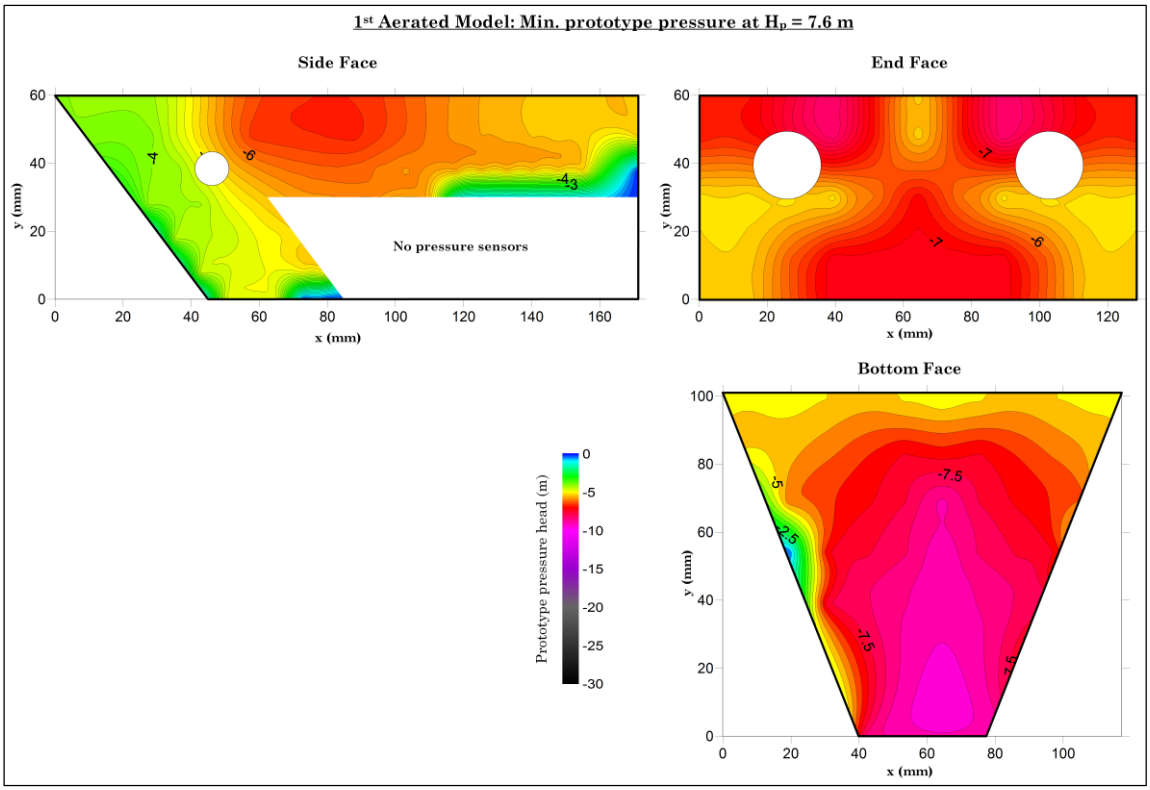

Figure 4-17: Contour plot of minimum prototype pressure on splitter faces of the 1st aerated model at H_p = 7.6 m

From Figure 4-16 it is clear that for the design head of 6.7 m, the aerated pressure situation was much more favourable than that of the unaerated model. The lowest prototype pressure was measured at the centre of the bottom face at -3.7 m. This is well within the cavitation threshold of -7 m.

At the maximum measured prototype head of 7.6 m, cases of severe negative pressure were measured. On the end and bottom faces respectively, prototype pressures of -8.2 m and -8.9 m were measured. The locations of these measurements are evident by the red and pink zones on the end and bottom faces in Figure 4-17. The side face showed the most improvement. The lowest measured prototype pressure was -6.7 m, within the cavitation threshold of -7 m.

It was concluded that the pressure increased sufficiently with the inclusion of the 1st aerated model's Ø20 mm air vents. Up to the design spillway head of 6.7 m (q_p = 40 m²/s) and above to 7.1 m (q_p = 45 m²/s), no cavitation should occur as all measured pressures were within the pressure limit of -7 m as set by Chadwick *et al.* (2013). At the maximum prototype spillway head of 7.6 m (q_p = 50 m²/s), however, severe cases of negative pressure were measured that could lead to cavitation if the air concentration is too low.

4.3.2. Air Concentration

In order to determine the cavitation risk of the 1st aerated model at the maximum prototype spillway head, the air concentration was measured at the same places as with the unaerated model. The average air concentrations are contained in Table 4-9 and graphically presented in Figure 4-18.

Table 4-9: Air concentration of the 1st aerated model

H_p (m)	1.9	2.9	3.7	4.4	5.0	5.6	6.1	6.7	7.1	7.6
Bottom (%)	99	100	100	100	100	100	100	99	94	83
End (%)	100	100	100	99	98	95	89	79	59	46
Side (%)	99	99	98	98	97	87	56	21	9	6

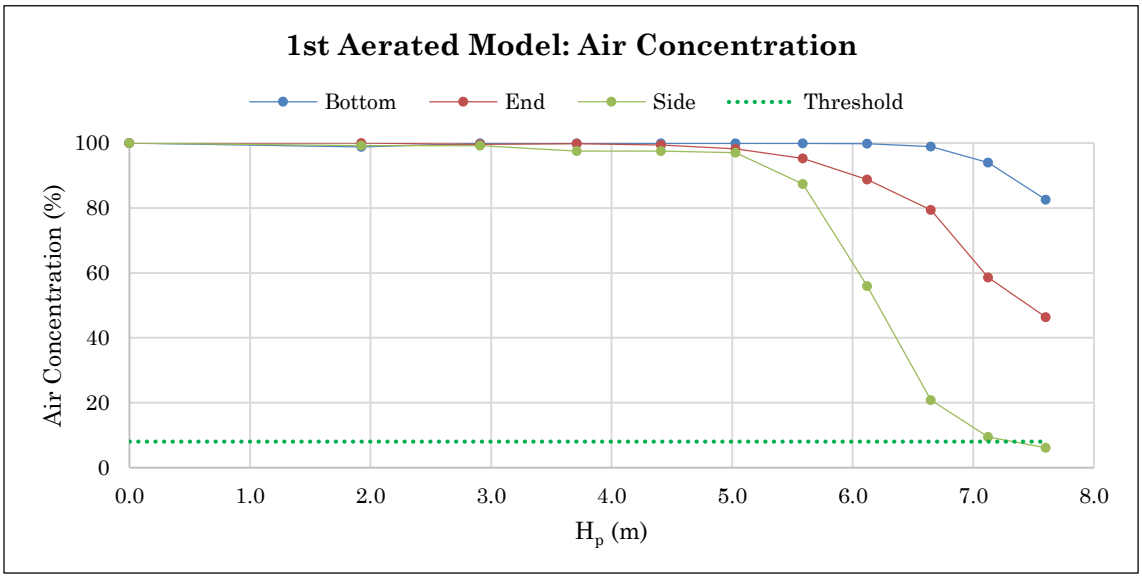

Figure 4-18: 1st Aerated model air concentration

As with the unaerated model, the air concentrations of the 1st aerated model generally decreased with increasing spillway head. At the higher heads, the increased water depth approaching the splitters caused the side streams to hit the probe's needle when measuring the side position. This caused the measured air concentration at the side to drop to 9% at 7.1 m spillway head and to 6% at the maximum spillway head of 7.6 m. The air concentration of the end and bottom measurements were very high for all spillway heads.

4.3.3. Aeration Duct Performance

In order to evaluate the performance of the aeration duct, the air velocity in the shaft, the air discharge from the air vents and the water inflow into the air vents was analysed simultaneously. It was found that the water inflow caused a drop in air discharge, and in turn a decrease in air velocity in the shaft. By designing the air vents to control the air discharge rather than the aeration duct, the air discharge could be linked to the spillway head. As mentioned, the air velocity in the aeration shaft was measured in ft/min and converted to m/s in prototype scale. This was then used to determine the air discharge per splitter over a range of spillway heads. The water inflow into the air vents was determined by measuring the drainage from the aeration duct.

4.3.3.1. Air Velocity

Table 4-10 contains the prototype air velocities for the 1st aerated model for a range of spillway heads. This is graphically shown in Figure 4-19.

Table 4-10: Air velocity in aeration shaft of the 1st aerated model – prototype scale

H_p (m)	1.9	2.9	3.7	4.4	5.0	5.6	6.1	6.7	7.1	7.6
$(v_{air})_{avg}$ (m/s)	2.42	4.18	3.84	4.13	**4.97**	4.77	4.52	4.04	3.74	3.51
$(v_{air})_{max}$ (m/s)	3.19	5.71	5.19	5.09	**6.58**	5.68	5.49	4.90	5.18	4.55

Note: Values in **bold** indicate maximum air velocity

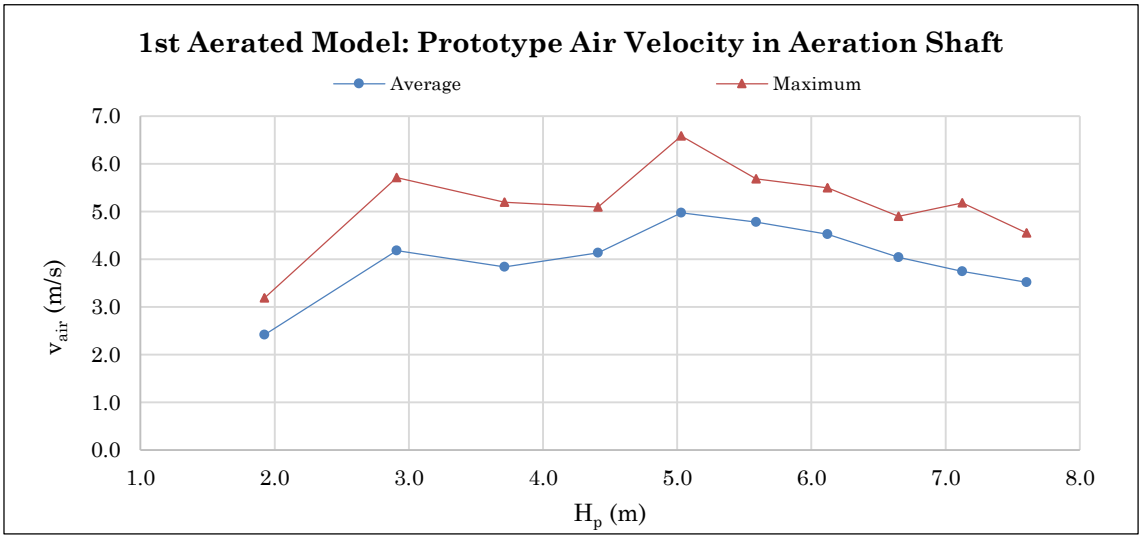

Figure 4-19: Prototype air velocity in the aeration shaft of the 1st aerated model

As expected, the air velocity increased with increasing spillway head because of decreasing splitter pressure. But, interestingly, the velocity profile flattened out at heads over 3.0 m, and decreased with spillway heads over 5.0 m. This unexpected phenomenon can be explained by the water drainage from the duct and an increase in maximum pressure at the air vent positions.

The maximum air velocity of 6.58 m/s occurred at a prototype spillway head of 5.0 m. This is equivalent to 23.7 km/h and equates to a Beaufort number of 4. In practical terms, wind with a BN of 4 is described as a moderate breeze (see Table 2-2 on page 19).

4.3.3.2. Air Discharge per Splitter

Using the model shaft's inside diameter of 110 mm, the intake air discharge into the aeration duct, Q_{intake}, was calculated using Eq. (4-1):

$$Q_{intake} = A_{shaft} \times v_{air} \quad (4\text{-}1)$$

where the prototype cross-sectional area of the aeration shaft, A_{shaft}, was calculated as 3.80 m².

This was converted to air discharge per splitter, Q_{air}, by equally dividing the intake air discharge between the number of splitters as described in 3.5.6, to produce the values in Table 4-11.

Table 4-11: Prototype air discharge per splitter for the 1st aerated model

H_p (m)	1.9	2.9	3.7	4.4	5.0	5.6	6.1	6.7	7.1	7.6
Q_{air} (m³/s)	2.30	3.97	3.65	3.93	4.73	4.54	4.30	3.83	3.56	3.34

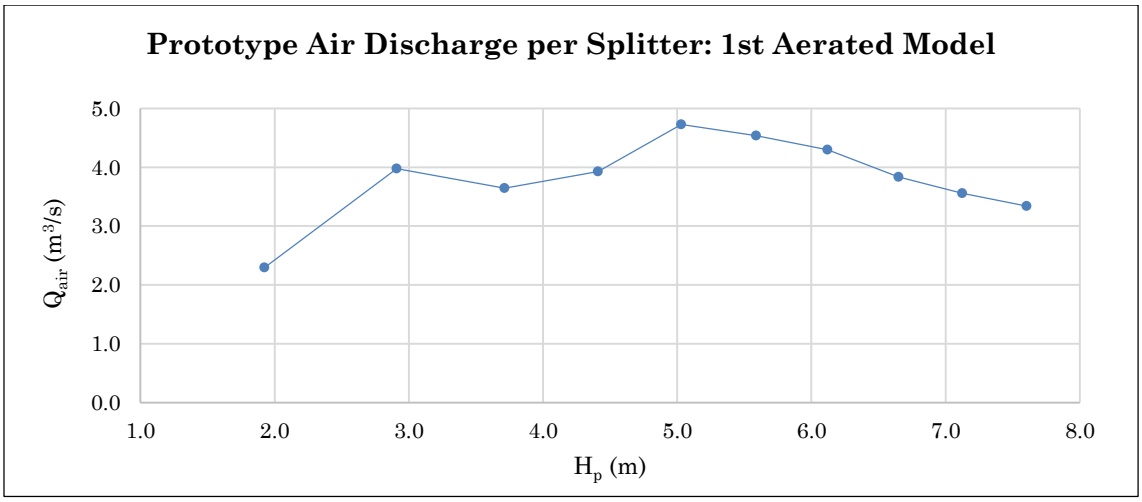

Figure 4-20: Prototype air discharge per splitter of the 1st aerated model

As expected, the shape of the air discharge plot in Figure 4-20 is the same as that of the air velocity in Figure 4-19 since the conversion to air discharge was linear. As mentioned, the reason for the decrease in air velocity and therefore air discharge was due to water inflow into the air vents and an increase in maximum pressure at the position of the vents.

4.3.3.3. Drainage from Aeration Duct

As mentioned, at prototype spillway heads equal to and greater than 6.7 m, the study found that water flowed into the air vents and needed to be drained. This was not catastrophic but it did, however, cause a drop in air velocity within the aeration shaft. The air velocity was not measured while draining the water from the duct. If the drainage cap was removed, the majority of air would flow into the big hole thus created and effectively nullify any air velocity measurements in the shaft.

Table 4-12: Prototype drainage discharge from aeration duct – 1st aerated model

H_p (m)	6.7	7.1	7.6
Q_{drain} (m³/s)	0.030	0.112	0.286

As defined in Section 3.5.7, the water inflow per splitter was calculated by dividing the drainage discharge by the number of splitters in the system. The water inflow values for the 1st aerated model are included in Table 4-13:

Table 4-13: Prototype water inflow per splitter – 1st aerated model

H_p (m)	6.7	7.1	7.6
Q_{inflow} (m³/s)	0.008	0.028	0.071

The water inflow is considerably less than the air discharge namely by a factor of about 50, indicating that the air discharge did not decrease with increasing heads solely because of the inflow of water. The large variance of pressure at high heads meant that air was being sucked out and pushed back into the air vents in rapid succession. The turbulence created by the splitters caused water to sometimes join the air being pushed back into the air vents, and thus accumulating in the duct.

4.4. Results of the 2nd Aerated Model

The aim of the 2nd aerated model was to determine the effect of larger air vents on the cavitation risk of Roberts splitters and was therefore similar to the 1st aerated model in every way except that the air vents were larger. The Ø20 mm main air vents of the 1st aerated model were enlarged to Ø23 mm and the Ø10 mm side vents enlarged to Ø11.5 mm. This equates to prototype dimensions of Ø460 mm and Ø230 mm respectively. The aeration duct was kept unchanged as it was originally designed for the larger air vents (see Section 3.3.3). The size of the air vents was limited by the placement of the pressure sensors on the end face of the splitter.

The same testing procedure was followed as the 1st aerated model, testing pressure, air concentration and aeration duct performance at the same positions for the same spillway heads.

4.4.1. Local Pressures

In order to determine the effect of larger air vents on pressure around the splitter, the results for the design head of 6.7 m and the maximum head of 7.6 m were summarised together. The minimum, probable minimum, average and maximum values were taken for all sensors of each individual face, included in Table 4-14 and graphically presented in Figure 4-21 to Figure 4-24.

Table 4-14: Summarised prototype pressure of each splitter face of the 2nd aerated model

	H_p	Prototype pressure (m)			
		Min.	Prob. Min.	Avg.	Max.
End face	**6.7**	-1.089	-0.652	-0.022	2.708
	7.6	-5.111	-1.881	-0.149	5.437
Bottom Face	**6.7**	-2.318	-1.318	0.869	8.105
	7.6	-8.235	-4.683	0.845	12.599
Side Face	**6.7**	-1.776	-0.794	-0.338	0.427
	7.6	-3.422	-2.081	-0.844	0.728
Side Bottom Face	**6.7**	-1.296	-1.046	-0.394	0.451
	7.6	-3.094	-1.980	-0.875	0.836

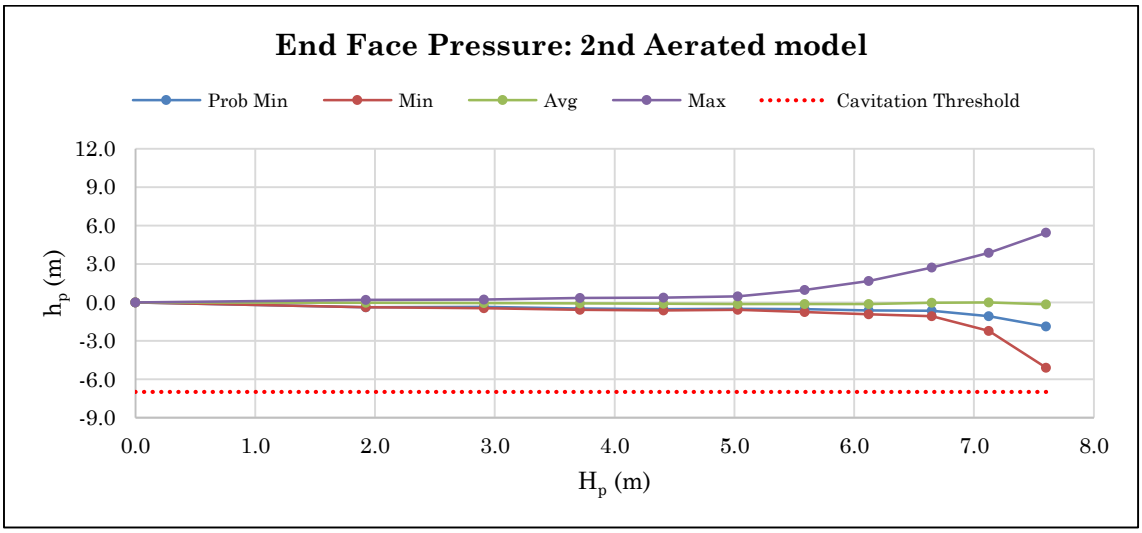

Figure 4-21: Summarised prototype pressure on end face – 2nd Aerated model

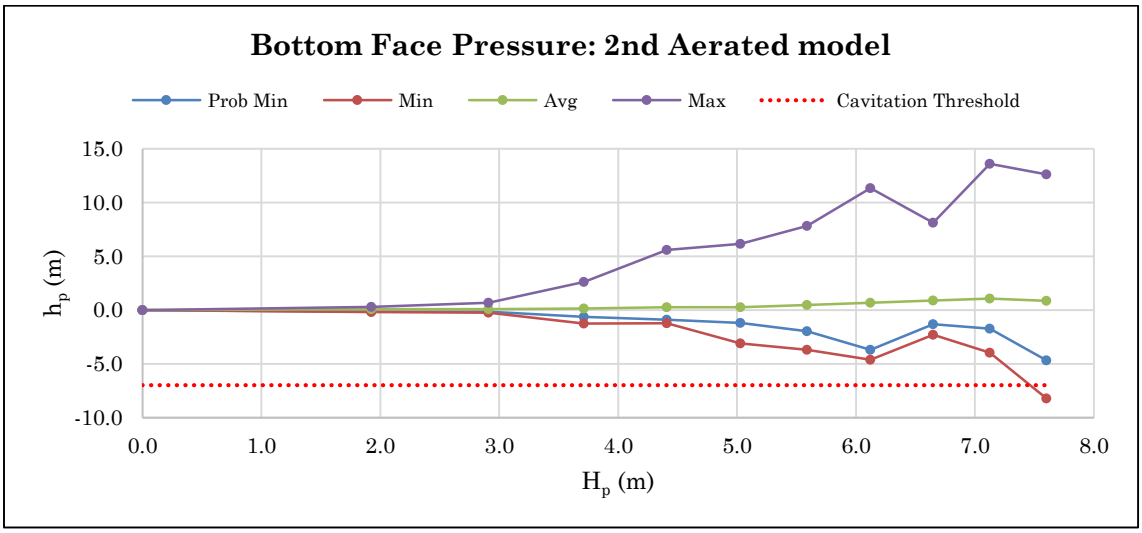

Figure 4-22: Summarised prototype pressure on bottom face – 2nd Aerated model

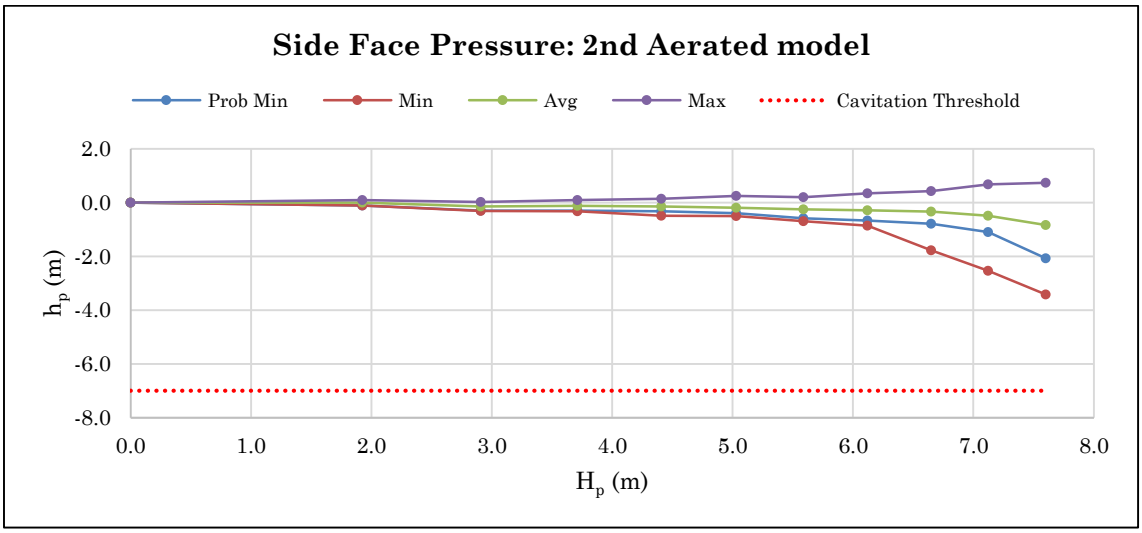

Figure 4-23: Summarised prototype pressure on side face – 2nd Aerated model

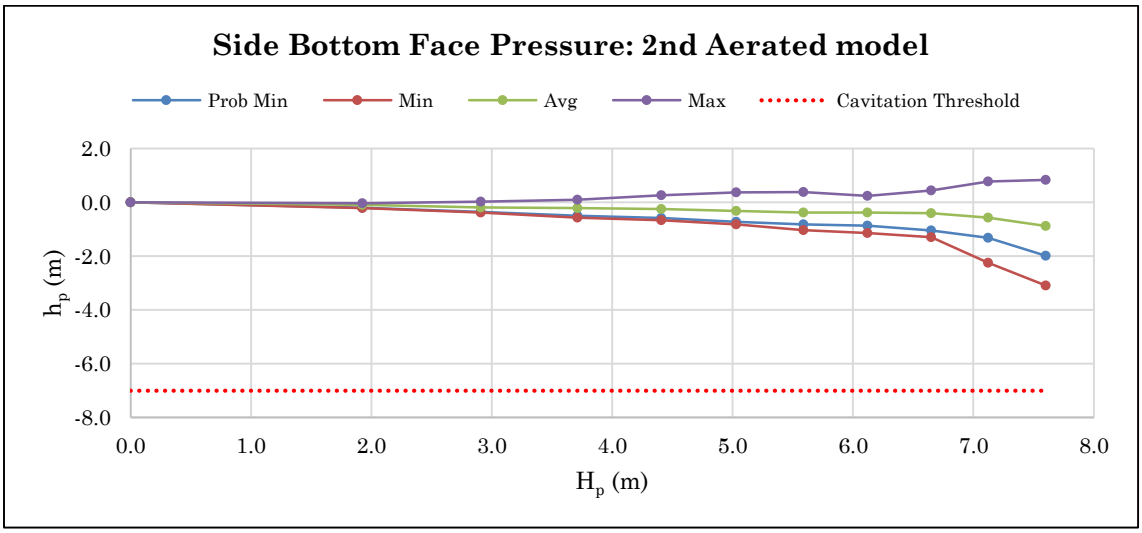

Figure 4-24: Summarised prototype pressure on side bottom face – 2nd Aerated model

The shapes of the plots in Figure 4-21 to Figure 4-24 indicate that the variance of the pressure gradually increased for increasing spillway head, with the exception being the bottom face. Again, with the exception of the bottom face at the maximum spillway head, the minimum of pressures on the splitter faces remain well above the cavitation threshold of -7 m atmospheric. The exact location of the severe negative pressure of the bottom face can clearly be distinguished on the 2D contour plot in Figure 4-26 by the bright red zone in the middle of the bottom face.

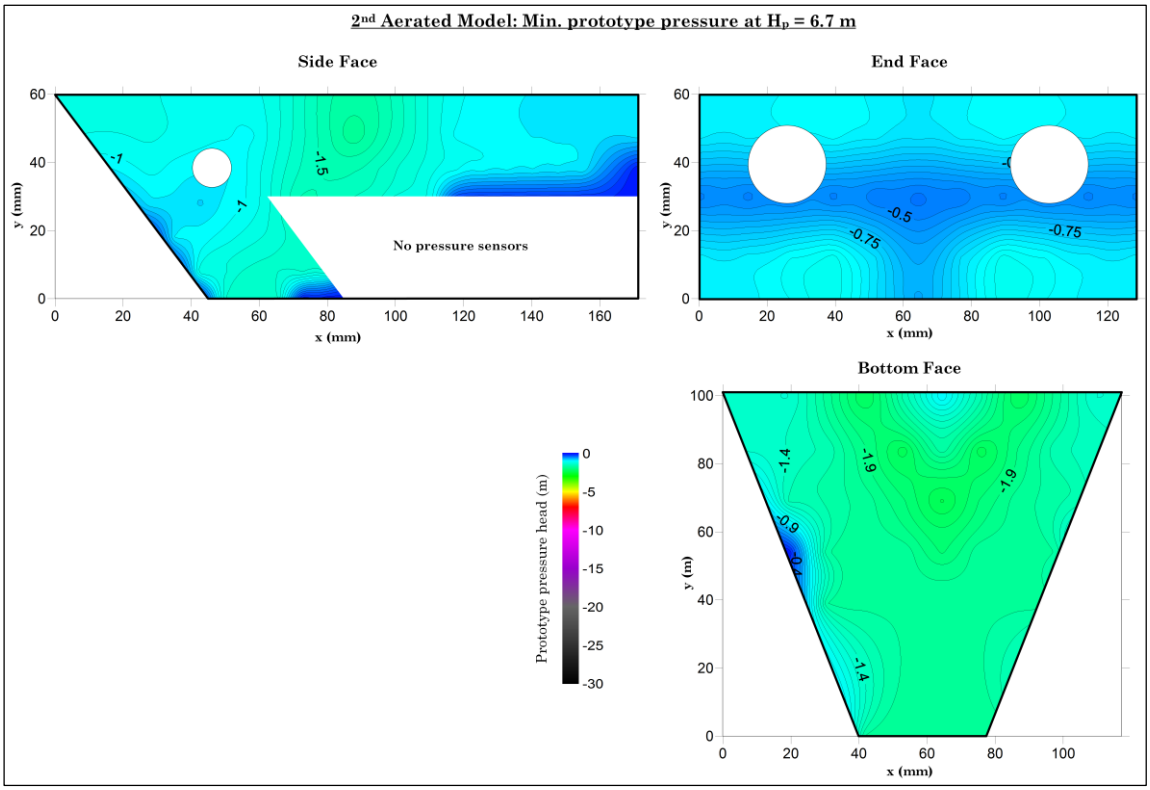

Figure 4-25: Contour plot of minimum prototype pressure on splitter faces of the 2nd aerated model at H_p = 6.7 m

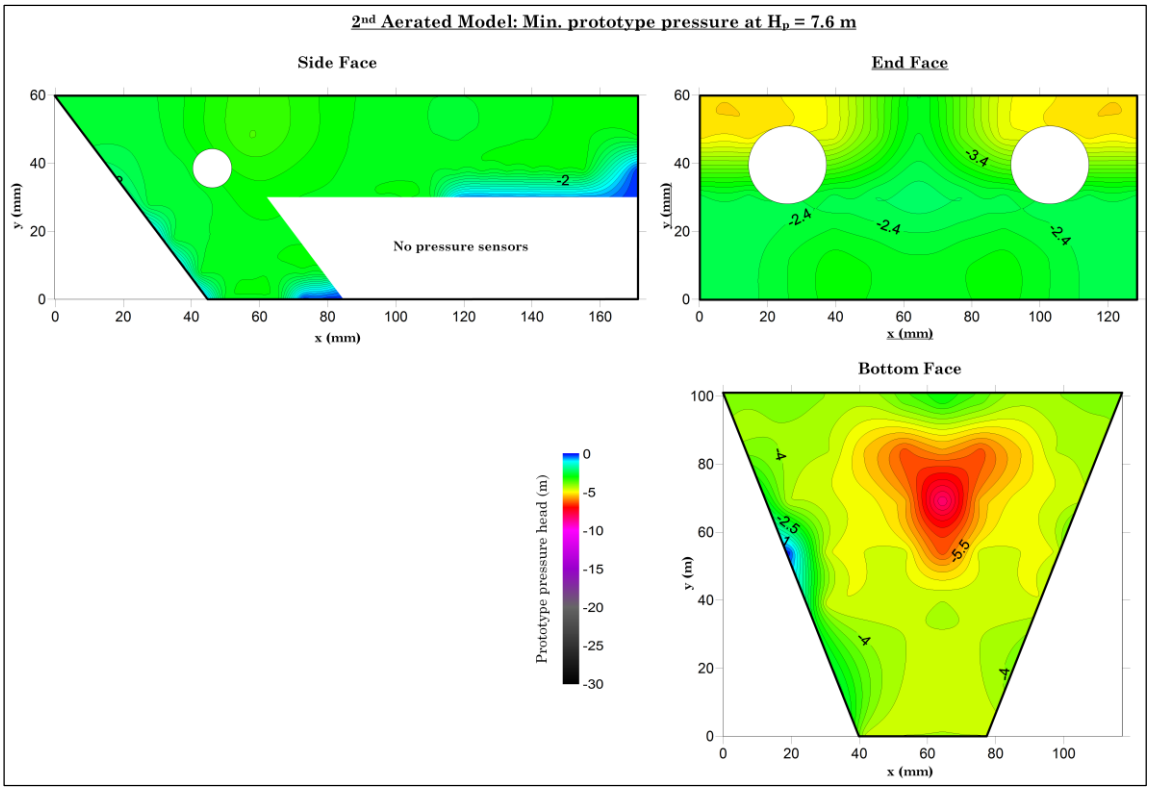

Figure 4-26: Contour plot of minimum prototype pressure on splitter faces of the 2nd aerated model at H_p = 7.6 m

From Figure 4-25 it is clear that no severe negative pressure existed on the splitter at the design head of 6.7 m. The absolute value and spread of the negative pressures are, however, similar to those of the 1st aerated model (see Figure 4-16). This indicated that there is no apparent reason to design larger air vents for Roberts splitters operated up to, but not exceeding its design head. At the maximum spillway head of 7.6 m, the minimum prototype pressure at sensor D4 in the middle of the bottom face was measured at -8.2 m, 1.2 m below the cavitation threshold (see Figure 4-26). The top corners of the end face also showed signs of exaggerated negative pressure, but within the cavitation threshold. It should however be noted that the spread of the severe negative pressures is greatly reduced from that of the 1st aerated model (see Figure 4-17), an indication that larger air vents is advantageous in mitigating any risk of cavitation to Roberts splitters operated at heads exceeding its design head by no more than 13%. A complete comparison of the pressures of all models is contained within Section 4.5.4.

4.4.2. Air Concentration

The air concentrations of the 2nd aerated model, as measured at the three positions defined in Section 3.5.4.4, are given in Table 4-15 and graphically presented in Figure 4-27.

Table 4-15: Air concentration of the 2nd aerated model

H_p (m)	1.9	2.9	3.7	4.4	5.0	5.6	6.1	6.7	7.1	7.6
Bottom (%)	100	100	100	100	100	100	99	98	90	83
End (%)	100	100	99	99	97	97	97	64	56	41
Side (%)	100	99	98	98	96	68	11	2	1	1

Figure 4-27 shows that the air concentration decreased similarly to that of the 1st aerated model at high spillway heads. The air concentration measured at the side dropped to nearly 0% as the side stream from the splitter flowed straight into the air probe's needle. There was not a significant improvement in air concentration, supporting the hypothesis that the air pocket provides the biggest mitigation to cavitation.

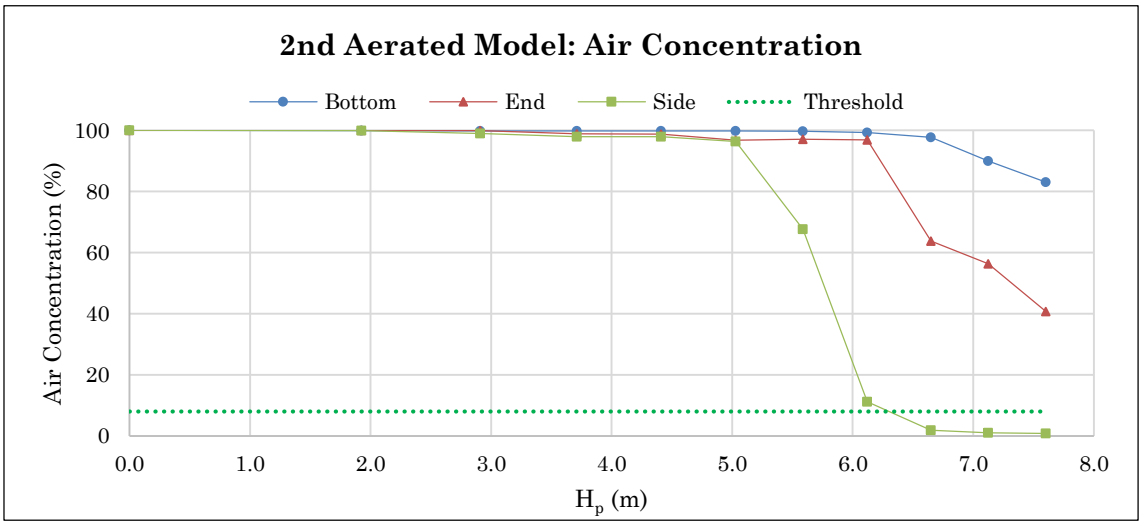

Figure 4-27: 2nd Aerated model air concentration

4.4.3. Aeration Duct Performance

The performance of the aeration duct was measured in exactly the same manner as the 1st aerated model. The air discharge per splitter can be compared with the water inflow per splitter to determine the effectiveness of the air vents.

4.4.3.1. Air Velocity

The air velocity in the aeration shaft is contained within Table 4-16 and presented in Figure 4-28.

Table 4-16: Air velocity in aeration shaft of the 2nd aerated model – prototype scale

H_p (m)	1.9	2.9	3.7	4.4	5.0	5.6	6.1	6.7	7.1	7.6
$(v_{air})_{avg}$ (m/s)	2.75	7.07	7.44	8.23	**9.36**	9.03	9.05	8.00	5.08	5.21
$(v_{air})_{max}$ (m/s)	3.40	8.20	8.58	9.61	**11.09**	10.98	10.15	9.25	6.06	6.48

Note: **Bold** values indicate maximum air velocity

The air velocity increased considerably with the introduction of flow over the spillway up to the maximum at a head of 5.0 m, but then plateaued until dropping at spillway heads greater than the design head. The shape of the plot in Figure 4-28 is similar to that of the 1st aerated model, but more exaggerated. At heads of 5.0 to 5.6 m, the measured air velocities were much higher than that of the 1st aerated model. The drop in air velocity can again be attributed to the inflow of water into the air vents and the high variance in pressure at the end face of the splitter. This is described in more detail in Section 4.5.5. The maximum prototype air velocity of 11.09 m/s (39.9 km/h) at a spillway head of 5.0 m is equivalent to a Beaufort number of 6, describing a strong breeze. This is still lower than the maximum comfortable air velocity as prescribed by Lee (1999).

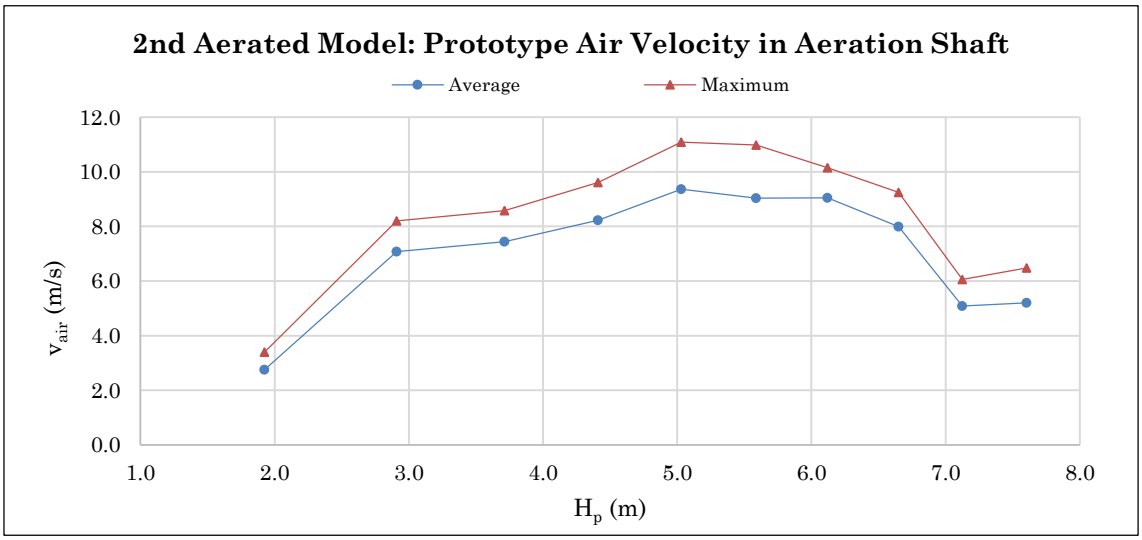

Figure 4-28: Prototype air velocity in aeration shaft of 2nd aerated model

4.4.3.2. Air Discharge per Splitter

The air velocity was converted to air discharge per splitter using the same basis as in Section 4.3.3.2. Table 4-17 and Figure 4-29 contains the prototype air discharge per splitter.

Table 4-17: Prototype air discharge per splitter for the 2nd aerated model

H_p (m)	1.9	2.9	3.7	4.4	5.0	5.6	6.1	6.7	7.1	7.6
Q_{air} (m³/s)	2.62	6.72	7.07	7.82	8.90	8.58	8.60	7.60	4.83	4.95

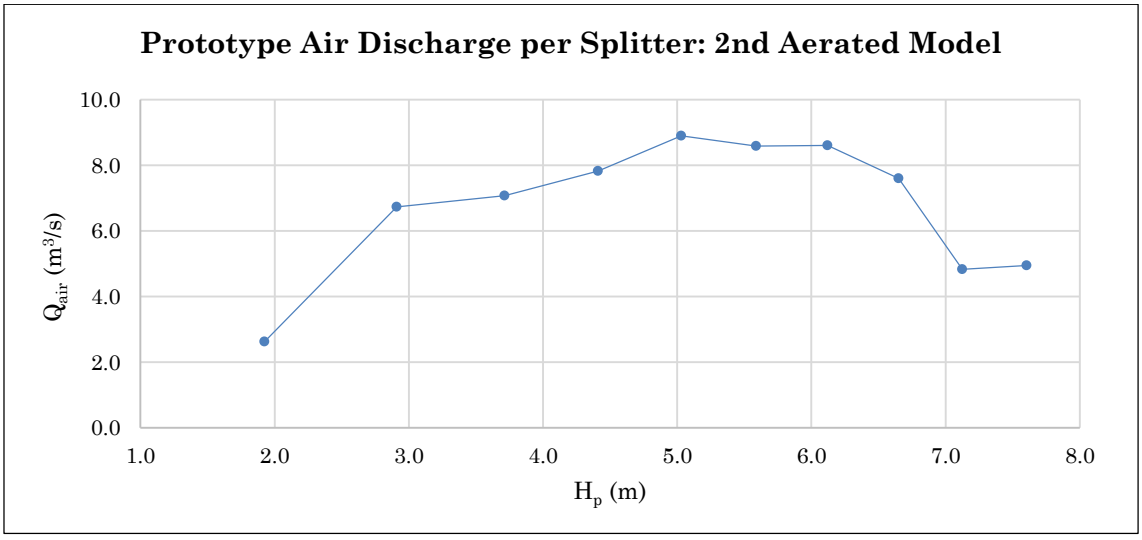

Figure 4-29: Prototype air discharge per splitter of the 2nd aerated model

The air discharge plot showed exactly the same shape as that of the air velocity, increasing with increasing spillway heads up to 5.0 m and then declining as the head increased to the maximum of 7.6 m.

4.4.3.3. Drainage from Aeration Duct

As with the 1st aerated model, it was found that at high spillway heads water entered into the air vents and had to be drained from the aeration duct. The drainage rates of the 2nd aerated model are shown in Table 4-18:

Table 4-18: Prototype drainage discharge from aeration duct – 2nd aerated model

H_p (m)	6.7	7.1	7.6
Q_{drain} (m³/s)	0.037	0.146	0.366

Again, the water inflow was calculated by arguing that the four splitters attributed equally to the drainage discharge from the aeration duct. The prototype water inflow per splitter contained in Table 4-19 is equal to the drainage discharge divided by four.

Table 4-19: Prototype water inflow per splitter – 2nd aerated model

H_p (m)	6.7	7.1	7.6
Q_{inflow} (m³/s)	0.009	0.037	0.092

4.5. Analysis and Discussion of Results

In order to accurately determine the effect of aeration through internal ducts on the local pressures of Roberts splitters, the results of the three hydraulic models were compared, analysed and discussed in this section following a brief discussion of each model.

4.5.1. Brief Discussion on the Unaerated Model and the Drowning of Splitters

A common theme with the results of the unaerated model tests was the severe change in conditions from spillway heads less than the design head of 6.7 m, to spillway heads equal to and greater than 6.7 m. The pressure around the entire splitter dropped considerably to below the cavitation threshold of -7 m atmospheric, and the air concentration decreased to zero. Figure 4-30 shows the prototype pressure and air concentration of the entire splitter. The probable minimum pressure of all 25 pressure sensors and the average air concentration of all three measured positions were calculated to provide this visual illustration of the drop in performance of the splitters.

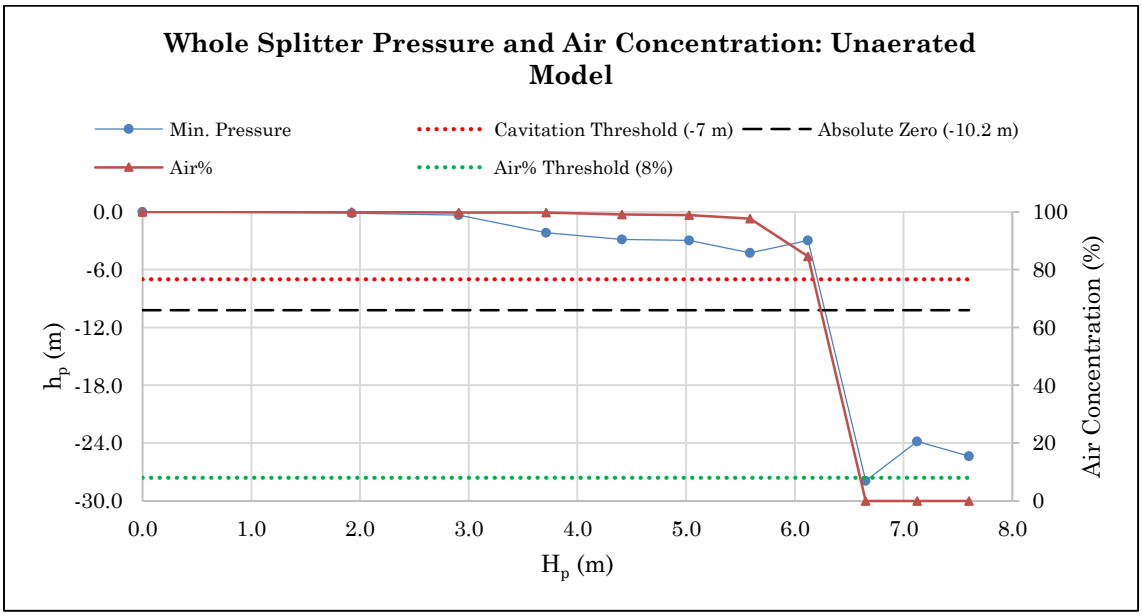

Figure 4-30: Prototype pressure and air concentration of whole splitter – unaerated model

From Figure 4-30 it is clear that the probable minimum pressure of the entire splitter drops to well below the cavitation threshold of -7 m atmospheric (Chadwick *et al.*, 2013) and that the air concentration drops to below the 8% needed to alleviate cavitation (Chanson, 1992). It was concluded that at flows higher than 35 m²/s and at spillway heads equal to and greater than the design head, the cavitation risk of unaerated Roberts splitters is so high it can be deemed inevitable.

4.5.1.1. Drowning of Roberts Splitters

Jordaan (1989) stated that the energy-dissipating performance of Roberts splitters drops when the splitters become drowned at the critical head of 1.2 times the design head. The unaerated model tests found that this critical head was reached at the design head of 6.7 m and not at $1.2H_D$. Roberts (1943) was the first person to prescribe the critical head of $1.2H_D$, but also limited the use of unaerated Roberts splitters to spillway heads of only 3.0 m. Figure 4-31 (a) and (b), and Figure 4-32 (a) and (b) show photographs of unaerated model tests nos. 7 and 8 respectively. Test no. 7 had a prototype spillway head of 6.1 m, less than the H_D of 6.7 m and test no. 8 was at the design head of 6.7 m.

An air pocket can clearly be seen in the boil downstream of the splitters in Figure 4-31. The results indicate that this air pocket greatly alleviated severe negative pressures on the splitters. This was due to the compressibility of air in comparison to water. If air was present within the flow, it absorbed the extreme pressure fluctuations caused by the

turbulent flow around the splitters by compressing and expanding accordingly. In contrast, if the air pocket was absent, as is the case with the drowned splitters, the extreme pressure fluctuations were transferred to the surface of the splitters by the incompressible water.

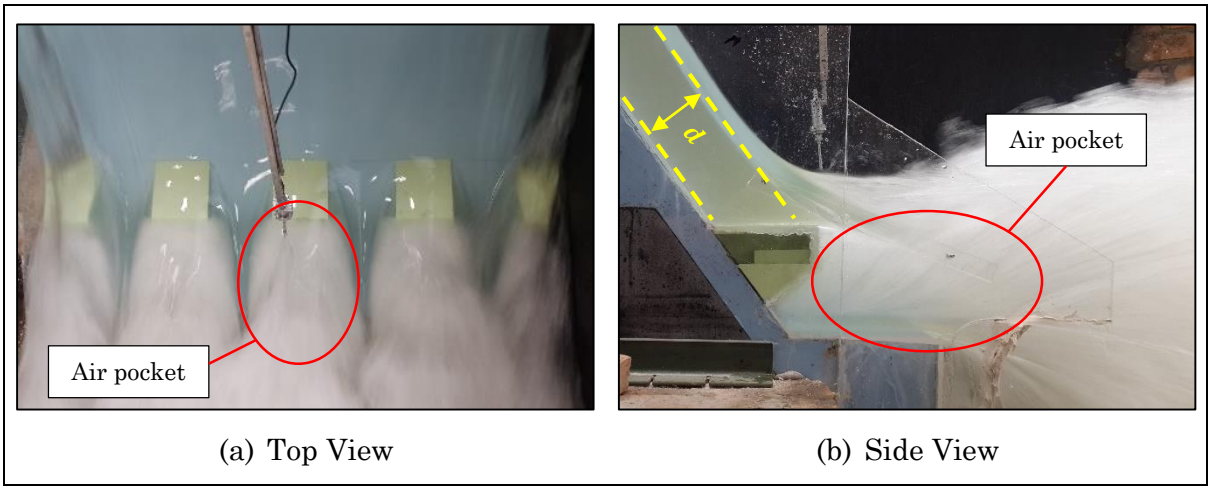

Figure 4-31: Photographs showing normal operation of Roberts splitters – Test no. 7: H_p = 6.1 m (< H_D)

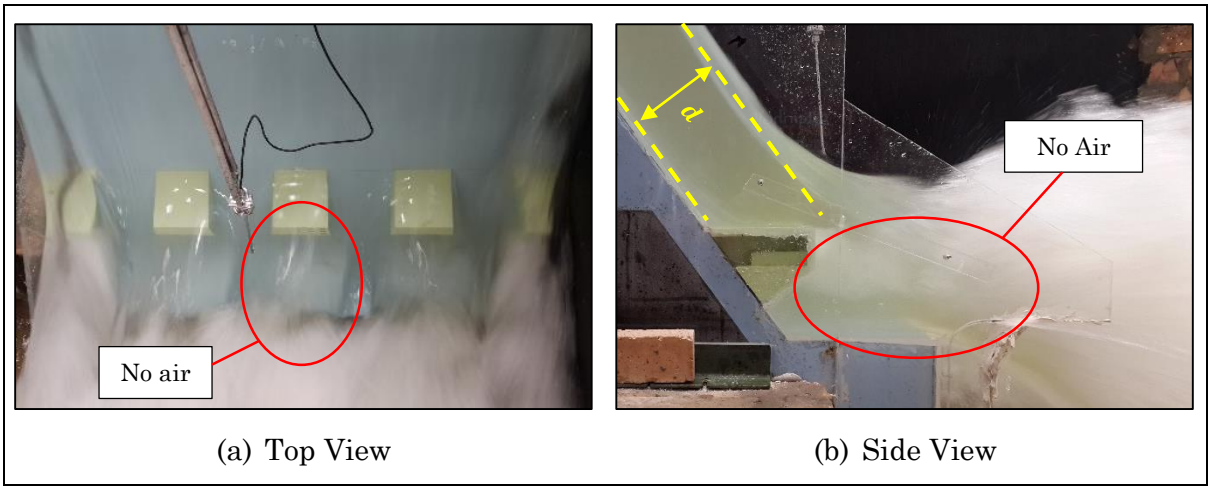

Figure 4-32: Photographs showing drowned operation of Roberts splitters – Test no. 8: H_p = 6.7 m (= H_D)

Note the illustration of *d* in Figure 4-31 (b) and Figure 4-32 (b) does not include the water flowing up against the Perspex viewing pane. The dark sheet of water included between the two illustrative yellow dashed lines is representative of the water depth across the whole spillway width.

The study found that the drowning of the splitters commenced at a critical flow depth *d* approaching the splitters, and that the relationship between *d* and the projected height of the splitters played a role. This is also evident from Figure 4-32. The projected height

of the splitters was defined as L_{proj} and is related to the length of the splitters L and the downstream slope of the spillway θ, and can be calculated as follows (see Figure 4-33):

$$L_{proj} = L \times \sin(\theta) \tag{4-2}$$

In the case of the studied hydraulic model, the prototype spillway slope was 0.75:1 (H:V), equal to a slope of θ = 53.1°, and the prototype length of the splitters was 3.425. This gave a projected splitter height of L_{proj} = 2.740 m.

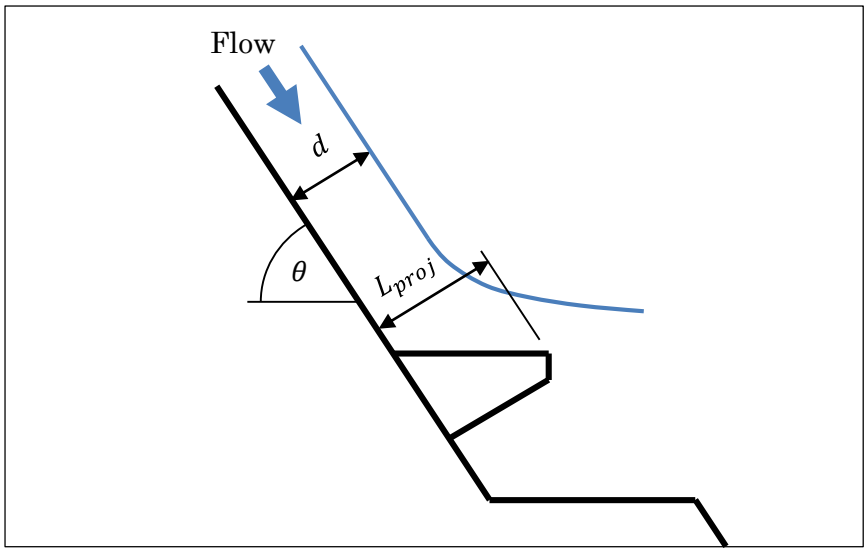

Figure 4-33: Definition of d and L_{proj} on a cross-section of a splitter

Using simple energy equations, the depth of flow was calculated from the spillway head H, the spillway unit discharge q and the height of the splitters below the spillway crest P:

$$H + P = d + \frac{(q/d)^2}{2 \cdot g} \tag{4-3}$$

From the depth of flow, the relationship of d/L_{proj} was obtained and plotted in Figure 4-34 against the spillway head to determine when the splitters would become drowned. The plot of H_p/L_{proj} is included for convenience. Note that the usage of this relationship to determine the point at which Roberts splitters will start to drown is subject to the discharge coefficient of the analysed spillway. Using the observation that the splitter became drowned at the prototype design spillway head of 6.7 m, from Figure 4-34 it can be concluded that for high design spillway heads of around 6.7 m, Roberts splitters will become drowned at a point where H/L_{proj} is equal to 2.4 and d/L_{proj} is equal to 0.84.

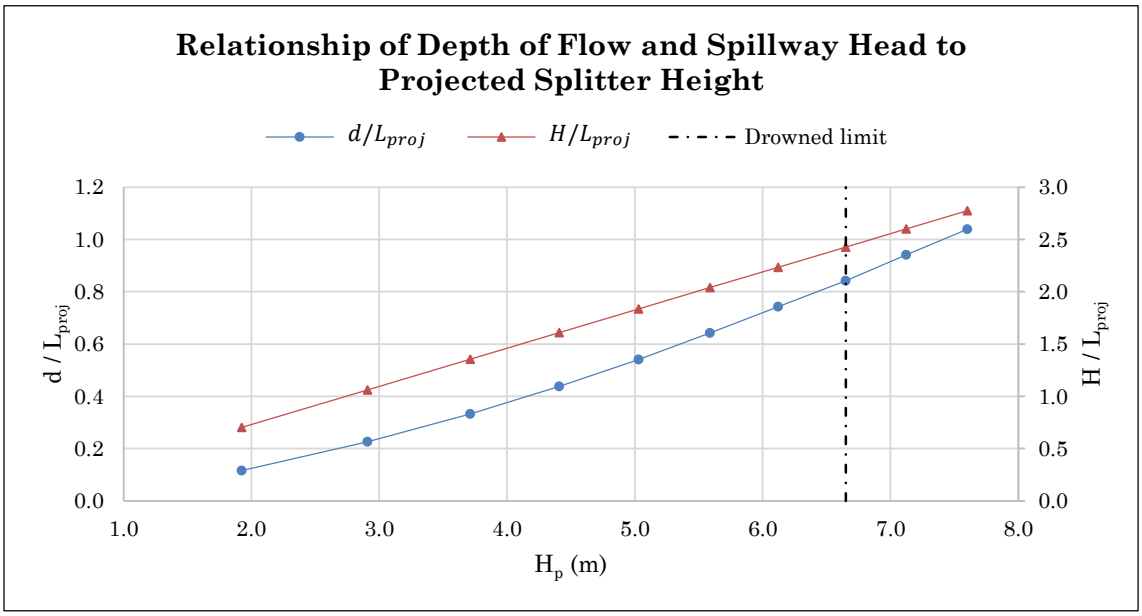

Figure 4-34: Relationship of depth of flow and spillway head to the projected splitter height

Thus, if the flow was deep enough to effectively flow over the splitters without projecting away, it would flush the air pocket downstream of the step causing severe pressure conditions around the step as no air is present to absorb the negative pressures. Figure 4-35 shows a close-up photograph of the splitters at the design head of 6.7 m, showing the lack of an air pocket downstream of the splitters.

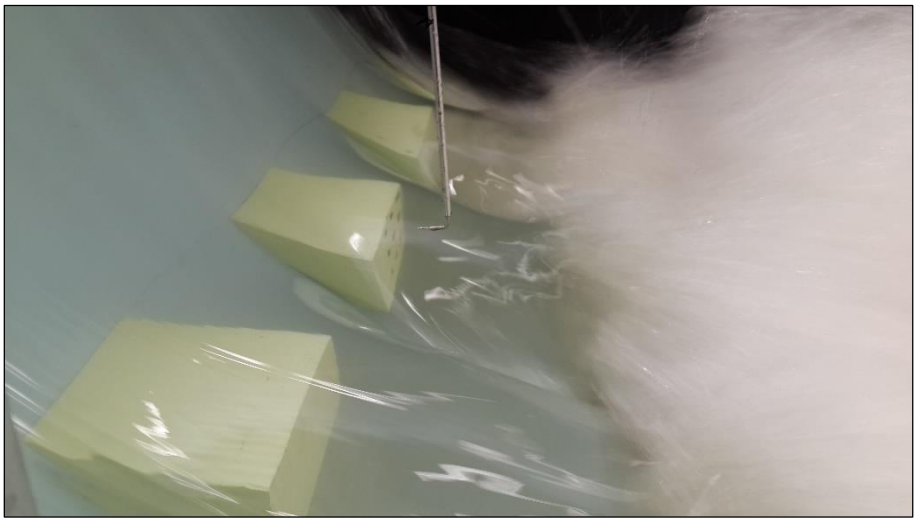

Figure 4-35: Photograph showing lack of air downstream of splitters of the unaerated model – H_p = 6.7 m

4.5.1.2. Entrainment of Air

In Figure 4-31, the splitters operated normally as described in Section 2.2.2, with the rotating columns of water projected by the splitter entraining large amounts of air from underneath the step. This air entrainment is needed for effective energy dissipation downstream as the projected jet of water falls to the plunge pool (Roberts, 1943), and is shown in Figure 4-36. The side streams from the splitters hit the step and move inward toward the centre of the splitter, hitting each other and moving upward and outward, producing a rotating column of water from each splitter.

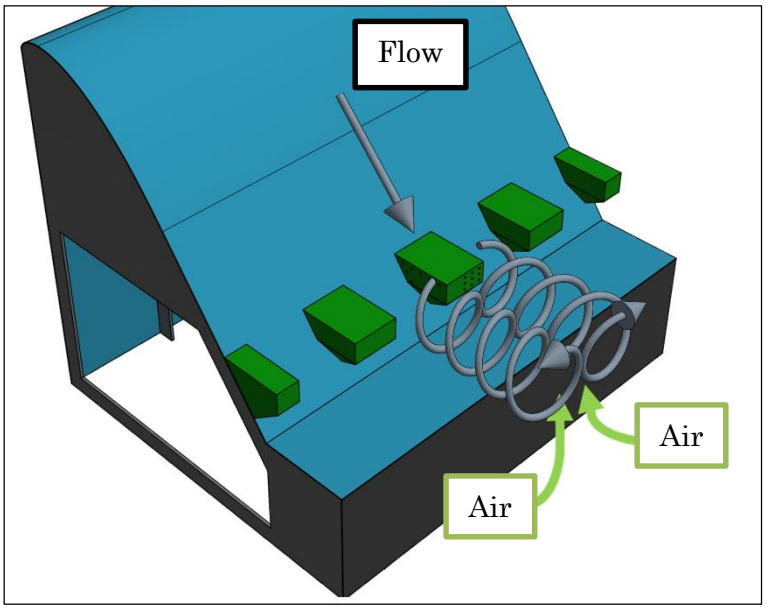

Figure 4-36: Air entrainment through rotating columns of water

While operating normally, the air pocket downstream of the splitters was fed by the air entrainment mechanism of the splitters. At relatively lower water velocities, the air pocket was kept in place immediately downstream of the splitters, increasing the air concentration and dynamic fluid pressure around the splitters. In the case of the drowned splitter, with higher velocities and greater flow depth approaching the splitters, the air pocket was flushed downstream, but the water followed the same streamlines as with the normal operating conditions in Figure 4-36. Air was still entrained from underneath the step, but could not readily establish the air pocket, as can be seen in Figure 4-32 (b). This resulted in zero air concentration around the splitter and very severe negative pressures. The zero air concentration is evident in Figure 4-35 where the geometry of the splitter appears distorted due to refraction.

It appeared that in order to alleviate the severe negative pressures around the splitters, the air pocket had to be kept immediately downstream of the splitters. As mentioned, this was done by introducing aeration through air vents on the splitters.

4.5.2. Brief Discussion on the 1st Aerated Model

The overall pressure situation of the 1st aerated model improved from that of the unaerated model, indicating that air vents were necessary to avoid cavitation risks at high spillway heads. Figure 4-37 shows the minimum prototype pressure measured on the whole splitter and the average air concentration of the flow around the splitter.

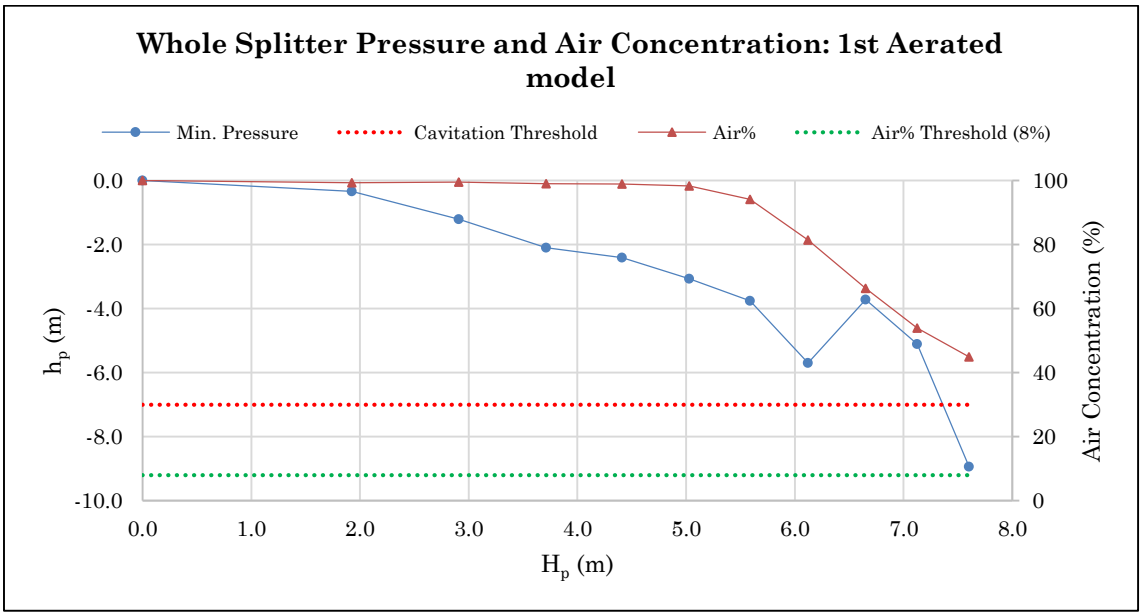

Figure 4-37: Prototype pressure and air concentration of whole splitter – 1st aerated model

Even though the minimum pressure dropped below the cavitation threshold of -7 m atmospheric, the air concentration remained above the necessary 8% to avoid cavitation (Chanson, 1992).

The drop in air concentration was not as severe as that of the unaerated model. This is because even though the splitter became drowned according to the criteria set in Section 4.5.1.1, the air pocket stayed immediately downstream of the splitters. This is evident from the photograph in Figure 4-38 of the 1st aerated model in operation at H_p = 7.6 m, equivalent to q_p = 50 m²/s. Note that the flow depth of the sheet of water approaching the splitters is slightly greater than the projected height of the splitters, but by feeding the air pocket with air from the vents, it was not flushed downstream of the step as was the case with the unaerated model at the maximum spillway head of 7.6 m. It was

observed that the air pocket was still being pushed downstream by the high velocity flow approaching the splitters, as with the unaerated model, but as it was fed by the air vents, the air pocket continuously re-established downstream of the splitters.

With the air pocket in place, air was naturally entrained by the rotating columns of water from the splitters. This led to the hypothesis that once the air pocket was established downstream of the splitter, it just needed to be fed and kept in place. The air pocket would improve the air concentration and pressure situation around the splitter considerably. The energy dissipation advantages of this operational improvement were inconclusive as the downstream scouring effects of the splitters and the energy dissipation were never tested due to the size of the model.

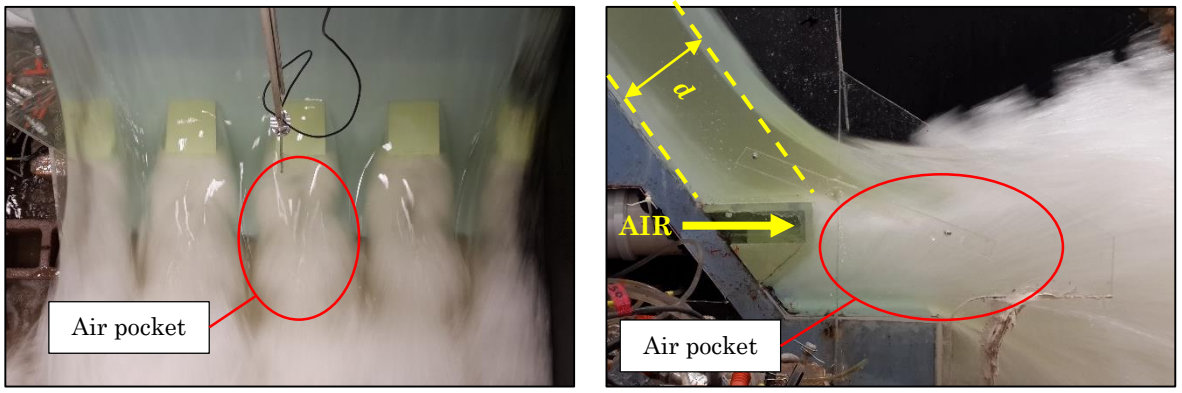

(a) Top View (b) Side View

Figure 4-38: Photograph showing air pocket downstream of splitters of the 1st aerated model at H_p = 7.6 m

The air vents and aeration duct performed sufficiently by increasing the pressures around the splitters and the average air concentration of the flow around the splitters. The performance of the air vents is described in more detail later in Section 4.5.5, considering and comparing both aerated models.

4.5.3. Brief Discussion on the 2nd Aerated Model

The minimum prototype pressure of the whole splitter of the 2nd aerated model decreased with increasing spillway head, and only dropped below the cavitation threshold of -7 m at the maximum prototype spillway head of 7.6 m. The air concentration around the splitter remained high, despite having decreased with increasing spillway head. The average air concentration of the whole splitter remained above 40% for all spillway heads. This is illustrated in Figure 4-39.

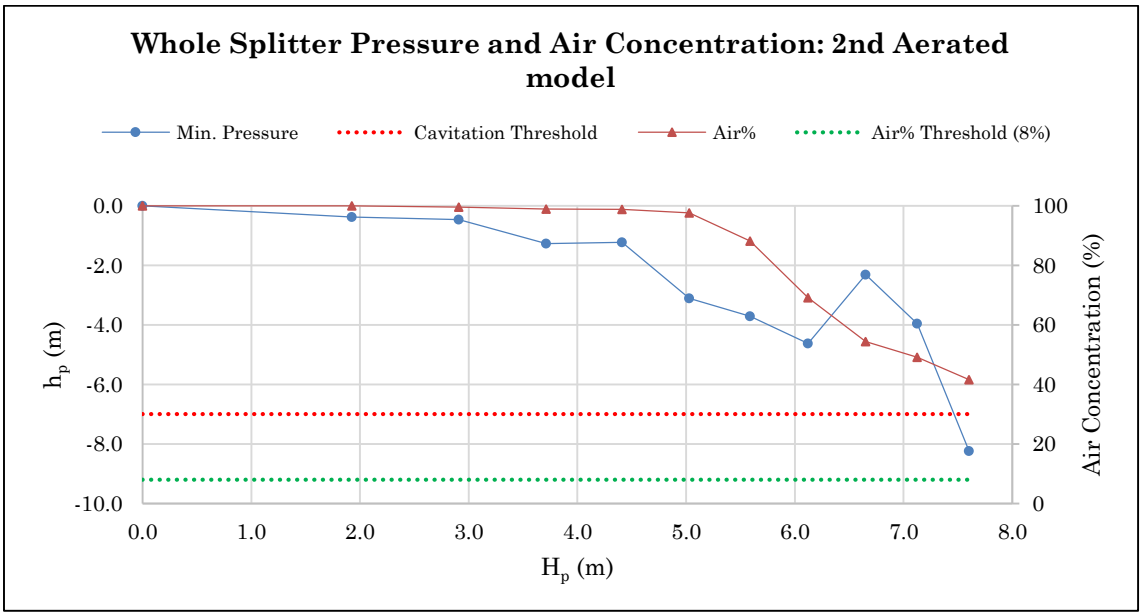

Figure 4-39: Prototype pressure and air concentration of whole splitter – 2nd aerated model

The combination of pressure and air concentration suggested that cavitation would not be a problem if large air vents are used. The high air concentration was due to the air pocket downstream of the splitter. As with the 1st aerated model, the air pocket was pushed downstream by the high velocity flow of the design head and above. As with the 1st aerated model, however, the air pocket was continuously fed by the larger air vents and this kept it in position. Figure 4-40 shows photographs of the top view and side view of test no. 66 at a prototype spillway head of 7.6 m. In these photographs, the air pocket is clearly visible even though the approach flow depth was greater than the projected splitter height indicating the splitters were drowned.

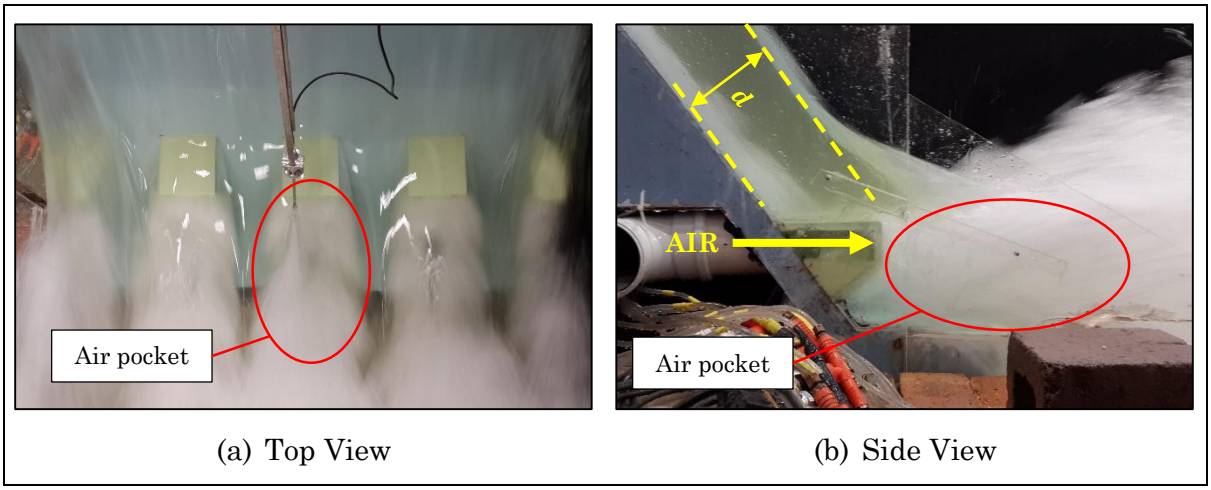

Figure 4-40: Photograph showing air pocket downstream of splitters of the 2nd aerated model at H_p = 7.6 m

4.5.4. Comparison of Local Pressures and Air Concentration

Figure 4-41 contains the comparison of prototype minimum pressures of the whole splitter and Figure 4-42 shows the air concentration for each model. The models behaved similarly for heads up to 6.1 m in terms of pressure and air concentration. However, at the design head of 6.7 m and above, the splitters became drowned (as discussed in Section 4.5.1.1) and the unaerated splitters showed a severe drop in pressure and air concentration.

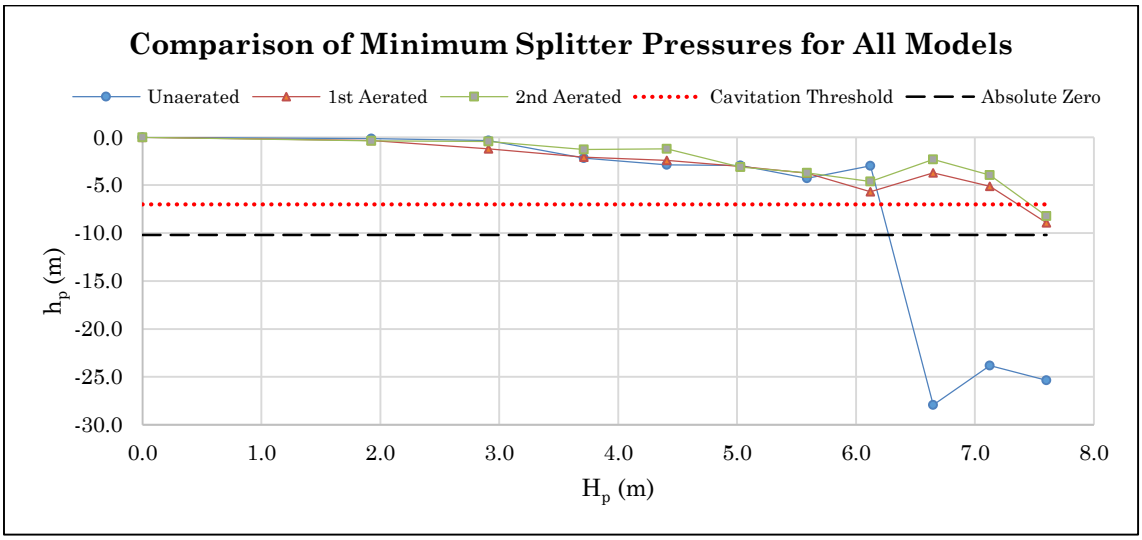

Figure 4-41: Comparison of splitter minimum pressures of all models

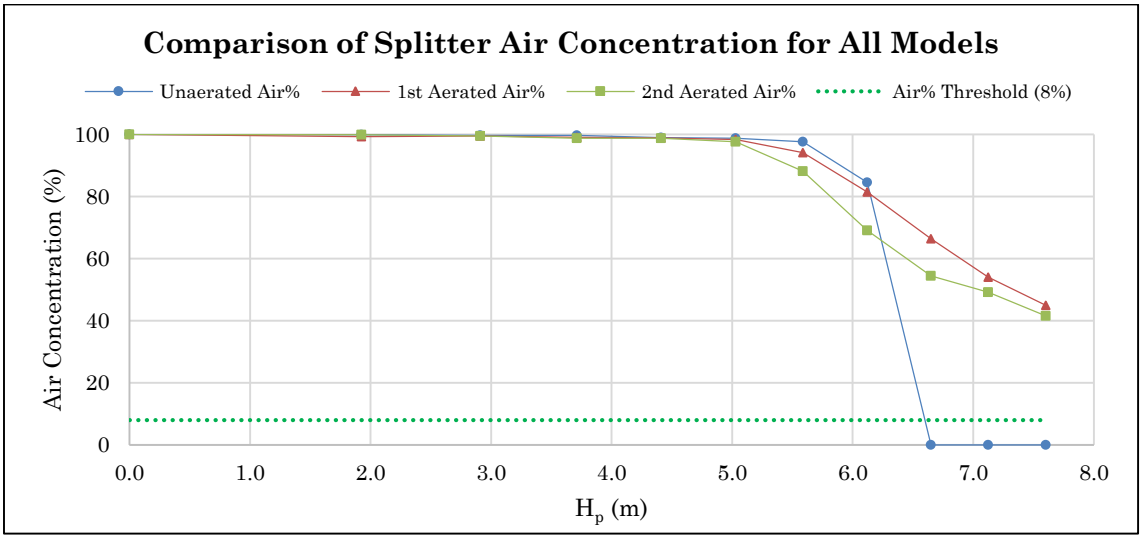

Figure 4-42: Comparison of splitter average air concentration for all models

The normal air pocket found in the boil immediately downstream of the splitters was flushed downstream of the step and the characteristic air entrainment mechanism of Robert splitters was not as effective in this state as intended by Roberts (1943).

Pressure was assumed to be vacuum (-10.2 m) on the side face as -27.9 m was measured. Adding to this the 0% air concentration, cavitation was inevitable.

The air vents of the aerated models provided much needed air supply to the splitters in this drowned state. The air pocket was continuously re-established and the pressure conditions improved considerably, as evident from Figure 4-41. The change in minimum pressures for each aerated model from the unaerated model is shown in Table 4-20:

Table 4-20: Change in prototype pressure from the unaerated model in metres

H_p (m)	1.9	2.9	3.7	4.4	5.0	5.6	6.1	6.7	7.1	7.6
1st Aerated	-0.2	-0.9	+0.1	+0.5	-0.1	+0.5	-2.7	+24.2	+18.7	+16.4
2nd Aerated	-0.2	-0.1	+0.9	+1.7	-0.2	+0.6	-1.7	+25.6	+19.9	+17.1

At spillway heads equal to and greater than the design spillway head of 6.7 m, the change in prototype pressure is clearly evident and beneficial. The air concentration still decreased for the increasing spillway head, but did not drop below 40%. In only one location, a prototype pressure less than the cavitation limit of -7 m as prescribed by Chadwick *et al*. (2013), was recorded. However, according to Chanson's (1992) findings, this is acceptable given that the air concentration in the flow at this point is greater than 8%.

In order to determine the effect of larger air vents, the summarised prototype pressures of the two aerated model's splitters are plotted in Figure 4-43.

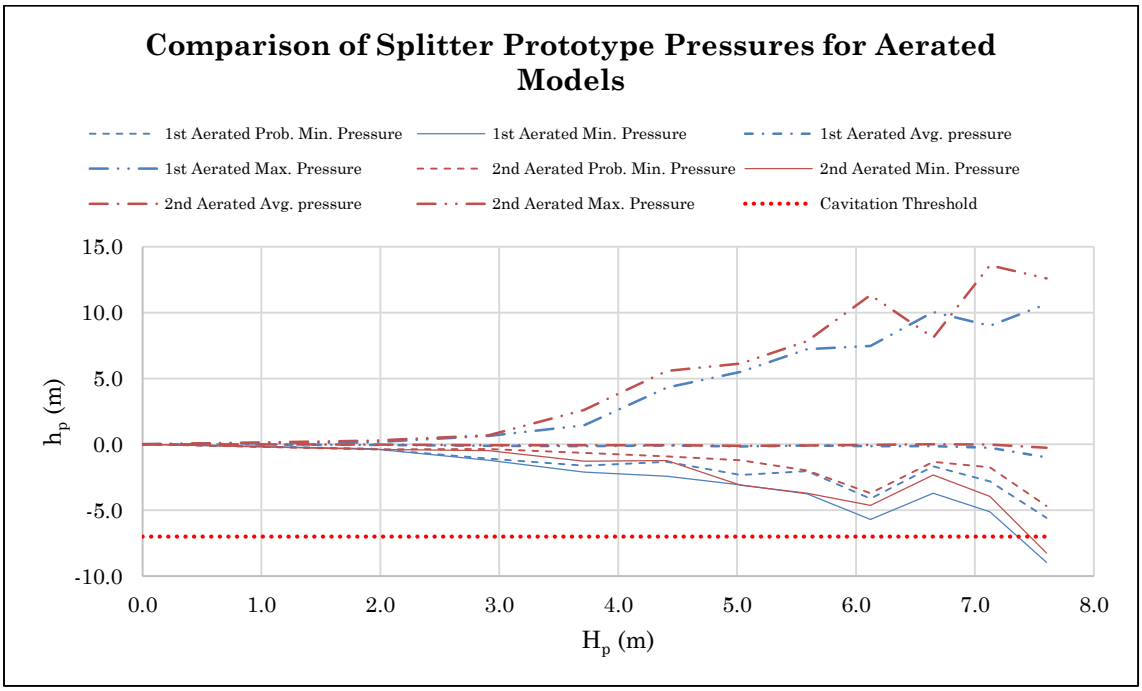

Figure 4-43: Comparison of the pressure of the aerated models

From Figure 4-43 it can be seen that the minimum, probable minimum, average and maximum pressures increased slightly from the 1st aerated to the 2nd aerated model. The benefit of both air vent designs is, however, evident when considering the minimum pressure distribution on the faces of the splitter for the design head of 6.7 m and the maximum head of 7.6 m, included in Figure 4-44 and Figure 4-45 respectively (both on Page 124).

Regarding the pressure distributions of the design head of 6.7 m in Figure 4-44, it was noted that the severe pressure situation of the unaerated model was completely alleviated by both the aerated models. There was, however, no significant difference between the pressure distributions of the two aerated models. As mentioned in Section 4.4.1, this indicated that there is no apparent advantage in terms of pressure distribution to designing larger air vents for Roberts splitters operated up to, but not exceeding its design head.

At the maximum head of 7.6 m, however, the spread and distribution thereof is significantly different (see Figure 4-45). Note the large spread of pressure equal to or less than -7 m on all splitter faces of the 1st aerated model (the red areas on the contour plots). This is greatly reduced in the 2nd aerated model to only a single zone on the bottom face, giving strong reason to design larger air vents for Roberts splitters in the event that the design head is exceeded by up to 13%.

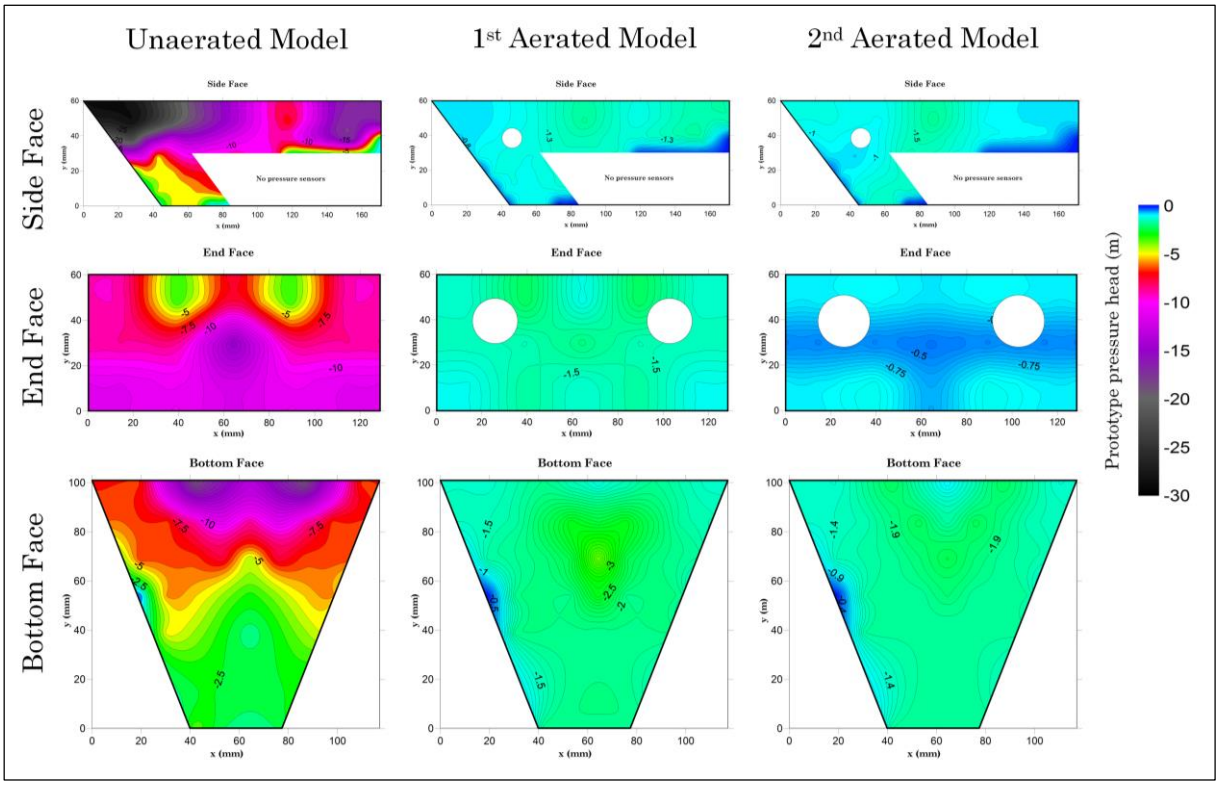

Figure 4-44: Pressure distribution on the splitter for all models at H_p = 6.7 m

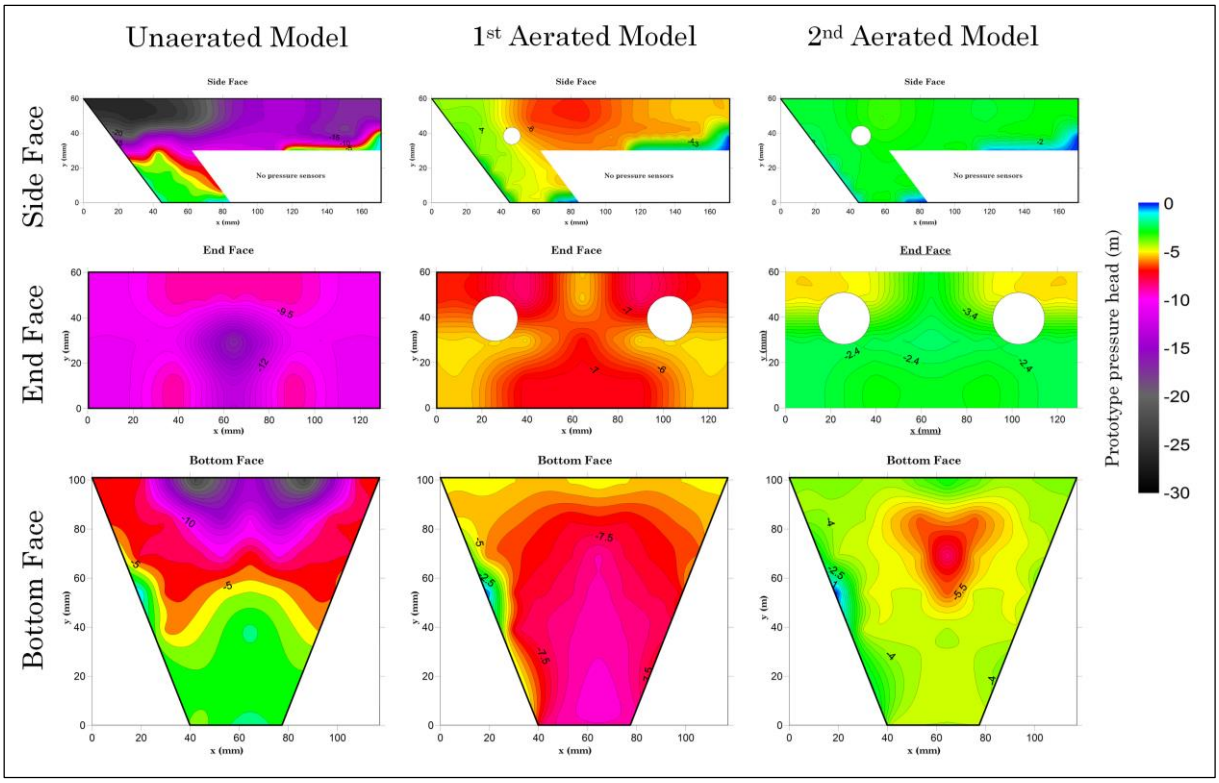

Figure 4-45: Pressure distribution on the splitter for all models at H_p = 7.6 m

4.5.5. Discussion on Aeration Duct Performance

The next consideration in deciding on the appropriate size of the air vents is the aeration duct performance in terms of air discharge and water inflow per splitter. Figure 4-46 shows the prototype air discharge and the water inflow per splitter for all tested spillway heads. It is evident that the decrease in air discharge at heads greater than 5.0 m and more prominently at heads greater than 6.0 m, is linked to the increase in water inflow at the same heads.

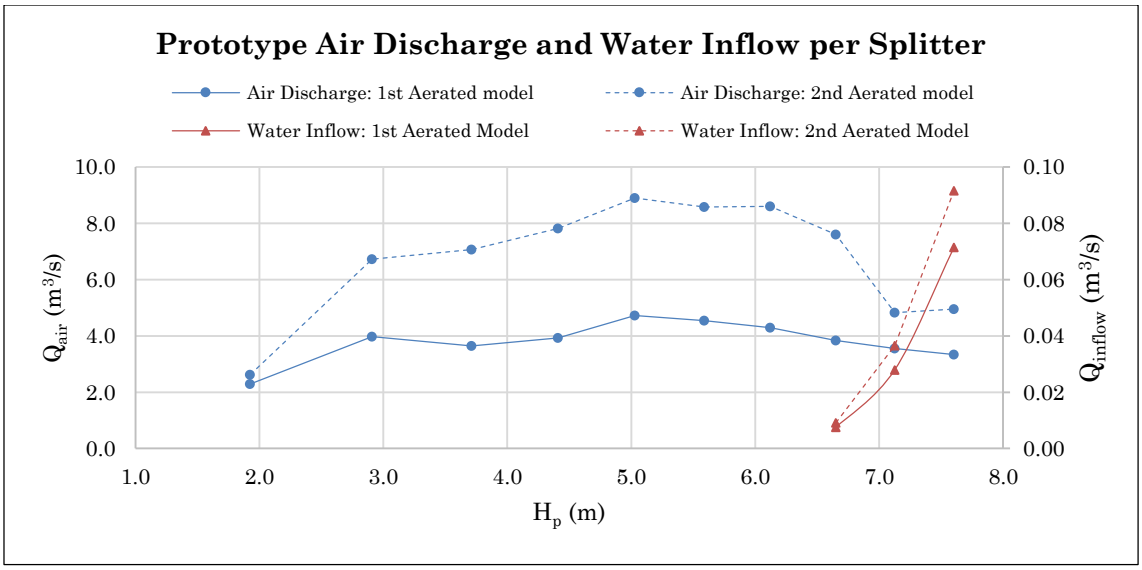

Figure 4-46: Prototype air discharge and water inflow per splitter for both aerated models

As the movement of air and water through the air vents is caused by the pressure differential between the outside and inside of the air vents, and the pressure on the inside of the vents was kept at atmospheric, the measured pressure at the air vent positions was analysed to find the solution.

The prototype pressures at the main air vents were interpolated from the values of pressure sensors A2, A3, B2 and B3, and the pressure of the side air vents were interpolated from sensors E4, E5 and E6. By taking the minimum, average and maximum of these interpolated sets of data, Figure 4-47 and Figure 4-48 were produced.

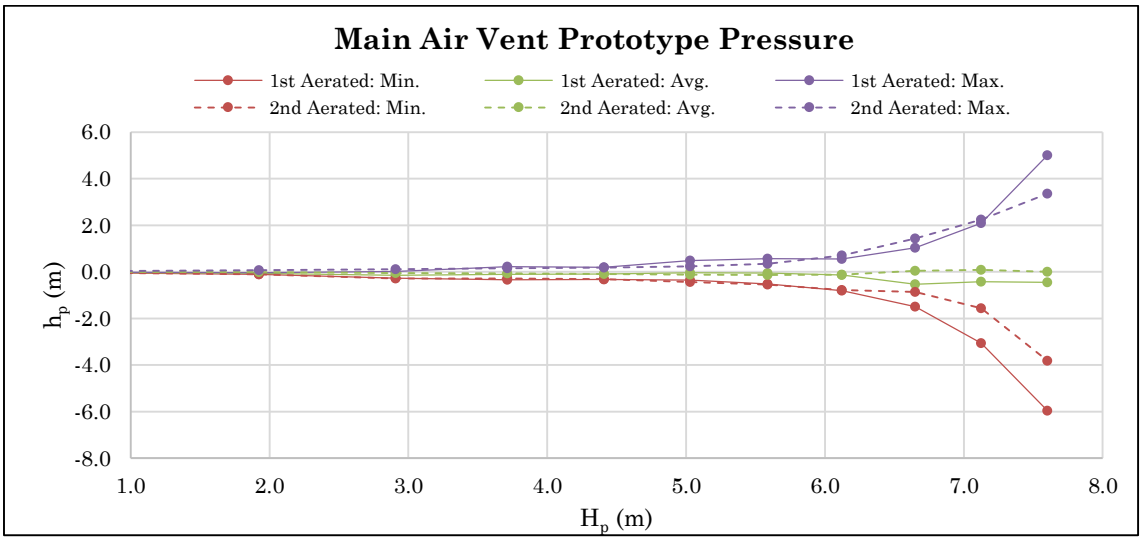

Figure 4-47: Prototype pressure at the main air vents of both aerated models

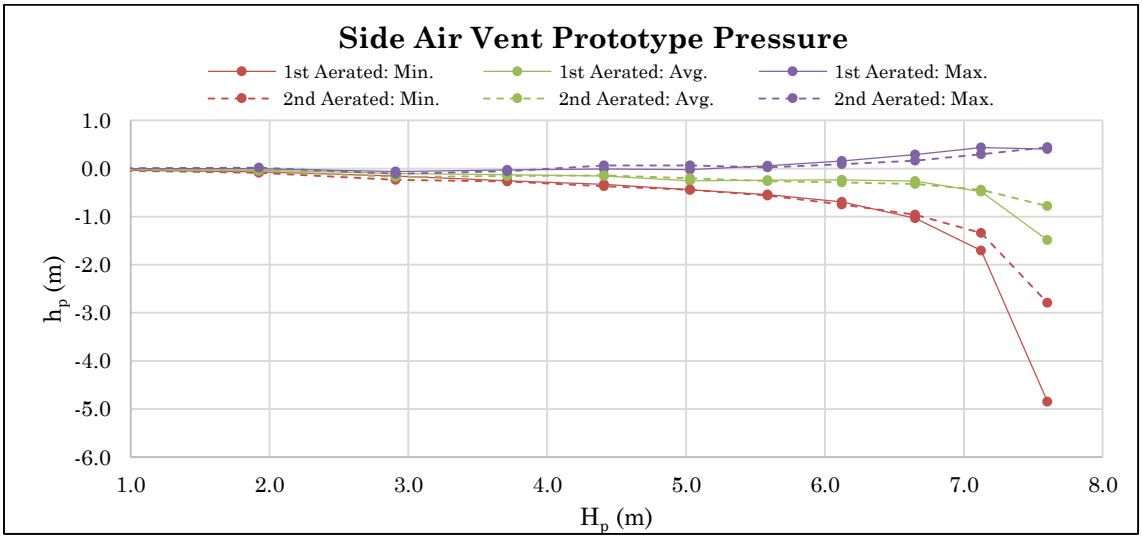

Figure 4-48: Prototype pressure at the side air vents of both aerated models

In Figure 4-47 and Figure 4-48, the negative pressures relate to air being discharged from the air vents, and the positive pressure relates to water that flowed into the vents. It must be noted that the minimum and maximum pressure values in these figures represent pressure peaks. There were several positive peaks and several negative peaks. Each of these peaks would induce a burst of air discharge or a burst of water inflow. Air and water never continuously or steadily flowed through the air vents.

The large increase in air discharge of the 2nd aerated model from that of the 1st aerated model at heads between 2.0 m and 7.0 m can be explained by the similarity of the pressure results at the air vents. If the pressures at the air vents were to be equal, then the larger cross-sectional area of the Ø23 mm vents would produce a greater volume of air per given time. Referring to the higher heads of 7.1 m and 7.6 m within Figure 4-47

and Figure 4-48, the pressure at the air vents of the 2nd aerated model increased from that of the 1st aerated model, causing a decrease in air demand. The larger air vents still resulted in an increase in air discharge, as can be seen in Figure 4-46, but the decreased demand meant that the difference between the two aerated models is not as great as is the case with the heads less than 7.0 m.

Referring to Figure 4-46, small amounts of water only started sporadically flowing into the air vents at spillway heads equal to and greater than 6.7 m, the same head as when the splitters became drowned. As mentioned, the inflow of water is due to peaks of positive pressure at the air vents. From observations during the tests it was found that almost zero water flowed into the side vents. This is partly due to the size of the side vents being half of that of the main vents, but mostly due to absence of notable positive pressure at the side vents, as can be seen in Figure 4-48. During the aerated tests, the sides of the splitters produced surprisingly stable and predictable pressure results, especially considering that during the unaerated model tests, the pressures on the side were the most severe of all tests.

4.6. Conclusions from the Results of the Hydraulic Model Tests

The results of the hydraulic model tests were summarised into the following brief conclusions:

Unaerated Model Tests

- During the unaerated model tests, the splitters became drowned when the following limits were exceeded:
  i. $H_p \geq$ the design spillway head of H_D = 6.7 m;
  ii. $d/L_{proj} \geq 0.84$;
  iii. $H/L_{proj} \geq 2.4$;
- When the splitters were drowned during the unaerated model tests, very severe negative pressures occurred on all faces of the splitter. The minimum measured prototype pressure during these tests was -27.9 m atmospheric. This is significantly lower than the absolute zero pressure of -10.2 m, effectively indicating vacuum conditions;
- The average air concentration of the unaerated model dropped to 0% when the splitters were drowned;

- The cavitation risk for unaerated Roberts splitters is extremely high at $q_p \geq$ 40 m²/s and at $H_p \geq$ the design head of 6.7 m;

Pressure and Air Concentration of the Aerated Model Tests

- During the aerated model tests, severe pressure and air concentration conditions were greatly alleviated, and the cavitation risk was essentially lowered to zero;
- The minimum measured prototype pressure was -8.9 m atmospheric during the 1st aerated model tests and -8.2 m atmospheric during the 2nd aerated model tests. Both of these occurred at H_p = 7.6 m;
- The lowest average air concentration was 45% for the 1st aerated model and 42% for the 2nd aerated model. Once again, both of these instances occurred at H_p = 7.6 m;
- At H_D = 6.7 m, there was no advantage in terms of pressure to the larger air vents of the 2nd aerated model, but however, at H_p = 7.6 m the pressure conditions were significantly improved by the larger air vents;

Aeration Duct Performance of the Aerated Model Tests

- The maximum air discharge per splitter was 4.73 m³/s and of the 1st aerated model and 8.90 m³/s for the 2nd aerated model. Both of these occurred at H_p = 5.0 m;
- At a spillway head of 6.1 m, small amounts of water started to flow into the air vents, lowering the air discharge per splitter at H_p = 7.6 m to 3.34 m³/s for the 1st aerated model and to 4.95 m³/s for the 2nd aerated model;
- The maximum water inflow per splitter occurred at H_p = 7.6 m for both aerated models. This was 0.071 m³/s for the 1st aerated model and 0.092 m³/s for the 2nd aerated model;
- The maximum prototype air velocity in the aeration gallery was 6.58 m/s (23.7 km/h) for the 1st aerated model and 11.09 m/s (39.9 km/h) for the 2nd aerated model. Both of these occurred at H_p = 5.0 m and are within the safety recommendations of Lee (1999).

CHAPTER 5
CONCLUSIONS

A hydraulic model study was performed to investigate the effects of aeration of Roberts splitters through an internal aeration gallery on the local splitter pressures. This was done to alleviate cavitation risks arising from severe negative pressure in flows with essentially zero air concentration. At very high spillway heads, higher than the design value, these conditions can occur and were indeed measured on the hydraulic model.

Three hydraulic models were constructed: a control model of unaerated Roberts splitters, the 1st aerated model where small air vents were included on the end and side faces of the splitters, and a 2nd aerated model where the air vents were enlarged.

The conclusions of the entire study can be divided into two parts: firstly, conclusions from the literature review, and then secondly, conclusions from the hydraulic model tests.

5.1. Conclusions from the Literature Review

The conclusions made from the literature gave important insight on what to expect during the set-up of the hydraulic model.

Roberts splitters as an energy-dissipating measure was developed in the 1930's by Lt. Col. D.F. Roberts for the uncontrolled spillway of the Loskop Dam (Van Vuuren, 2008). After the first usage of splitter aeration at the spillway of the Gariep Dam, and effectively increasing the maximum design head of the splitters to 7.3 m, Mason (1983) studied the five major prototype cases of Roberts splitters and recommended improvements to Roberts' (1943) original design procedure.

The splitter aeration system for the Gariep, Vanderkloof, Hazelmere and Victoria Dams consisted of air vents for each splitter individually being provided with air by larger air vents set below the step of the system. This however led to Jordaan's (1989) statement: 'the need or effectiveness of aeration by internal ducts has, however, not been proved conclusively', as the aeration galleries of these dams were not open to the atmosphere.

During model testing of the Wadi Dayqah Dam, it was found that opening the internal aeration gallery to the atmosphere benefited energy dissipation (Mason, 2016).

The inception of cavitation on the surface of hydraulic structure commences when the dynamic fluid pressure decreases to the vapour pressure of the fluid. For an ideal fluid at standard temperature and ambient atmospheric pressure, this would happen if the fluid pressure drops to 0.3 m absolute (-10.0 m atmospheric). In practice however, irregularities and undissolved gases within water can cause cavitation to commence at higher pressures. Chadwick *et al.* (2013) recommended an operating limit of -7 m atmospheric for any hydraulic structure to avoid cavitation. During the study, this limit of -7 m was adopted as the cavitation threshold.

Through thorough model studies, Chanson (1992) concluded that an average air concentration of between 4% and 8% in the flow close to the surface of a spillway or structure would mitigate the damaging effects of cavitation. Thus it was concluded that an air concentration of at least 8% at the splitters in the model would indicate that cavitation would have no damaging effect on the surface of the splitters.

5.2. Conclusions from the Hydraulic Model Tests

The conclusions from the results of the three hydraulic model tests can be summarised as follows:

Care must be taken when using the test results of the relevant model study, as all hydraulics and geometry of Roberts splitters are related to the depth of flow approaching the splitters, d, and not the spillway head H. For convenience, the prototype spillway head was used as the independent variable. As the depth of flow approaching the splitters is dependent on not only the spillway head, but also the unit discharge of the spillway, the discharge coefficient of a given spillway will influence the results of the Roberts splitters on that spillway. The discharge coefficient of the relevant model spillway was 2.262.

The measured rating curve deviated slightly from the theoretical one, producing a higher discharge coefficient at high spillway heads and a lower discharge coefficient at low spillway heads. As such, the measured values for H_p was used as the independent variable rather than the theoretical ones. The measured prototype design head at a prototype unit discharge of 40 m²/s was 6.7 m.

During the unaerated model tests, it was found that the splitter became drowned at the design spillway head of 6.7 m. When considering the depth of flow approaching the splitters d, and the spillway head H, it was concluded that a system of unaerated Roberts splitters be operated under the following rules to avoid drowning:

- $d/L_{proj} < 0.84$
- $H/L_{proj} < 2.4$

where L_{proj} is the projected height of the splitters in the direction of the flow, as described in Section 4.5.1.1.

During the drowning of the splitters, the pressure effectively reached vacuum. Prototype pressures well below the absolute zero pressure of -10.2 m was measured (-27.9 m atmospheric and -22.0 m atmospheric on the side and bottom faces of the splitter respectively), and indicated that the pressures were very close to vacuum. As the air pocket in the boil of the splitter was flushed downstream because of the drowning, the average air concentration around the splitter essentially dropped to 0%. These conditions would inevitably lead to cavitation damage to the splitters.

During both aerated model tests, it was found that even though the splitters became drowned according the rules stated above, the air pocket remained within the boil of the splitters as it was fed with air from the air vents. This increased the pressure and the air concentration considerably. At the design head of 6.7 m, the minimum measured prototype pressure was -3.7 m and -2.3 m for the 1st and 2nd aerated models respectively. However, at the maximum head of 7.6 m, the minimum measured prototype pressure was -8.9 m and -8.2 m for the 1st and 2nd aerated models respectively. Both of these measurements were taken on the bottom face of the splitter, where no air vents were placed. Placing air vents on the bottom face would alleviate these pressures, but the risk of increased water inflow into these vents due to very high positive pressure peaks could nullify their effect. Regarding the minimum pressures of -8.9 m and -8.2 m for the two aerated models, it was however concluded that cavitation would be avoided as the average air concentration around the splitters never dropped below 42% for both aerated models, considerably higher than the 8% needed according to Chanson's (1992) recommendations.

In reply to Jordaan's (1989) statement, the need for aeration to Roberts splitters by internal ducts has been conclusively proven by these results.

Even though the pressure distributions at the design head of 6.7 m were very similar for both aerated models, the severe negative pressure conditions of the 1st aerated model at the maximum spillway head of 7.6 m were significantly improved by the larger air vents of the 2nd aerated model (see Figure 4-44 and Figure 4-45 on page 124). This indicated that larger air vents are advantageous if severe negative pressure needs to be alleviated at spillway heads greater than the design head, and at high unit discharges approaching 50 m²/s. The larger air vents had the following prototype dimensions:

- $\emptyset_{main} = 0.46\ m$
- $\emptyset_{side} = 0.23\ m \quad (\emptyset_{side} = 0.5 \cdot \emptyset_{main})$

This equated to the following design relationships for the model:

- $\emptyset_{main} = 0.2 \cdot d_D$
- $\emptyset_{side} = 0.5 \cdot \emptyset_{main}$

During both aerated model tests it was found that the air discharge from the splitters increased with increasing prototype spillway heads, peaking at H_p = 5.0 m, before decreasing for higher heads. For the 1st aerated model, the peak air discharge, Q_{air}, at H_p = 5.0 m was 4.73 m³/s before decreasing to 3.34 m³/s at H_p = 7.6 m. For the 2nd aerated model, a greater air discharge was measured over the entire range of heads. The peak air discharge, Q_{air}, at H_p = 5.0 m was 8.90 m³/s before decreasing to 4.95 m³/s at H_p = 7.6 m.

The observed decrease in air discharge was due to more regular and higher positive pressure peaks during the high head flows, at the air vent positions. This resulted in less air being discharged from the vents and also small sporadic bursts of water inflow into the vents. The small bursts of water accumulated within the aeration duct, further lessening the total air discharge through the duct. The four splitters of the model equally contributed to a peak prototype drainage discharge from the aeration duct of 0.286 m³/s and 0.366 m³/s for the 1st and 2nd aerated models respectively. Both of these peaks occurred at H_p = 7.6 m. The peak water inflow per splitter was 0.071 m³/s for the 1st aerated model, and 0.092 m³/s for the 2nd aerated model.

The safety of the aeration gallery for human observation during floods is guaranteed when using a safety factor of 2.0 to dimension the gallery for air flow to the air vents. The maximum recorded air velocity was 11.09 m/s, and was measured at H_p = 5.0 m

during the 2nd aerated model tests. This is equivalent to a strong breeze with a Beaufort number of 6. From Section 2.2.3.4, this would suggest that a person would still be able to move comfortably and conveniently inside the aeration gallery. If smaller safety factors were to be used in practice, the expected air velocity can be determined using the air discharge per splitter as a starting point.

In summary, the inclusion of air vents in Roberts splitters and an aeration gallery open to the atmosphere increased the effective operating spillway head to 7.6 m, 13.4% greater than the design head of 6.7 m, indicating that the design flood can be marginally underestimated with a degree of safety. The maximum measured unit discharge that was safely passed over the spillway was 50 m^2/s, which is significantly more than the 12 m^2/s limit set by Roberts (1943) (see section 2.2.4.1: Spillway Head Limit) and the limit of 35 m^2/s as measured in this study for unaerated splitters.

The local minimum pressures increased considerably with the inclusion of aeration from effectively vacuum (-10.2 m) to -2.3 m at the design spillway head of 6.7 m (q = 35 m^2/s), an increase of 77%. At the maximum spillway head of 7.6 m (q = 35 m^2/s), the local minimum pressures increased from effectively vacuum (-10.2 m) to -8.2 m, an increase of 20%. The risk of cavitation was completely mitigated at the maximum spillway head as the air concentration around the aerated splitters remained well above the 8% needed according to Chanson's (1992) recommendations.

As a closing remark, it was found that the main objective of the study was successfully achieved, as aeration of Roberts splitters, through an internal gallery, had a satisfactory effect on the local negative pressures around the splitters and sufficiently alleviated the cavitation risk at prototype unit discharges of up to 50 m^2/s. The secondary objective of the study was also achieved as the proposed aeration system performed satisfactorily. The recommendations on the application thereof are contained in Chapter 6.

CHAPTER 6

RECOMMENDATIONS

The recommendations arising from this hydraulic study fall into two categories. Firstly, all practical recommendations made by the author on the effective usage of Roberts splitters in practice as an energy-dissipating measure on dam spillways are listed under Section 6.1, and finally, any recommendations on future research regarding Roberts splitters, or similar spillway crest splitters are contained in Section 6.2.

6.1. Practical Recommendations on the use of Roberts Splitters

Roberts splitters have been used successfully on more than 30 dams in South Africa and abroad as an energy-dissipating measure. The following recommendations and considerations on the system and the aeration thereof arise from this study:

- Unaerated Roberts splitters should not be operated at design spillway unit discharges of more than 35 m²/s. At design unit discharges of 40 m²/s, the design spillway head will become too high and drowning of the splitters will commence at the design head;
- The critical head, H_C, to avoid drowning of the splitters as recommended by Roberts (1943) is valid for all design heads, but it is further recommended that splitters be dimensioned according to the following criteria to avoid drowning of the splitter's air entrainment mechanism, where L_{proj} is the projected splitter height in the direction of the approaching flow, and d_C is the depth of flow approaching the splitters associated with the critical head H_C:
  i. $L_{proj}/d_C > 1.19$
  ii. $L_{proj}/H_C > 0.42$
- At spillway design heads greater than Roberts' (1943) limit of 3.0 m, aeration to the splitters is recommended to avoid probable cavitation;
- It is recommended that the aeration of Roberts splitters be via an internal aeration gallery open to the atmosphere, and not locally through air vents below

the step. This is due to water entering the air vents on the splitters that needs to be drained without affecting the air supply of the vents. Local air vents in the steps could be drowned by the water that needs to be drained, cutting off the air supply to the splitters air vents;

- The main cross-sectional area of the aeration gallery must be larger than the sum of the cross-sectional areas of all air vents, plus a safety factor. The optimal value of this safety factor is inconclusive, as a conservative factor of 2.0 was used in this hydraulic model study;
- The aeration gallery should be equipped with a suitable drainage channel with exit ports, covered by a safety grid, below the main cross-sectional area of the gallery;
- Finally, it is recommended that air vents be placed on the following locations (see Figure 6-1):
    i. Two main air vents on the end face of the splitters, centrally placed on each half-width of the face;
    ii. One side air vent on each side face of the splitter a distance of $\emptyset_{main}$ measured perpendicular from the spillway surface;
    iii. It is inconclusive whether to provide an air vent on the bottom face;

  and dimensioned according to the following relationships, where d_D is the design depth of flow approaching the splitters:
    i. $\emptyset_{main} = 0.2 \cdot d_D$
    ii. $\emptyset_{side} = 0.5 \cdot \emptyset_{main}$

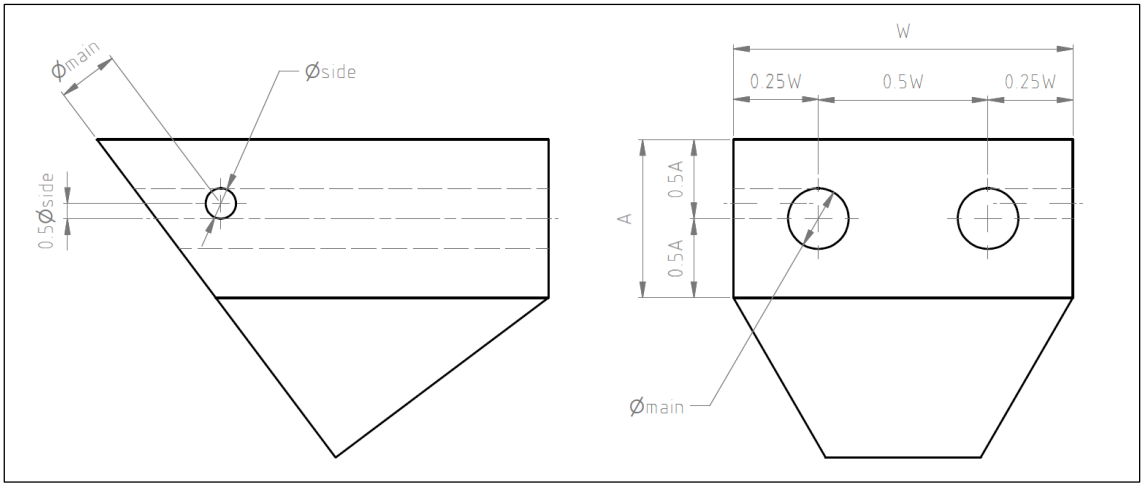

Figure 6-1: Recommended air vent positions

6.2. Recommendations for Future Research

The following recommendations are made for future research on the subject of Roberts splitters and the aeration thereof:

- Determine the effect of aeration of drowned splitters on the downstream energy dissipation, and the impact pressures of the projected jet on the apron of the dam. Jordaan (1989) mentions that unaerated drowned splitters have a considerable decrease in energy-dissipating performance. From the current study, there is reason to believe that this might be improved with the addition of air vents, as the normal air entrainment mechanism of the splitters was essentially restored during the aerated model tests;
- The current study was limited by the discharge capacity of the laboratory of 700 l/s and the 1 in 20 scale of the model, and used a design unit discharge of 40 m^2/s in order to evaluate the possibility of the underestimation of the design flood of a dam by a further 10 m^2/s. If practically possible, further increase the design prototype unit discharge of the model above 40 m^2/s and the maximum tested unit discharge above 50 m^2/s without increasing the scale factor above 1:20, and ideally without narrowing the model spillway width;
- Determine the minimum effective air vent dimensions to alleviate the severe pressure and air concentration conditions of drowned splitters. Only two air vent sizes were tested during the study, and therefore the optimal size remains to be found;
- Study the flow of air within the aeration gallery (possibly by means of CFD) with the goal of optimising the minimum dimensioning of the gallery in order to maintain air vent performance. The conservative safety factor of 2.0 used in the dimensioning of the aeration gallery can be decreased to a more optimal number;
- Uncertainty exists on the pressures of the step downstream of the splitters. The effect of aeration on these pressures can be studied with the goal of avoiding cavitation in this area. A large model is needed for this purpose, including the entirety of the spillway and the toe of the dam, as the air underneath the nappe of the projected jet played an important role in the aeration of the flow downstream of the step (see Section **Error! Reference source not found.**);

- If at all possible, undertake prototype measurements of air velocities and observations on air flow within the aeration gallery of an existing prototype case, such as the Gariep or Vanderkloof Dams, during a spilling event.
- Determine the maximum design head for unaerated splitters, above Roberts' (1943) limit of 3.0 m, in order to completely avoid any cavitation risks at this design head. Further determine an upper limit to additional head above the design head where cavitation would still be avoided.

REFERENCES

Acharjya, N. 2014, *A short trip to the Wadi Dayqah dam*, 1st edn, mymirusing.blogspot.co.za, Oman.

Amador, A., Sànchez-Juny, M. & Dolz, J. 2005, "Discussion of "Two-Phase Flow Characteristics of Stepped Spillways" by Robert M. Boes and Willi H. Hager", *Journal of Hydraulic Engineering,* vol. 131, no. 5, pp. 421-423.

Aurecon 2016, 20 April 2016-last update*, Berg Water Project, South Africa* [Homepage of Aurecongroup], [Online]. Available: http://www.aurecongroup.com/en/projects/water/berg-water-project.aspx [2016, 22 July].

Back, P.A.A., Frey, J.P. & Johnson, G. 1973, "P. K. le Roux Dam Spillway Design and Energy Dissipation", *Proc. 11th ICOLD Congress, Madrid, Spain,* vol. Q. 41, R. 76, no. II, pp. 1439-1468.

Back, P. & Mee, W. 1991, "The Victoria Project, Sri Lanka: Project Planning and Design of Victoria Dam", *Proceedings of the Institution of Civil Engineers,* vol. 90, no. 2, pp. 281-311.

Badenhorst, D. 2016, "Forward", *Appropriate technology to ensure proper Development, Operation and Maintenance of Dams in Developing Countries*, ed. L. Hattingh, South African Committee on Large Dams, Johannesburg, 18 May 2016, pp. iii.

Bird, J. & Wallace, P. 2001, "Dams and development–an insight to the report of the World Commission on Dams", *Irrigation and Drainage,* vol. 50, no. 1, pp. 53-64.

Bosman, E. & Basson, G.R. 2012, Investigation of Unsteady Flow Conditions at Dam Bottom Outlet Works Due to Air Entrainment During Gate Closure: Physical Modelling, Water Research Commission Report TT528-12, Republic of South Africa.

Calitz, G. 2014, *The Effect of Aeration on Local Negative Pressures of Roberts Splitters,* Final Year Research Dissertation. University of Stellenbosch.

Calitz, G. & Basson, G.R. 2015, "The Design of Roberts Splitters for Energy Dissipation at Dam Spillways", *Design and Construction of Hydraulic Structures Course,* University of Stellenbosch, Stellenbosch, September 2015, pp. 223.

Calitz, J.A. 2015, *Investigation of air concentration and pressures of a stepped spillway equipped with a crest pier*, Stellenbosch University.

Chadwick, A., Morfett, J. & Borthwick, M. 2013, *Hydraulics in civil and environmental engineering,* 5th edn, Taylor & Francis Group, Boca Raton, Florida.

Chanson, H. 2013, "Hydraulics of aerated flows: quid pro quo?", *Journal of Hydraulic Research,* vol. 51, no. 3, pp. 223-243.

Chanson, H. 2009, "Turbulent air – water flows in hydraulic structures: dynamic similarity and scale effects", *Environmental fluid mechanics,* vol. 9, no. 2, pp. 125-142.

Chanson, H. 1993, "Stepped spillway flows and air entrainment", *Canadian Journal of Civil Engineering,* vol. 20, no. 3, pp. 422-435.

Chanson, H. 1992, *Air Entrainment in Chutes and Spillways*, The University of Queensland - Department of Civil Engineering, Brisbane, Australia.

Chanson, H. 1988, *A study of air entrainment and aeration devices on a spillway model*, University of Canterbury, Christchurch, New Zealand.

Chen, Q., Dai, G. & Liu, H. 2002, "Volume of fluid model for turbulence numerical simulation of stepped spillway overflow", *Journal of Hydraulic Engineering,* vol. 128, no. 7, pp. 683-688.

Collier, M., Webb, R.H. & Schmidt, J.C. 1996, *Dams and rivers: a primer on the downstream effects of dams,* US Dept. of the Interior, US Geological Survey.

CSIR - Division of Earth, Marine and Atmospheric Science and Technology 1990, *Katse Dam 1:70 Hydraulic Model Tests*, Private - Lesotho Highlands Consultants.

Da Silva, A.M., Young, C.C. & Levitus, S. 1995, "Toward a revised Beaufort equivalent scale", *Proc. Int. COADS Winds Workshop,* Citeseer, pp. 270.

Denys, F.J.M. 2015, "Piano key weir spillway standard design principles", *Design and Construction of Hydraulic Structures*, ed. A. Bosman, Stellenbosch University, Stellenbosch, 28 September 2015, pp. 388.

Durieux, J.H. 2015, "Concrete Dam Design and Construction Considerations", *Design and Construction of Hydraulic Structures Course,* University of Stellenbosch, Stellenbosch, 2015/09/28, pp. 235.

DWS 2014, 8 March 2014-last update*, Midmar Dam: KwaZulu-Natal* [Homepage of Department of Water & Sanitation], [Online]. Available: http://www.ewisa.co.za/misc/DamKZNMidmar/MidmarDam.htm [2016, 22 July].

EDF 2016, 10 June 2016-last update*, Piano keys for reconfigured dam* [Homepage of EDF], [Online]. Available: https://www.edf.fr/en/the-edf-group [2016, 22 July 2016].

Elevatorski, E.A. 1959, *Hydraulic energy dissipators,* 1st edn, McGraw-Hill, New York.

Falvey, H. 1982, "Predicting cavitation in tunnel spillways", *International Water Power and Dam Construction,* vol. 34, no. 8.

Fraser, C.N. 2016, *Ski-Jump Energy Dissipation*, University of Stellenbosch.

Geringer, J.J. 2015, "Planning and Site Selection of Dams", *Design and Construction of Hydraulic Structures Course,* University of Stellenbosch, Stellenbosch, 2015/09/28, pp. 1.

Gleick, P.H. 2009, "Three Gorges Dam Project, Yangtze River, China" in *The world's water 2008–2009: the biennial report on freshwater resources* Island Press Washington DC, pp. 139-150.

Gonzalez, C.A. & Chanson, H. 2007, "Hydraulic design of stepped spillways and downstream energy dissipators for embankment dams", *Dam Engineering,* vol. 17, no. 4, pp. 223-244.

Google Earth. 2015, *Plover Cove Dam 22°27'51.65" N 114°15'37.11" E*, 2015/09/29 [Viewed 2016/06/22].

Hagen, D.J. 2015, "Earthfill Dam Design and Construction", *Design and Construction of Hydraulic Structures Course,* University of Stellenbosch, Stellenbosch, 2015/09/28, pp. 66.

Heller, V., Hager, W.H. & Minor, H. 2005, "Ski jump hydraulics", *Journal of Hydraulic Engineering,* vol. 131, no. 5, pp. 347-355.

Houston, K.L. 1983, "Hydraulic model study of Hyrum Dam auxiliary labyrinth spillway", *All US Government Documents (Utah Regional Depository)*, pp. 159.

ICOLD 2016, 2016/03/04-last update*, Purposes of Dams* [Homepage of International Commission on Large Dams], [Online]. Available: http://www.icold-cigb.org/GB/World_register/general_synthesis.asp [2016, 06/22].

Isaks, G. 2016, The aeration gallery of the Gariep Dam, personal interview by G. Calitz, 29 June.

Jackson, S. & Sleigh, A. 2000, "Resettlement for China's Three Gorges Dam: socio-economic impact and institutional tensions", *Communist and Post-Communist Studies,* vol. 33, no. 2, pp. 223-241.

Jordaan, J.M. 1989, "The Roberts Splitter: Fifty years on", *The Civil Engineer in South Africa,* vol. 31, no. 10, pp. 319-319-321.

Khatsuria, R.M. 2005, *Hydraulics of Spillways and Energy Dissipators,* 1st edn, Marcel Dekker, New York.

Langa, M.C. 2015, *Dam spillway energy dissipation by Roberts splitters: Study of cavitation and aeration requirement,* Final Year Research Dissertation. University of Stellenbosch.

Lee, H.S. 1999, *Assessment of potential aerodynamic effects on personnel and equipment in proximity to high-speed train operations*, U.S. Department of Transportation, Washington.

Lide, D.R. 2005, *Handbook of chemistry and physics,* CRC press, Florida.

Madamombe, L. 2002, *The Economic Development of the Kapenta Fishery Lake Kariba (Zimbabwe/Zambia)*, University of Tromsø.

Mason, P.J. 2016, Roberts Splitters, email to G. Calitz, 24 July. [Online] Available: 16451120@sun.ac.za.

Mason, P.J. 2012, "A guide to safe and cost effective spillways", *Hydro 2012: Symposium of The International Journal on Hydropower and Dams*, ed. P.J. Mason, International Journal on Hydropower and Dams, London, 29 October 2012, pp. 1.

Mason, P.J. 2004, *A guide to energy dissipaters*, HRW, London.

Mason, P.J. 1983, "Energy dissipating crest splitters for concrete dams", *International Water Power & Dam Construction,* vol. 35, no. 11, pp. 37-40.

May, R. 1987, "Cavitation in hydraulic structures: Occurrence and prevention".

Montgomery, D.C. & Runger, G.C. 2007, *Applied statistics and probability for engineers,* 4th edn, John Wiley & Sons, New Jersey.

Morris, J.D. 2012, 27 August-last update*, Cavitation* [Homepage of Institute for Creation Research], [Online]. Available: http://www.freerepublic.com/focus/f-news/2923323/posts [2016, 5 August].

Moyo, P. & Oosthuizen, C. 2009, "Dynamic testing of a concrete arch dam", *3rd International Operational Modal Analysis Conference*, ed. Curran Associates, IOMAC, L'Aquila, Italy, 4 May 2009, pp. 103.

Nikseresht, A.H., Talebbeydokhti, N. & Rezaei, M.J. 2013, "Numerical simulation of two-phase flow on step-pool spillways", *Scientia Iranica A,* vol. 20, no. 2, pp. 222-230.

Noret, C., Girard, J., Munodawafa, M. & Mazvidza, D. 2013, "Kariba dam on Zambezi river: stabilizing the natural plunge pool", *La Houille Blanche*, no. 1, pp. 34-41.

Novak, P., Moffat, A., Nalluri, C. & Narayanan, R. 2007, *Hydraulic structures,* 4th edn, Taylor & Francis, New York.

Roberts, C.P.R. 1980, *Hydraulic Design of Dams*, Department of Water Affairs, Forestry and Environmental Conservation, Pretoria.

Roberts, D.F. 1943, "The dissipation of the energy of a flood passing over a high dam", *Proceedings of the South African Society of Civil Engineers,* vol. XLI, no. 1, pp. 48-48-92.

Roberts, P.R. 2011, 2011/06/24-last update*, Beervlei Dam* [Homepage of Department of Water and Sanitation], [Online]. Available: http://www.ewisa.co.za/misc/DamECBeervlei/BeervleiDam.htm [2016, 06/22].

Roberts, P.R. 1977, "Energy dissipation by dam crest splitters", *The Civil Engineer in South Africa,* vol. 19, no. 11, pp. 263-263-264.

Robertson, G.K. 2014, *Labyrinth weir hydraulics: validation of CFD modelling*, Stellenbosch: Stellenbosch University.

Rogers, J.D. 2010, "Hoover Dam: Operational Milestones, Lessons Learned, and Strategic Import", *Hoover Dam: 75th Anniversary History Symposium,* ASCE, pp. 189.

Schnitter, N. 1994, *A History of Dams: The Useful Pyramids,* 1st edn, Balkema, Rotterdam.

Shah, Z. & Kumar, M.D. 2008, "In the midst of the large dam controversy: objectives, criteria for assessing large water storages in the developing world", *Water Resources Management,* vol. 22, no. 12, pp. 1799-1824.

Shand, M.J. 2015, "Energy dissipation at dams and outlet works design", *Design and Construction of Hydraulic Structures*, ed. Stellenbosch University, Stellenbosch University, Stellenbosch, 28 September 2015, pp. 174.

Tomita, Y. & Shima, A. 1986, "Mechanisms of impulsive pressure generation and damage pit formation by bubble collapse", *Journal of Fluid Mechanics,* vol. 169, pp. 535-564.

Tukey, J.W. 1977, "Box-and-whisker plots" in *Exploratory data analysis* Addison-Wesley MA, Reading, PA, pp. 39-43.

USBR 1987, *Design of Small Dams,* 3rd edn, United States Department of the Interior: Bureau of Reclamation.

Van Vuuren, L. 2011, "Blyderivierspoort - Dam of extraordinary beauty", *Water Wheel,* vol. 10, no. 6, pp. 30-32.

Van Vuuren, L. 2008, "Loskop Dam - Early Local Engineering Ingenuity: Water History", *Water Wheel,* vol. 7, no. 5, pp. 18-21.

vanderkloofdam.com 2014, 2014, March 23-last update, *About Vanderkloofdam*. Available: http://www.vanderkloofdam.co.za/about/ [2014, 2014, October 24].

Wood, I.R., Ackers, P. & Loveless, J. 1983, "General method for critical point on spillways", *Journal of Hydraulic Engineering,* vol. 109, no. 2, pp. 308-312.

Wright, H. 2006, *Protrusions on Stepped Spillways to Improve Energy Dissipation*, University of Stellenbosch.

PART II – APPENDICES

APPENDIX A
BACKGROUND ON DAMS

A.1. Brief History on Dam Construction

In the simplest sense, a dam is a structure to store water from a stream. It consists of the reservoir of water that is being contained by a dam structure (Chadwick *et al.*, 2013). Humans have been building dams in Cairo approximately 5000 years ago (Collier *et al.*, 1996).

The reasons for building these ancient dams ranged from flood control to irrigation, but remained very basic in nature, revolving around the needs of the settlements of those periods (Shah & Kumar, 2008). Today the list of reasons for building dams is long and complex – for water storage to serve municipal, agricultural and industrial needs; for flood control and improved navigation; for sediment trapping; for improvement of water quality; for electrical generation; for recreation, aesthetic, and wildlife requirements (Collier *et al.*, 1996). As dams became larger and more expensive, a few benefits only could not justify the construction thereof. Most dams built after 1950 had to serve a combination of purposes (Collier *et al.*, 1996).

Some very early civilisations considered the construction of dams a vital part of their technological progress. Even though not technically qualifying as dams, the earliest evidence of river engineering can be found among the ruins of irrigation canals in Mesopotamia, which are over 8000 years old (Shah & Kumar, 2008). The earliest functioning dams were in Jordan, Egypt and parts of the Middle East, which date back to at least 3000 BC (Shah & Kumar, 2008). Table A-1 shows a chronological list of ancient dams that were constructed before the birth of Christ (BC).

Table A-1: Chronological list of ancient dams (Schnitter, 1994, Shah & Kumar, 2008)

Year Completed (Approx.)	Country	Name of Dam	Type	Function	Purpose
3000 BC	Jordan	Jawa	Gravity	Reservoir	Water supply
2600 BC	Egypt	Sadd el-Kafara	Embankment	Reservoir	Flood control
2500BC	Baluchistan	Gabarbands	Gravity	Reservoir	Conservation

Table A-1: Chronological list of ancient dams (Schnitter, 1994, Shah & Kumar, 2008)

Year Completed (Approx.)	Country	Name of Dam	Type	Function	Purpose
1500 BC	Yemen	Marib	Embankment	Diversion	Irrigation
1260 BC	Greece	Kofini	Embankment	Diversion	Flood control
1250 BC	Turkey	Karakuyu	Embankment	Reservoir	Water supply
950 BC	Israel	Shiloah	Unknown	Reservoir	Water supply
703 BC	Iraq	Kisiri	Gravity	Diversion	Irrigation
700 BC	Mexico	Purron	Embankment	Reservoir	Irrigation
581 BC	China	Anfengtang	Embankment	Reservoir	Irrigation
370 BC	Sri Lanka	Panda	Embankment	Reservoir	Irrigation
275 BC	Sudan	Musawwarat	Embankment	Reservoir	Water supply

The number, size and complexity of dam construction increased with advances in science and technology. As such, the growth of large dams accelerated, especially during the nineteenth and mid-twentieth centuries (Shah & Kumar, 2008). In 1900, there were approximately 600 large dams in existence. The figure grew to nearly 5,000 large dams by 1950. According to the International Commission on Large Dams (ICOLD), the current number of large dams internationally is 58 402 (ICOLD, 2016).

In this time of population growth combined with industrial development and rapid urbanization, the acceleration of economic growth was not possible without the generation of power and availability of water for agriculture and domestic consumption. Thus, dam-construction was a critical requirement for meeting the growth requirements of all social and economic sectors (Shah & Kumar, 2008). By the turn of the 21st century, estimates suggested that nearly 30 - 40% of irrigated land worldwide relied on dams and that dams generated 19% of the world's electricity (Bird & Wallace, 2001).

A.2. Modern Definition of Large Dams

The International Commission on Large Dams (ICOLD) currently provides the most recent and widely accepted definition of large dams (ICOLD, 2016, Shah & Kumar, 2008). This definition has a minimum dam height of 15m (from the lowest foundation to the crest) as the major criterion (ICOLD, 2016, Shah & Kumar, 2008). There are however further criteria that would classify dams with a height between 10-15m as large dams. According to Shah & Kumar (2008) this is the case if:

1. The crest length is more than 500m;

2. The reservoir capacity is more than 1 million m^3;
3. The maximum flood is more than 2,000 m^3/s;
4. The foundations have complex problems;
5. The dam is an unusual design.

In South Africa the conventions of the South African National Committee on Large Dams (SANCOLD) are followed regarding the definition of large dams. The SANCOLD definitions are in close relations to those of ICOLD. As of May 2016, SANCOLD have included 1,114 large dams in the South African Register of Large Dams according to the following criteria (Badenhorst, 2016):

- The dam height must be at least 15 m above the lowest point of the foundation to be classified as a large dam.

Dams with heights between 5 m and 15 m impounding more than 3 million m^3 are also included in the register, but with limited statistical information.

A.3. Types of Dams

The classification of dams can be done in many ways. Dams can be classified according to its use, its construction material or according to the dam's safety legislation. Dams may be classified according to the broad functions they serve; this includes storage dams, flood detention dams and non-overflow dams (Wright, 2006, Calitz, 2014).

The most common classification is however, based upon the materials comprising the structure. The two main categories according to this classification are (a) embankment dams, and (b) concrete dams. By ICOLD's definition, an embankment dam is any dam built from earth or rocks and a concrete dam is any dam built from concrete (Hagen, 2015, Durieux, 2015).

Within these two main categories, dams are further classified according to their materials and structure. Below is a summarised list of embankment dam types classified according to their construction materials (Hagen, 2015):

- Earthfill (TE) embankment dam;
- Clay core rockfill (CCR) embankment dam;
- Concrete faced rockfill (CFR) embankment dam;
- Asphalt faced rockfill (AFR) embankment dam.

Below is a list of concrete dam types and their uses, defined according to construction materials and structural features (Durieux, 2015, Wright, 2006):

- Concrete gravity dam – for wide valleys;
- Concrete arch gravity dam – for relatively steep valleys;
- Concrete arch dam – for steep valleys with good foundations;
- Double curvature concrete arch dam – a very high dam for steep valleys with good foundations;
- Composite dam – for relatively wide valleys;
- Concrete arch dam with abutments – for relatively wide valleys with good foundations;
- Concrete buttress dam – for versatile valley shapes;
- Concrete multiple cylindrical arch dam – for wide valleys;
- Masonry multiple arch dam – for wide valleys with good foundations.

A.4. The Purpose of Dams

In the simplest sense, a dam is any structure, for instance a wall, built in a valley or gorge with the purpose of storing water behind it. A dam consists of the reservoir of water that is being impounded by a dam structure (Chadwick *et al.*, 2013). A natural stream or river can flow in this valley, or in the case of off-channel storage dams no natural stream or river exists and water is often pumped into the reservoir. Some of the earliest evidence of dam building by humans dates back approximately 5000 years to Cairo, Egypt (Collier *et al.*, 1996).

The reasons for building these ancient dams ranged from flood control to irrigation, but remained very basic in nature, revolving around the needs of the settlements of those periods (Shah & Kumar, 2008). Today the list of reasons for building dams is long and complex – for water storage to serve municipal, agricultural and industrial needs; for flood control and improved navigation; for sediment trapping; for improvement of water quality; for electrical generation; for recreation, aesthetic, and wildlife requirements (Collier *et al.*, 1996). As dams became larger and more expensive, the construction thereof could not be justified by only a few benefits. Most dams built after 1950 had to serve a combination of purposes (Collier *et al.*, 1996).

Modern dams can serve a multitude of purposes including, but not limited to the following (Geringer, 2015):

A.4.1. Water Supply for Domestic and Industrial Use

Because of increasing urbanisation, population growth and industrial growth, this remains one of the main purposes of dams. Even in ancient times, this was an integral reason for the construction of dams, as seen by the construction of the Ajilah Dams on the Kosr River in Iraq, dating back to 694 BC to accommodate the water demands of Niniveh (Schnitter, 1994). An example of a very unconventional water supply dam is the Plover Cove Dam in Hong Kong. Completed in 1968, the Plover Cove Dam (Figure A-1) is built in the seawater bay formed by two landmasses. Upon completion, the seawater was drained and the reservoir was allowed to fill with the fresh water runoff of the area. After its 1973 raising the dam increased in capacity from 170 million m^3 to 230 million m^3 (Geringer, 2015).

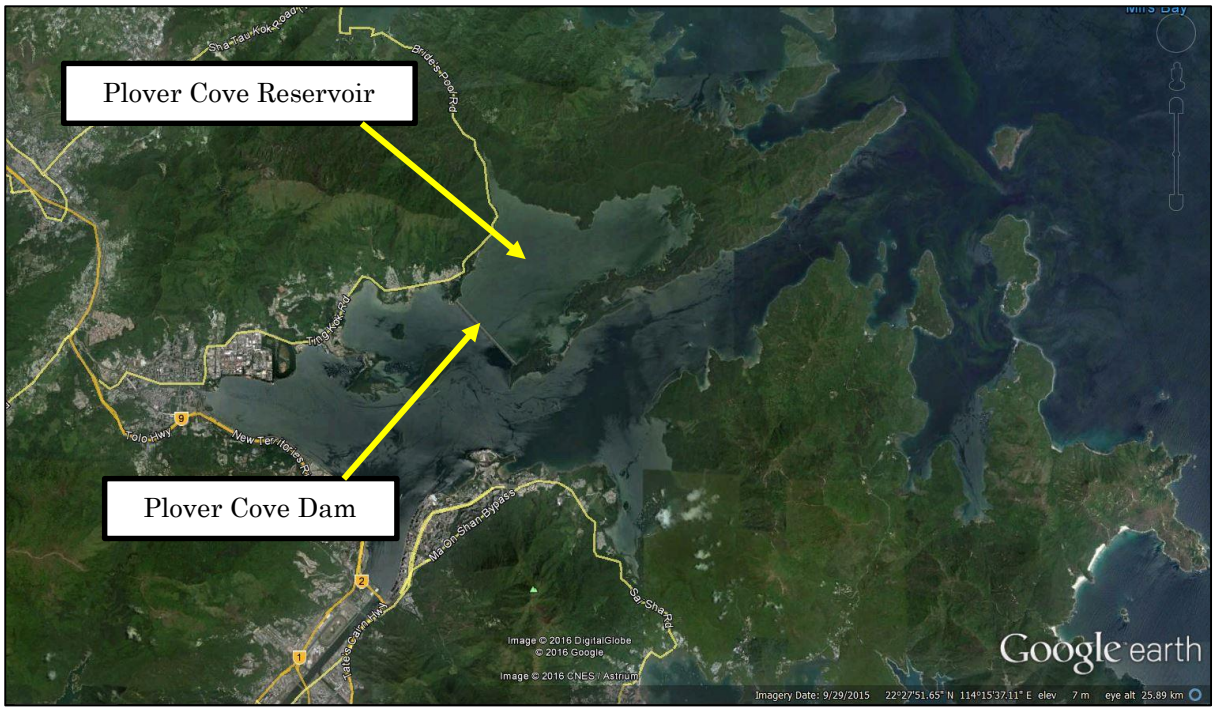

Figure A-1: Aerial Photograph of Plover Cove Dam (Google Earth, 2015)

A.4.2. Generation of Hydropower

In modern times, the provision and use of environmentally friendly renewable energy has come to the fore. This means that the generation of electricity through hydropower has become probably the second main purpose for the construction of dams, especially in countries where an abundance of water exists. The biggest dam in the world, in terms of power generation, is the Three Gorges Dam in the Yangtze River valley in China. It currently has a capacity of 22,400 MW, surpassing the 14,000 MW capacity of the Itaipu Dam in Brazil (Jackson & Sleigh, 2000, Gleick, 2009).

In South Africa, and elsewhere in the world, where the topography lends itself to it, pump-storage schemes have been constructed to generate power during peak periods by discharging water from a higher reservoir to a lower one. During off-peak periods where electricity demand is low, the water can be pumped back to the top reservoir preparing the scheme once more for high demand peak periods. The Drakensberg Pump-Storage Scheme is an example where these types of dams have been utilised in South Africa (Geringer, 2015).

A.4.3. Irrigation Water Supply

The construction of dams for this purpose has decreased in recent times due to more efficient irrigation. Irrigation does however remain one of the main reasons for dam construction. The Loskop Dam, in Mpumalanga, is an example of a South African dam primarily built for the irrigation of the surrounding farmland (Geringer, 2015). The Loskop Dam was also the first dam where Roberts splitters were used on its spillway (Van Vuuren, 2008).

A.4.4. Flood Protection

The usage of dams for flood protection is common worldwide, but in most cases such dams are built as multipurpose dams. For example, the Gariep and Vanderkloof Dams are both built to provide irrigation and power generation, but also to provide flood protection to the lower Orange River. The Beervlei Dam (Figure A-2), located in the Eastern Cape, South Africa, is an excellent example of a dam solely built for the purpose of flood protection. The Karoo sediments in the valley are very saline and thus the runoff is not suited for storage (Roberts, 2011). The operation of the dam relies on the reservoir to be as empty as possible before a flood event and that the resulting floodwater be used as fast as possible afterwards.

Figure A-2: The Beervlei Dam – an example of a flood protection dam (Roberts, 2011)

A.4.5. Military Defence

Dams can be built to prevent navigation on rivers, therefor protecting inland cities from enemy fleets. Reports suggest that Alexander the Great destroyed all the Persian weirs in the Tigris River built for this purpose upon his return from India in 324 BC (Geringer, 2015).

A.4.6. Reclamation of Land

Dams can be built to restore a previously eroded valley to its former topography and shape by retaining the sediment of a river or stream. In South Africa, the Department of Agriculture's Land Conservancy Section provides legislation to continue building dams to reclaim land (Geringer, 2015).

A.4.7. Fisheries

In South Africa, there exists many dams with the purpose of providing fishing opportunity. This ranges from rainbow trout and largemouth bass dams on private farms to dams aimed at commercially breeding catfish as a food supplement (Geringer, 2015). In most cases however, fisheries are created naturally after impoundment. It is reported that more than 25,000 tonnes of kapenta fish are caught annually in the

Kariba Dam on the Zimbabwean border with Zambia for commercial purposes (Madamombe, 2002). This is besides the Kariba Dam being a premier sport fishing lake.

A.4.8. Environmental Purposes

Despite the general view that dams negatively affect the environment through flooding and abnormally cooler discharges, there are instances where dams are built to protect the environment. In the mining industry, dams are used to impound contaminated chemical water and prevent it from joining a natural watercourse. The same approach is followed in preventing raw sewage effluent from re-entering a natural watercourse.

A.4.9. Diversion / Abstraction

River abstraction is a very effective means to obtain water from a river. It is often needed to create a reservoir in the river in order to create enough head for the inlets of diversion canals on the river bank(s) or to accommodate the requirements of abstraction pumps. These weirs can be as low as 1 m or as high as 50 m. The Katse Dam, with a wall height of 185 m (CSIR - Division of Earth, Marine and Atmospheric Science and Technology, 1990), can be seen as an extreme case of a dam built for river diversion as it is essentially diverting water from Lesotho to South Africa (Geringer, 2015).

A.4.10. Aesthetic Appeal

Even from ancient times aesthetic appeal has driven the intentional formation of lakes and bodies of water within urbanised environments. In modern times, the Centurion Lake (Gauteng, South Africa) serve as an example of an aesthetic body of water to enhance the experience at nearby shopping malls and apartments. However, careful planning of such dams is needed as in the case of the Centurion Lake, sedimentation problems have completely spoiled the aesthetic appeal of the lake (Geringer, 2015).

A.4.11. Improvement of River Navigation

The water levels in several rivers have been raised through the building of dams, with the main purpose of making them more navigable. In many instances these dams also had good potential for power generation as water storage within the said river was not deemed a discernible objective. On the other hand, storage dams have been built on rivers to feed separate navigation canals (Geringer, 2015). Examples of rivers where navigation have been improved through damming include the Rhine, Danube, Dnepr, Volga, Hudson and Tigris. In order to navigate rivers that have been dammed, a ship

lock is needed. Therefor the location for such a dam is an important consideration in the design process, as a suitable site for a ship lock must be available.

A.4.12. Tailings Dams

The tailings dams of mines are usually constructed on level ground. If, however, more or less level ground is not available, the spoils of the mining activity are stored in conventional reservoirs, designed in a valley or gorge. These dams have traditionally been raised to accommodate the increase in storage demands of these mines. An example of a tailings dam is the Sheep Creek Dam, proposed for the Echo Bay Mines in Alaska. A roller compacted concrete (RCC) dam was selected and designed as a 60 m high 3-phased arch-gravity dam to be raised initially to 82 m and finally to 99 m (Geringer, 2015).

A.4.13. Recreation

It is rare that the purpose for the construction of a dam is solely recreational. Recreational activities and the provision thereof are normally only considered close to, or after, the commissioning of a dam. The Water Resource Management Plan's (WRMP) policies of the DWS are used to zone South African state dams for recreational purposes (Geringer, 2015).

A.4.14. Cofferdams

A cofferdam is a temporary dam structure built to isolate part or all of main dam site. This is done to divert a watercourse so the foundations of the main dam can duly be constructed. Cofferdams differ in size and is dependent on the size of the flood in question, usually the 6-month to 2-year flood, depending on the construction time of the dam. Because of this variability, different types of dams are common, ranging from RCC dams to thin concrete arch dams, to the most common type, the embankment dam. The height of a cofferdam can be immense to ensure safety and a due construction time frame for the main dam, as was the case for the Three Gorges Dam, where some of the cofferdams had heights in excess of 100 m (Geringer, 2015).

A.4.15. Tailpond Dams

The purpose of a tailpond dam is to raise the tailwater level at very high dams with ski jump, orifice outlet or free overfall type spillways, where excessive downstream scouring and erosion might be a problem resulting from the impacts of the plunging jets. To avoid any risk of undermining of the main dam's structure, a tailpond dam is designed in close

relations to the spillway of the main dam (Geringer, 2015). Although dwarfed by the main dam, tailpond dams can be quite large and could still fall into many definitions of a large dam, requiring all the due attention and safety precautions. The scouring force of the Katse Dam spillway's plunging jet required the construction of a 35 m high tailpond dam (CSIR - Division of Earth, Marine and Atmospheric Science and Technology, 1990).

APPENDIX B
BACKGROUND ON DAM SPILLWAYS

B.1. Dam Spillways

As mentioned in Chapter 1 the main report, spillways are chutes or channels, designed to safely discharge a dam's excess flood water back into the river valley to avoid damage, and ultimately failure, of the dam by overtopping (Chadwick *et al.*, 2013). Any spillway can be operated in one of two ways: either controlled or uncontrolled. A controlled spillway usually has crest gates or sluices somewhere present to enabled the volume of discharge to be controlled and throttled according to the demand of the downstream river or to effectively route a severe flood event. An uncontrolled spillway is exactly the opposite, where there are no such devices present and the excess water is allowed to freely discharge at certain, predefined stages (Geringer, 2015).

The different types of dam spillways are listed and briefly described below (Chadwick *et al.*, 2013, Geringer, 2015):

B.1.1. Ogee Spillway

The ogee spillway is by far the most common type of spillway used, as it is easy to construct and can be effectively used for a wide range of hydraulic conditions (Chadwick *et al.*, 2013). An ogee spillway basically comprises a steeply sloping open channel, with a rounded crest at its entry. The open channel's profile resembles that of the nappe formed from a sharp-crested weir. The trajectory of the nappe will vary with the head H above the crest of the ogee. This implies that for the design head H_d, there will only be one correct ogee profile. The entire crest section will be designed specifically for the design head of the spillway. The shape of the ogee may however, be designed for lower discharges than that of the design head. This practice is described in Section 2.3.1 of the main report. Below the crest section is the steeply sloping 'face' followed by the 'toe'. With general ogee spillways the toe will be curved to form a tangent to the apron at the base of the dam (Chadwick *et al.*, 2013). The point of tangency (Figure B-1) marks the

point at which the slope of the crest section matches the downstream slope θ, normally expressed in terms of horizontal dimension against vertical dimension (H:V). An ogee spillway is normally used on concrete gravity and arch-gravity dams, and may sometimes be found on composite dams (Geringer, 2015).

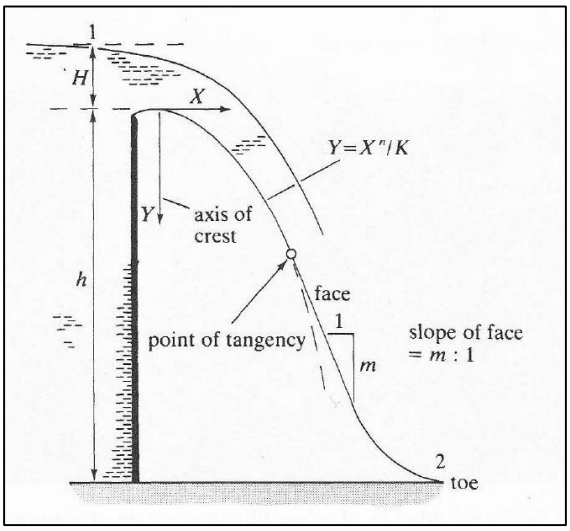

Figure B-1: Typical section of an ogee spillway (Chadwick *et al.*, 2013)

B.1.2. Free Overfall Spillway

A free overfall spillway is common on high arch dams where the discharge falls freely to a plunge pool downstream of the dam. The underside of the nappe is supported by air and must be ventilated sufficiently to avoid a fluctuating and pulsating jet (Geringer, 2015). The biggest risk associated with free overfall spillways is the possibility of scour within the plunge pool. If not designed properly or not monitored continuously, this could lead to catastrophic damage through undermining of the foundations of the dam. An example of a scour hole that must be monitored continuously to avoid failure of the dam is that of the Kariba Dam (Noret *et al.*, 2013). Figure B-2 shows the free overfall spillway of the 72 m high Roode Elsberg Dam in the Western Cape of South Africa.

Figure B-2: Spillway of the Roode Elsberg Dam (Moyo & Oosthuizen, 2009)

B.1.3. Stepped Spillway

Since ancient times, stepped spillways have been used, but have recently seen a considerable revival in terms of design consideration as the construction thereof is fairly simple and very cost effective for a roller compacted concrete (RCC) dam (Wright, 2006). A further advantage of the stepped spillway is the considerable energy dissipation caused by the steps, resulting in cheaper energy-dissipating devices at the toe of the dam (Geringer, 2015). The discharge capacity of the spillway is the main disadvantage as it is limited by cavitation risks to about 30 m^2/s (Wright, 2006).

B.1.4. Side-channel Spillway

This spillway type consists of an upstream weir at the side of the dam, turning the flow at a sharp angle (commonly 90°) to follow a steep chute back to the river. A side channel spillway is most suited to embankment dams with solid rock at its flanks (Geringer, 2015). The Berg River Dam in the Western Cape of South Africa (Figure B-3) is a modern embankment dam where a side channel spillway with modified splitters has been used (Aurecon, 2016, Calitz & Basson, 2015).

Figure B-3: Side channel spillway with modified splitters at the Berg River Dam (Aurecon, 2016)

B.1.5. Trough Spillway

A trough spillway is similar to a side channel spillway, with the main difference being that it is not situated on the flank of a dam due to the absence of suitable founding rock conditions. The Inyaka Dam in Mpumalanga in South Africa is equipped with a trough spillway (Geringer, 2015).

B.1.6. Morning Glory Spillway

A morning glory spillway, or shaft spillway, consists of a vertical shaft situated within the impoundment followed by an almost horizontal conduit extending under or through the dam wall structure back to the river channel downstream of the toe of the dam. At its intake, it has a horizontal rim designed to accommodate discharges of up to 1400 m^3/s. Blockage of the intake or shaft can be a serious risk, considerably lowering the discharge capacity and as such, auxiliary spillways and/or breaching sections (fuse plugs) should be used in conjunction with a morning glory spillway (Geringer, 2015).

B.1.7. Labyrinth Spillway

The main goal of a labyrinth spillway is to increase the crest length of a weir or dam crest with its zig-zag shape. This advantage diminishes as the total head on the crest increases. Generally, labyrinth spillways are used as weirs, with the Douglas weir on the Vaal River in South Africa being an example. A labyrinth spillway can be built on top of existing dam spillways to increase the reservoir's storage capacity while decreasing the head of the existing design flood and keeping freeboard requirements similar. If this is done properly, the non-overspill crests of dams needn't be raised while

effectively increasing the storage capacity of the reservoir. A South African example of this is the 3.5 m heightening of the Midmar Dam in KwaZulu-Natal in 2003 (Geringer, 2015), shown in Figure B-4.

Figure B-4: The labyrinth spillway of the Midmar Dam (DWS, 2014)

B.1.8. Piano Key Weir

Piano key weirs or spillways are a very modern type of spillway, only being developed in the late 1990's. It is effectively a modified type of labyrinth weir, and can be used for the same reasons, including heightening a dam while keeping the total head the same. Although comprehensive understanding of these structures are very limited, it has been used in several countries, including South Africa at the Hazelmere Dam in KwaZulu-Natal (Denys, 2015). Figure B-5 shows the piano key spillway of the Malarce Dam in France.

Figure B-5: The piano key spillway of the Malarce Dam in France (EDF, 2016)

B.1.9. Orifice Spillway

An orifice spillway is an opening in the dam wall with a controlling valve or gate. Its dissimilar to a morning glory spillway in the fact that it is not situated at the full supply level, and can thus discharge floods at different supply levels. It is mostly found in thin arch dams, such as the Cahora Bassa Dam in Mozambique (Geringer, 2015) and the Kariba Dam on the border of Zimbabwe and Zambia (Noret *et al.*, 2013). Figure B-6 shows a cross-section through the orifice spillway of the Kariba Dam. Note how the scour hole deepened though more than 40 years of continued spilling.

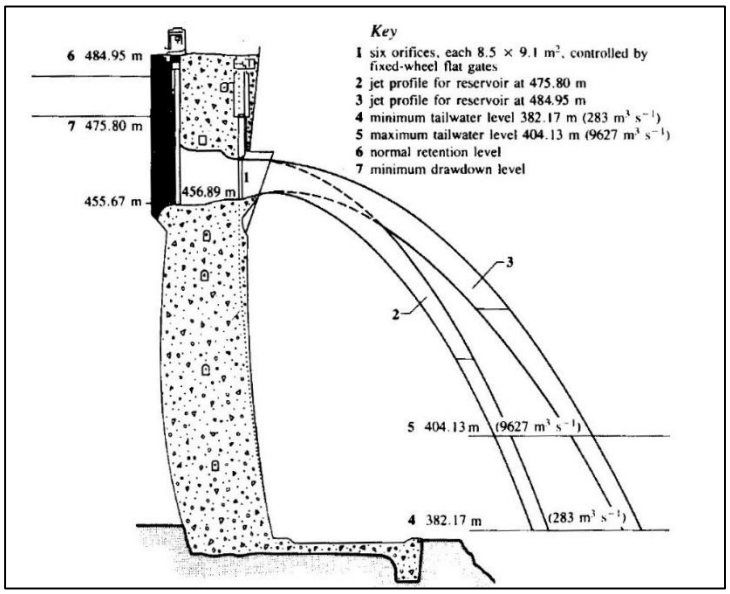

Figure B-6: Cross-section of the orifice spillway of the Kariba Dam (Novak *et al.*, 2007)

B.1.10. Saddle Spillway

Sometimes it is not possible to provide a spillway within the river section of the dam, and, if the local topography allows it, a saddle spillway can be built on a depression of the watershed adjacent to the dam section. A saddle spillway would comprise of a low weir-like spillway structure discharging the design flood down a chute to either the main river valley or side tributary. The Goedertrouw Dam in KwaZulu-Natal, South Africa, is an example where a saddle spillway is used (Geringer, 2015).

APPENDIX C
BACKGROUND ON ENERGY DISSIPATORS

C.1. Energy-Dissipating Measures on Dam Spillways

Although velocities within dam reservoirs remain negligibly small, the fluid still contains large amounts of potential energy directly proportional to the height of the dam. During floods, and in particular during spilling, the high potential energy of the reservoir changes to kinetic energy on the spillway (very high velocities and supercritical flow (Chadwick *et al.*, 2013)), and needs to be dissipated in order to safely discharge the fluid back into a waterway. Energy-dissipating measures are designed to safely convert the high kinetic energy of the fluid into heat and back to potential energy at the much lower tailwater level of the dam (Shand, 2015). These measures vary, but in principle all aim to break up the streams of water in some way or another by creating turbulence. This can happen anywhere on the spillway, including at the top near the crest, at the bottom close to the toe of the dam and even further way from the dam in mid-air. Below are examples of energy dissipators:

- Deflector buckets / Ski-jump deflector (Shand, 2015)
- Stilling basins / Hydraulic jump basins (USBR, 1987)
- Submerged buckets / Roller buckets (USBR, 1987, Shand, 2015)
- Stepped or baffled chutes (Mason, 2012, Wright, 2006)
- Crest splitters / Roberts splitters (Roberts, 1943, Mason, 1983, Mason, 2012)

Below are short descriptions of these energy-dissipating measures:

C.1.1. Deflector Buckets / Ski-jump Deflectors

Ski-jumps are intended to deflect flow with high velocities into the air to fall in a plunge pool some distance away and well below the end of the spillway and the toe of the dam (Shand, 2015). During the time the flow travels through the air, air is entrained into the jet. This reduces the scour potential of the jet as it impacts into the plunge pool (Heller

et al., 2005). Shand (2015) states that the simple Veronese formula is frequently used to predict the scour depth of the hole created by the discharge jet within the plunge pool. With low flows erosion below the end of the spillway can be a problem if insufficient protection exists. This is due to the lack of flow velocity causing the deflector bucket to perform properly. Figure C-1 below shows a simple diagram of a ski-jump energy dissipator.

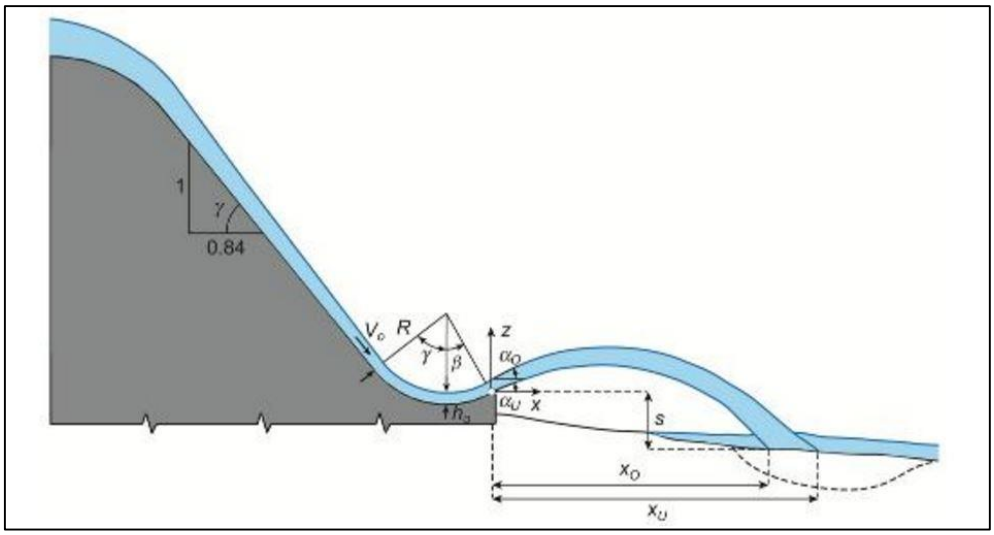

Figure C-1: Ski-jump energy dissipator (Heller *et al.*, 2005)

C.1.2. Stilling Basins / Hydraulic Jump Basins

A stilling basin is an energy dissipator situated at the toe of the dam, with a long chute feeding it at the upstream end. The use of a hydraulic jump is a natural and efficient way to dissipate energy over a wide range of Froude numbers. The use of United States Bureau of Reclamation's (USBR) stilling basins encourages a stable hydraulic jump to form and if designed properly, will efficiently convert supercritical flow to subcritical flow within the structure before safely discharging to the natural outlet watercourse (Shand, 2015). The USBR comprehensively tested a wide range of Froude numbers to develop a series of stilling basin configurations. Figure C-2 shows a USBR Type III stilling basin, designed to dissipate energy of flows with a Froude number greater than 4.5 and velocities less than 18 m/s. Note the teeth or splitters incorporated in the design, a principle similar to Roberts splitters. There have been several cases of cavitation within these structures. Cavitation is one of the major limiting factors of stilling basins and it has been stated by Mason (2012) that stilling basins operate optimally when the head difference between the reservoir level and the downstream tailwater level is less than 50 m.

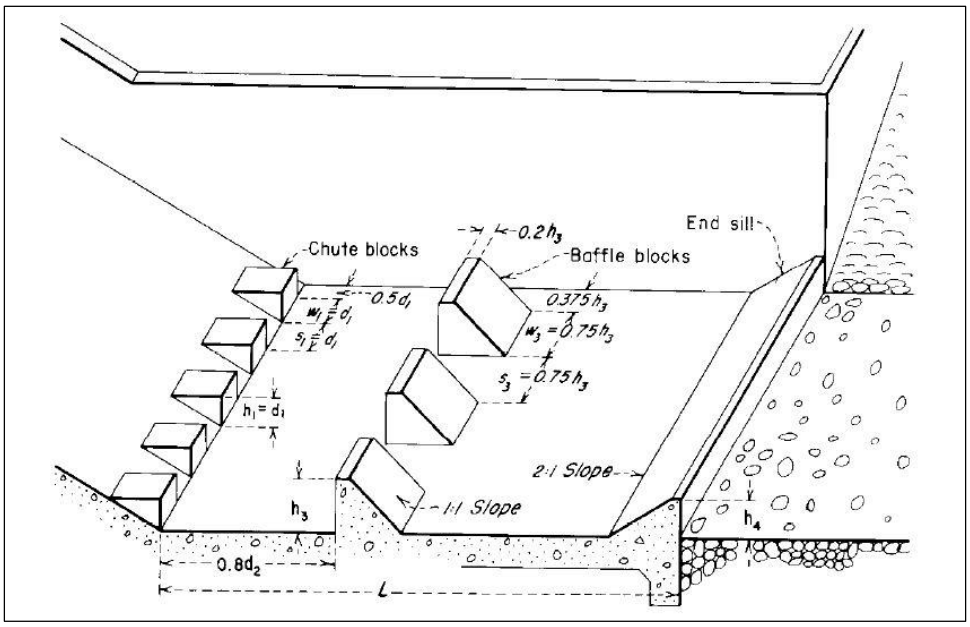

Figure C-2: USBR Type III stilling basin (USBR, 1987)

C.1.3. Submerged Buckets / Roller Buckets

Submerged buckets are similar to stilling basins, except that it is submerged. Thus, when the tailwater level is too high for a stable hydraulic jump to form within a stilling basin, a roller bucket like the one in Figure C-3 can be used. Once again the USBR tested and implemented these type of energy dissipators, and generalised two types of roller buckets: (a) solid type roller buckets and (b) slotted type roller buckets (USBR, 1987). Figure C-3 is an example of a slotted type roller bucket. As with the aforementioned stilling basin, note the presence of "teeth" or slots, with the potential of cavitation, limiting the design discharge of these structures.

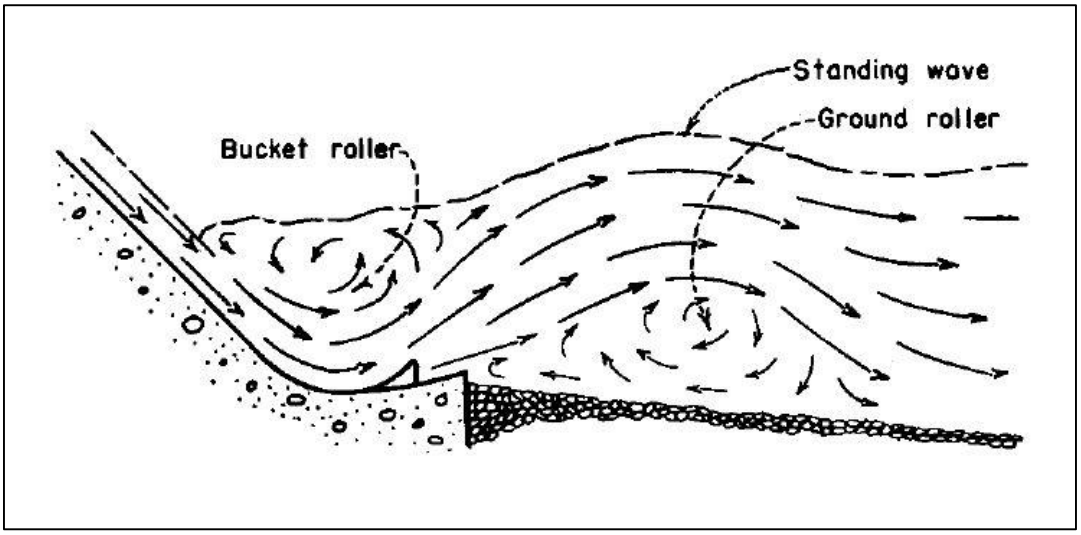

Figure C-3: USBR slotted type roller bucket (USBR, 1987)

C.1.4. Stepped or Baffled Chutes

Stepped or baffled chutes are designed to dissipate energy as water flows down them, leaving minimal energy at the end of the spillway left to dissipate, normally by means of a stilling basin or roller bucket. Stepped chutes encourages two distinct flow regimes: (a) nappe flow and (b) skimming flow (Mason, 2012). Nappe flow at lower flows. During nappe flow, the water cascades down each step separately as a series of waterfalls, dissipating energy each separate time until it reaches the bottom. Skimming flow occurs at higher flows, including the design discharge of the spillway. During skimming flow, the water skims over the steps, forming rotating vortices within the triangular depressions of the steps. During skimming flow, the energy dissipates gradually down the chute, with a lot more residual energy left at the bottom. Because of this, stepped chutes are generally designed with a second energy-dissipating structure at the end of the chute or spillway. Figure C-4 shows the stepped spillway of the Opuha Dam in New Zealand, with the simple stilling basin visible at the end of the chute.

Figure C-4: Stepped spillway of the Opuha Dam in New Zealand (Gonzalez & Chanson, 2007)

C.1.5. Crest Splitters / Roberts Splitters

Dam crest splitters, or Roberts splitters, has been proven to be an effective energy dissipation measure as it has been effectively used, even before 1989, on more than 30 dams worldwide (Jordaan, 1989). The total structure consists of a specific arrangement of splitters or “teeth” and a continuous step directly downstream of these splitters. They work together to disperse the flow that approaches from an upstream ogee crest, creates

severe turbulence and projects a highly aerated jet of water away from the toe of the dam to a plunge pool well below, limiting scour potential. It is a very versatile setup as it has been used on both arch and gravity dams as well as concrete spillways of embankment dams. It has also been used with gated and ungated spillways (Mason, 1983). Figure C-5 shows the Roberts splitters on the spillway of the Blyderivierspoort Dam in Mpumalanga, South Africa. The Blyderivierspoort Dam is 66 m high with a spillway capacity of 2 350 m^3/s, equivalent to a unit discharge of 26.1 m^2/s (Roberts, 1977). A detailed discussion on Roberts splitters is contained in the main report under Section 2.2.

Figure C-5: Roberts splitters on the spillway of the Blyderivierspoort Dam (Van Vuuren, 2011)

APPENDIX D
USBR (1987) OGEE DESIGN PROCEDURE

D.1. Design Procedure

The United States Department of the Interior Bureau of Reclamation (USBR) prescribes the following method of designing the nappe-shape of the ogee spillway. This method is widely used in South Africa and internationally.

The following symbols bears importance in the design (USBR, 1987):

Table D-1: Symbols used in USBR ogee design method

Symbol	Meaning
Q	Discharge over spillway
H_0	Design head
H_e	Actual observed head (total energy head)
C_0	Design constant
C_e	Effective constant
h_a	Additional head (incl. velocity head)
g	Gravitational constant (9.81 m/s^2)
K	Downstream profile constant
n	Downstream profile constant

Table D-2: Dimensions used in the USBR ogee design method

Symbol	Dimension
b	Effective spillway width
P	Upstream dam height
R_1	Upstream profile dimension
R_2	Upstream profile dimension
Y_C	Upstream profile dimension
X_1	Upstream profile dimension
X_C	Upstream profile dimension

The objective of this method is to obtain the perfect ogee nappe shape for a specific design head. The economy of the design can be greatly increased by using a design head that is less than the actual head or the maximum expected head. Increased discharges for the full range of heads can be obtained by using a smaller design head. The increase in capacity makes it possible to achieve economy by reducing either the crest length or the maximum surcharge head (USBR, 1987).

Tests have shown that the sub atmospheric pressures on a nappe-shaped crest do not exceed about one-half the design head when the design head is not less than about 75 % of the maximum head i.e. $H_e/H_0 \leq 1.33$. For most conditions in the design of spillways, these negative pressures will be small, and they can be tolerated because they will not approach absolute pressures that can induce cavitation (USBR, 1987).

The basic stepwise design process follows. Note that all figures used in the design of the ogee spillway according to the USBR method can be found in Section D.2.

1. The following variables must be defined to start the process:
    a. The design discharge Q of the proposed spillway;
    b. The width b of the proposed spillway;
    c. The upstream dam height P;
    d. Assuming a value for $P/H_0 \geq 2.5$ makes the design simpler as C_0 can easily be obtained as 2.175. In any case, this must be checked afterwards or iterated to find the correct value for C_0.
2. From Figure D-1, find the value of C_0 by using the value of P/H_0;
3. For economic purposes, assume $H_e/H_0 = 1.33$ (or any other value) and use Figure D-2 to obtain C_e/C_0;
4. Using Figure D-3 to Figure D-5, obtain other ratio's to adjust C_0 for any other characteristics of the proposed spillway;
5. Adjust C_0 accordingly;
6. Using the adjusted value of C_0, use the following equation to solve for H_e:

$$Q = CbH_e^{3/2} \tag{D-1}$$

7. Once H_e is determined again use the ratio of $H_e/H_0 = 1.33$ to determine the design head H_0;

8. Calculate h_a using the formula:

$$h_a = \frac{q^2}{2g(P + h_0)^2} \tag{D-2}$$

9. Determine the ratio h_a/H_0;
10. Use Figure D-6 to find the values of K and n.
11. Use K and n to determine the downstream crest profile using the equation:

$$\frac{y}{H_0} = -K\left(\frac{x}{H_0}\right)^n \tag{D-3}$$

    With x and y being the coordinates of the downstream profile using the axes shown in Figure D-8;

12. With the known design head H_0, all the necessary dimensions of the upstream profile of the crest can be determined using Figure D-7.

For the design of the toe of the spillway, special consideration must be shown as the flow will be highly critical. The flow must ideally be deflected or 'guided' to a horizontal direction into the apron or stilling basin. This will result in very high thrust forces on the base and the side walls of the spillway. These forces can be roughly estimated by using momentum equations (Chadwick *et al.*, 2013).

D.2. Figures

The following figures are used in the USVR (1987) design method for ogee spillways.

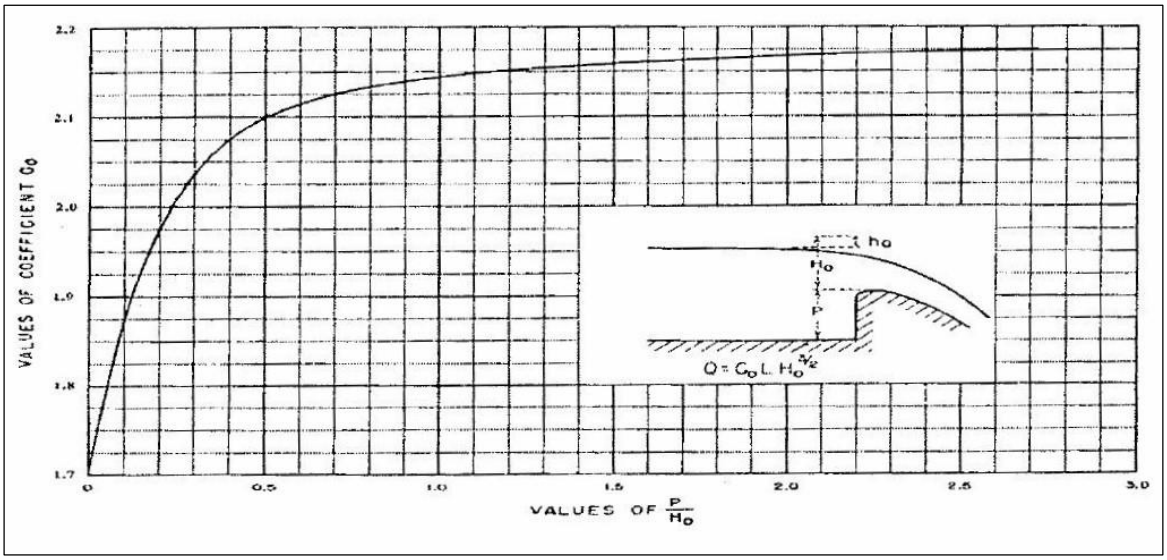

Figure D-1: Discharge coefficient for vertical-faced ogee crest (USBR, 1987)

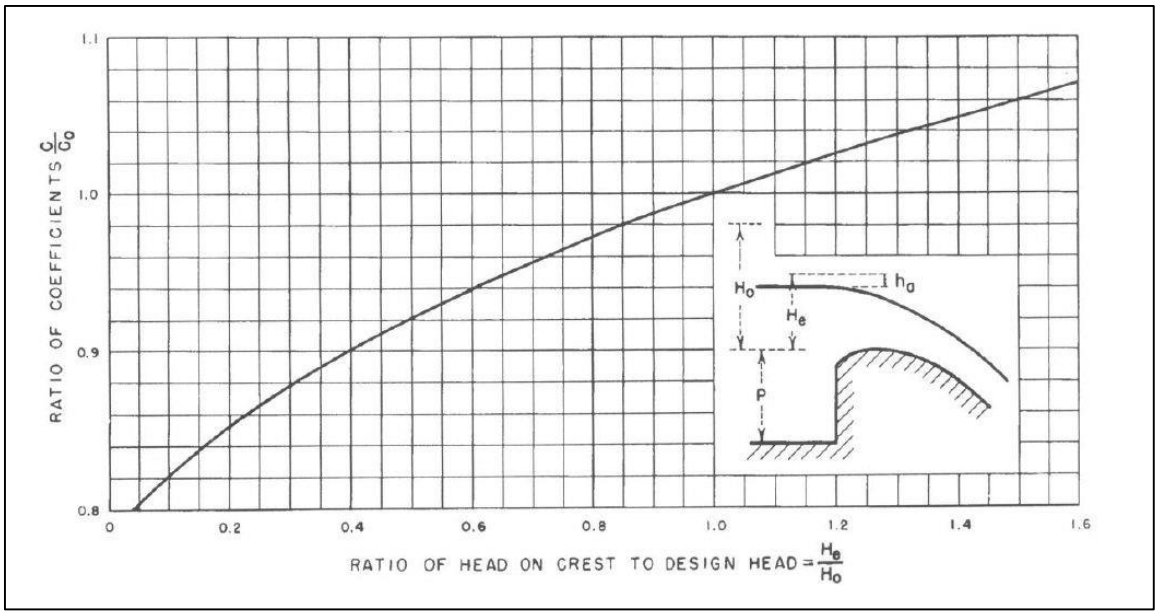

Figure D-2: Discharge coefficients for other than design head (USBR, 1987)

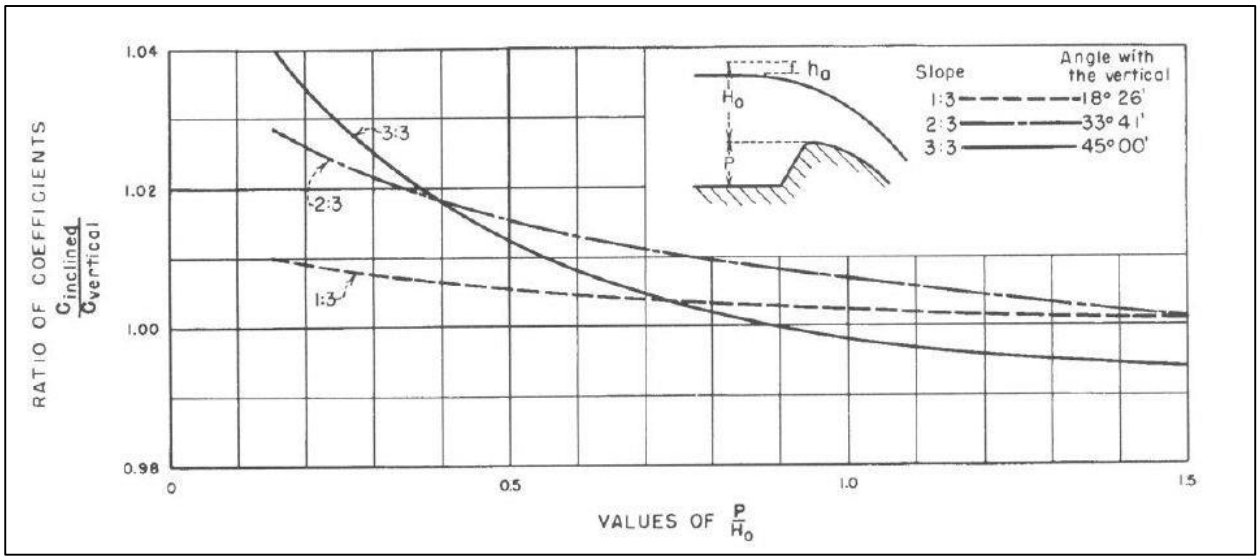

Figure D-3: Discharge coefficients for ogee crest with sloping upstream face (USBR, 1987)

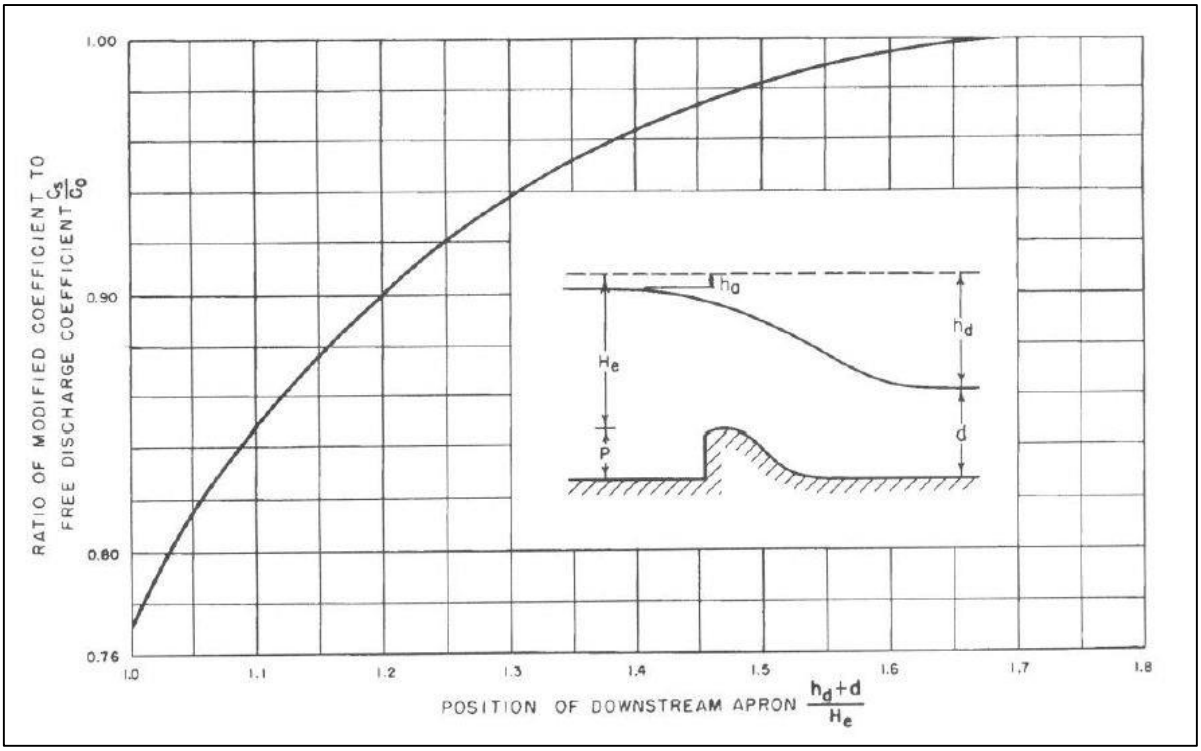

Figure D-4: Discharge coefficients resulting from apron effects (USBR, 1987)

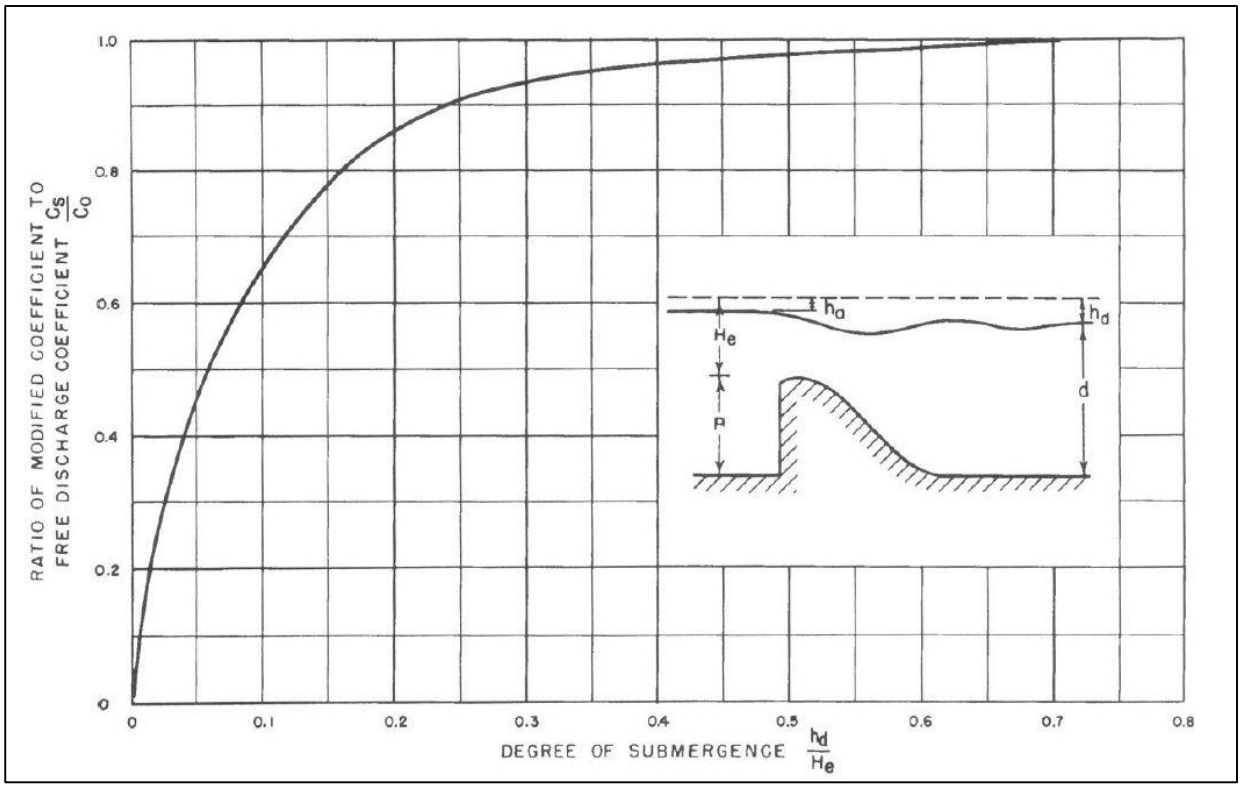

Figure D-5: Discharge coefficients from tailwater effects (USBR, 1987)

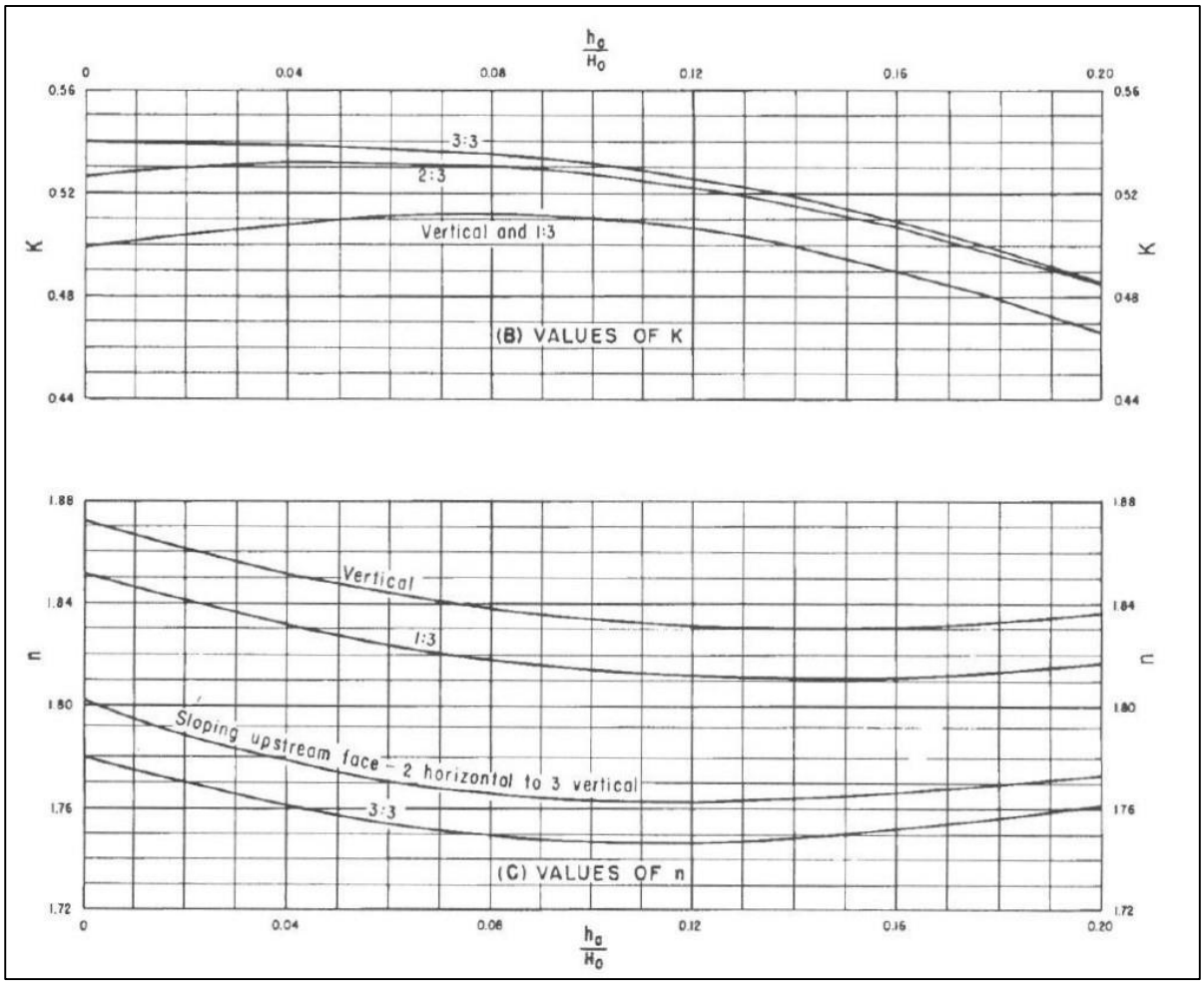

Figure D-6: Coefficients to obtain downstream ogee profile (USBR, 1987)

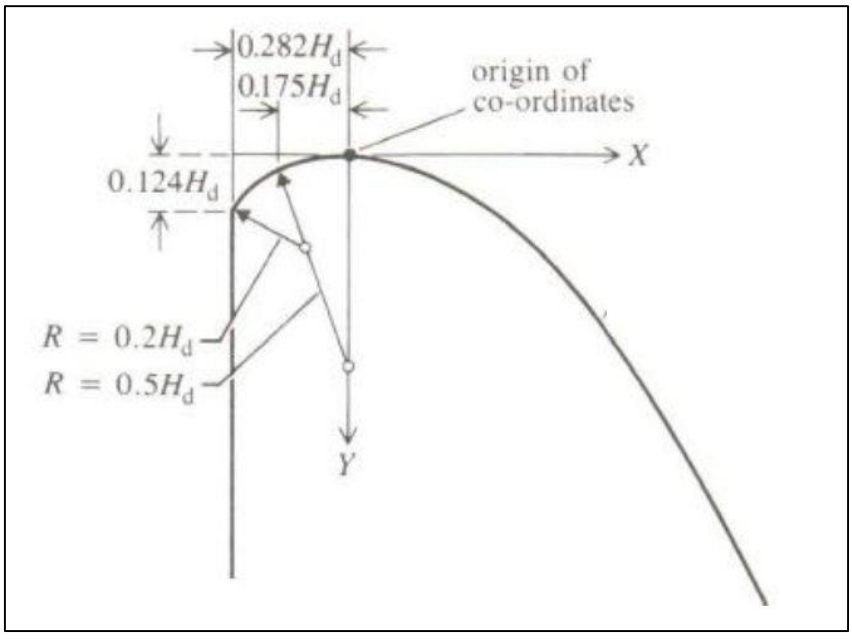

Figure D-7: Profile upstream of crest (USBR, 1987)

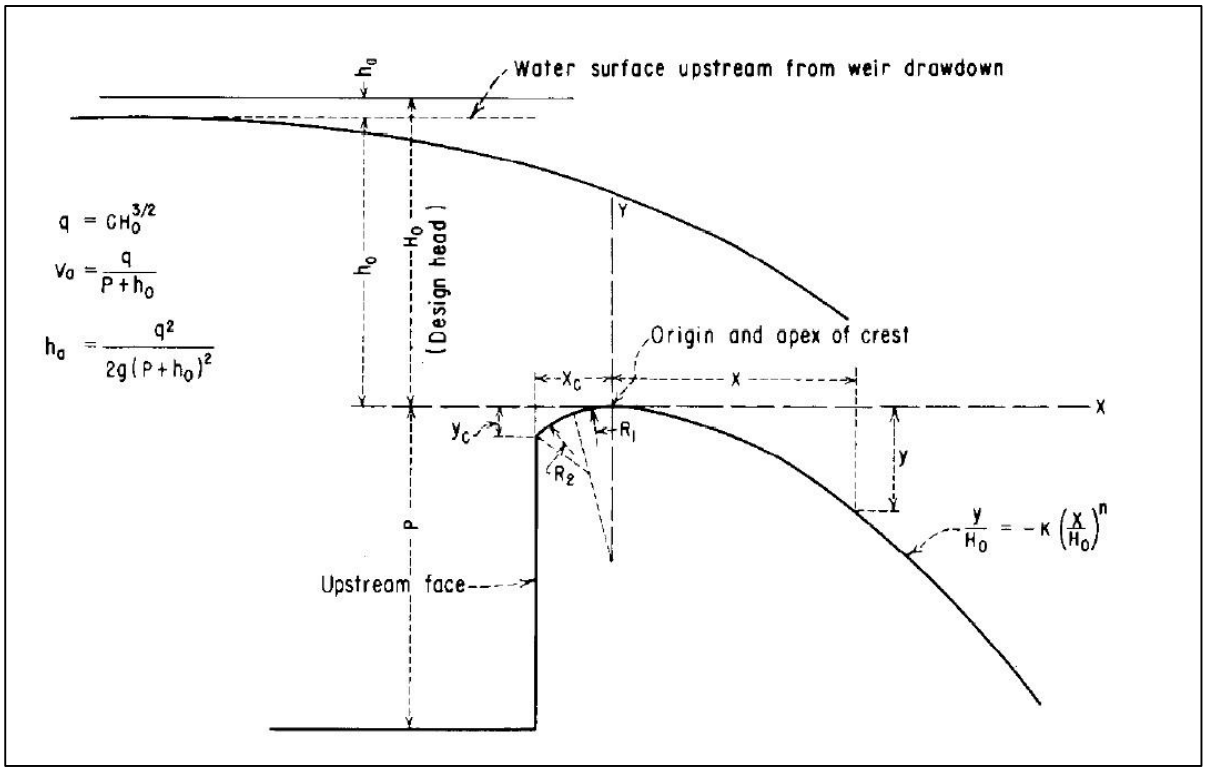

Figure D-8: Elements of ogee crest profile (USBR, 1987)

APPENDIX E
MODEL DESIGN

All as built design drawings of the model is contained in Appendix F.

E.1. Ogee Design

The ogee spillway of the model was designed according to the USBR (1987) procedure given in Appendix D. A short overview of an ogee spillway is contained in the background information on dam spillways in Appendix B.

Table E-1: Model ogee spillway design

Ogee Spillway Design according to USBR					
Step no.		Parameter	**Value**		*Reference*
1		Scale - 1 : x	**20**		
		Qm	**0.537**	m3/s	
		Qp	**960.0**	m3/s	
		b	**1.2**	m	
		qm	**0.447**	m2/s	
		qp	**40.0**	m2/s	*given*
		C0	**2.175**		*Fig 1.9-1 (w. P/H0 > 3.0)*
		H0	**0.255**	m	
		*3*H0*	*0.764*	m	
		He	*0.339*	m	
		*3*He*	*1.018*	m	
2		He/H0	**1.333**		*choose*
	>	Ce/C0	**1.040**		*Fig 1.9-2 (w. He/H0 = 1.333)*
3		Q=C0*Ce/C0 *L*He^(3/2)			
	>	He	**0.3394**	m	
	>	H0 = He/1.33	**0.2545**	m	
4		P/H0	**3.0**	m	*given*

	P (from P/H0)	**0.764**	m	
	Min P (To fit in Splitters)	**1.039**	m	
	P	**1.039**	m	
	Freeboard	**0.200**	m	
	P + He	**1.379**	m	
	P + He + Freeboard	**1.579**	m	
5	**Ogee Shape using H0**			
	H0	**0.255**	m	
	ha= q^2/2g(P+h0)^2			*[1]*
	he + ha = He			*[2]*
	he	**0.334**	m	*choose*
>	ha	**0.005**	m	*from [1]*
>	ha	**0.005**	m	*from [2]*
	ha/H0	**0.0212**		
>	K	**0.507**		*fig1.7-1 (w. ha/H0 = 0.01)*
>	n	**1.855**		*fig1.7-1 (w. ha/H0 = 0.01)*
	y/H0 = -K(x/H0)^n			*equation 6*
	See 'Ogee using H0' sheet			*from equation 6*
	R1	**0.051**	m	*from Figure 1*
	R2	**0.127**	m	*from Figure 1*
	Yc	**0.032**	m	*from Figure 1*
	X1	**0.045**	m	*from Figure 1*
	Xc	**0.072**	m	*from Figure 1*
	R1	**50.91**	mm	
	R2	**127.27**	mm	
	Yc	**31.56**	mm	
	X1	**44.54**	mm	
	Xc	**71.78**	mm	

Table E-2: Ogee crest shape coordinates

x (mm)	y (mm)
0.0	0.000
10.0	-0.318
20.0	-1.152
30.0	-2.444
40.0	-4.168
50.0	-6.305
60.0	-8.842
70.0	-11.769
80.0	-15.078
90.0	-18.759
100.0	-22.809
110.0	-27.220
120.0	-31.987
130.0	-37.108
140.0	-42.576
150.0	-48.389
160.0	-54.543
170.0	-61.035
180.0	-67.862
190.0	-75.021
200.0	-82.510
210.0	-90.326
220.0	-98.467
230.0	-106.931
240.0	-115.715
250.0	-124.818
260.0	-134.237
270.0	-143.972
280.0	-154.020
290.0	-164.379
300.0	-175.048
310.0	-186.026
320.0	-197.311
330.0	-208.901
340.0	-220.796
350.0	-232.994
360.0	-245.493
370.0	-258.293
380.0	-271.626
390.0	-284.959
400.0	-298.293
410.0	-311.626
420.0	-324.959
430.0	-338.293
440.0	-351.626
956.0	-1039.00

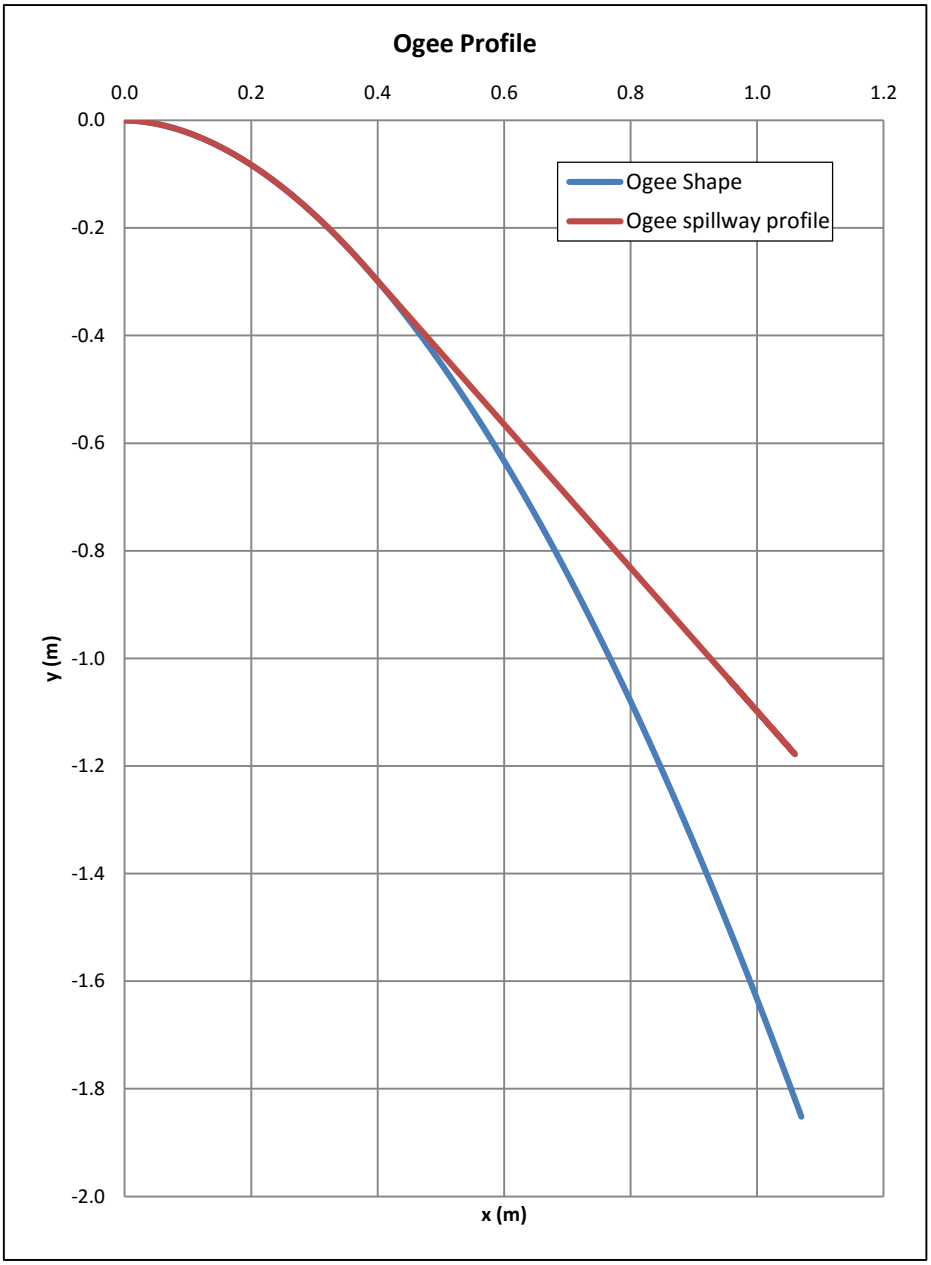

Figure E-1: Ogee shape and spillway profile

E.2. Roberts Splitters

Roberts splitters as an energy-dissipating structure and its design procedure is set out in Section 2.2 of the main report. Here follows the complete design of the Roberts splitters on the hydraulic model.

Table E-3: General parameters of model splitters design

For parameter definitions, see Section 2.2.5 and Figure 2-12		
General Information		
Scale:	1:	20
No. of cycles in model		4

Table E-4: Design parameters for model Roberts splitters

Parameter	Prototype	Model	Unit	(measured from toe of dam)		
Dam height	20.789	1.039	MASL			
b	24.000	1.200		*Model spillway width*		
B	48.000	2.400	m	*Bay width*		
Hd	6.788	0.339	m	**Rmax**	**18.483**	**m**
Slope	0.750	0.75:1	(H:V)	**Rmin**	**5.557**	**m**
θ	53.130	53.130	degrees			
θ	0.927	0.927	rad			
Q	960.000	0.537	m3/s			
qw	20.000	0.224	m2/s			
ks	0.00020	0.000010	m			
y tailwater	0	0	m	Status of Design:		OK

Table E-5: Model splitters design procedure

	Design Procedure				
(i)					
	Hd	6.788	0.339	m	
	Hc	8.145	0.407	m	
	Ha	1.851	0.093	m	
(ii)					
	x + y =	27.576	1.379	m	
	4Hd =	27.150	1.358	m	
	x + y > 4Hd ?	OK			
(iii)					
	Choose N	8		splitters	(number of splitters in BAY)
	B/N	6.000	0.300	m/splitter	

	W	2.575	0.129	m	
	S	3.425	0.171	m	
	T	3.425	0.171	m	
	L	3.425	0.171	m	
(iv)					
	Ls	4.8	0.240	m	(Select *Ls* so that: $1.25 < Ls/L < 1.5$)
	Ls/L	1.402			
	Check Ls/L	OK			
(v)					
	P	10.9639	0.548	m	(Choose *P*, and check *W* in (v) against *W* in (iii))
	W tolerance	*0.01*	0.001	*m*	
	Hc/P	0.743			
	W/P	0.235			(from Figure 1.4-2)
	W	2.575	0.129	m	(*W* in (v) is suitable)
(vi)					
	x	17.751	0.888	m	
	y	9.825	0.491	m	
(vii)					
	C	14.389	0.719	m	
	C/Hd	2.120			
	f	0.979			(from Figure 1.4-3)
	Rmax	18.483	0.924	m	
	Rmin	5.557	0.278	m	

E.3. Aeration Vents

The aeration vents of the splitters were designed according to the Gariep Dam's splitter aeration vents.

Table E-6: Aeration vents design

Aeration Calcs				
First Calcs: Based on Gariep Dam Roberts, P. R. 1977. Energy Dissipation by Dam Crest Splitters				
Gariep Dam Proportions	H0		**7.300**	m
	H_prf	Satisfactory Performance	**8.300**	m
	H_act	Maximum Head	**9.100**	m
Splitter Dimensions	W		**3.400**	m
	S			
	T		**3.200**	m
	L		**3.200**	m
	Ls		**3.400**	m
	Ø_end		**0.600**	m
	Ø_side		**0.300**	m
		Ø_end/W	**0.176**	17.65%
		Ø_side/W	**0.088**	8.82%
		Ø_end/L	**0.188**	18.75%
		Ø_side/L	**0.094**	9.38%
		Ø_end/H0	**0.082**	8.22%
		Ø_side/H0	**0.041**	4.11%
Based on H- ratio of Gariep Dam				
Prototype Dims	H0		**5.091**	m
	Ø_end		**0.418**	m
	Ø_side		**0.209**	m
Model Dims	Ø_end		**20.92**	mm
	Ø_side		**10.46**	mm
Based on W				
	W		**128.755**	mm
	Ø_end		**22.722**	mm
	Ø_side		**11.361**	mm
Area				
	Height		**60.000**	mm
	H/W		**0.466**	

H_gar	**1.584**	m
A_gar	**5.387**	m2
A_air_gariep (both)	**0.565**	m2
A_face_gariep	**5.387**	m2
A_air/A_face	**0.105**	10.50%
A_face_model	**0.008**	m2
A_air	**0.001**	m2
r_air	**0.011**	
Ø_end	**0.023**	m
	22.722	mm

APPENDIX F
DESIGN DRAWINGS OF THE MODEL

F.1. Design Drawings

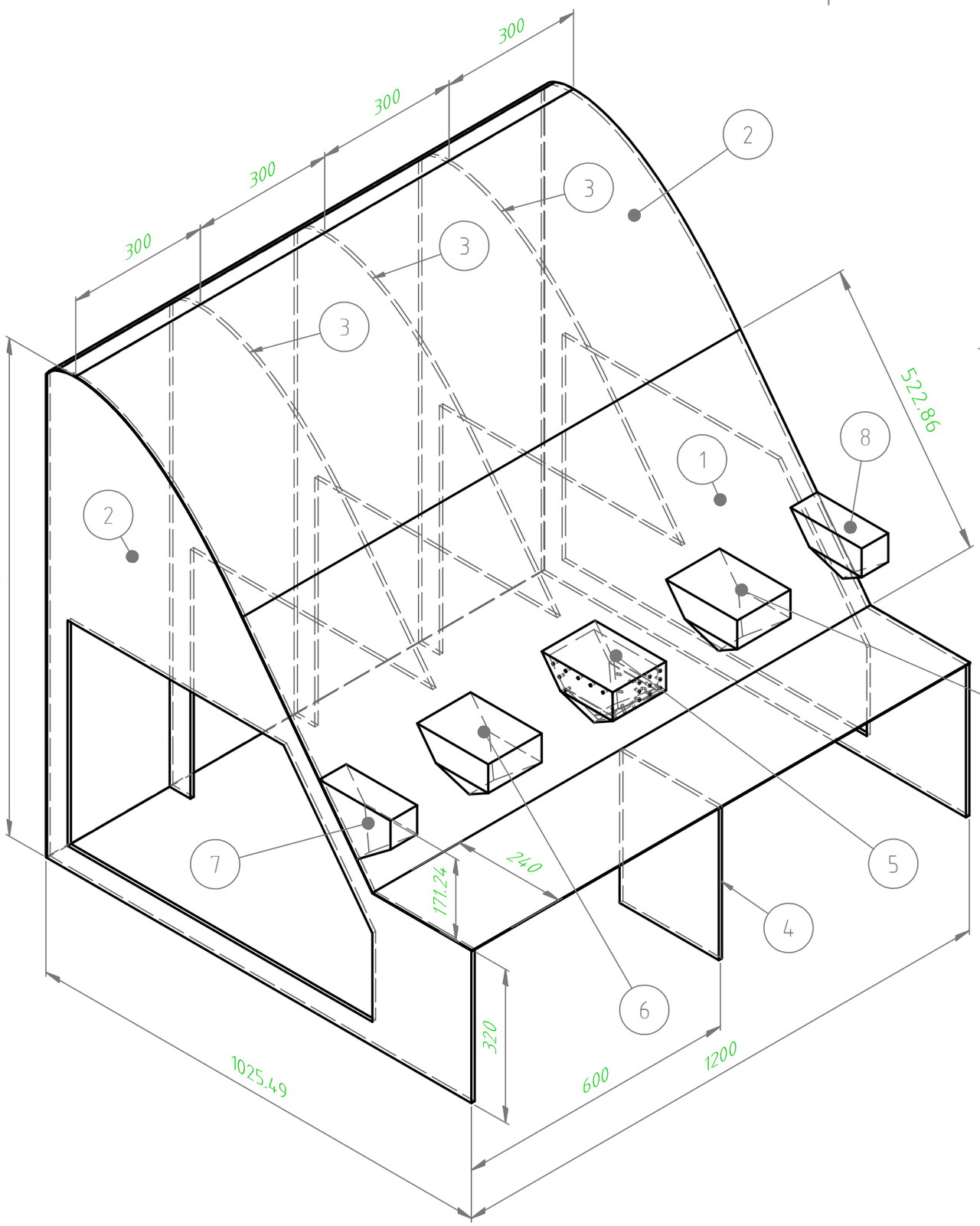

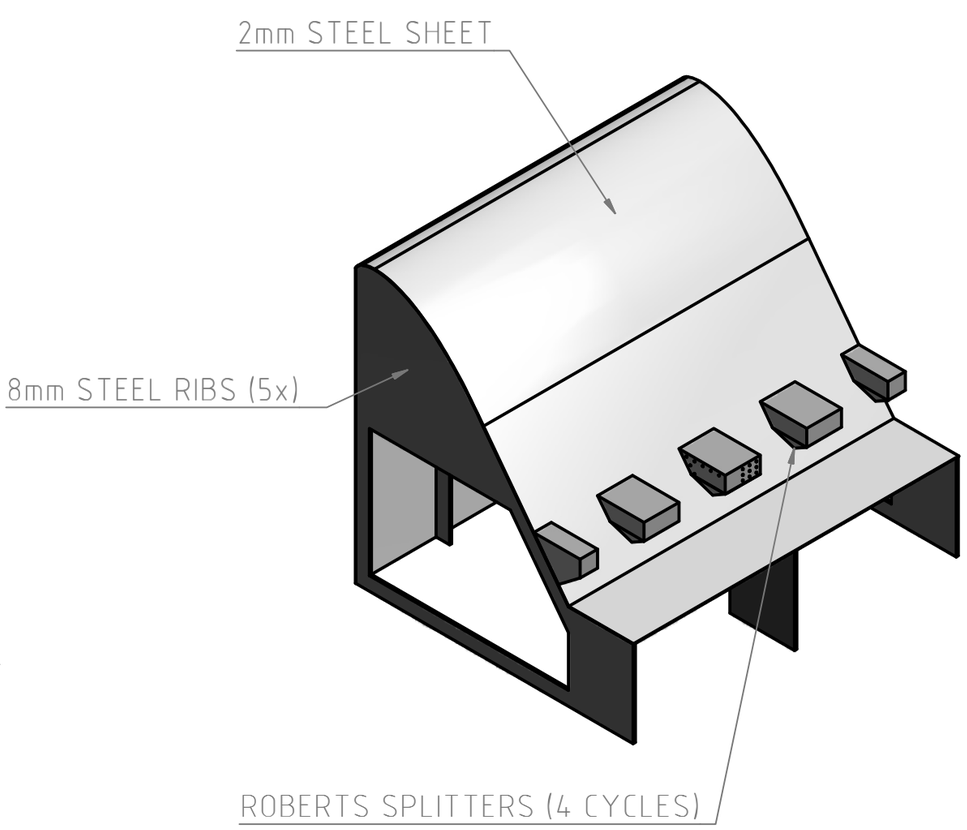

PARTS LIST		
ITEM	QTY	PART NUMBER
1	1	OGEE SHEET
2	2	SIDE RIB
3	3	CENTRE RIB
4	1	STEP SUPPORT
5	1	CENTRE SPLITTER ASSEMBLY
6	2	FULL SPLITTER
7	1	LEFT HALF SPLITTER
8	1	RIGHT HALF SPLITTER

FILE NAME	FSCM NO	SHEET	SCALE 1 : 8
SIZE A3			
DRAWN 2015-11-19 Gerard Calitz			
CHECK			
APPR.			
ISSUED			
REV			
CONTRACT NO		DWG NO	GC-M01-ASM00

Model 01
Complete Assembly - Ogee with Splitters

PRESSURE SENSORS TO BE PLACED ON CENTRE SPLITTER AT SPECIFIED LOCATIONS

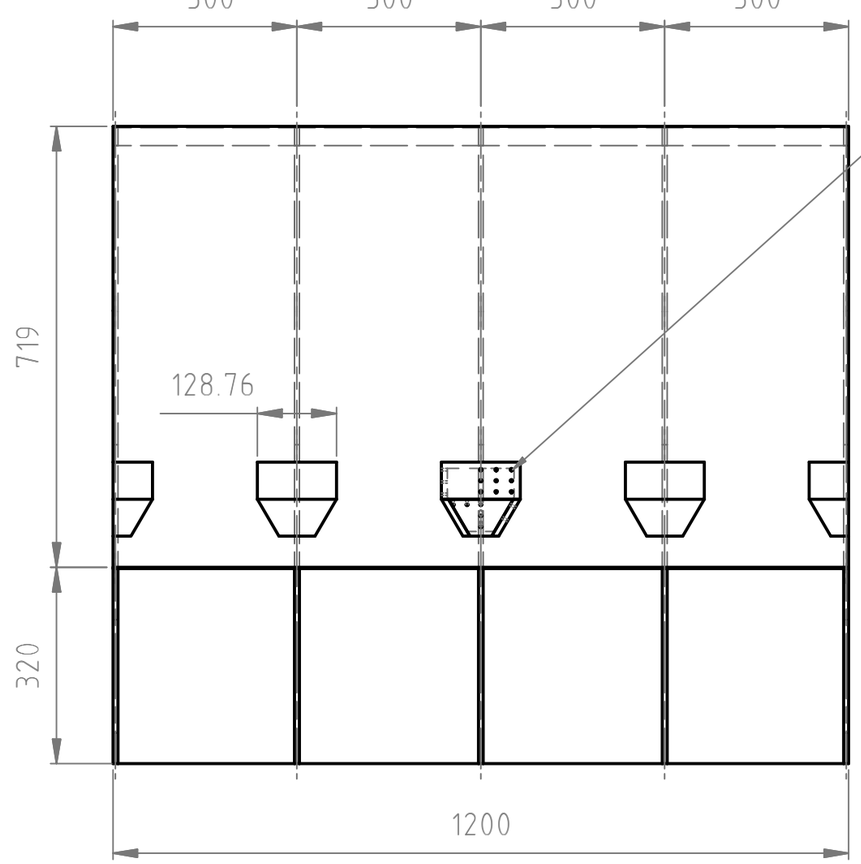

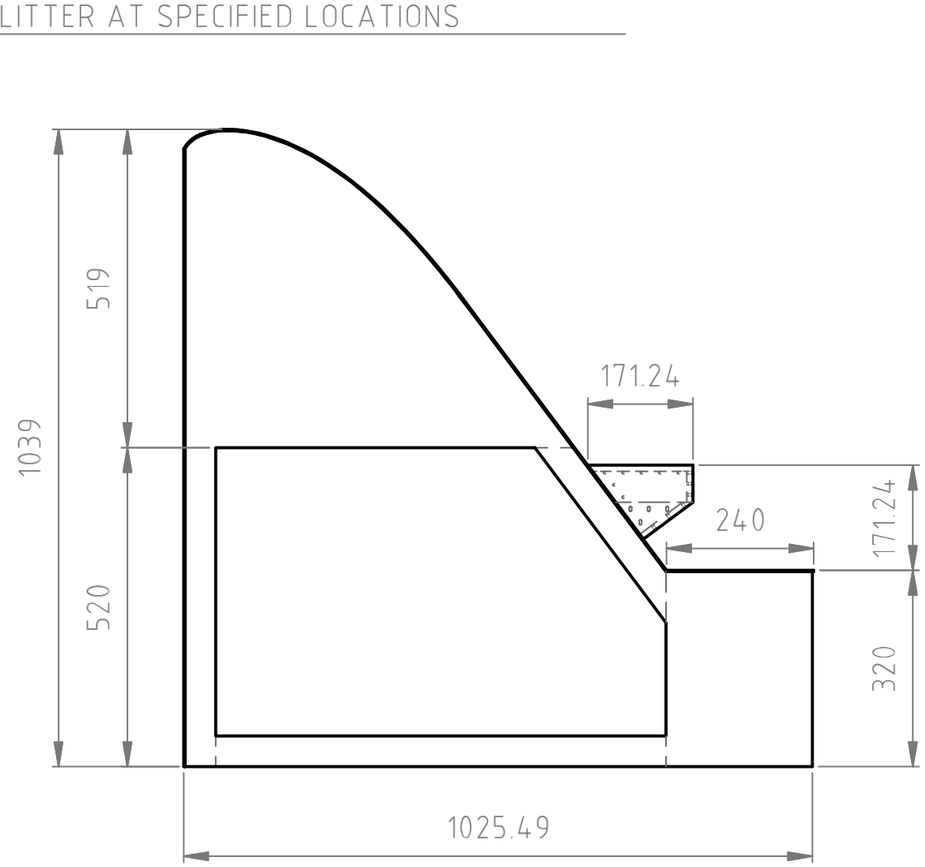

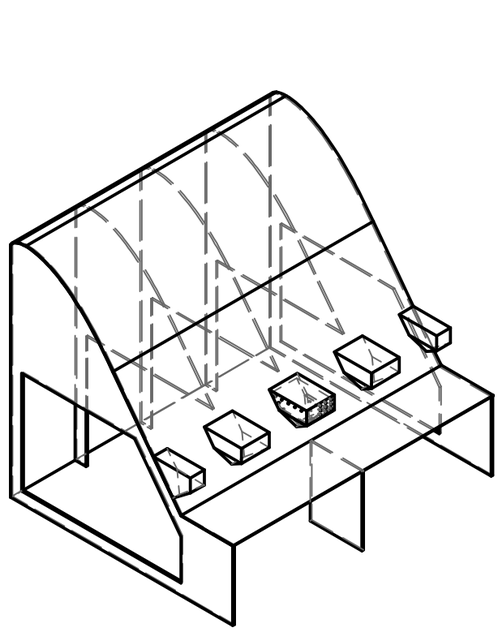

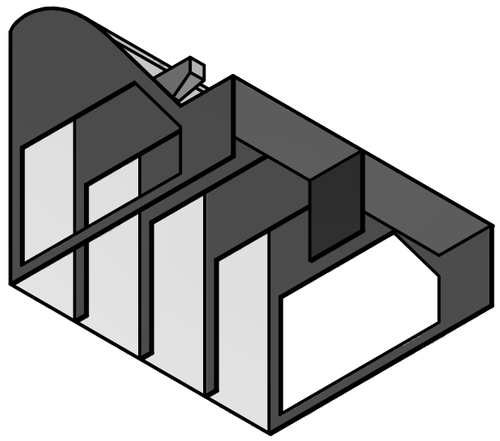

FILE NAME	FSCM NO	SHEET	SCALE 1 : 10
SIZE A3			
DRAWN 2015-11-19 Gerard Calitz			
CHECK			
APPR.			
ISSUED			
REV			
CONTRACT NO			

Model 01
Complete Assembly - Ogee with Splitters

DWG NO
GC-M01-ASM01

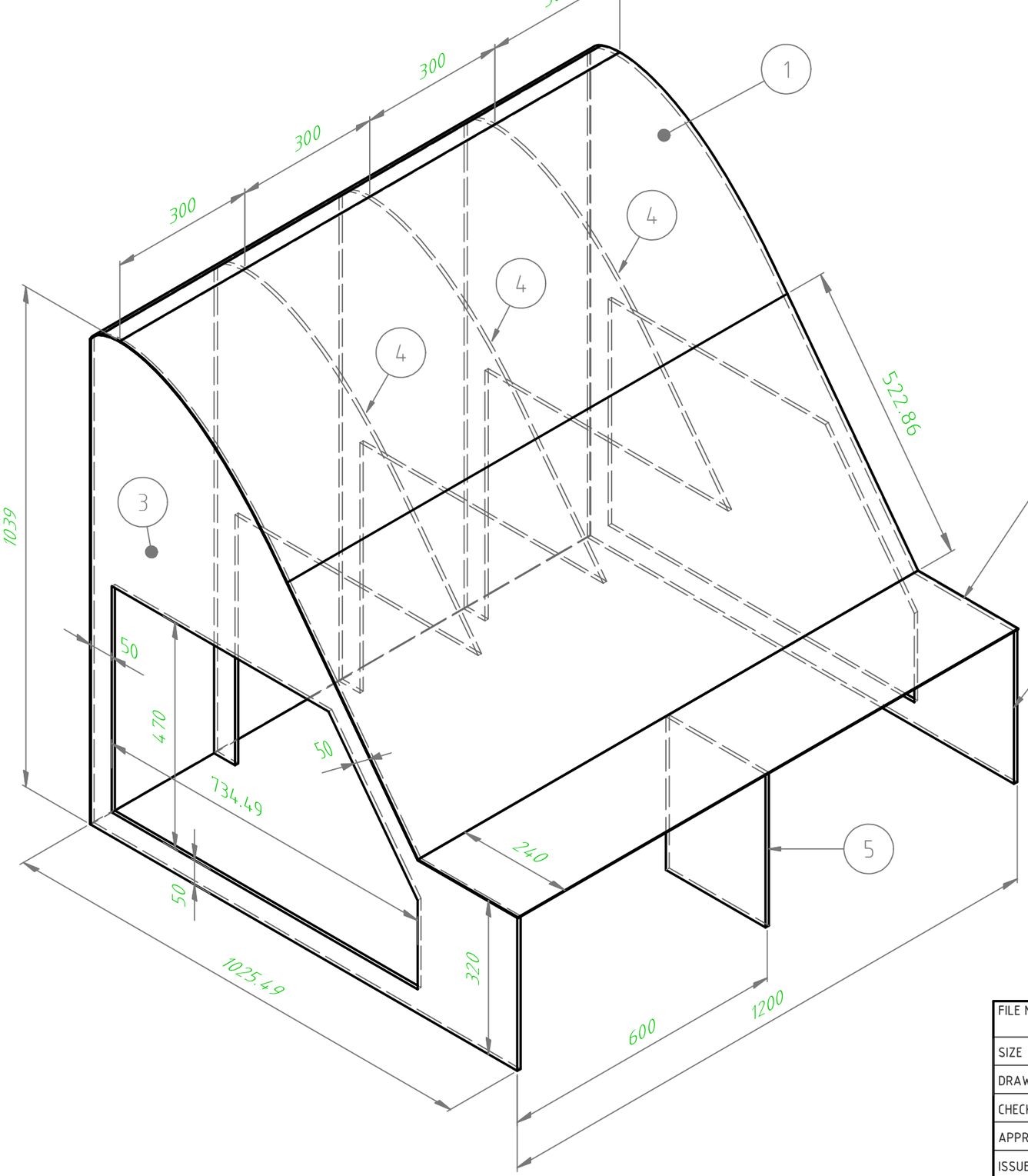

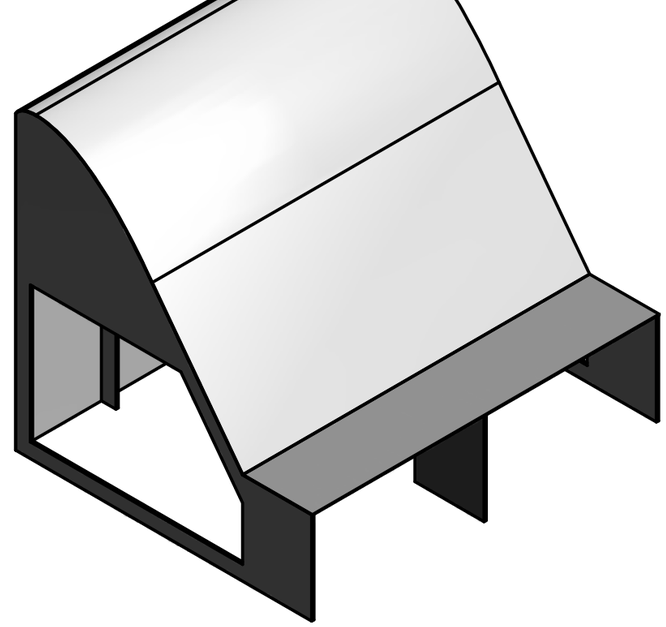

Parts List		
ITEM	QTY	PART NUMBER
1	1	2mm OGEE SHEET
2	1	2mm FLAT STEP SHEET
3	2	8mm SIDE RIB
4	3	8mm CENTRE RIB
5	1	8mm STEP SUPPORT

FILE NAME	FSCM NO	SHEET	SCALE 1 : 8
SIZE A3			
DRAWN 2015-08-17 Gerard Calitz			
CHECK			
APPR.			
ISSUED			
REV			
CONTRACT NO			

Ogee Model 01

Ogee Spillway with Ribs

DWG NO GC-M01-OG00

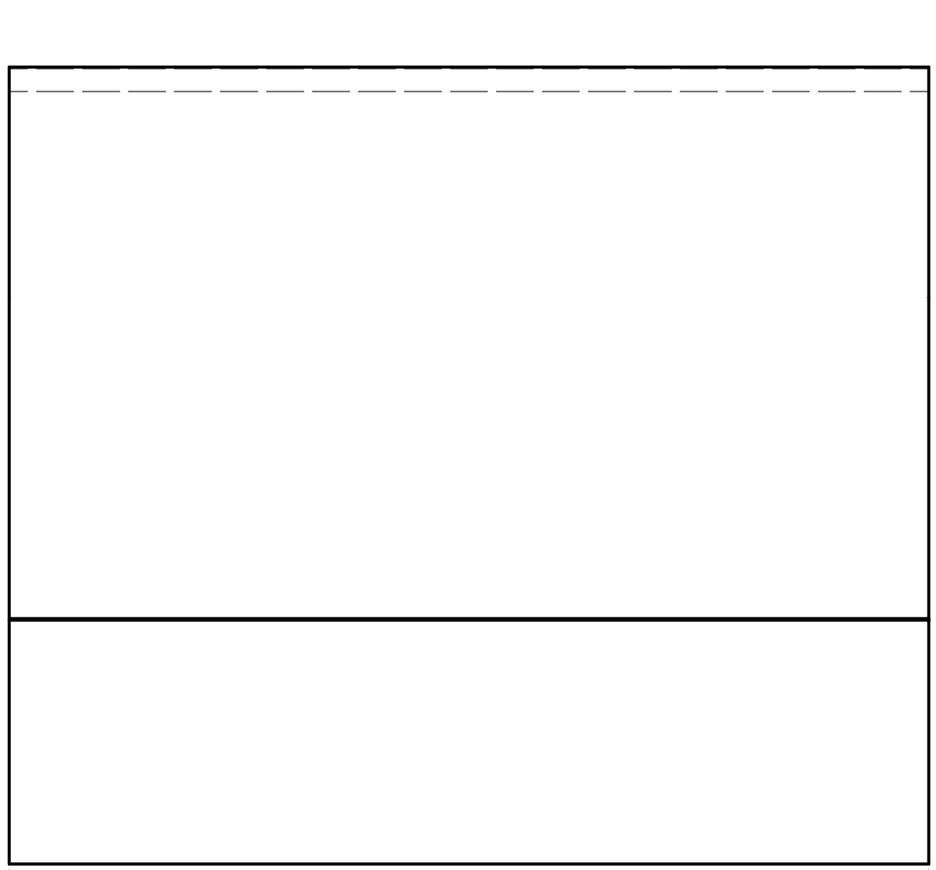

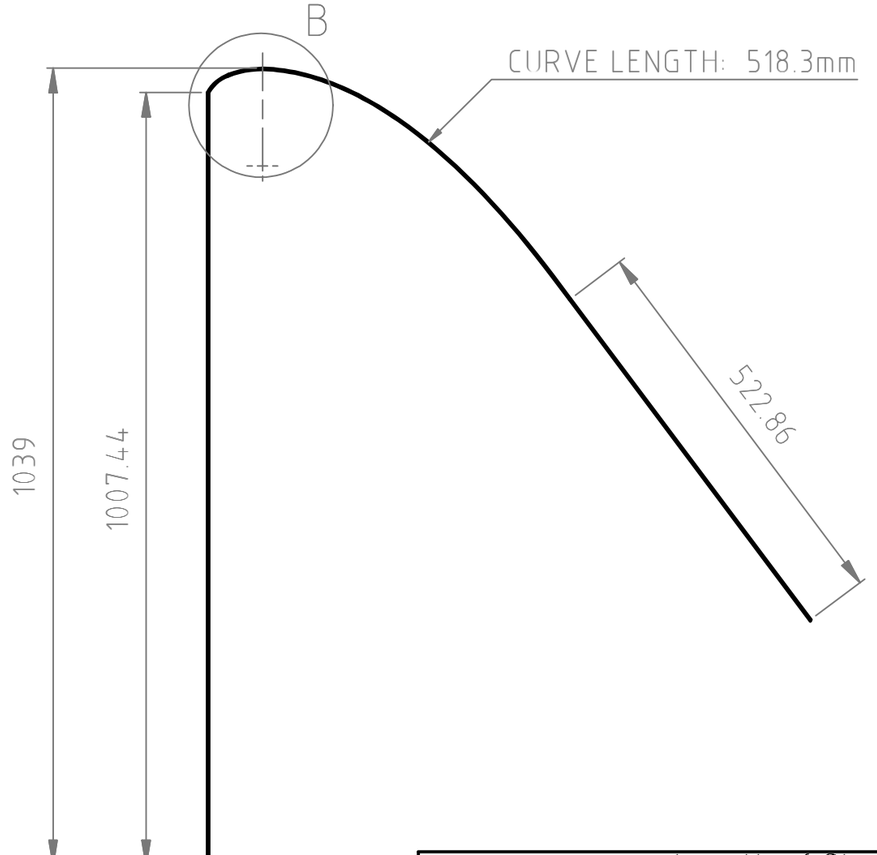

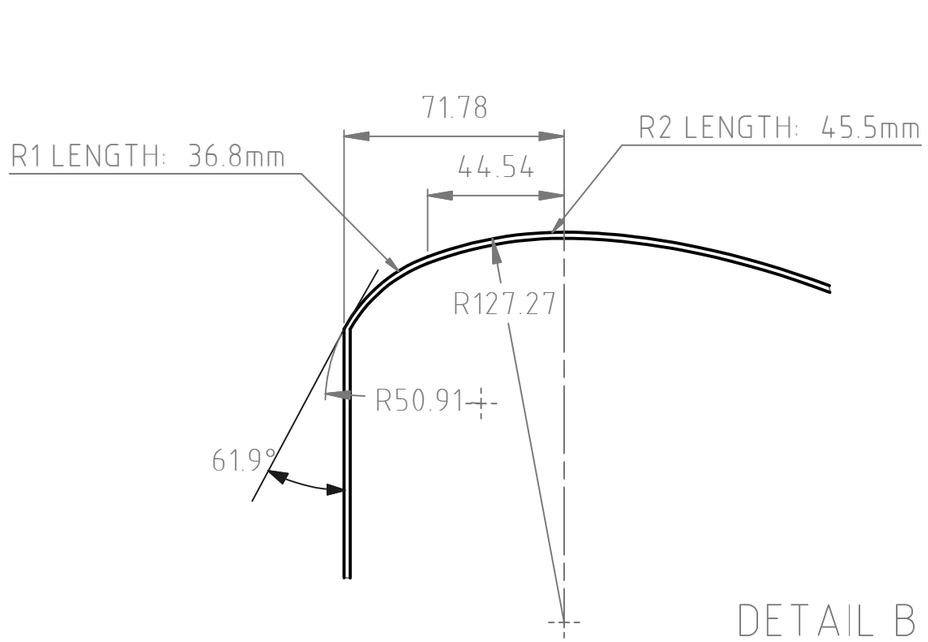

DETAIL B (1 : 2)

Length of Sheet	
Property	Length (mm)
Upstream Straight	1007.44
Upstream R1 (R50.91)	36.78
Upstream R2 (R127.27)	45.50
Downstream Curve	518.34
Downstream Straight	522.86
TOTAL	2130.92
2mm FLAT SHEET SIZE	2130.92 x 1200

Parts List		
ITEM	QTY	PART NUMBER
1	1	2mm OGEE SHEET

FILE NAME	FSCM NO	SHEET	SCALE 1 : 8
SIZE A3			
DRAWN 2015-08-17 Gerard Calitz			
CHECK			
APPR.			
ISSUED			
REV			
CONTRACT NO			

Ogee Model 01
2mm Ogee Sheet

DWG NO
GC-M01-OG01

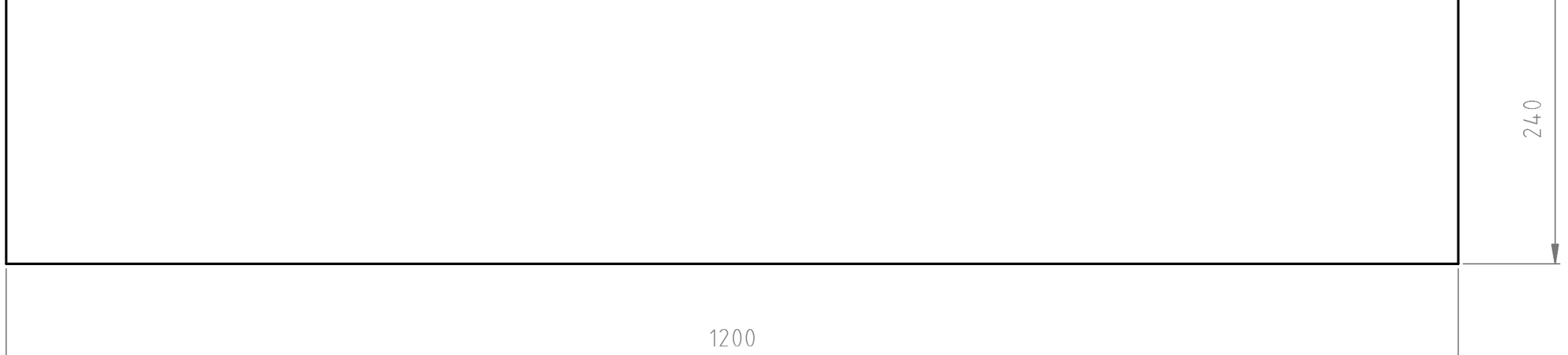

Parts List		
ITEM	QTY	PART NUMBER
2	1	2mm FLAT STEP SHEET

FILE NAME	FSCM NO	SHEET	SCALE 1 : 4
SIZE A3			
DRAWN 2015-08-17 Gerard Calitz			
CHECK			
APPR.			
ISSUED			
REV			
CONTRACT NO			

Ogee Model 01
2mm Flat Sheet for Step

DWG NO
GC-M01-OG02

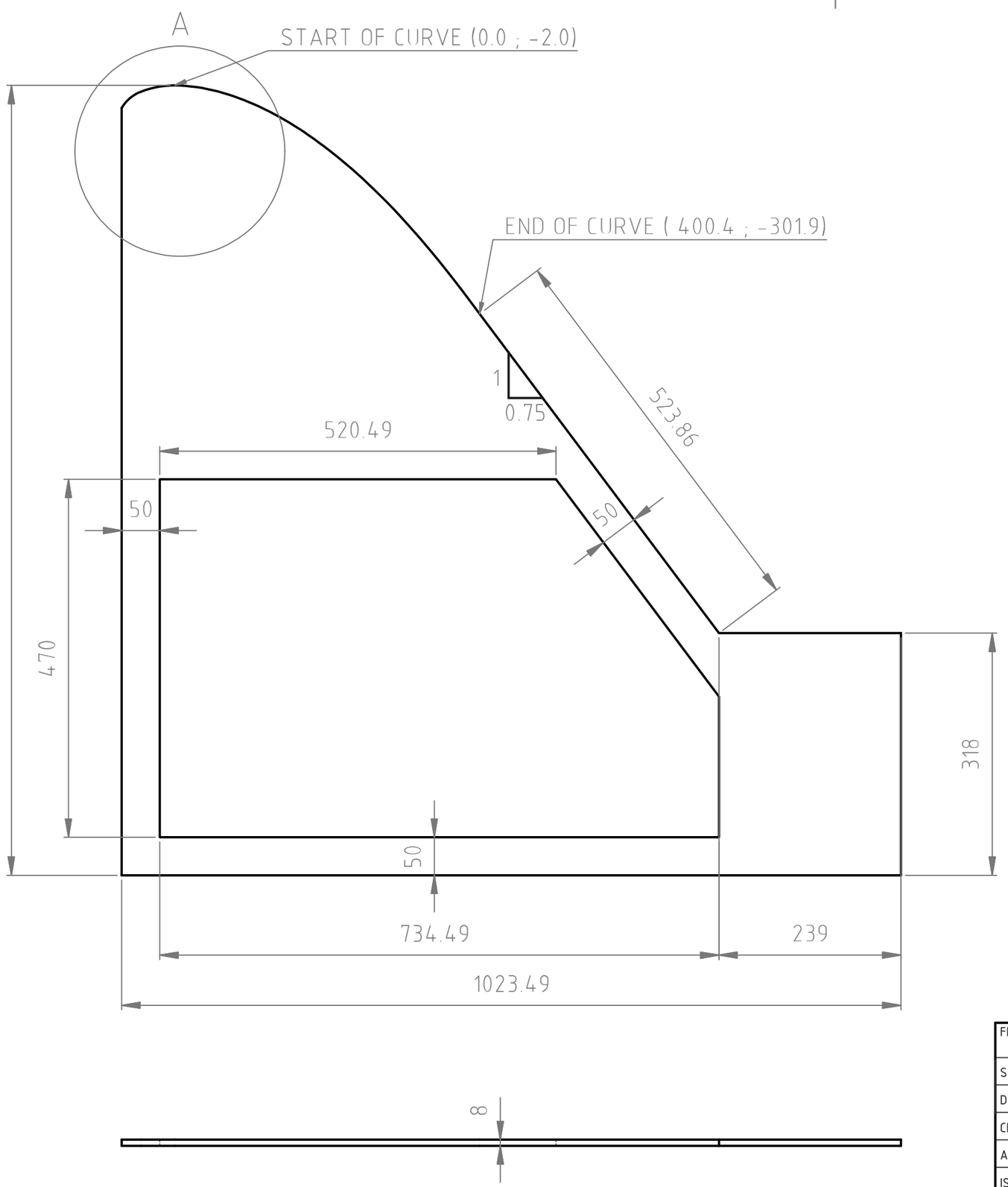

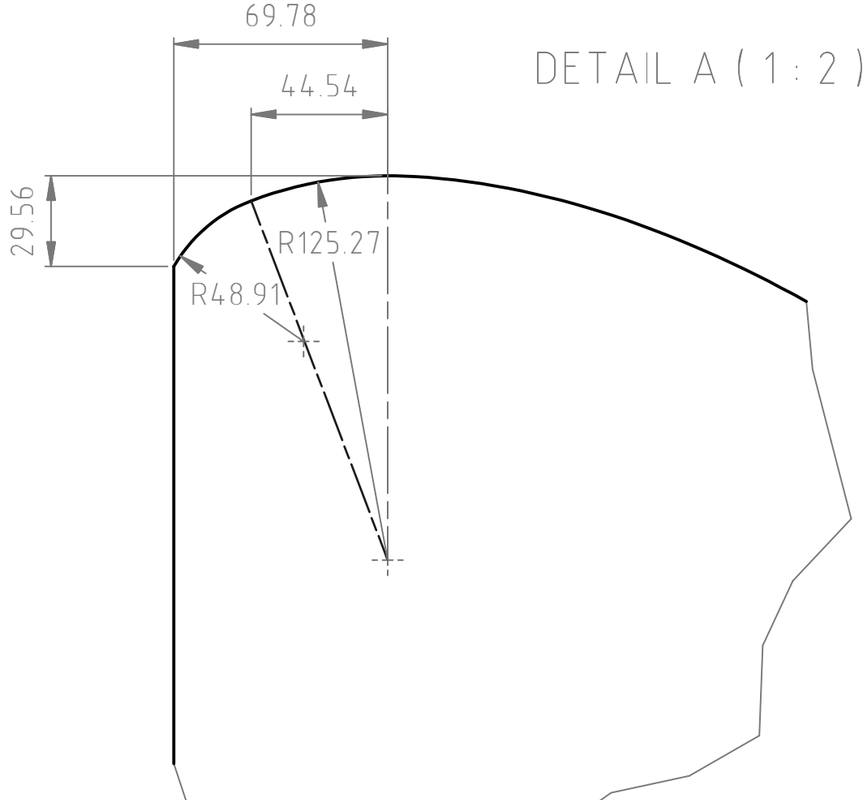

DETAIL A (1 : 2)

Parts List		
ITEM	QTY	PART NUMBER
3	2	8mm SIDE RIB

FILE NAME	FSCM NO	SHEET	SCALE 1 : 6
SIZE A3			
DRAWN 2015-08-17 Gerard Calitz			
CHECK			
APPR.			
ISSUED			
REV			
CONTRACT NO			

Ogee Model 01
8mm Side Rib (x2)

DWG NO
GC-M01-OG03

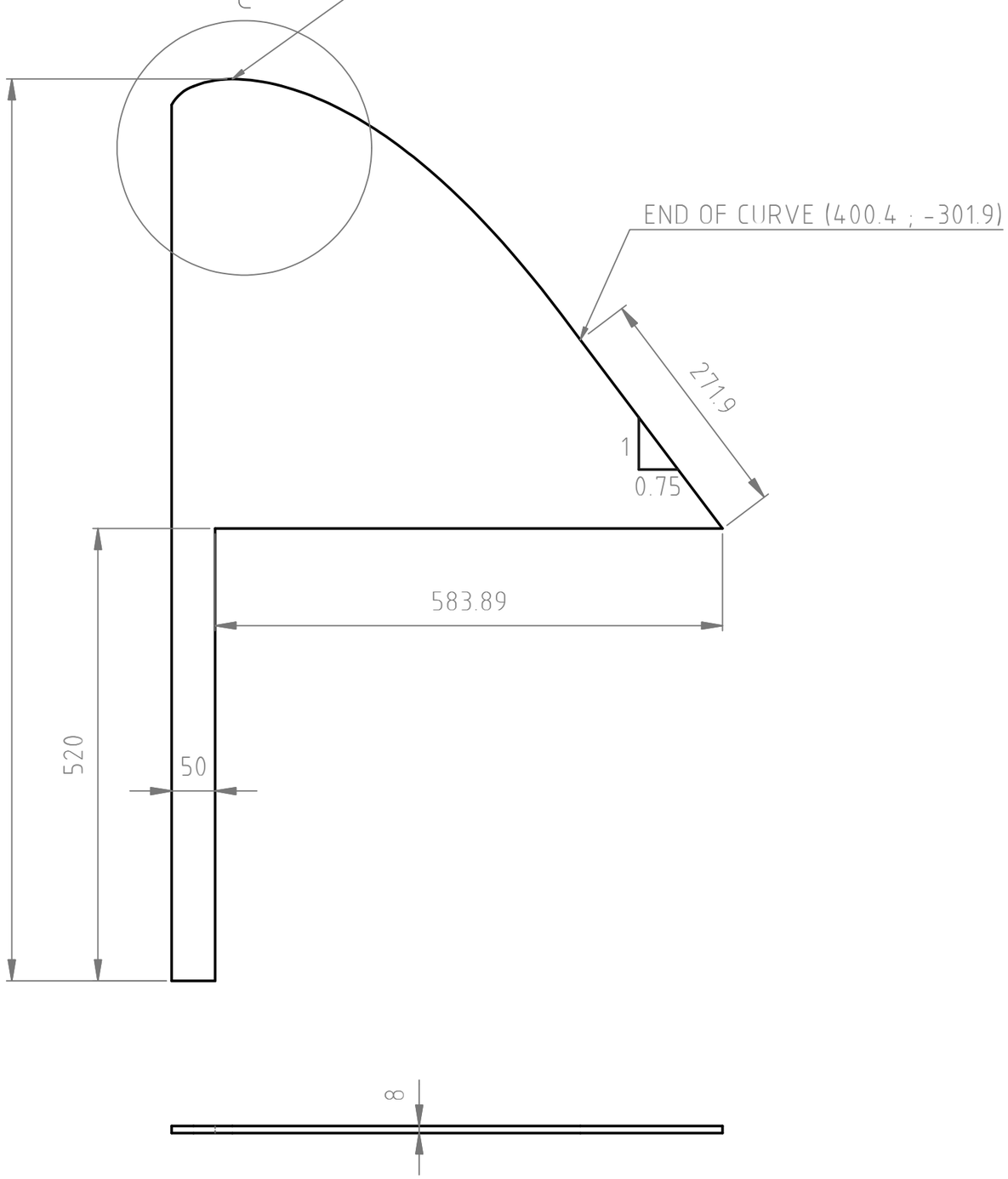

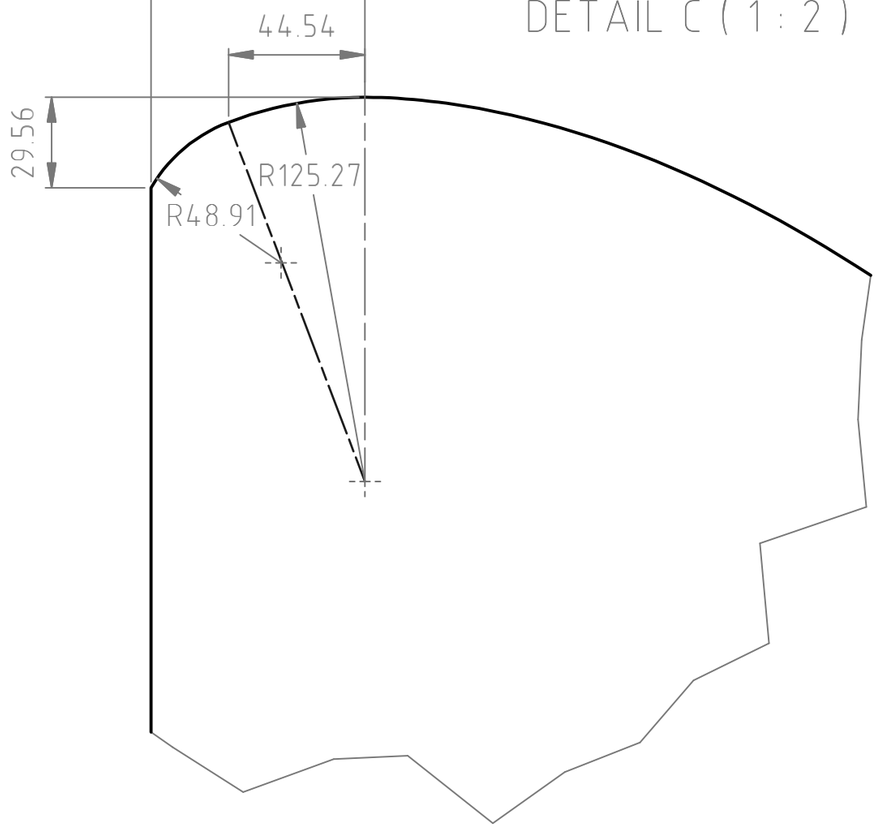

Parts List		
ITEM	QTY	PART NUMBER
4	3	8mm CENTRE RIB

FILE NAME	FSCM NO	SHEET	SCALE 1 : 6
SIZE A3			
DRAWN 2015-08-17 Gerard Calitz			
CHECK			
APPR.			
ISSUED			
REV			
CONTRACT NO		DWG NO	GC-M01-OG04

Ogee Model 01
8mm Centre Rib (x3)

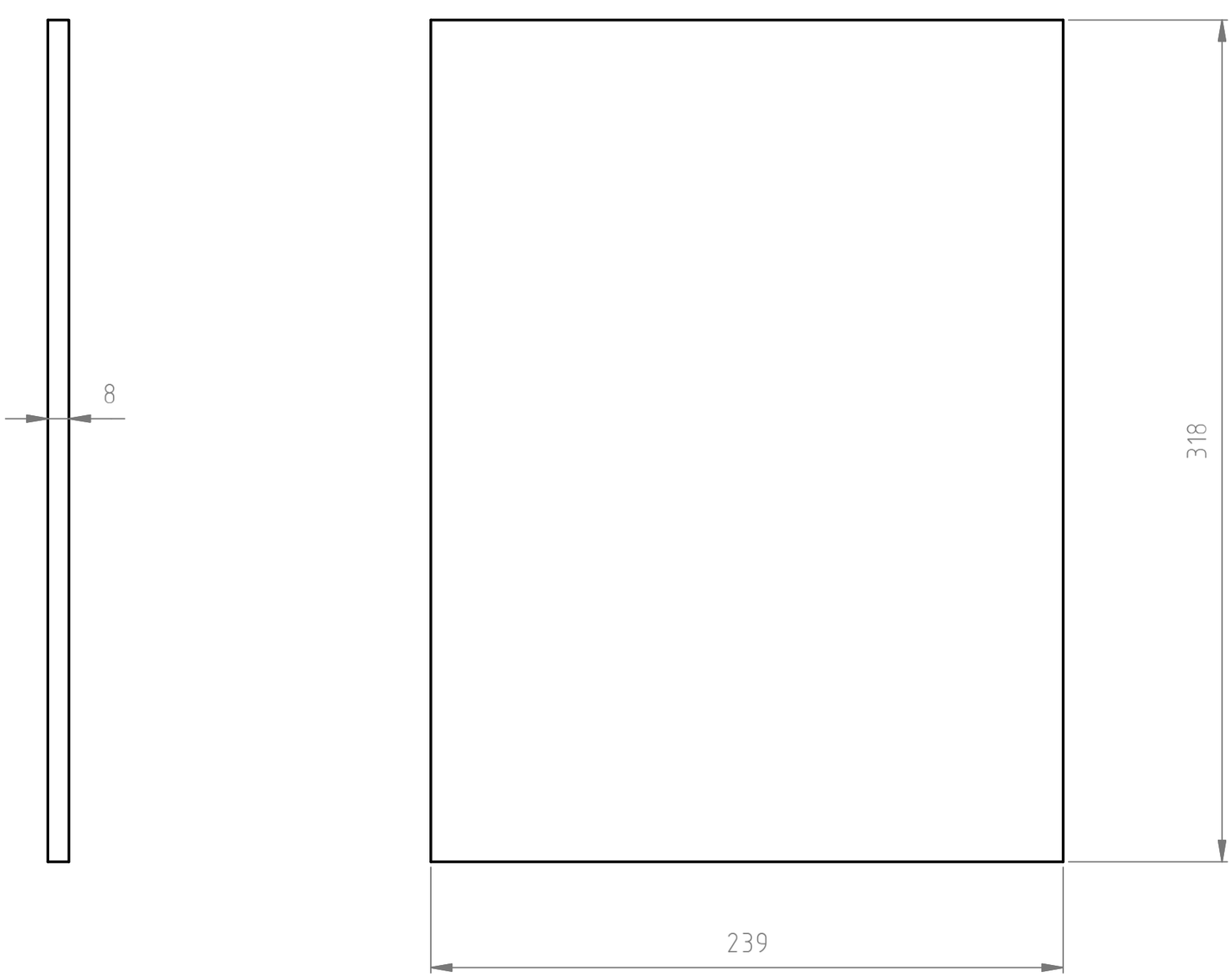

Parts List		
ITEM	QTY	PART NUMBER
5	1	8mm STEP SUPPORT

FILE NAME	FSCM NO	SHEET	SCALE 1 : 2
SIZE A3			
DRAWN 2015-08-17 Gerard Calitz			
CHECK			
APPR.			
ISSUED			
REV			
CONTRACT NO			

Ogee Model 01
8mm Step Support

DWG NO
GC-M01-OG05

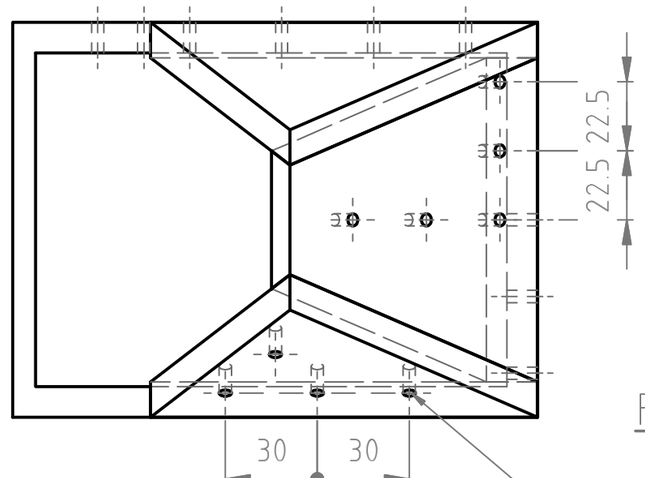

BOTTOM VIEW

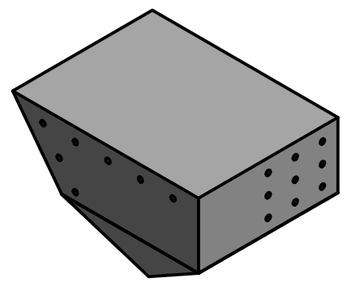

For position of pressure sensors,

see Drawing no's: GC-M01-SPL01 & 02

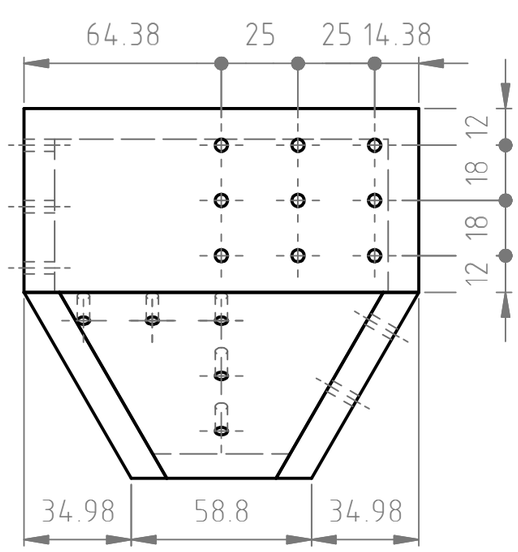

FRONT VIEW

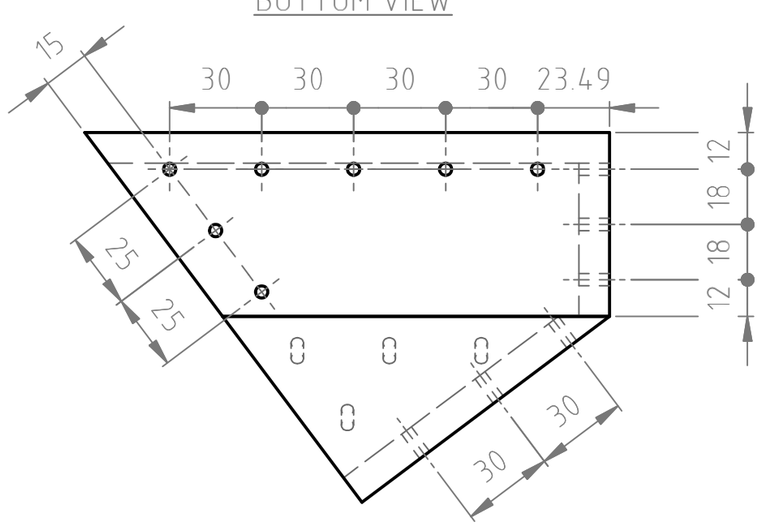

SIDE VIEW

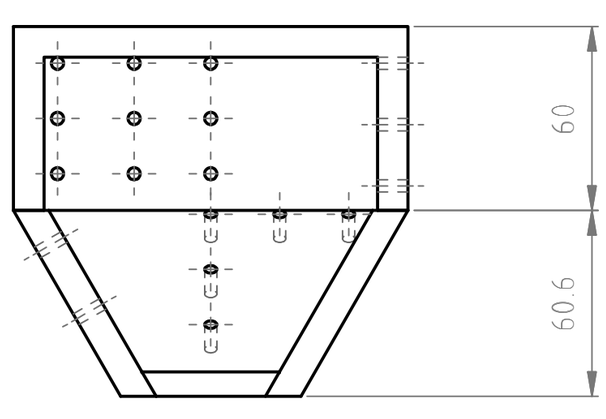

BACK VIEW

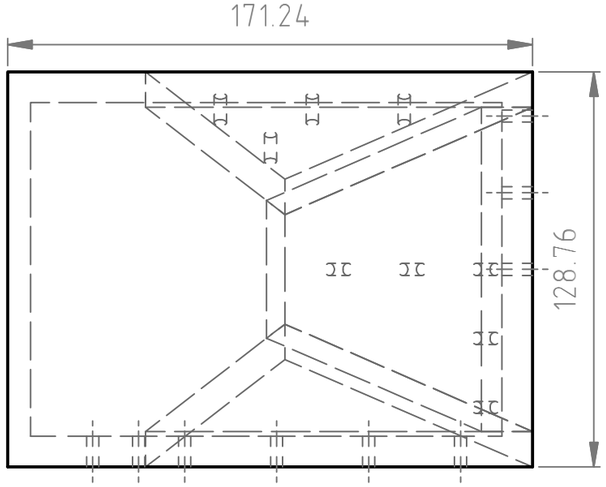

TOP VIEW

The 25 holes are desirable position for pressure sensors

The specific holes to be used must be discussed

FILE NAME	FSCM NO	SHEET	SCALE 1 : 2
SIZE A3			
DRAWN 2015-11-16 Gerard Calitz			
CHECK			
APPR.			
ISSUED			
REV			
CONTRACT NO			

Model 01

Centre Splitter Assembly

DWG NO GC-M01-SPL00

CENTRE SPLITTER - TOP PART

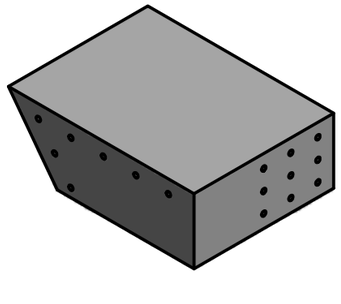

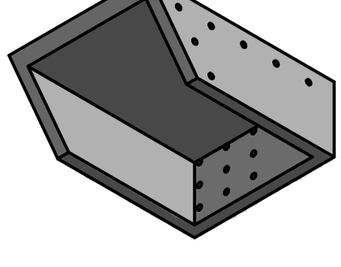

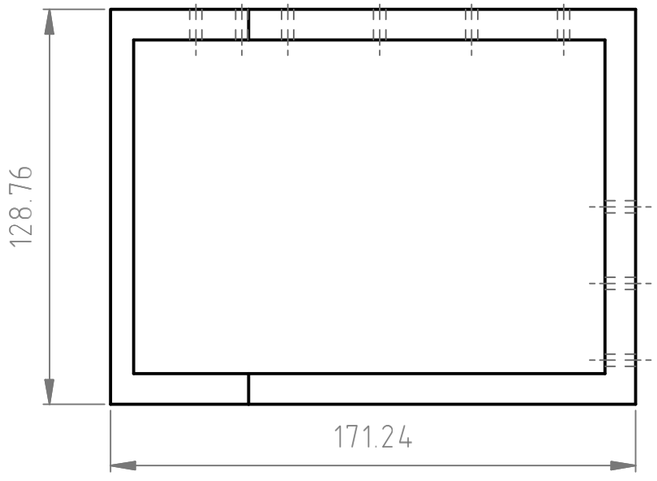

BOTTOM VIEW

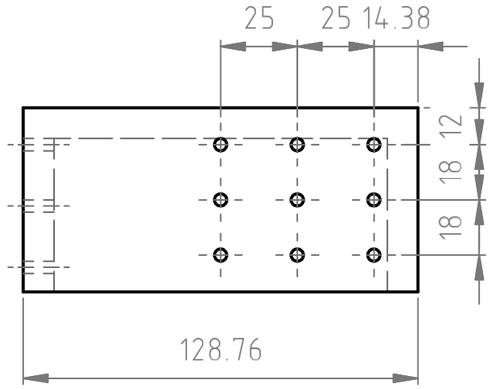

FRONT VIEW

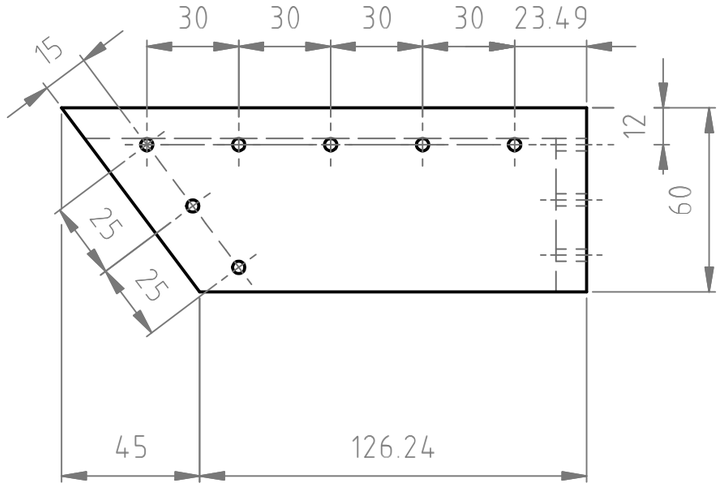

SIDE VIEW

CENTRE SPLITTER - BOTTOM FRONT PART

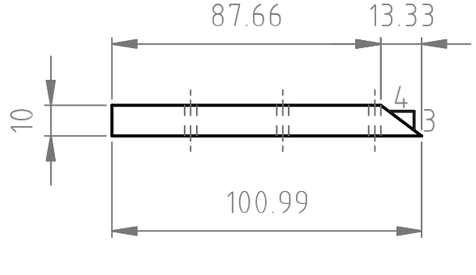

SIDE VIEW

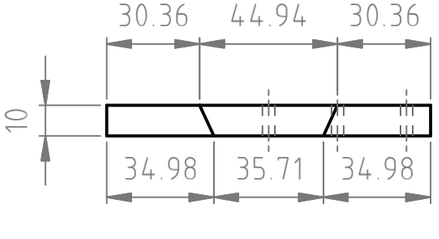

FRONT VIEW

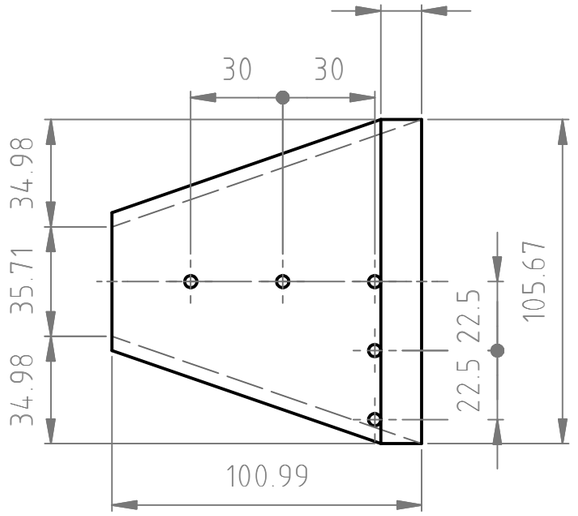

TOP VIEW

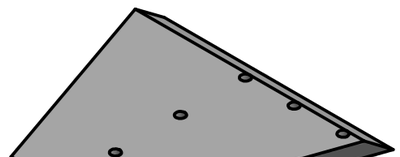

FILE NAME	FSCM NO	SHEET	SCALE 1 : 2
SIZE A3			
DRAWN 2015-11-16 Gerard Calitz			
CHECK			
APPR.			
ISSUED			
REV			
CONTRACT NO			

Model 01

Centre Splitter Parts (01)

DWG NO

GC-M01-SPL01

CENTRE SPLITTER - BOTTOM LEFT PART

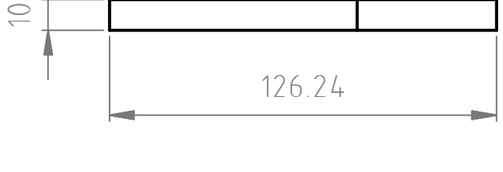

BOTTOM VIEW

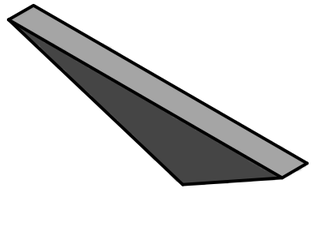

FRONT VIEW

SIDE VIEW

CENTRE SPLITTER - BOTTOM RIGHT PART

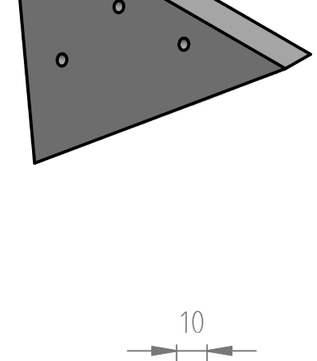

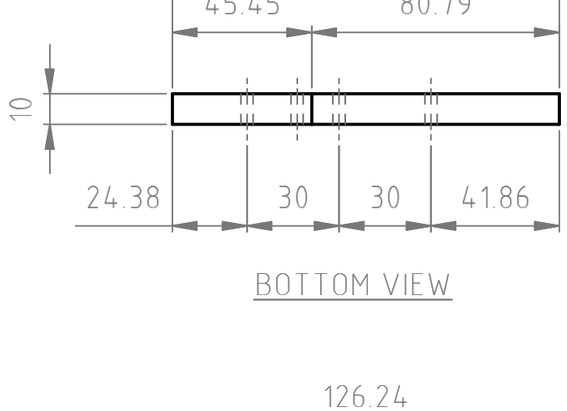

BOTTOM VIEW

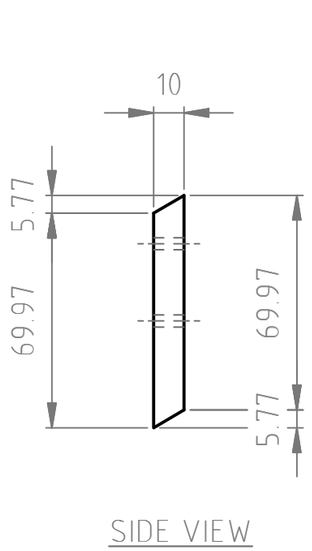

SIDE VIEW

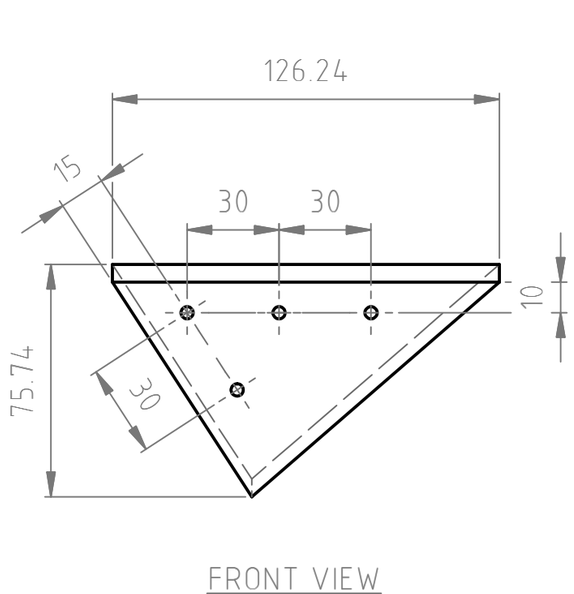

FRONT VIEW

FILE NAME	FSCM NO	SHEET	SCALE 1 : 2
SIZE A3			
DRAWN 2015-11-19 Gerard Calitz			
CHECK			
APPR.			
ISSUED			
REV			
CONTRACT NO		DWG NO GC-M01-SPL02	

Model 01
Centre Splitter Parts (02)

Stellenbosch University https://scholar.sun.ac.za

LEFT HALF SPLITTER

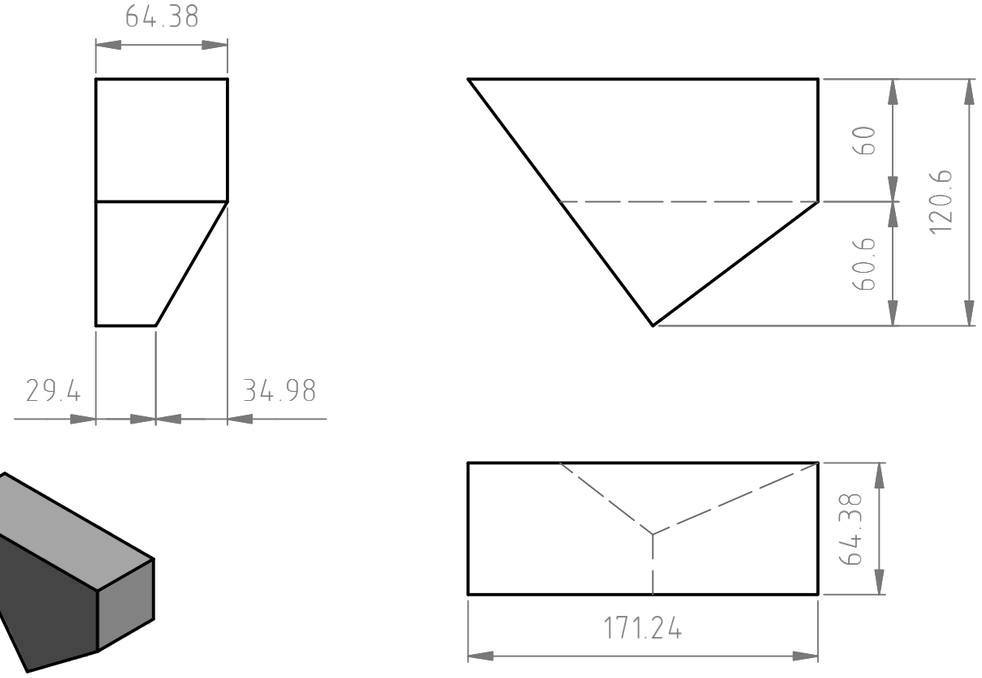

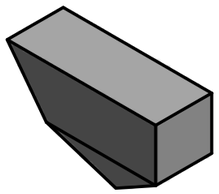

RIGHT HALF SPLITTER

FULL SPLITTER

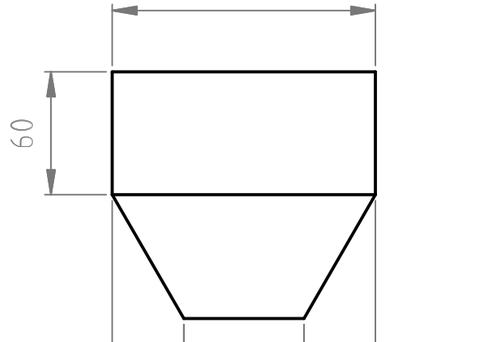

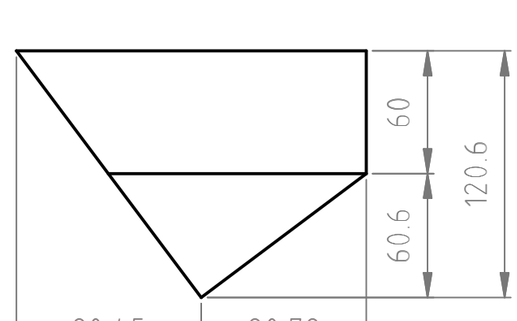

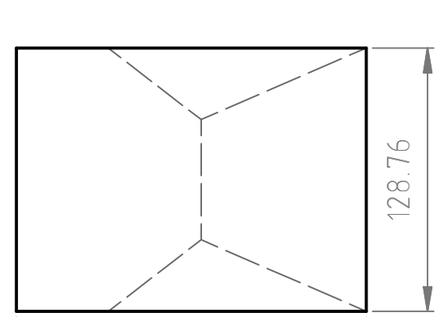

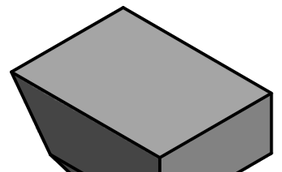

The left and right half splitters can be made by cutting a full splitter in half.

Ensure that the width of the cut is as small as possible

FILE NAME	FSCM NO	SHEET	SCALE 1 : 3
SIZE A3			
DRAWN 2015-11-19 Gerard Calitz			
CHECK			
APPR.			
ISSUED			
REV			
CONTRACT NO			

Model 01
Other Splitters

DWG NO
GC-M01-SPL03

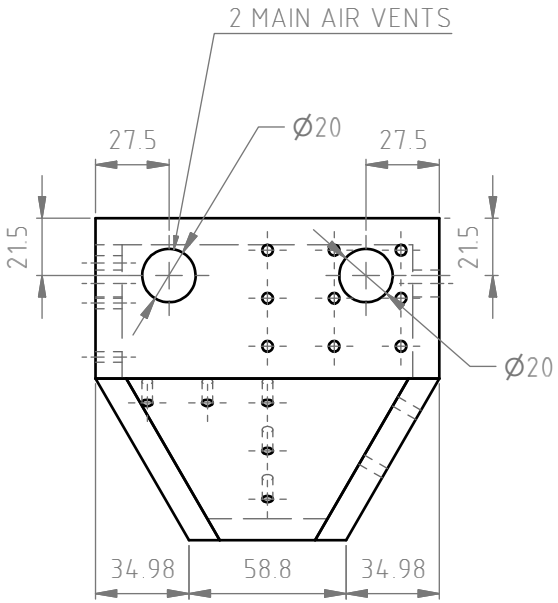

FRONT VIEW

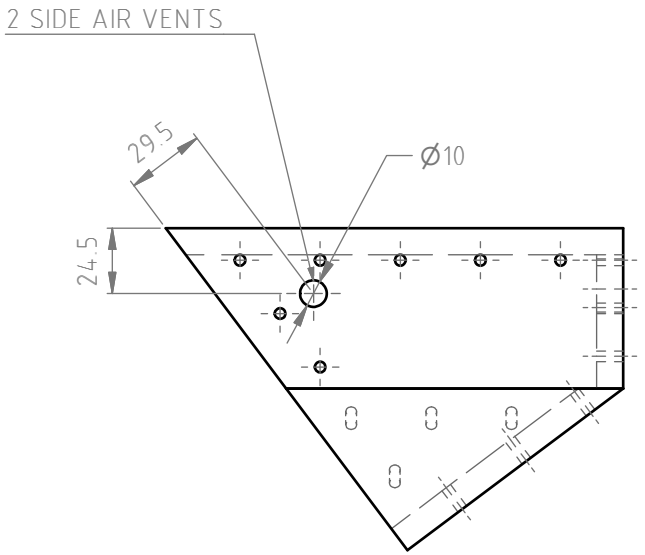

SIDE VIEW

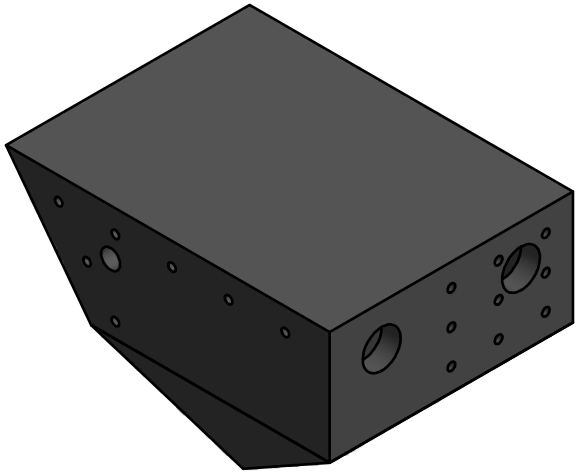

FILE NAME	FSCM NO	SHEET	SCALE 1 : 2
SIZE A3			
DRAWN 2016-08-13 Gerard Calitz			
CHECK			
APPR.			
ISSUED			
REV			
CONTRACT NO			

Model 02

Centre Splitter Assembly

DWG NO

GC-M02-SPL00

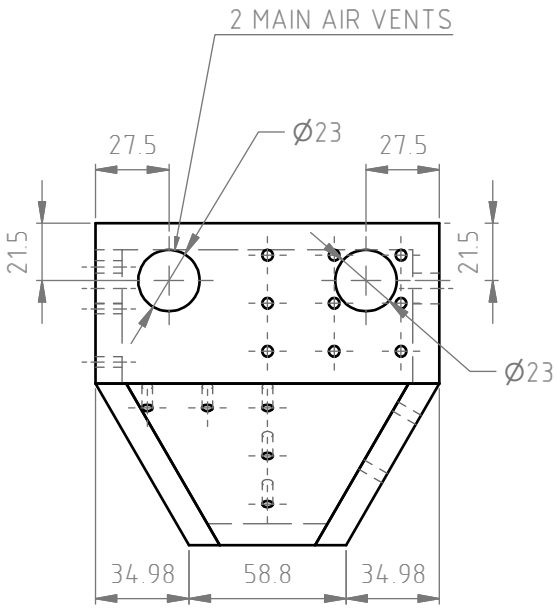

FRONT VIEW

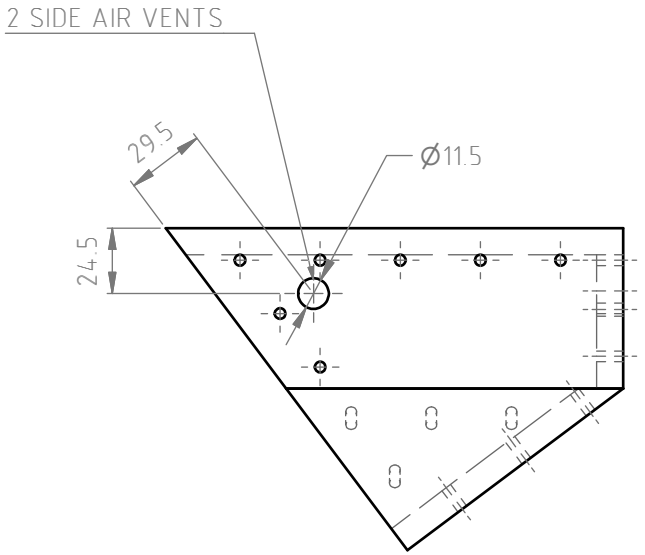

SIDE VIEW

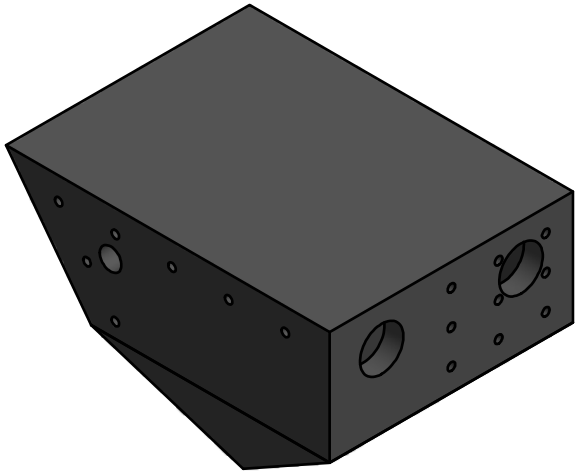

FILE NAME	FSCM NO	SHEET	SCALE 1 : 2
SIZE A3			
DRAWN 2016-08-13 Gerard Calitz			
CHECK			
APPR.			
ISSUED			
REV			
CONTRACT NO			

Model 03
Centre Splitter Assembly

DWG NO
GC-M03-SPL00

F.2. As Built Ogee Spillway

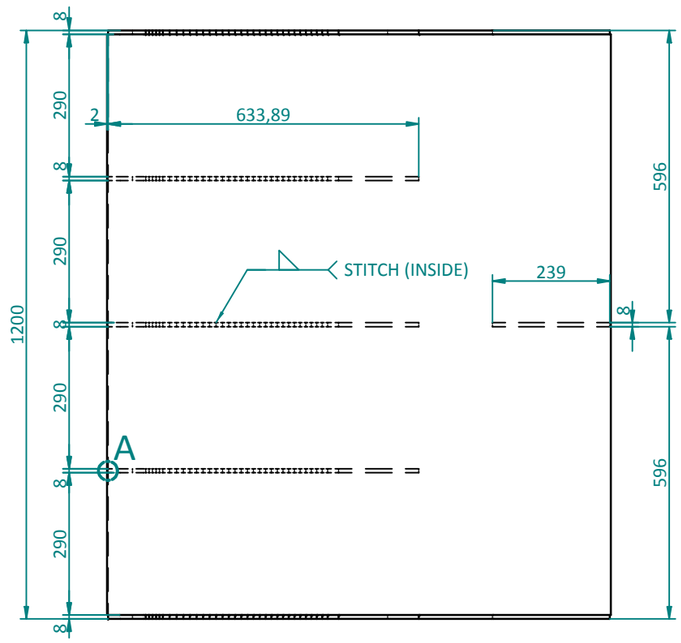

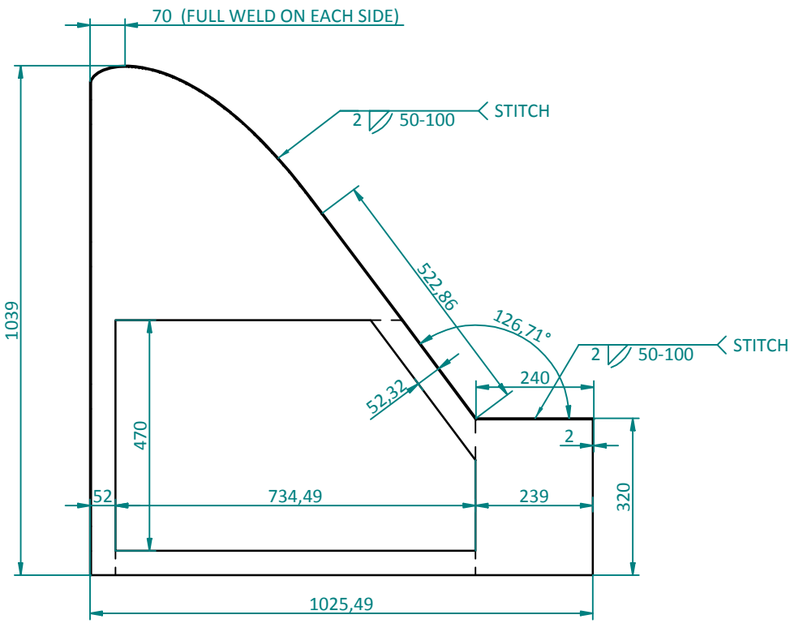

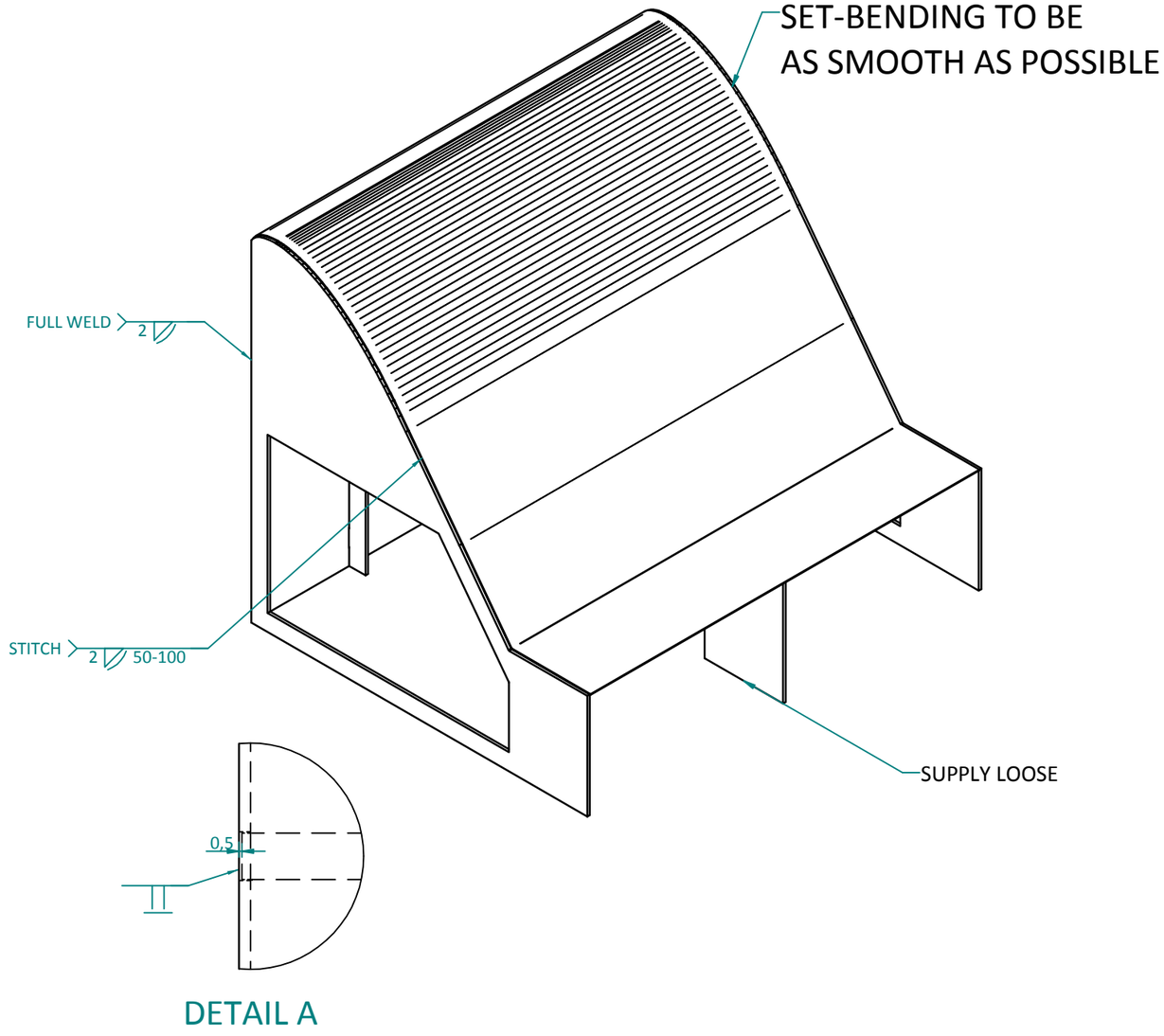

DETAIL A

DRAWN: sjvvuuren
CHECKED BY:
DATE: 2015/09/07
CHECKED DATE:

REVISIONS

REV	DATE	BY	DESCRIPTION

Tolerance Class	Linear Dimensions								Angular Dimensions			Straightness, flatness & parallelism							
	Range of nominal sizes, l, in mm								Range of nominal sizes, l, in mm (length or shorter leg)			Range of nominal sizes, l, in mm (relates to longer side of the surface)							
	2 to 30	>30 to 120	>120 to 400	>400 to 1000	>1000 to 2000	>2000 to 4000	>4000 to 8000	>8000 to 12000	UP to 400	>400 to 1000	>1000	>30 to 120	>120 to 400	>400 to 1000	>1000 to 2000	>2000 to 4000	>4000 to 8000	>8000 to 12000	
	Tolerance, t, in mm								Range of nominal sizes, Δα (in degrees and minutes)			Tolerance, t, in mm							
	± 1	± 2	± 2	± 3	± 4	± 6	± 8	± 10	± 45	± 30	± 20	1	1.5	3	4.5	6	8	10	
Welded Construction Tolerances DIN & ISO 13920																			

Permissible deviations in mm for range	Linear Tolerance Class M (medium)	Angular Tolerance Class M (medium)
0.5 - 3	± 0.1	± 0.1°
3 - 6	± 0.1	± 0.1°
6 - 30	± 0.2	± 0°-30'
30 - 120	± 0.3	± 0°-20'
120 - 400	± 0.5	± 0°-10'
400 - 1000	± 0.8	± 0°-05'
1000 - 2000	± 1.2	-
2000 - 4000	± 2.0	-

DIN & ISO 2768 Machining Tolerance

THIRD ANGLE

A3

CLIENT: UNIVERSITEIT STELLENBOSCH

TITLE: OGEE

FABRINOX

PART No.	000-0R00	FABRINOX DOCUMENT REV	00
STOCK No.	UNI003-00002421	CLIENT DOCUMENT REV	A
DRAWING No.	01-000	SCALE: NTS	SHEET No. 1 / 7

FILE LOCATION: G:\Acc Receivable\UNI003 - Universiteit Stellenbosch\Technical Info (drawings)\UNI003-00002421\UNI003-00002421-01-000.dft

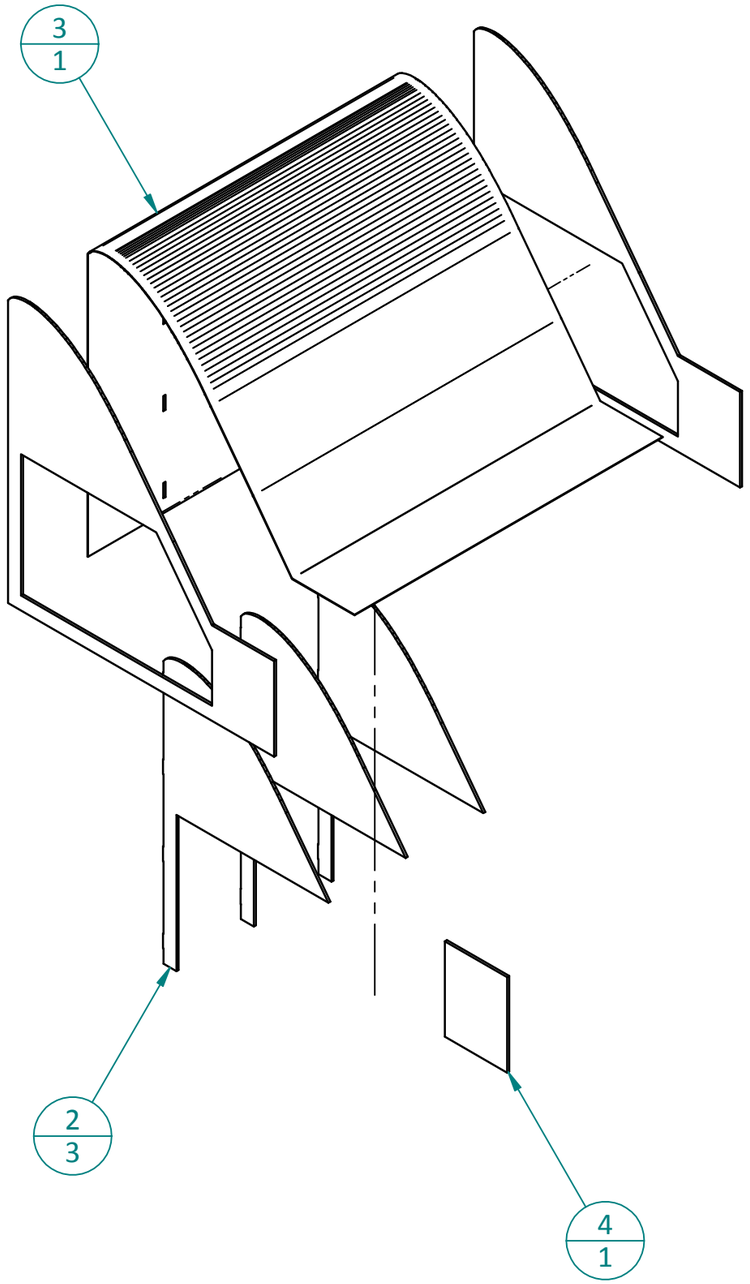

Item Number	File Name (no extension)	Material	Material Thickness	Quantity
1*	0001-2R00	MildSteel	8.00 mm	2
2	0002-2R00	MildSteel	8.00 mm	3
3	0004-2R00	MildSteel	2.00 mm	1
4	0003-2R00	MildSteel	8.00 mm	1

CHECKED DATE:

CHECKED BY:

DATE: 2015/09/07

DRAWN: sjvvuuren

REVISIONS

REV	DATE	BY	DESCRIPTION

Tolerance Class	Linear Dimensions								Angular Dimensions			Straightness, flatness & parallelism							
	Range of nominal sizes, l, in mm								Range of nominal sizes, l, in mm (length or shorter leg)			Range of nominal sizes, l, in mm (relates to longer side of the surface)							
	2 to 30	>30 to 120	>120 to 400	>400 to 1000	>1000 to 2000	>2000 to 4000	>4000 to 8000	>8000 to 12000	UP to 400	>400 to 1000	>1000	>30 to 120	>120 to 400	>400 to 1000	>1000 to 2000	>2000 to 4000	>4000 to 8000	>8000 to 12000	
	Tolerance, t, in mm								Range of nominal sizes, Δα (in degrees and minutes)			Tolerance, t, in mm							
	± 1	± 2	± 2	± 3	± 4	± 6	± 8	± 10	± 45	± 30	± 20	1	1.5	3	4.5	6	8	10	
Welded Construction Tolerances DIN & ISO 13920																			

Permissible deviations in mm for range	Linear Tolerance Class M (medium)	Angular Tolerance Class M (medium)
0.5 - 3	± 0.1	± 0.1°
3 - 6	± 0.1	± 0.1°
6 - 30	± 0.2	± 0°-30'
30 - 120	± 0.3	± 0°-20'
120 - 400	± 0.5	± 0°-10'
400 - 1000	± 0.8	± 0°-05'
1000 - 2000	± 1.2	-
2000 - 4000	± 2.0	-

DIN & ISO 2768 Machining Tolerance

THIRD ANGLE

A3

CLIENT: UNIVERSITEIT STELLENBOSCH

TITLE: OGEE

FABRINOX

PART No.	000-0R00	FABRINOX DOCUMENT REV	00
STOCK No.	UNI003-00002421	CLIENT DOCUMENT REV	A
DRAWING No.	02-000	SCALE: NTS	SHEET No. 2 / 7

FILE LOCATION: G:\Acc Receivable\UNI003 - Universiteit Stellenbosch\Technical Info (drawings)\UNI003-00002421\UNI003-00002421-01-000.dft

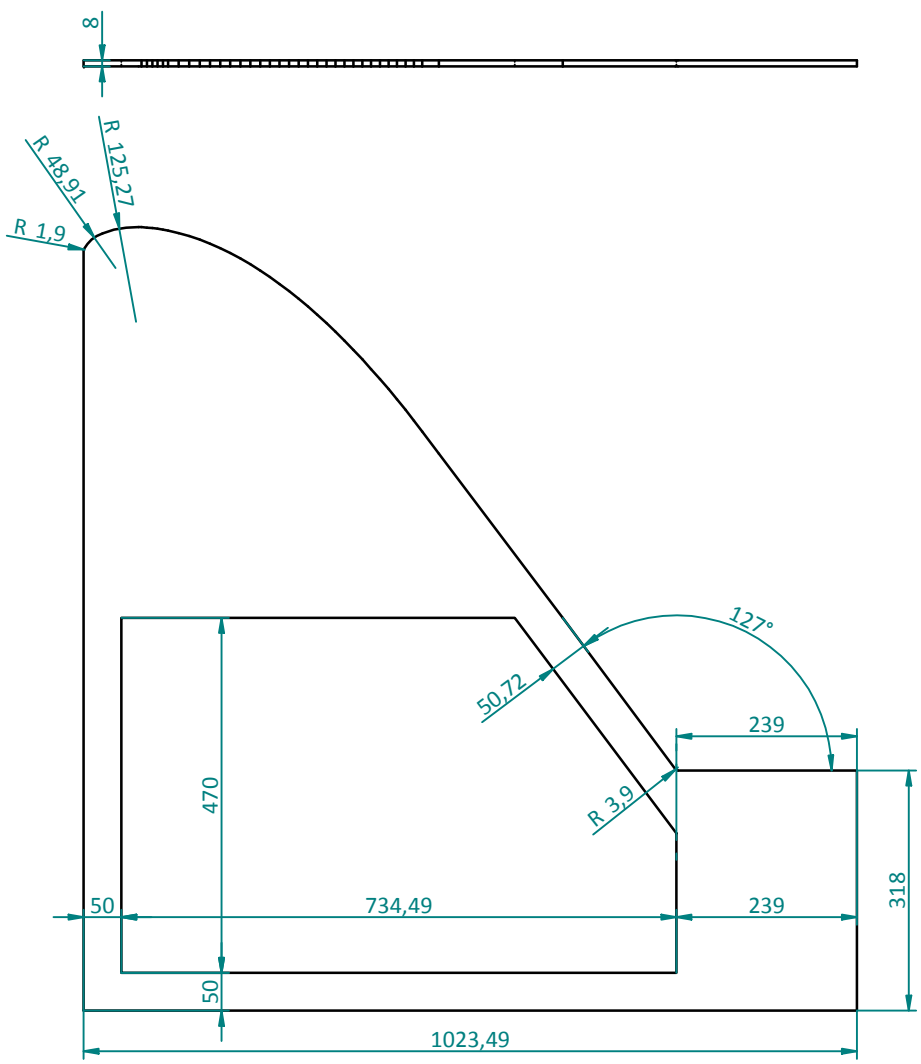

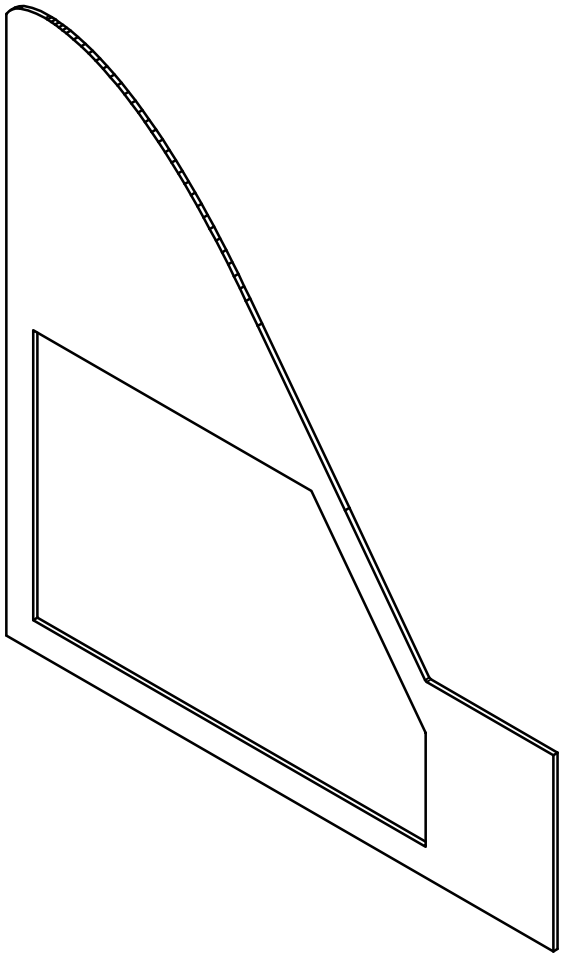

File Name (no extension)	Material	Material Thickness
0001-2R00	MildSteel	8.00 mm

CHECKED BY & DATE:

DATE: 2015/09/07

DRAWN: sjvvuuren

Permissible deviations in mm for range	Linear Tolerance Class M (medium)	Angular Tolerance Class M (medium)
0.5 - 3	± 0.1	± 0.1°
3 - 6	± 0.1	± 0.1°
6 - 30	± 0.2	± 0°-30'
30 - 120	± 0.3	± 0°-20'
120 - 400	± 0.5	± 0°-10'
400 - 1000	± 0.8	± 0°-05'
1000 - 2000	± 1.2	-
2000 - 4000	± 2.0	-

DIN & ISO 2768 Machining Tolerance

REVISIONS

REV	DATE	BY	DESCRIPTION

THIRD ANGLE

A4

CLIENT: UNIVERSITEIT STELLENBOSCH

TITLE: OGEE

FABRINOX

PART No.	0001-2R00	FABRINOX DOCUMENT REV	00
STOCK No.	UNI003-00002421	CLIENT DOCUMENT REV	A
DRAWING No.	03-0001	SCALE: NTS	SHEET No. 3 / 7

FILE LOCATION: G:\Acc Receivable\UNI003 - Universiteit Stellenbosch\Technical Info (drawings)\UNI003-00002421\UNI003-00002421-01-000.dft

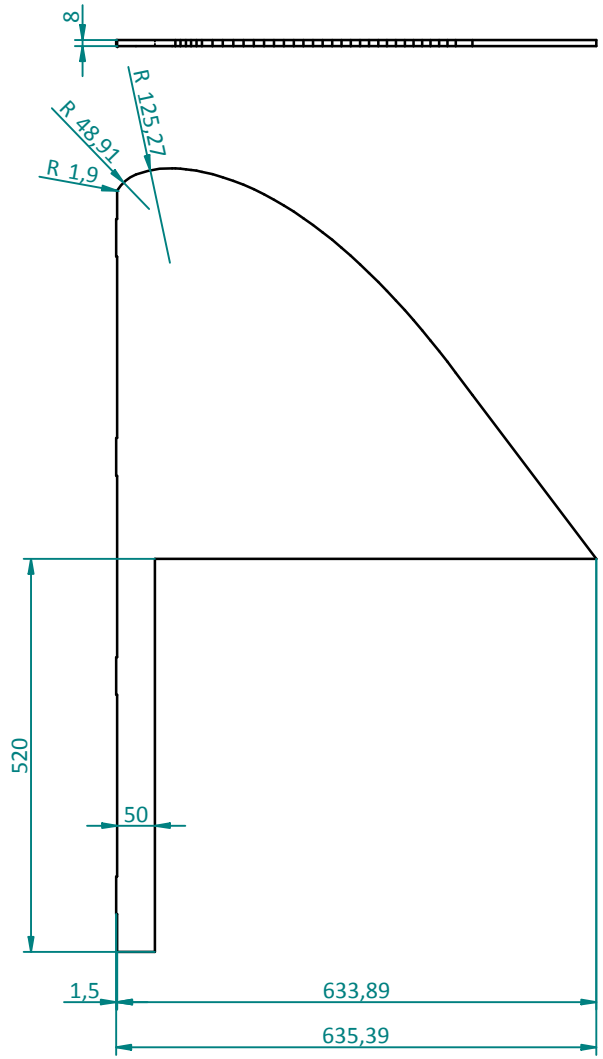

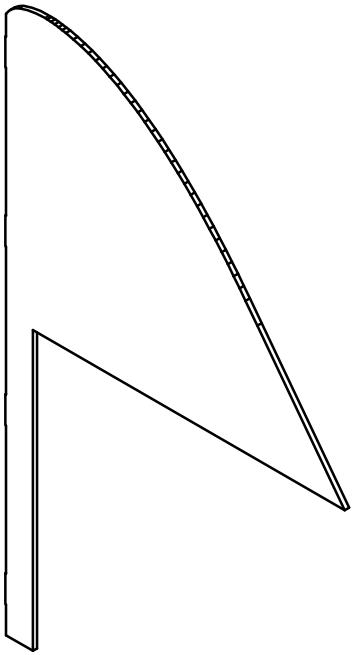

NO CORNER TREATMENT

File Name (no extension)	Material	Material Thickness
0002-2R00	MildSteel	8.00 mm

CHECKED BY & DATE:

DATE: 2015/09/07

DRAWN: sjvvuuren

Permissible deviations in mm for range	Linear Tolerance Class M (medium)	Angular Tolerance Class M (medium)
0.5 - 3	± 0.1	± 0.1°
3 - 6	± 0.1	± 0.1°
6 - 30	± 0.2	± 0°-30'
30 - 120	± 0.3	± 0°-20'
120 - 400	± 0.5	± 0°-10'
400 - 1000	± 0.8	± 0°-05'
1000 - 2000	± 1.2	-
2000 - 4000	± 2.0	-

DIN & ISO 2768 Machining Tolerance

REVISIONS

REV	DATE	BY	DESCRIPTION

THIRD ANGLE

A4

CLIENT: UNIVERSITEIT STELLENBOSCH

TITLE: OGEE

FABRINOX

PART No.	0002-2R00	FABRINOX DOCUMENT REV	00
STOCK No.	UNI003-00002421	CLIENT DOCUMENT REV	A
DRAWING No.	04-0002	SCALE: NTS	SHEET No. 4 / 7

FILE LOCATION: G:\Acc Receivable\UNI003 - Universiteit Stellenbosch\Technical Info (drawings)\UNI003-00002421\UNI003-00002421-01-000.dft

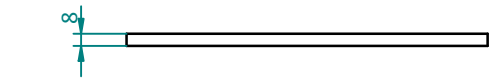

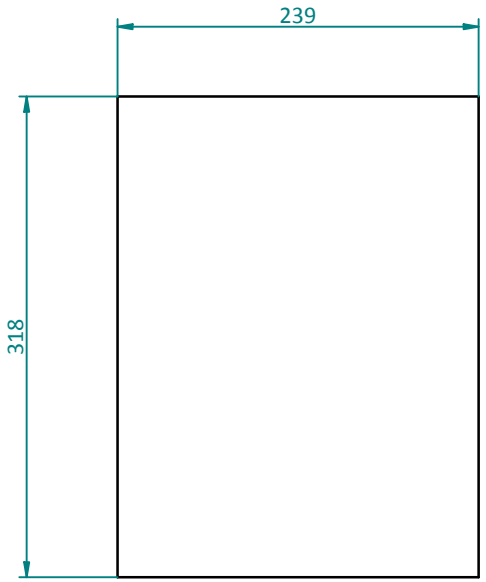

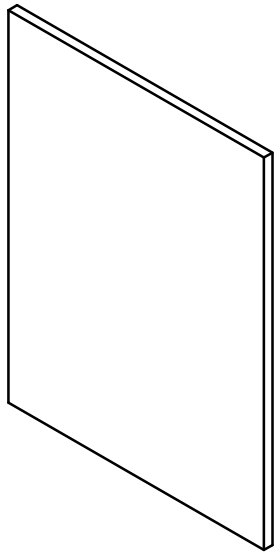

CHECKED BY & DATE:

DATE: 2015/09/07

DRAWN: sjvvuuren

File Name (no extension)	Material	Material Thickness
0003-2R00	MildSteel	8.00 mm

Permissible deviations in mm for range	Linear Tolerance Class M (medium)	Angular Tolerance Class M (medium)
0.5 - 3	± 0.1	± 0.1°
3 - 6	± 0.1	± 0.1°
6 - 30	± 0.2	± 0°-30'
30 - 120	± 0.3	± 0°-20'
120 - 400	± 0.5	± 0°-10'
400 - 1000	± 0.8	± 0°-05'
1000 - 2000	± 1.2	-
2000 - 4000	± 2.0	-

DIN & ISO 2768 Machining Tolerance

REVISIONS

REV	DATE	BY	DESCRIPTION

THIRD ANGLE

A4

CLIENT: UNIVERSITEIT STELLENBOSCH

TITLE: OGEE

FABRINOX

PART No.	0003-2R00	FABRINOX DOCUMENT REV	00
STOCK No.	UNI003-00002421	CLIENT DOCUMENT REV	A
DRAWING No.	05-0003	SCALE: NTS	SHEET No. 5 / 7

FILE LOCATION: G:\Acc Receivable\UNI003 - Universiteit Stellenbosch\Technical Info (drawings)\UNI003-00002421\UNI003-00002421-01-000.dft

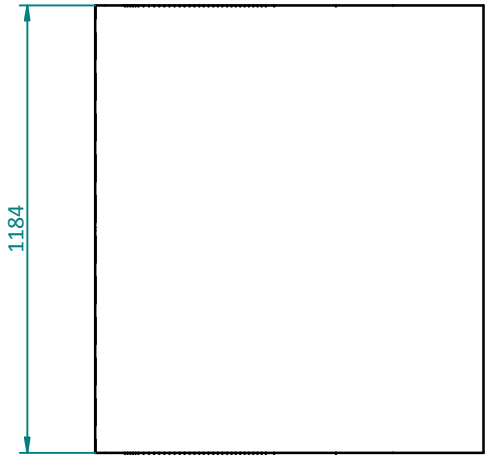

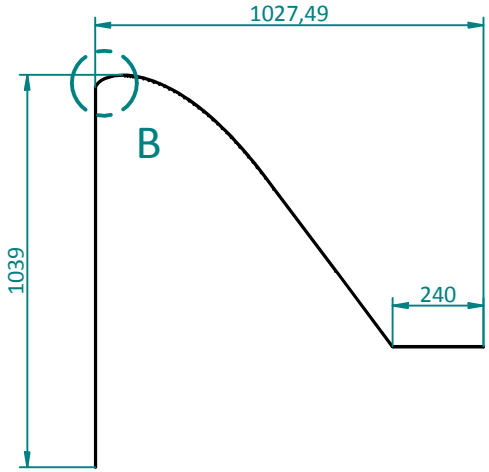

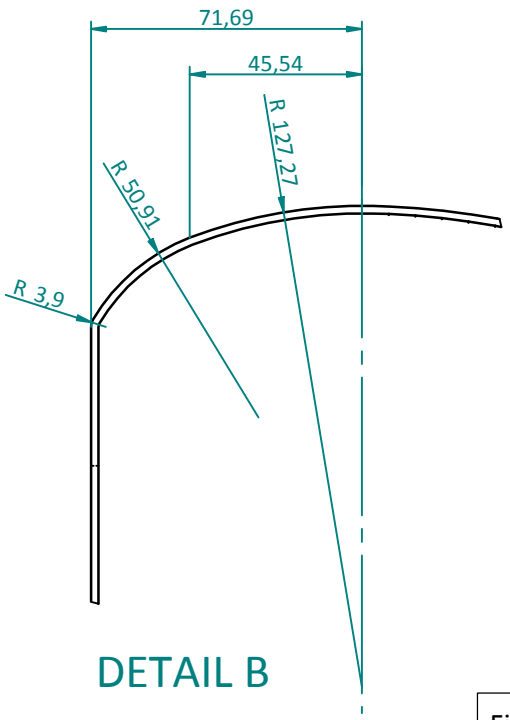

DETAIL B

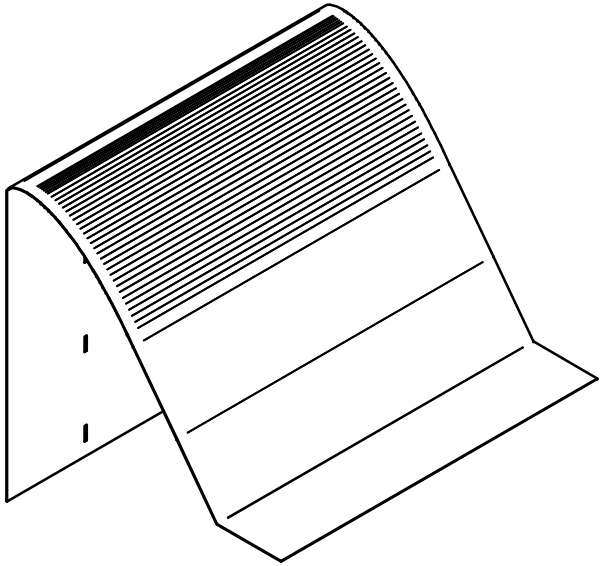

CHECKED BY & DATE:

DATE: 2015/09/07

DRAWN: sjvvuuren

File Name (no extension)	Material	Material Thickness
0004-2R00	MildSteel	2.00 mm

Permissible deviations in mm for range	Linear Tolerance Class M (medium)	Angular Tolerance Class M (medium)
0.5 - 3	± 0.1	± 0.1°
3 - 6	± 0.1	± 0.1°
6 - 30	± 0.2	± 0°-30'
30 - 120	± 0.3	± 0°-20'
120 - 400	± 0.5	± 0°-10'
400 - 1000	± 0.8	± 0°-05'
1000 - 2000	± 1.2	-
2000 - 4000	± 2.0	-

DIN & ISO 2768 Machining Tolerance

REVISIONS

REV	DATE	BY	DESCRIPTION

THIRD ANGLE

A4

CLIENT: UNIVERSITEIT STELLENBOSCH

TITLE: OGEE

FABRINOX

PART No.	0004-2R00	FABRINOX DOCUMENT REV	00
STOCK No.	UNI003-00002421	CLIENT DOCUMENT REV	A
DRAWING No.	06-0004	SCALE: NTS	SHEET No. 6 / 7

FILE LOCATION: G:\Acc Receivable\UNI003 - Universiteit Stellenbosch\Technical Info (drawings)\UNI003-00002421\UNI003-00002421-01-000.dft

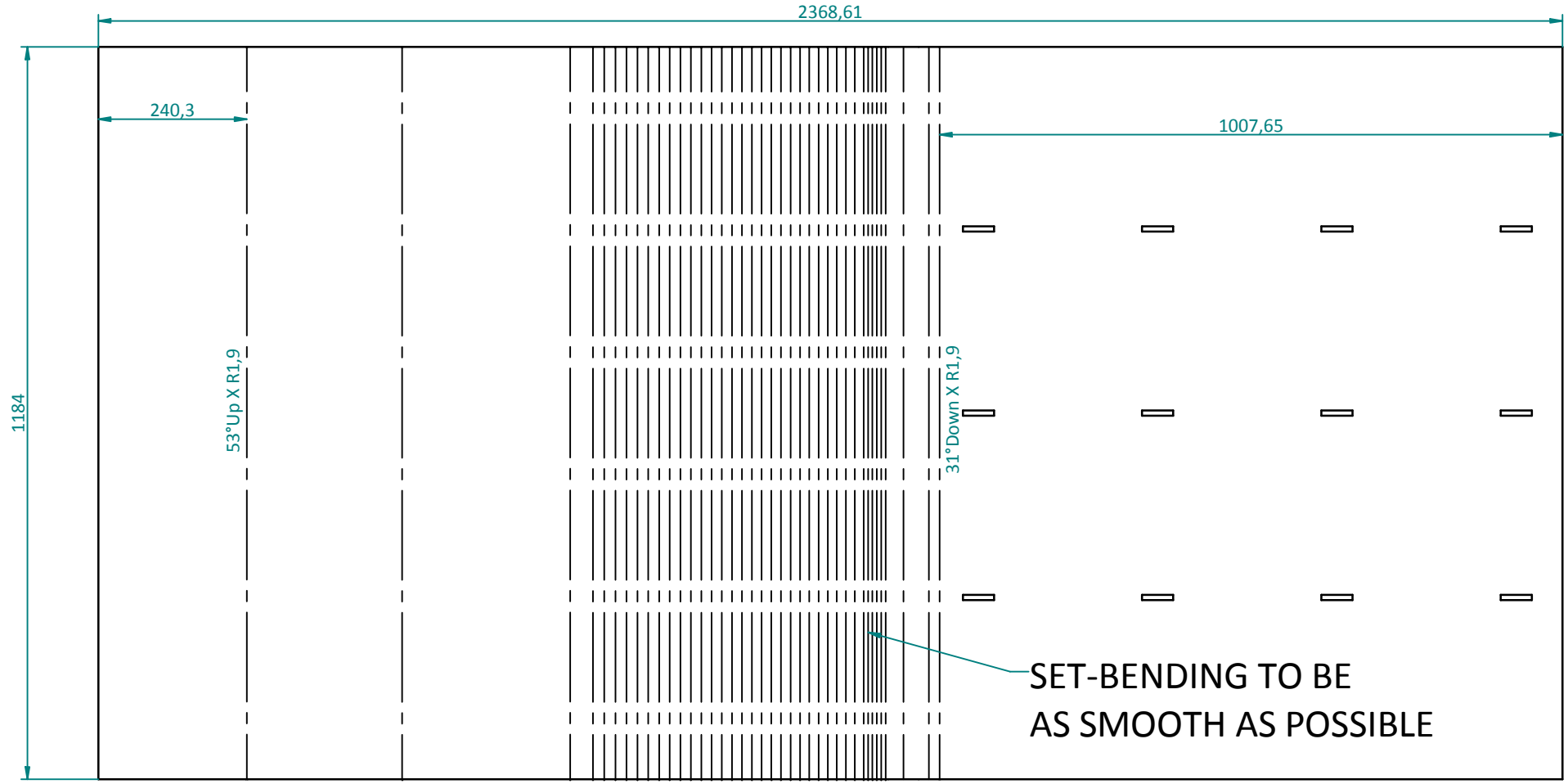

NO CORNER TREATMENT

File Name (no extension)	Material	Material Thickness
0004-2R00	MildSteel	2.00 mm

CHECKED BY & DATE:

DATE: 2015/09/07

DRAWN: sjvvuuren

Permissible deviations in mm for range	Linear Tolerance Class M (medium)	Angular Tolerance Class M (medium)
0.5 - 3	± 0.1	± 0.1°
3 - 6	± 0.1	± 0.1°
6 - 30	± 0.2	± 0°-30'
30 - 120	± 0.3	± 0°-20'
120 - 400	± 0.5	± 0°-10'
400 - 1000	± 0.8	± 0°-05'
1000 - 2000	± 1.2	-
2000 - 4000	± 2.0	-

DIN & ISO 2768 Machining Tolerance

REVISIONS

REV	DATE	BY	DESCRIPTION

THIRD ANGLE

A4

CLIENT: UNIVERSITEIT STELLENBOSCH

TITLE: OGEE

FABRINOX

PART No.	0004-2R00	FABRINOX DOCUMENT REV	00
STOCK No.	UNI003-00002421	CLIENT DOCUMENT REV	A
DRAWING No.	07-0004	SCALE: NTS	SHEET No. 7 / 7

FILE LOCATION: G:\Acc Receivable\UNI003 - Universiteit Stellenbosch\Technical Info (drawings)\UNI003-00002421\UNI003-00002421-01-000.dft

APPENDIX G
COMPLETE TESTING SCHEDULE

The tests were performed according to the schedule set out within these tables.

G.1. Unaerated Model

Table G-1: Test conditions - Unaerated model with splitter 1 (14 pressure sensors)

Test no.	q_p (m²/s)	Q_m (l/s)	H_m (mm)	Air% and photographs	Comments
1	5	67.1	94	Yes	
2	10	134.2	145	Yes	
3	15	201.2	186	Yes	
4	20	268.3	222	Yes	
5	25	335.4	255	Yes	
6	30	402.5	285	Yes	
7	35	469.6	313	Yes	
8	40	536.7	339	Yes	
9	45	603.7	364	Yes	
10	50	670.8	388	Yes	
11	30	402.5	285	Yes	Repeatability test
12	30	402.5	285	Yes	Repeatability test
13	40	536.7	339	Yes	Repeatability test
14	40	536.7	339	Yes	Repeatability test

Table G-2: Test conditions – Unaerated model with splitter 2 (11 pressure sensors)

Test no.	q_p (m²/s)	Q_m (l/s)	H_m (mm)	Air% and photographs	Comments
15	5	67.1	94	No	
16	10	134.2	145	No	
17	15	201.2	186	No	
18	20	268.3	222	No	
19	25	335.4	255	No	
20	30	402.5	285	No	
21	35	469.6	313	No	
22	40	536.7	339	No	
23	45	603.7	364	No	
24	50	670.8	388	No	

Table G-2: Test conditions – Unaerated model with splitter 2 (11 pressure sensors)

Test no.	q_p (m²/s)	Q_m (l/s)	H_m (mm)	Air% and photographs	Comments
25	30	402.5	285	No	Repeatability test
26	30	402.5	285	No	Repeatability test
27	40	536.7	339	No	Repeatability test
28	40	536.7	339	No	Repeatability test

G.2. 1st Aerated Model

Table G-3: Test conditions – 1st Aerated model with splitter 1 (14 pressure sensors)

Test no.	q_p (m²/s)	Q_m (l/s)	H_m (mm)	Air% and photographs	Comments
29	5	67.1	94	Yes	
30	10	134.2	145	Yes	
31	15	201.2	186	Yes	
32	20	268.3	222	Yes	
33	25	335.4	255	Yes	
34	30	402.5	285	Yes	
35	35	469.6	313	Yes	
36	40	536.7	339	Yes	
37	45	603.7	364	Yes	
38	50	670.8	388	Yes	
39	30	402.5	285	Yes	Repeatability test
40	30	402.5	285	Yes	Repeatability test
41	40	536.7	339	Yes	Repeatability test
42	40	536.7	339	Yes	Repeatability test

Table G-4: Test conditions – 1st Aerated model with splitter 2 (11 pressure sensors)

Test no.	q_p (m²/s)	Q_m (l/s)	H_m (mm)	Air% and photographs	Comments
43	5	67.1	94	No	
44	10	134.2	145	No	
45	15	201.2	186	No	
46	20	268.3	222	No	
47	25	335.4	255	No	
48	30	402.5	285	No	
49	35	469.6	313	No	
50	40	536.7	339	No	
51	45	603.7	364	No	
52	50	670.8	388	No	

Table G-4: Test conditions – 1st Aerated model with splitter 2 (11 pressure sensors)

Test no.	q_p (m²/s)	Q_m (l/s)	H_m (mm)	Air% and photographs	Comments
53	30	402.5	285	No	Repeatability test
54	30	402.5	285	No	Repeatability test
55	40	536.7	339	No	Repeatability test
56	40	536.7	339	No	Repeatability test

G.3. 2nd Aerated Model

Table G-5: Test conditions – 2nd Aerated model with splitter 1 (14 pressure sensors)

Test no.	q_p (m²/s)	Q_m (l/s)	H_m (mm)	Air% and photographs	Comments
57	5	67.1	94	Yes	
58	10	134.2	145	Yes	
59	15	201.2	186	Yes	
60	20	268.3	222	Yes	
61	25	335.4	255	Yes	
62	30	402.5	285	Yes	
63	35	469.6	313	Yes	
64	40	536.7	339	Yes	
65	45	603.7	364	Yes	
66	50	670.8	388	Yes	
67	30	402.5	285	Yes	Repeatability test
68	30	402.5	285	Yes	Repeatability test
69	40	536.7	339	Yes	Repeatability test
70	40	536.7	339	Yes	Repeatability test

Table G-6: Test conditions – 2nd Aerated model with splitter 2 (11 pressure sensors)

Test no.	q_p (m²/s)	Q_m (l/s)	H_m (mm)	Air% and photographs	Comments
71	5	67.1	94	No	
72	10	134.2	145	No	
73	15	201.2	186	No	
74	20	268.3	222	No	
75	25	335.4	255	No	
76	30	402.5	285	No	
77	35	469.6	313	No	
78	40	536.7	339	No	
79	45	603.7	364	No	
80	50	670.8	388	No	

Table G-6: Test conditions – 2nd Aerated model with splitter 2 (11 pressure sensors)

Test no.	q_p (m²/s)	Q_m (l/s)	H_m (mm)	Air% and photographs	Comments
81	30	402.5	285	No	Repeatability test
82	30	402.5	285	No	Repeatability test
83	40	536.7	339	No	Repeatability test
84	40	536.7	339	No	Repeatability test

APPENDIX H
PRESSURE DATA

All prototype pressure results are contained within this appendix as graphs. The graphs contain the minimum, probable minimum, average and maximum of each sensor. For complete results in table format, please contact the author through the University of Stellenbosch's Civil Engineering Department.

All values on the x-axis denote prototype spillway head in metres, and values on the y-axis denote prototype pressure head in metres.

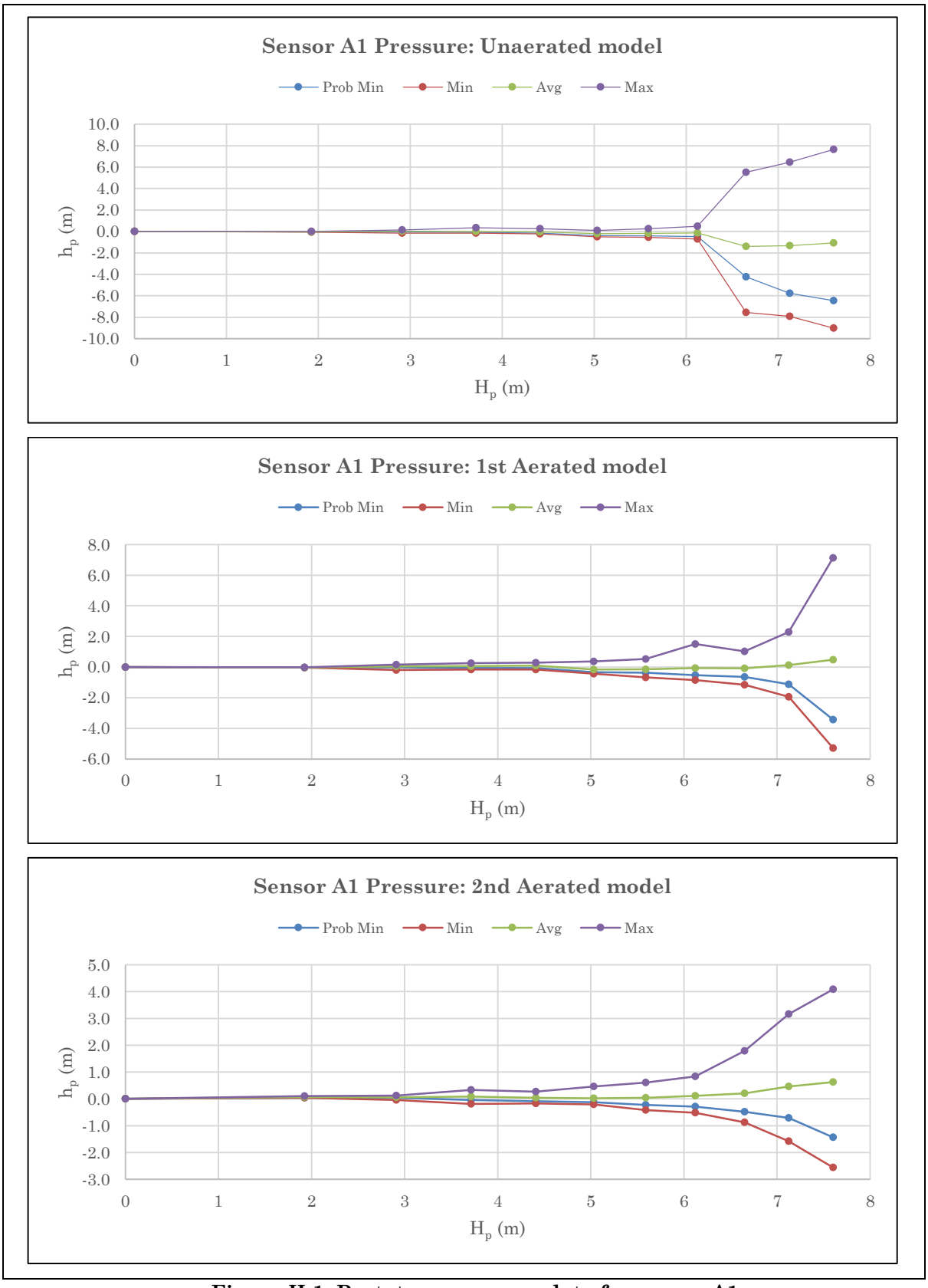

Figure H-1: Prototype pressure data for sensor A1

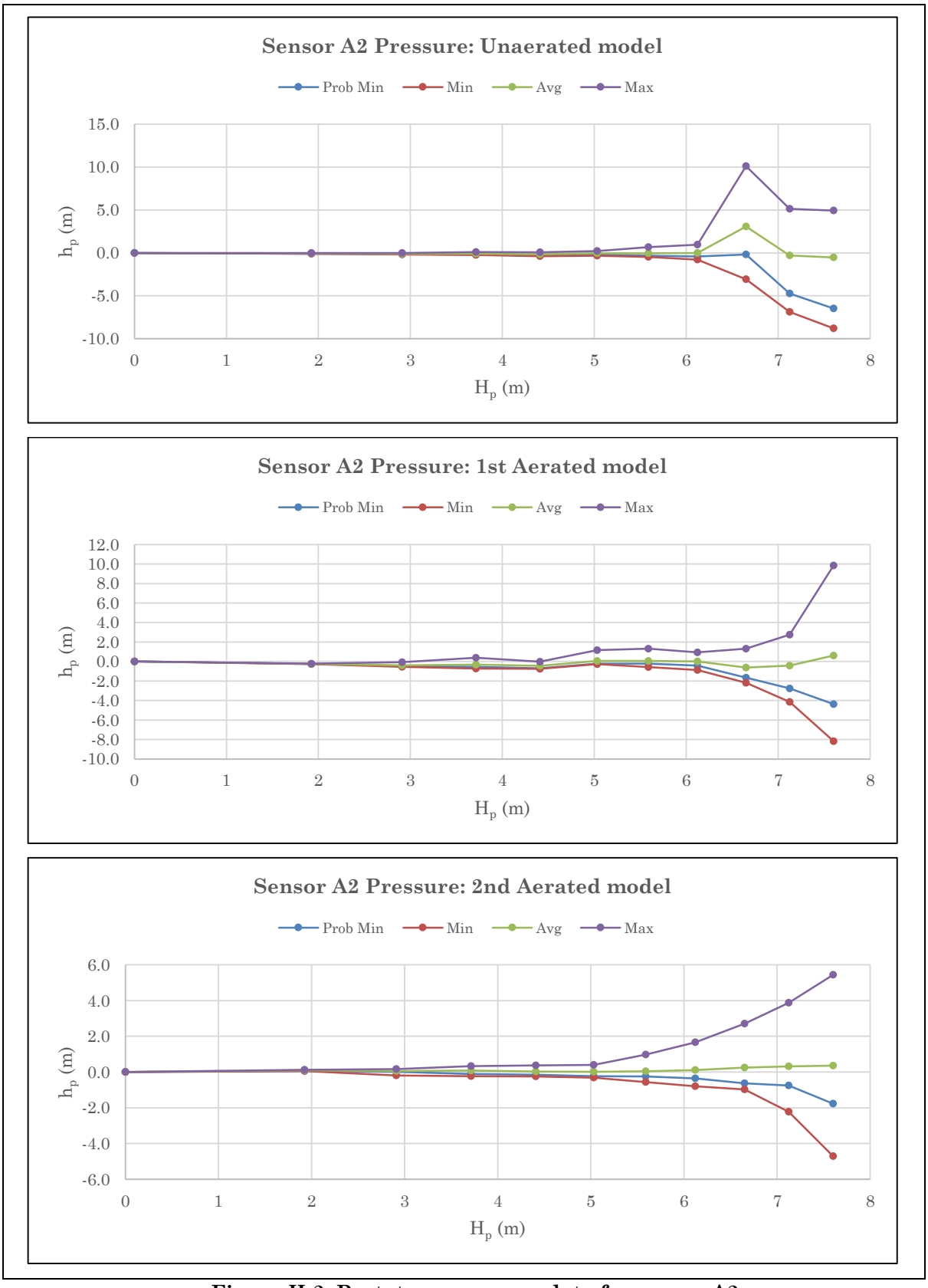

Figure H-2: Prototype pressure data for sensor A2

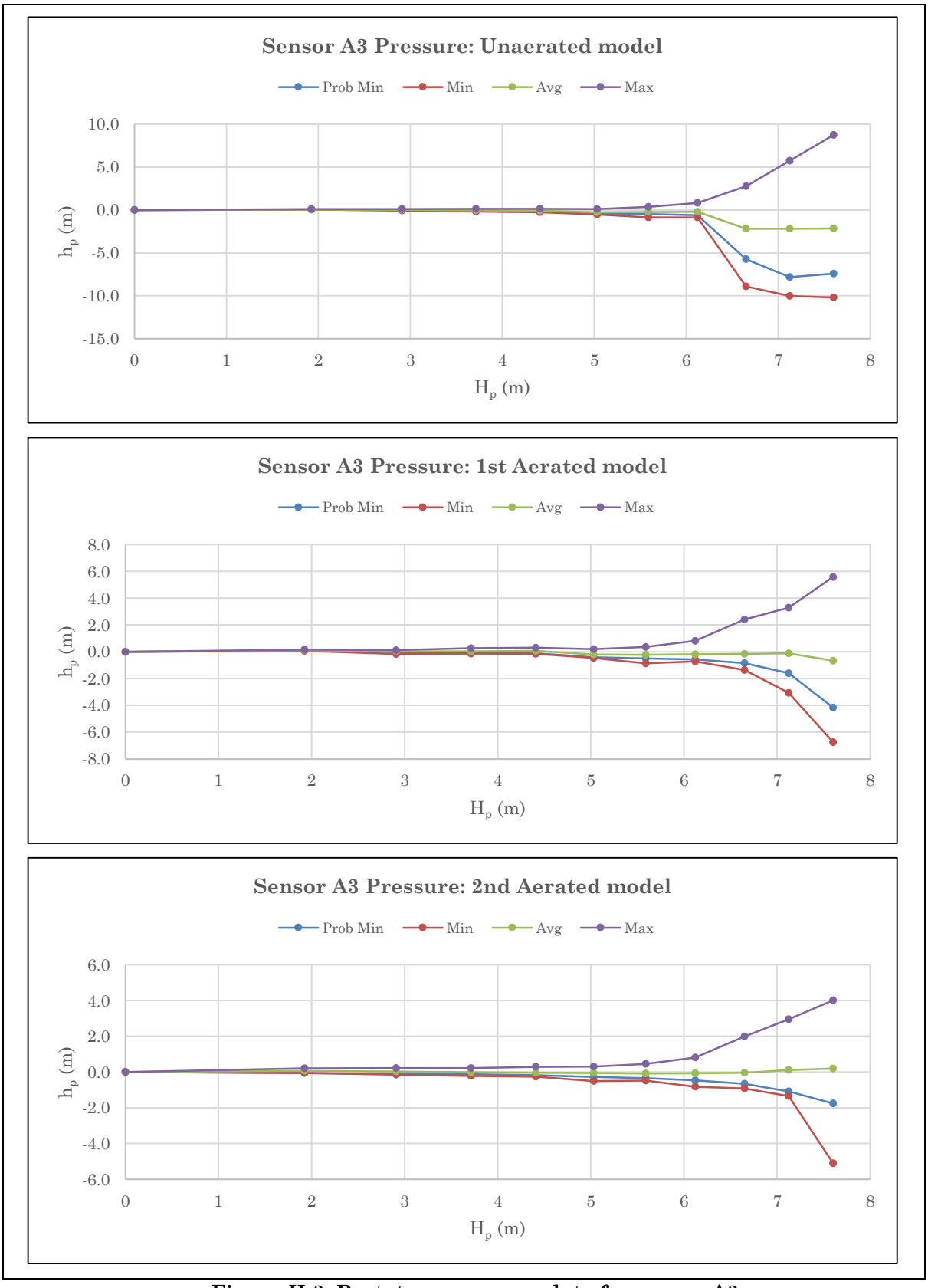

Figure H-3: Prototype pressure data for sensor A3

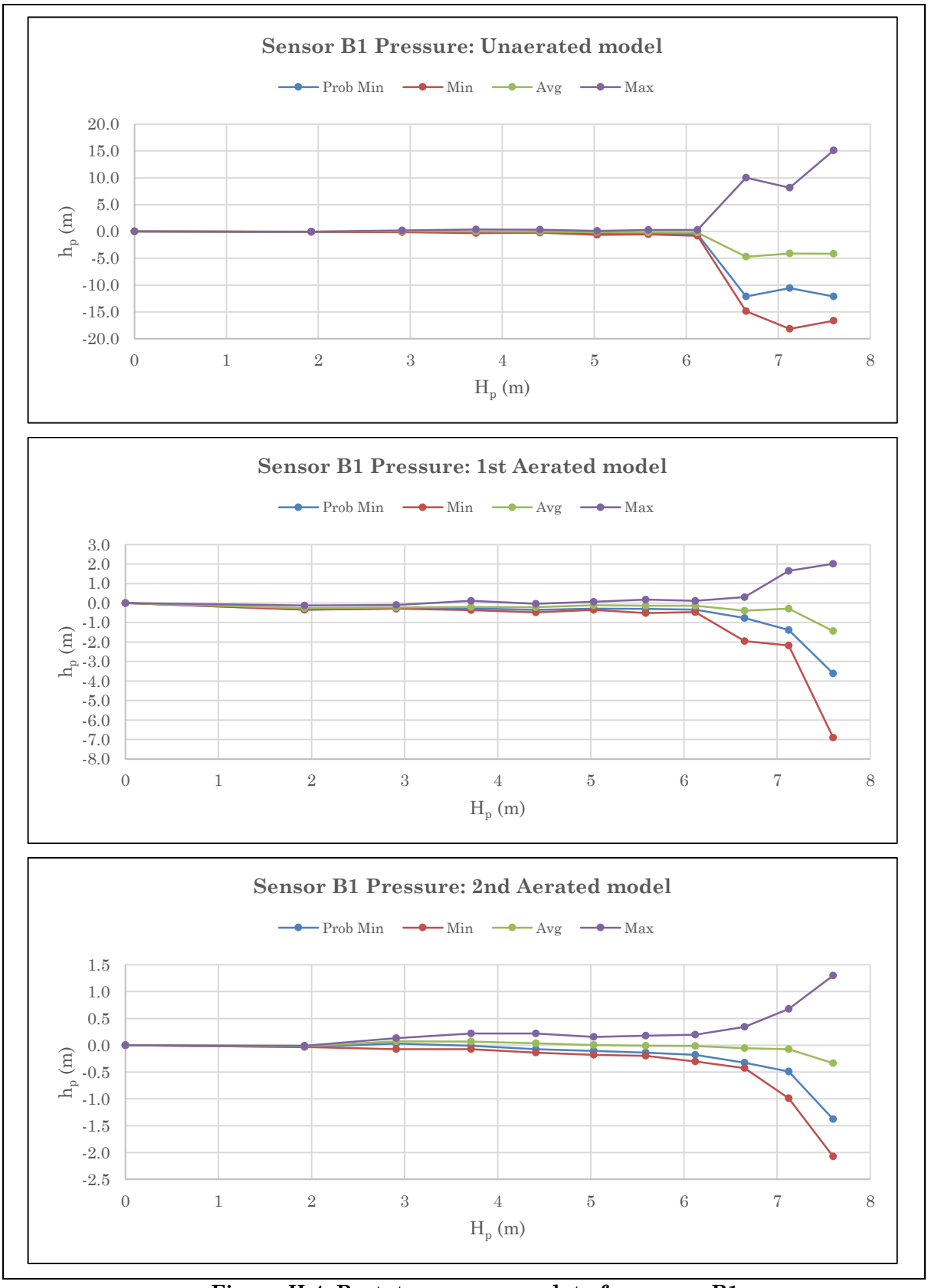

Figure H-4: Prototype pressure data for sensor B1

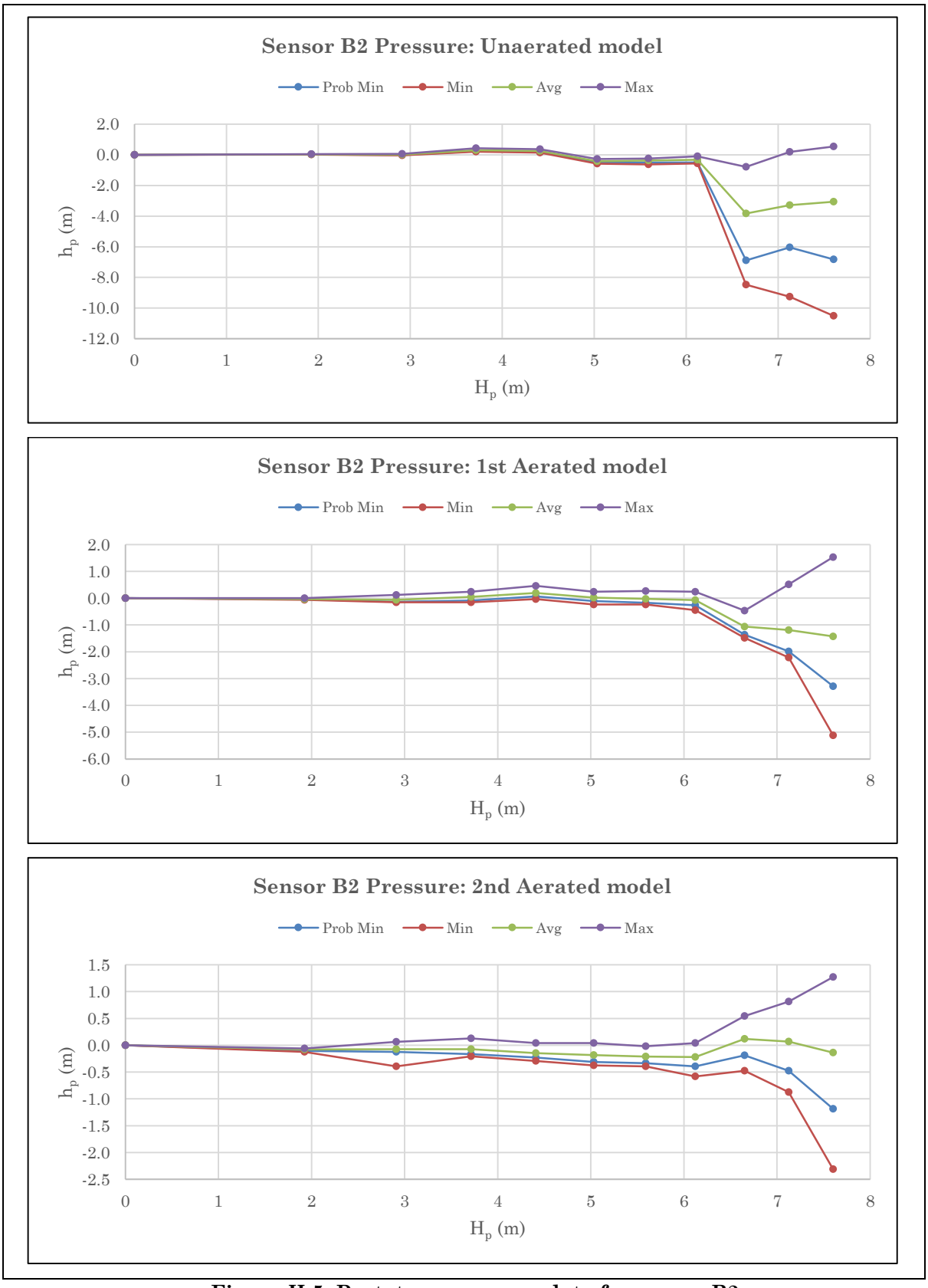

Figure H-5: Prototype pressure data for sensor B2

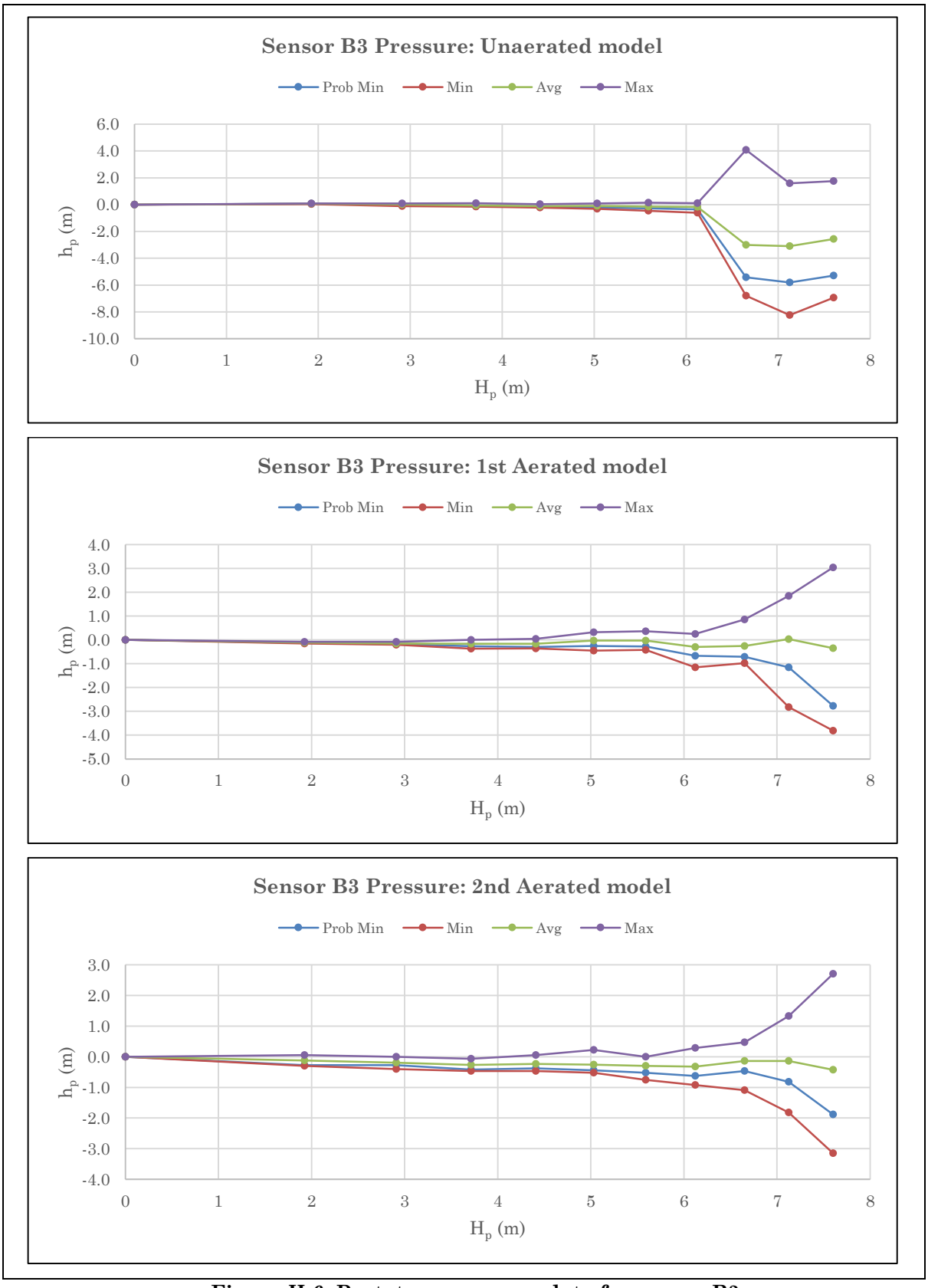

Figure H-6: Prototype pressure data for sensor B3

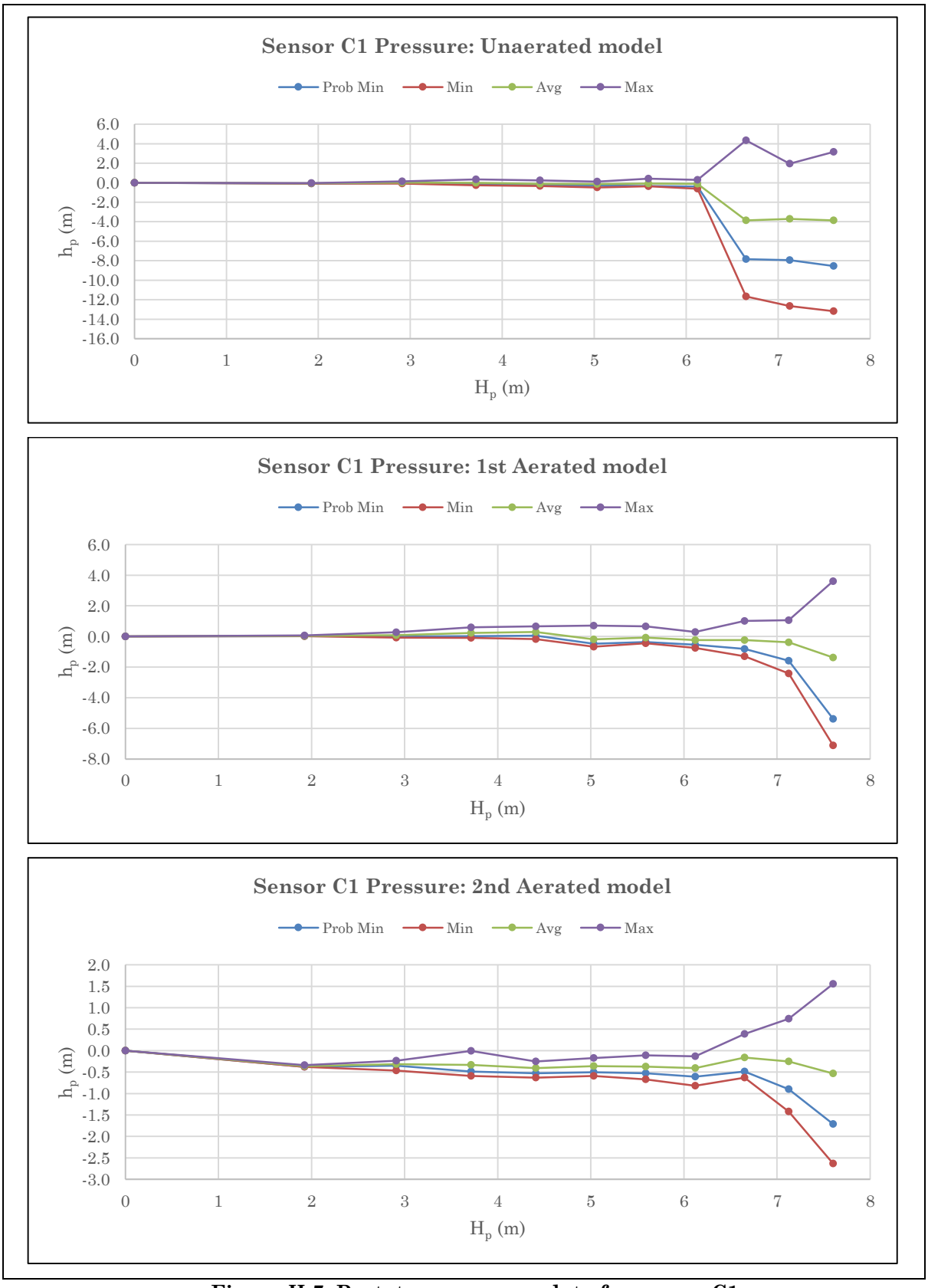

Figure H-7: Prototype pressure data for sensor C1

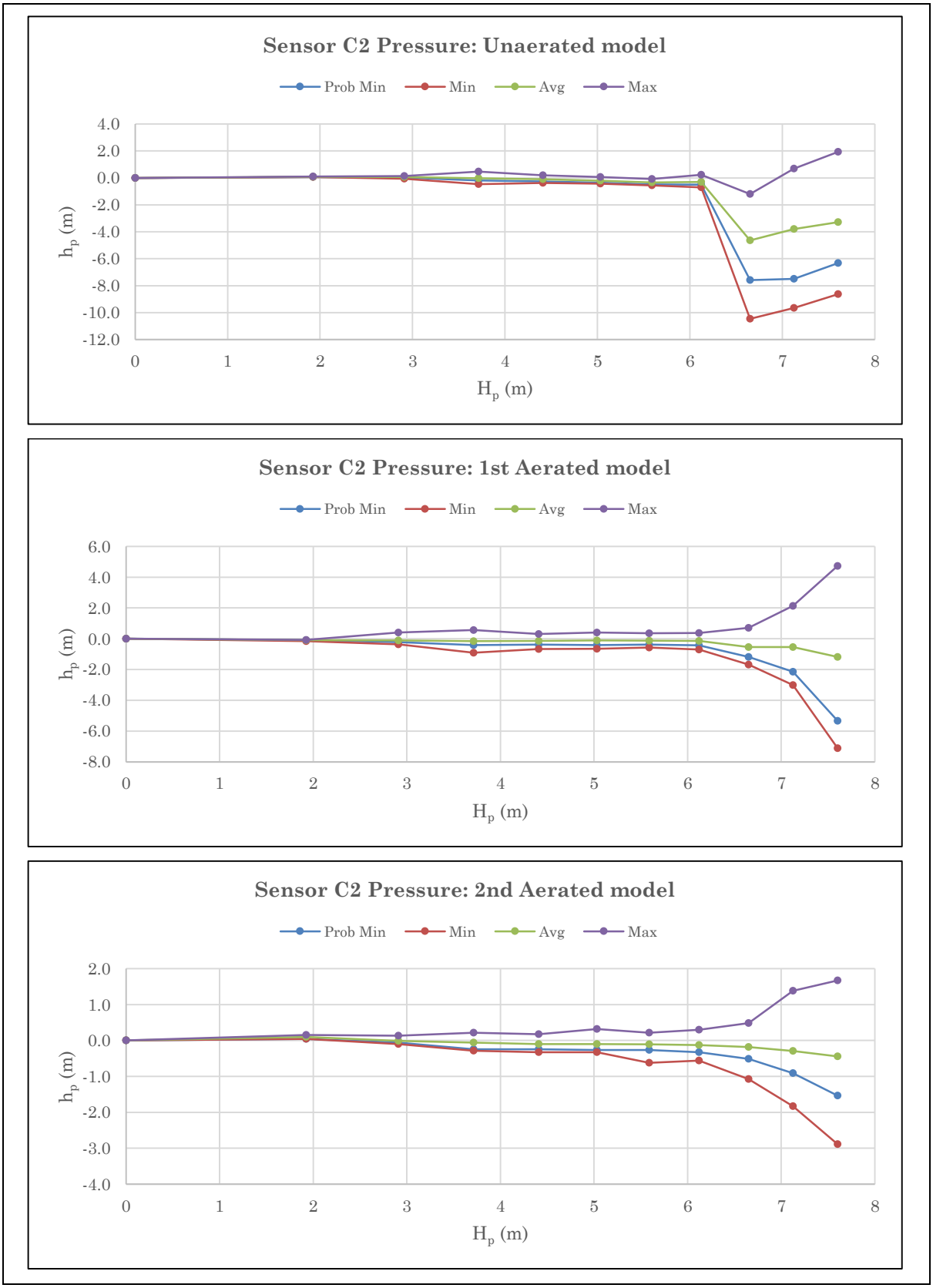

Figure H-8: Prototype pressure data for sensor C2

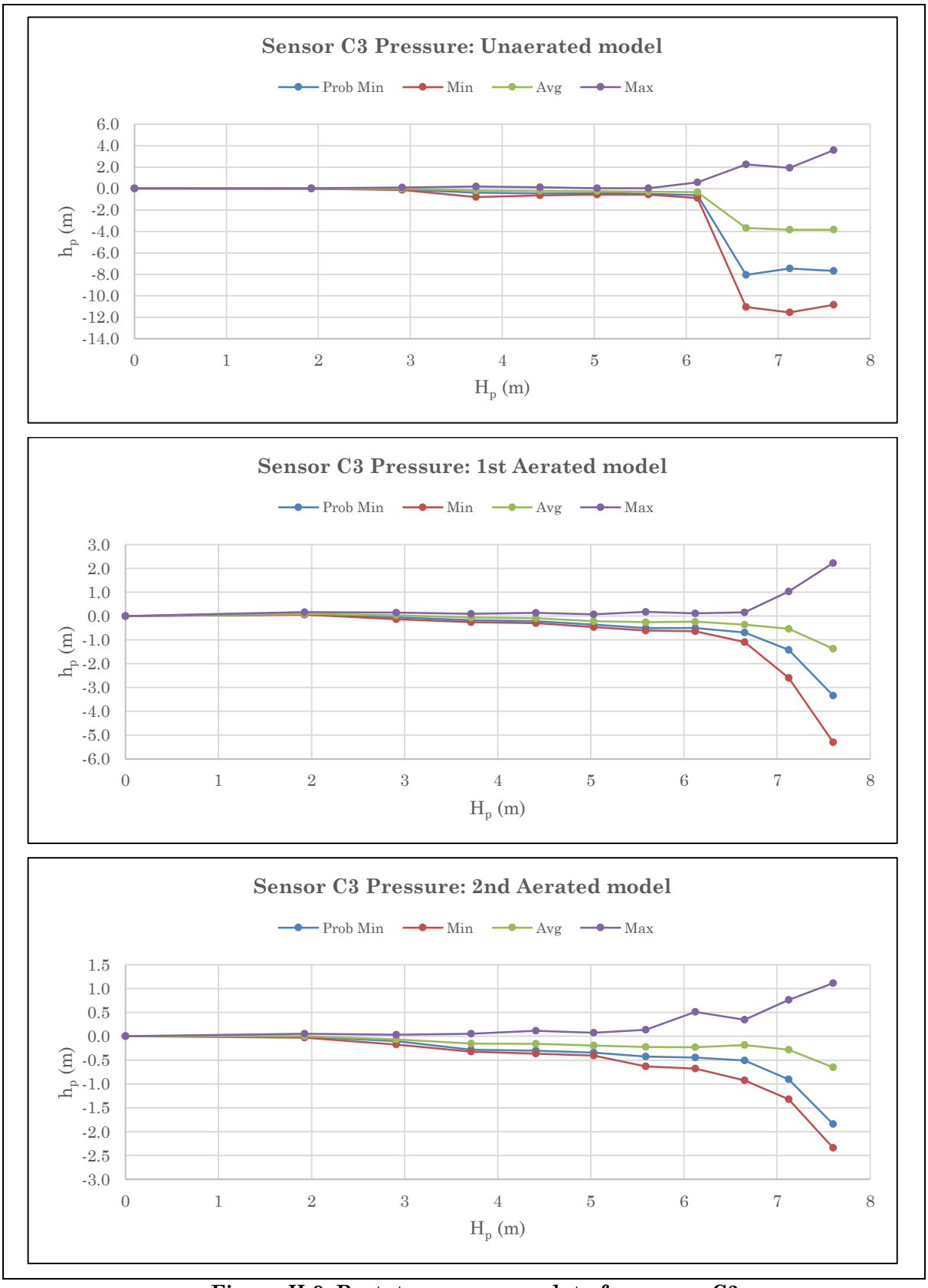

Figure H-9: Prototype pressure data for sensor C3

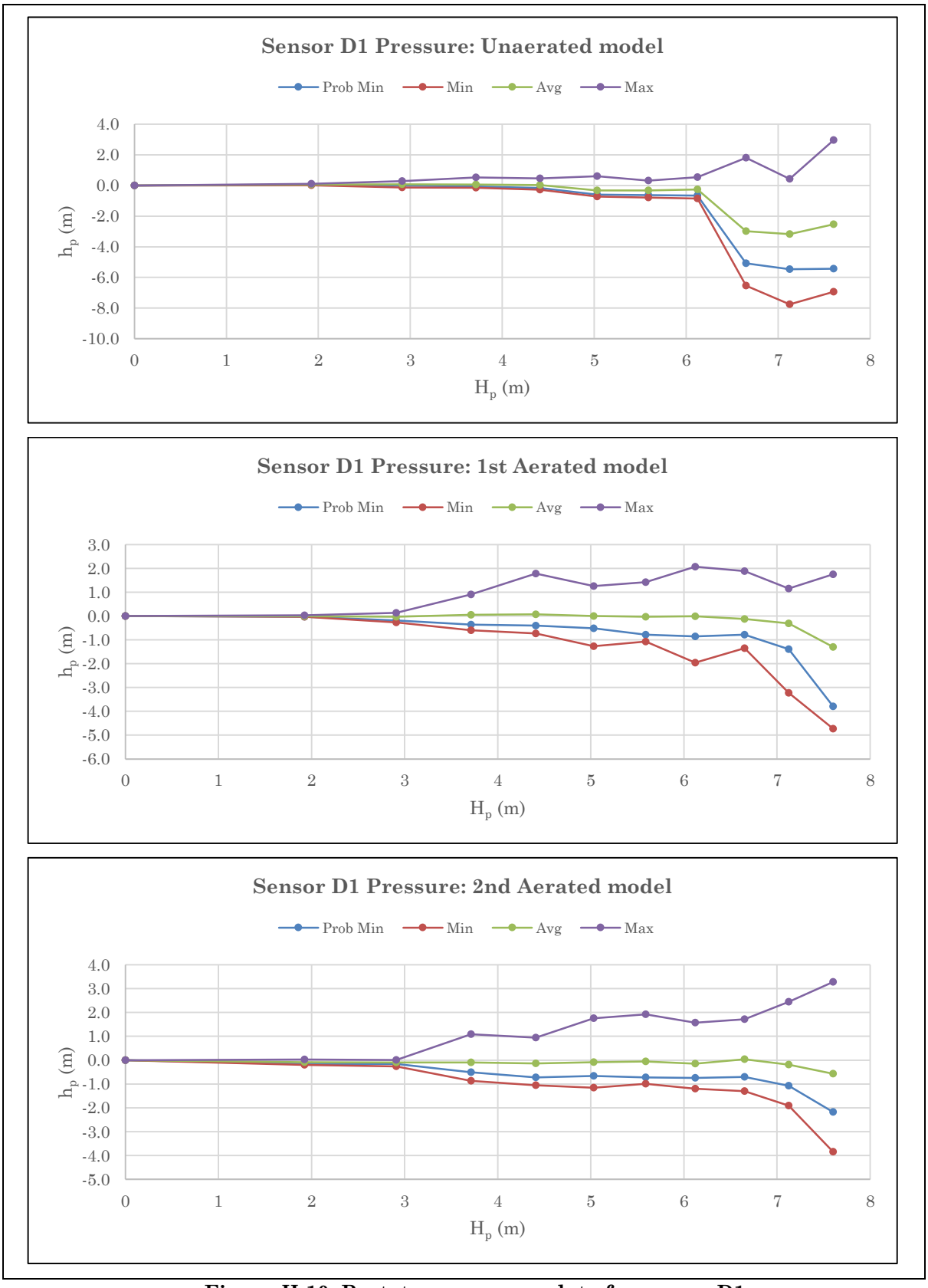

Figure H-10: Prototype pressure data for sensor D1

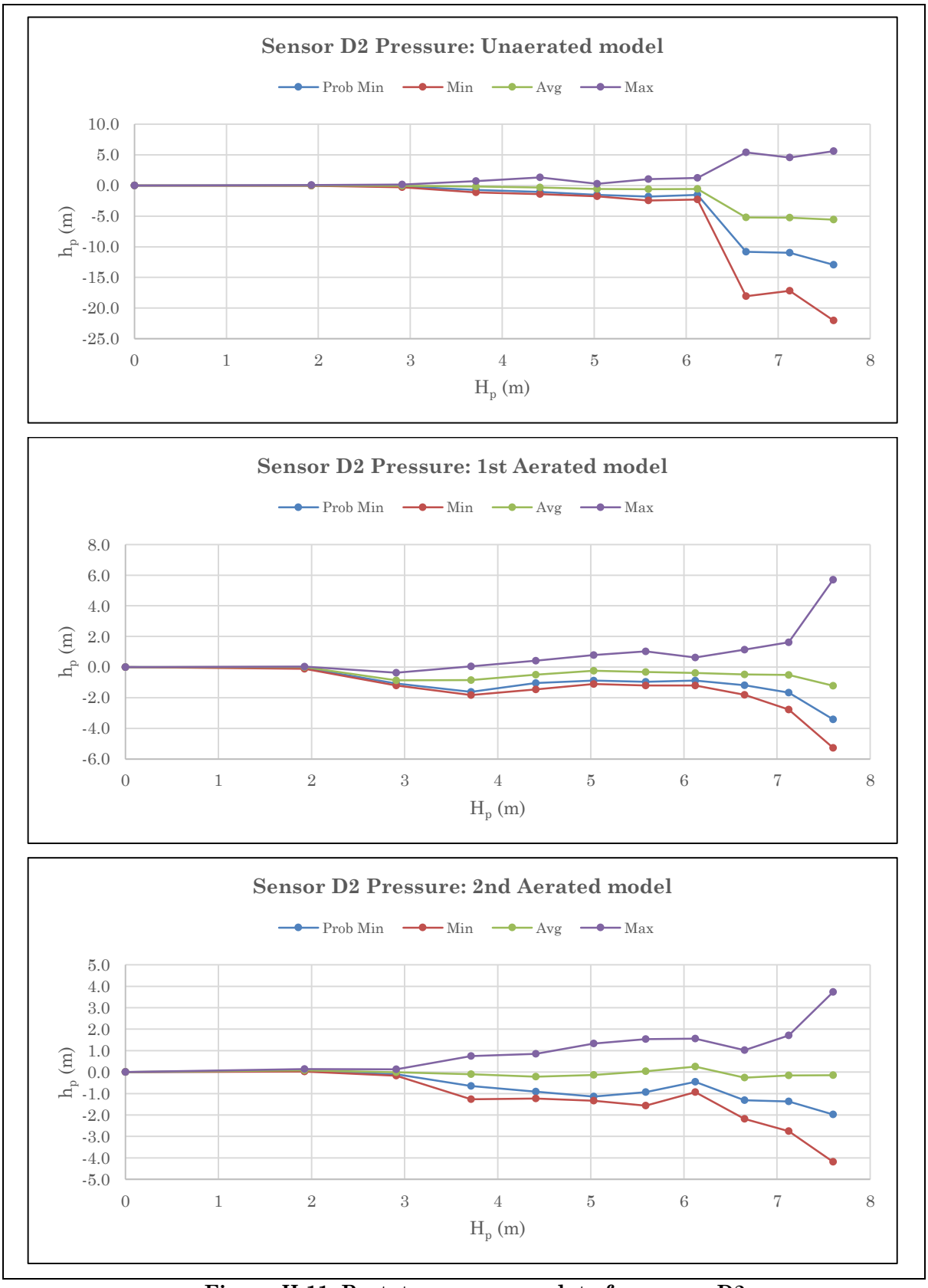

Figure H-11: Prototype pressure data for sensor D2

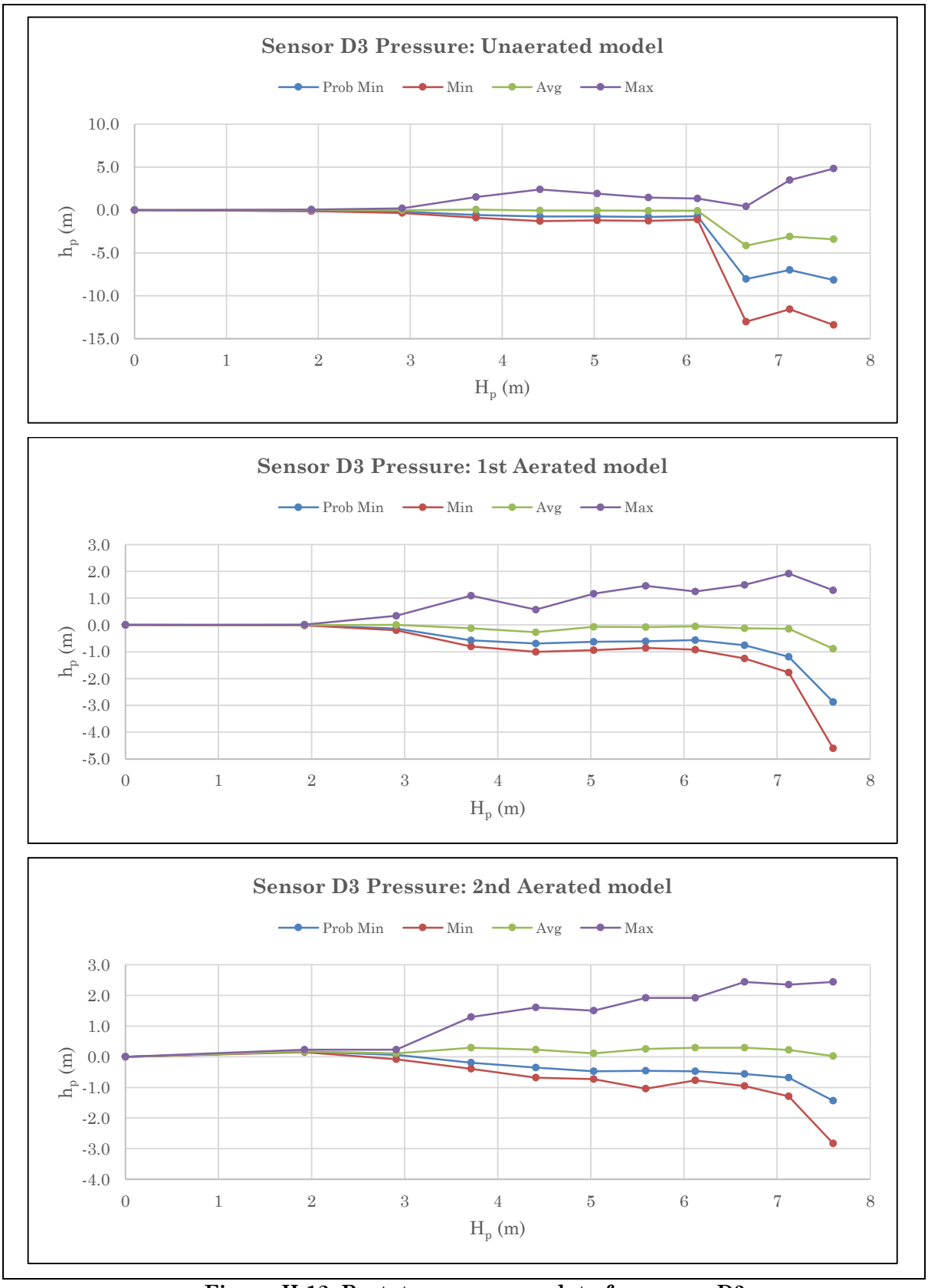

Figure H-12: Prototype pressure data for sensor D3

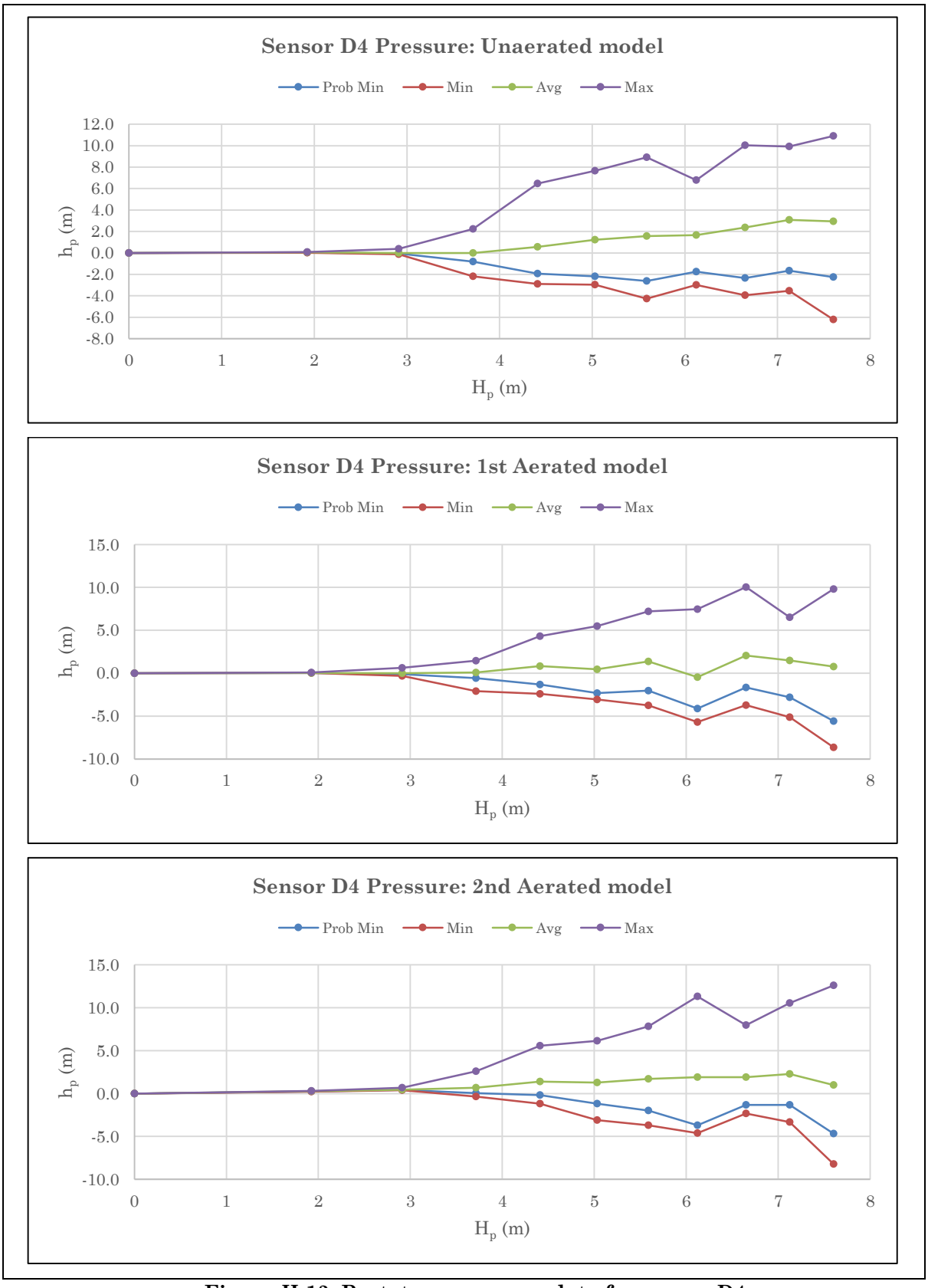

Figure H-13: Prototype pressure data for sensor D4

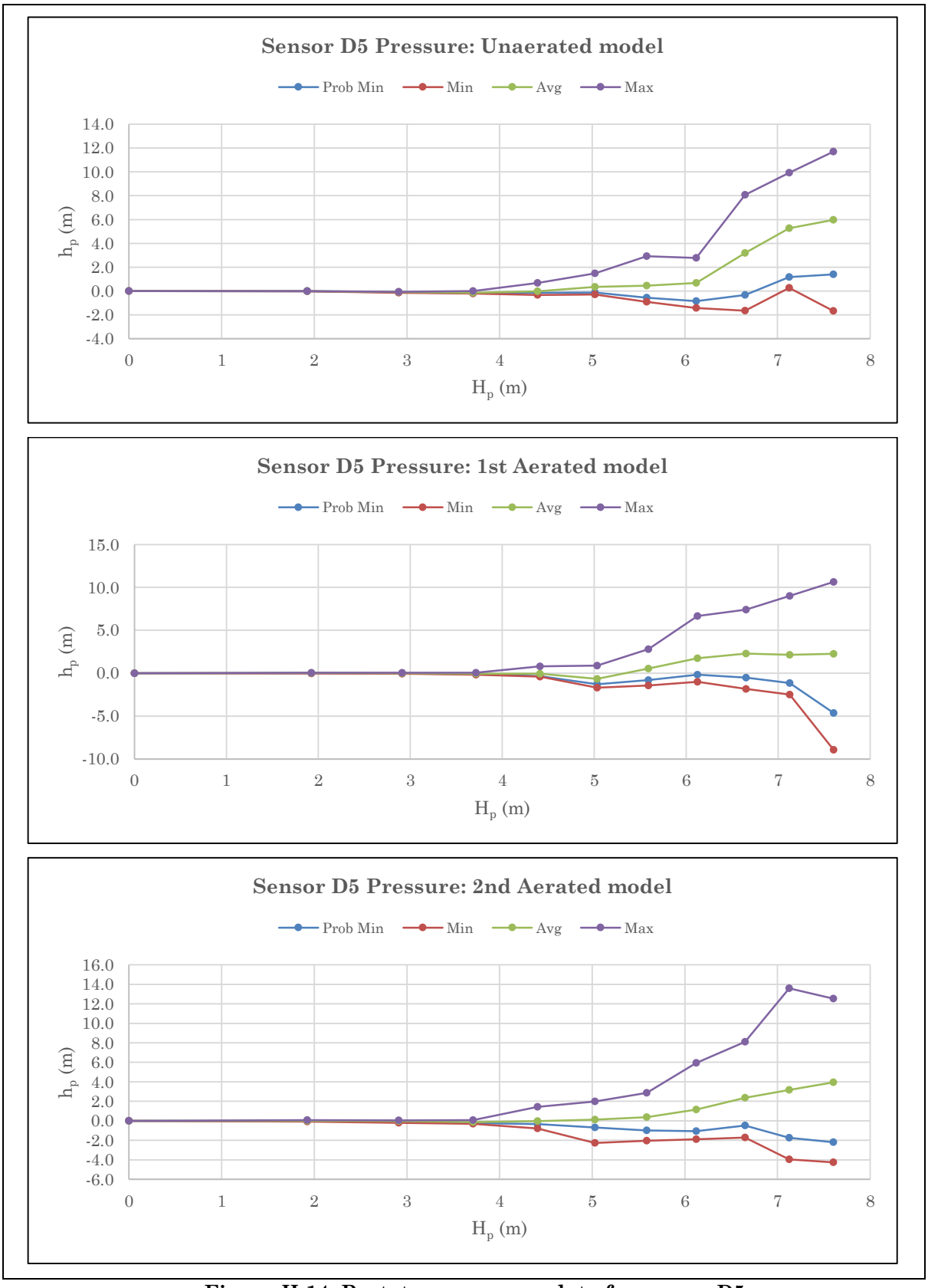

Figure H-14: Prototype pressure data for sensor D5

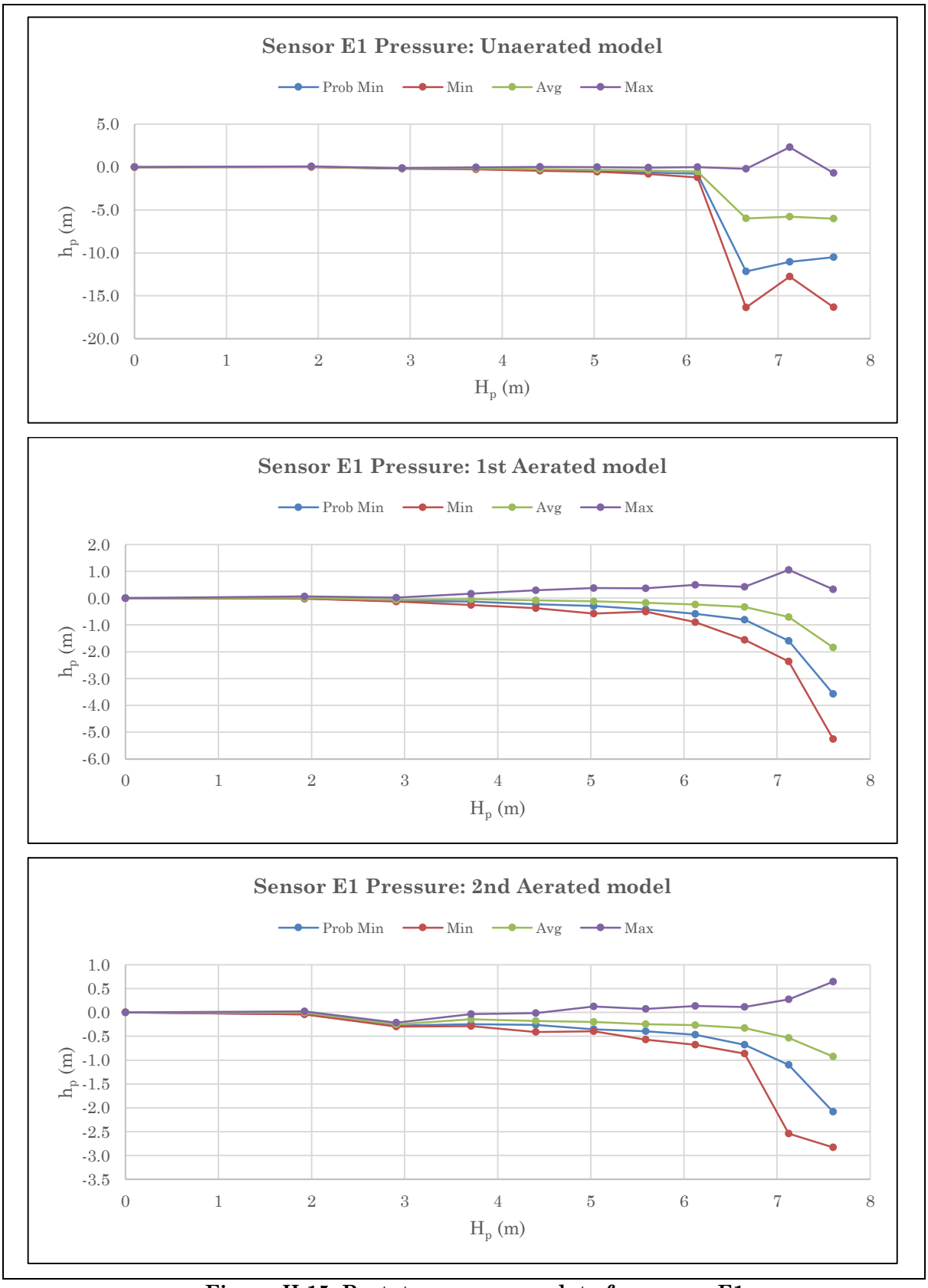

Figure H-15: Prototype pressure data for sensor E1

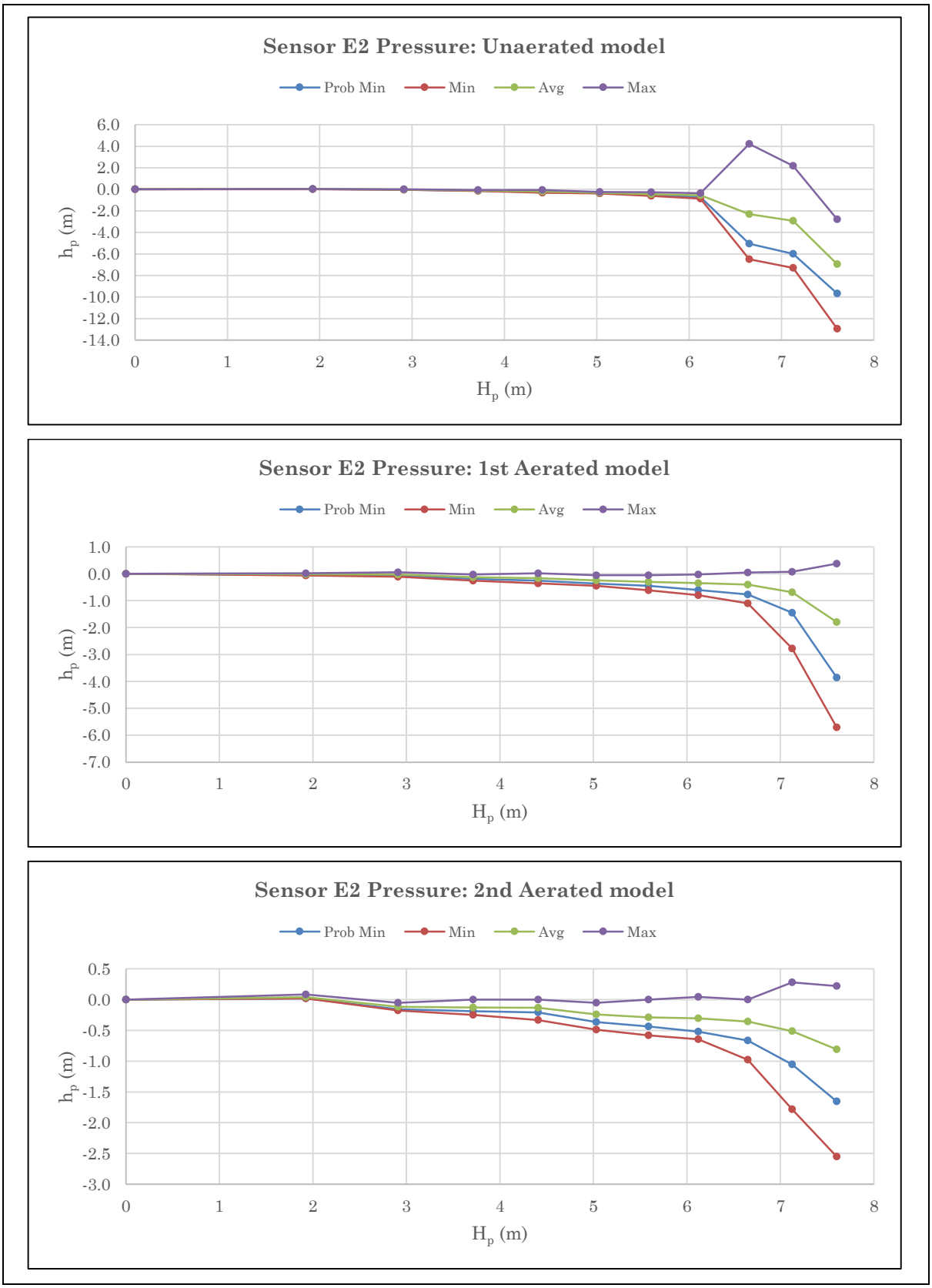

Figure H-16: Prototype pressure data for sensor E2

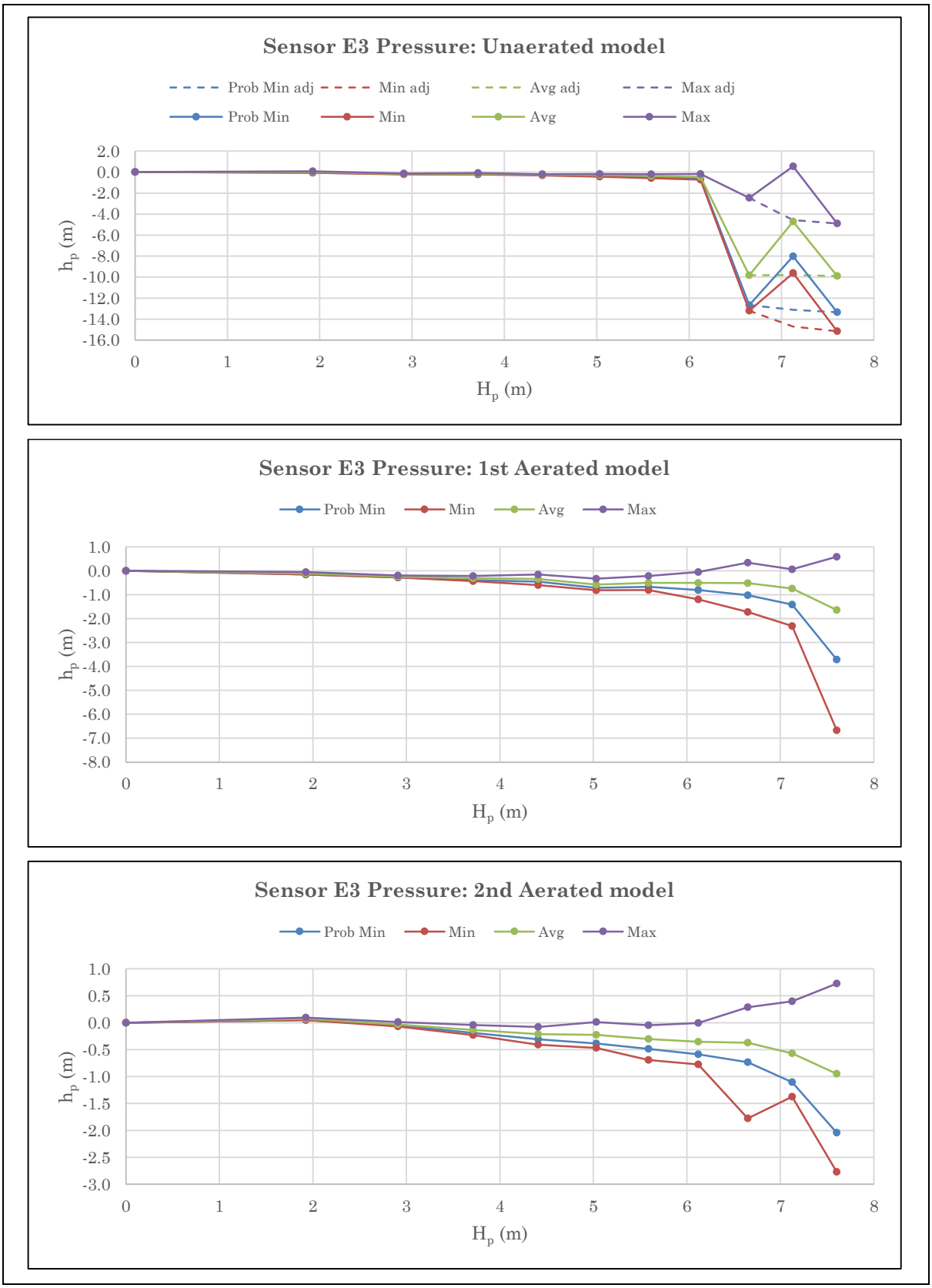

Figure H-17: Prototype pressure data for sensor E3

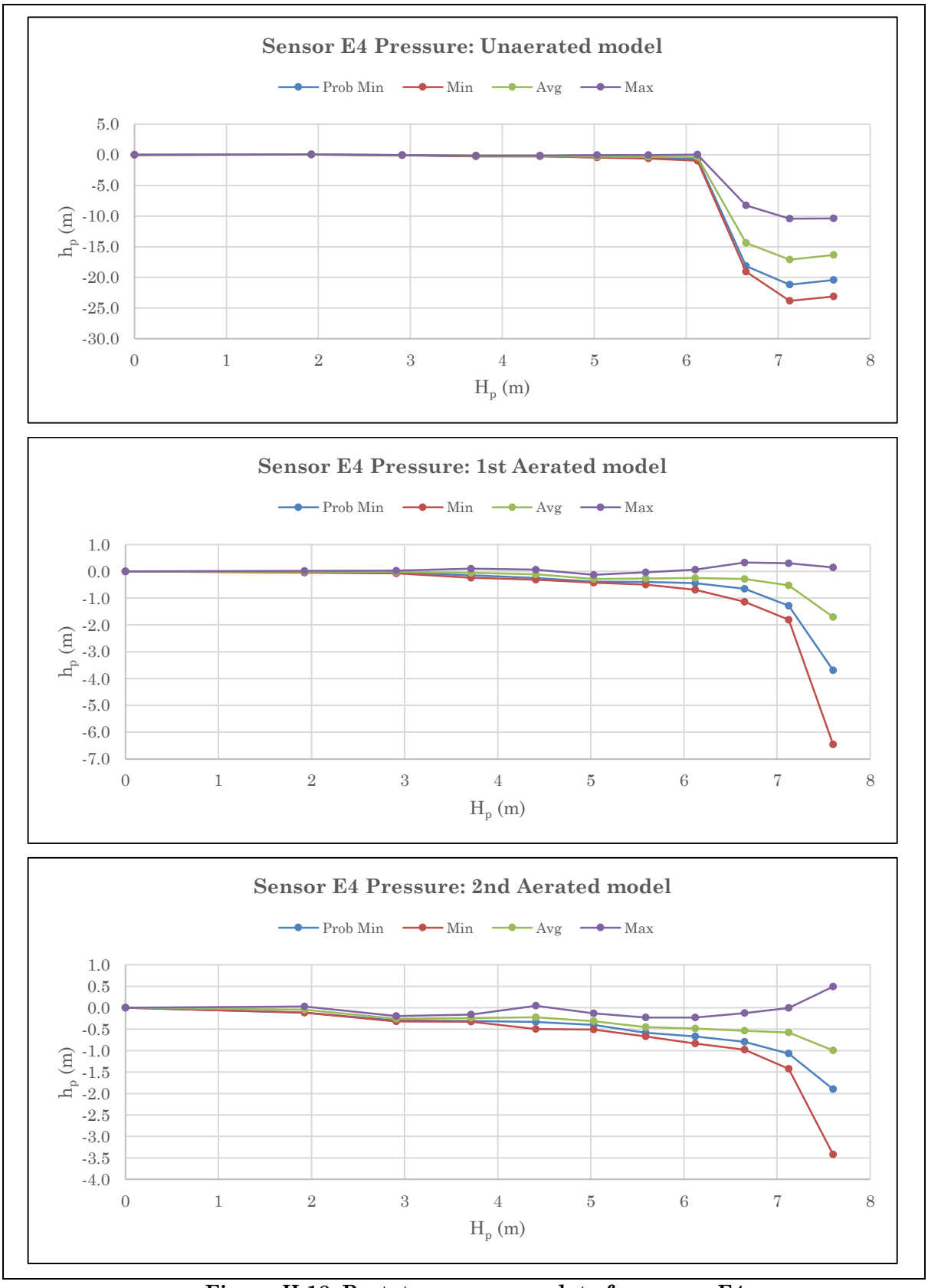

Figure H-18: Prototype pressure data for sensor E4

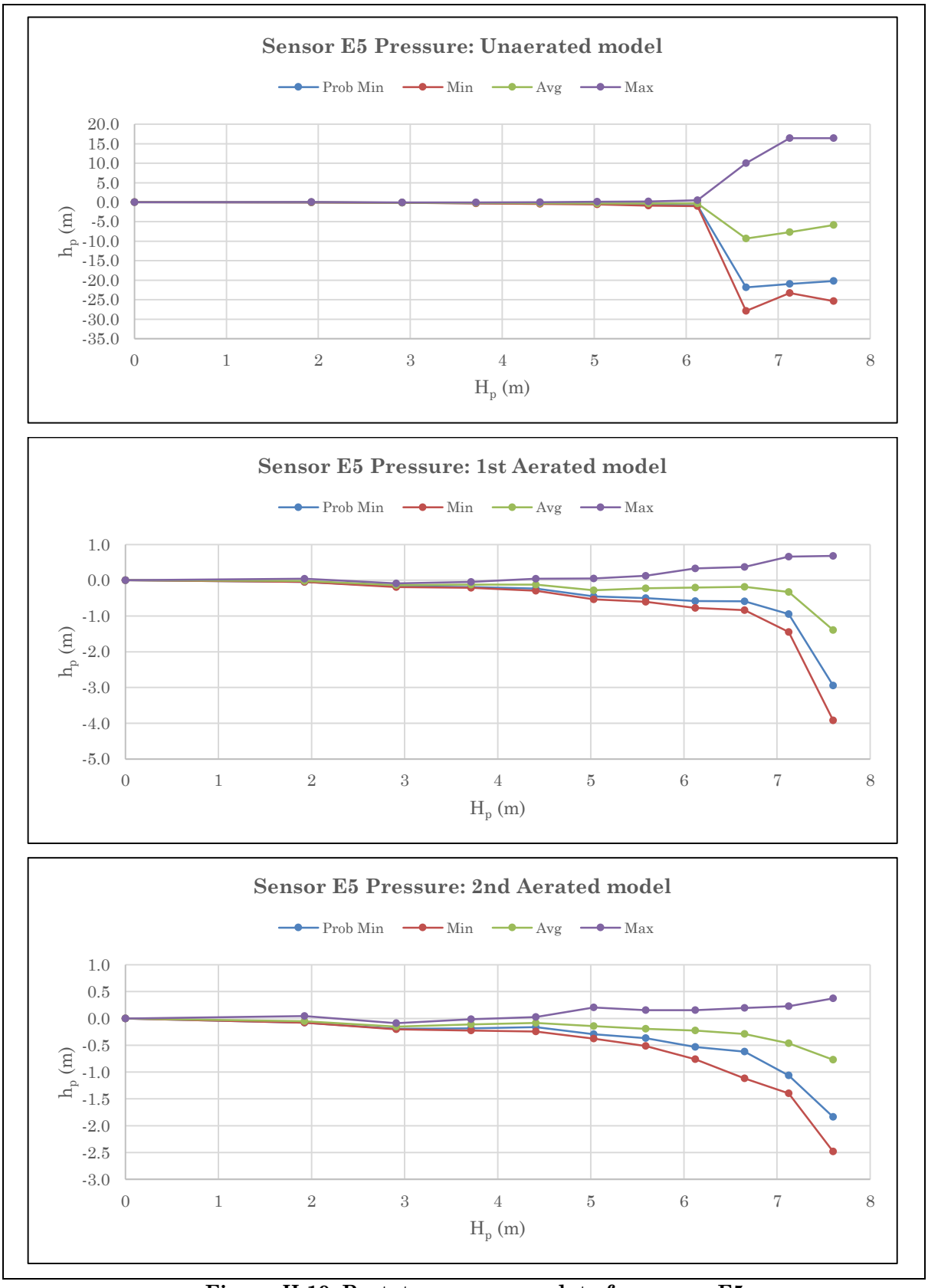

Figure H-19: Prototype pressure data for sensor E5

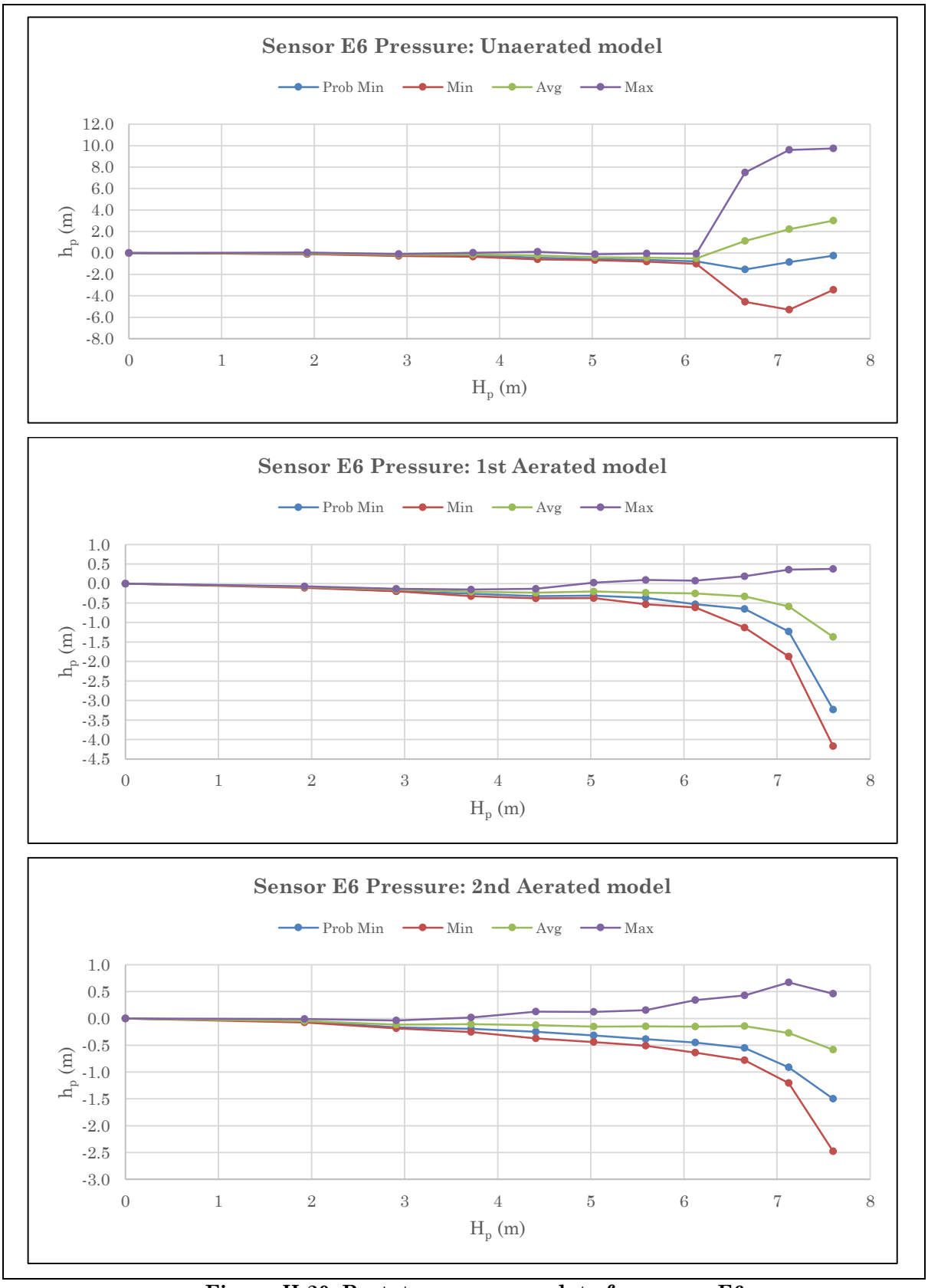

Figure H-20: Prototype pressure data for sensor E6

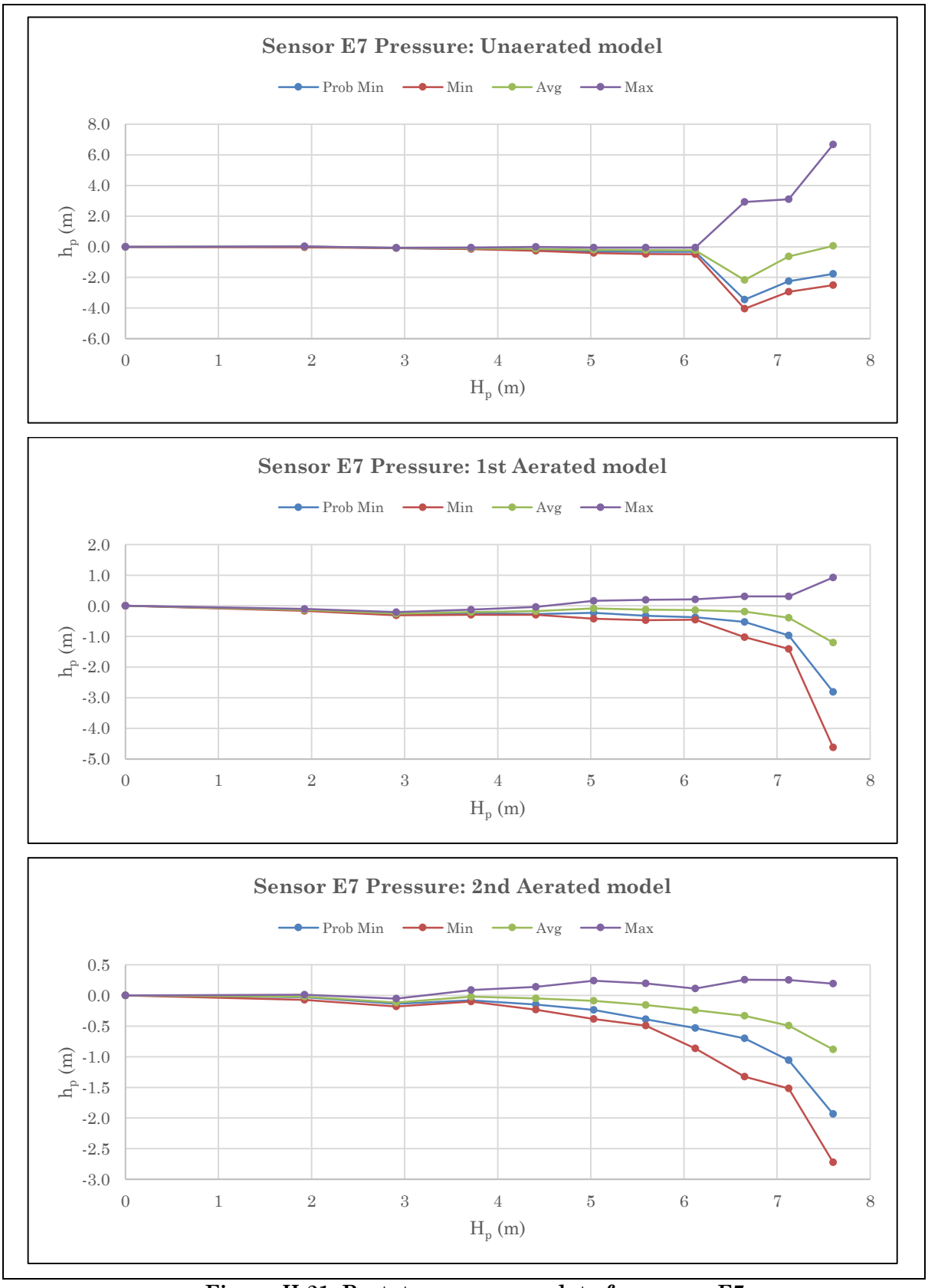

Figure H-21: Prototype pressure data for sensor E7

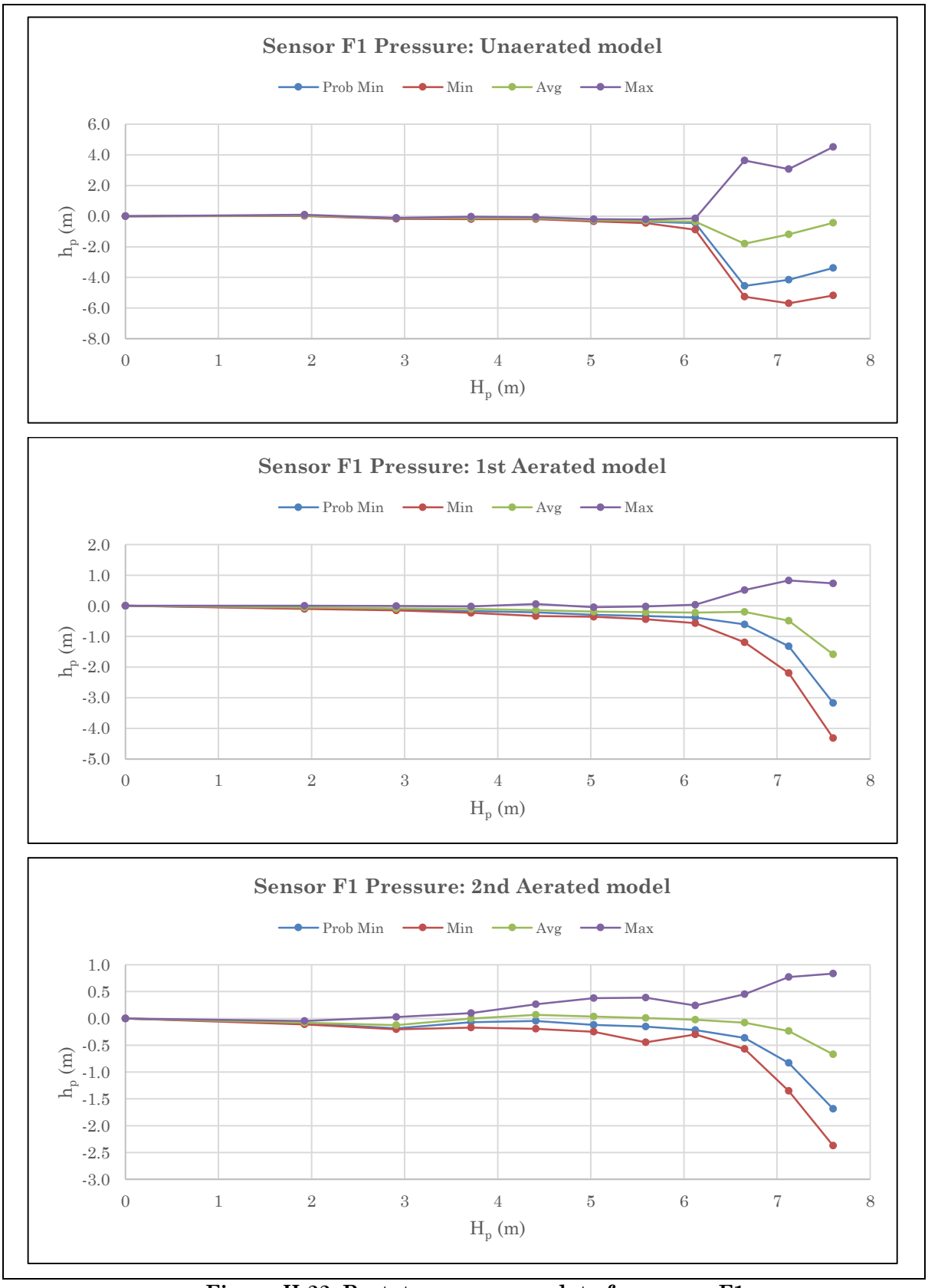

Figure H-22: Prototype pressure data for sensor F1

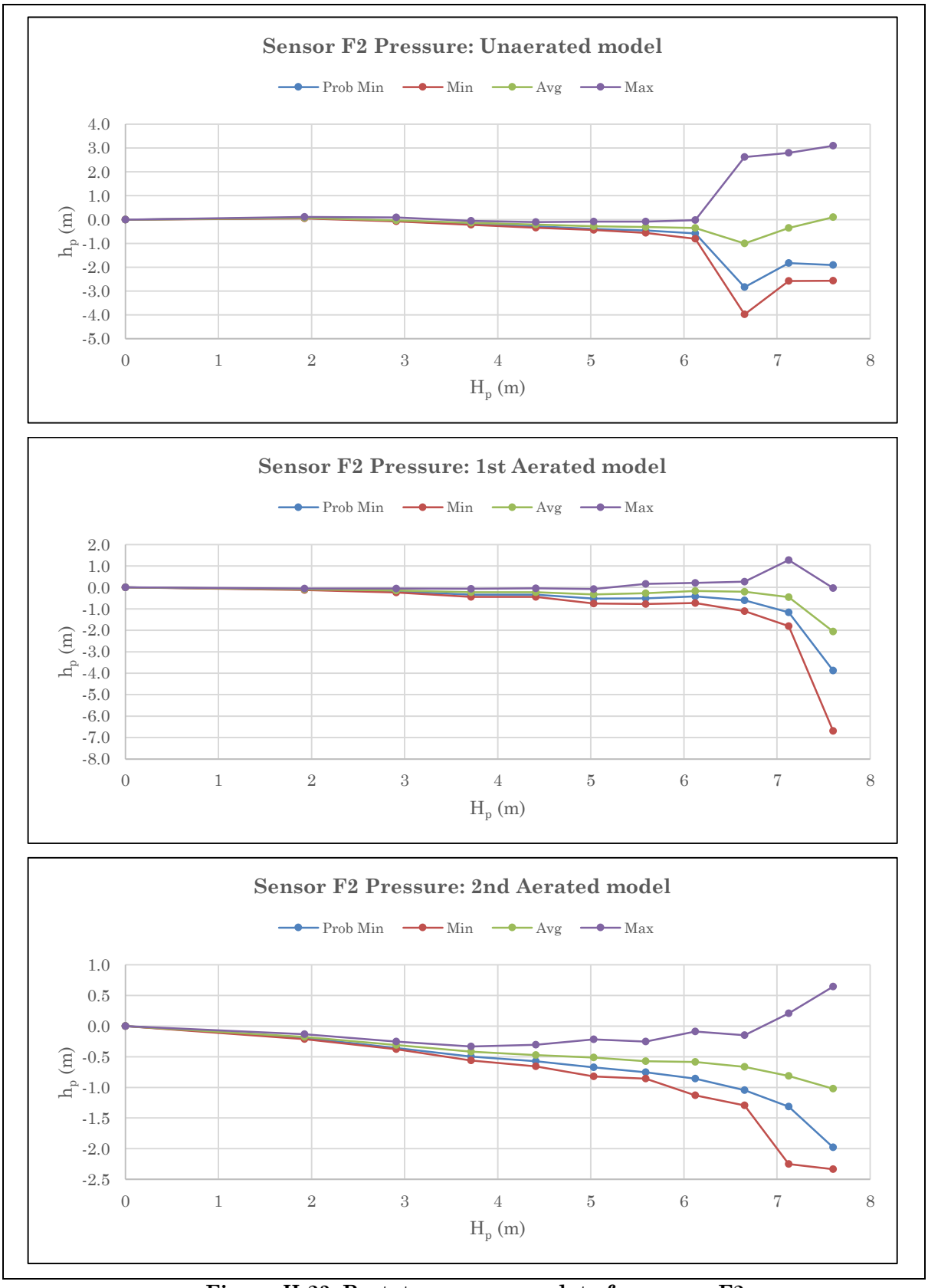

Figure H-23: Prototype pressure data for sensor F2

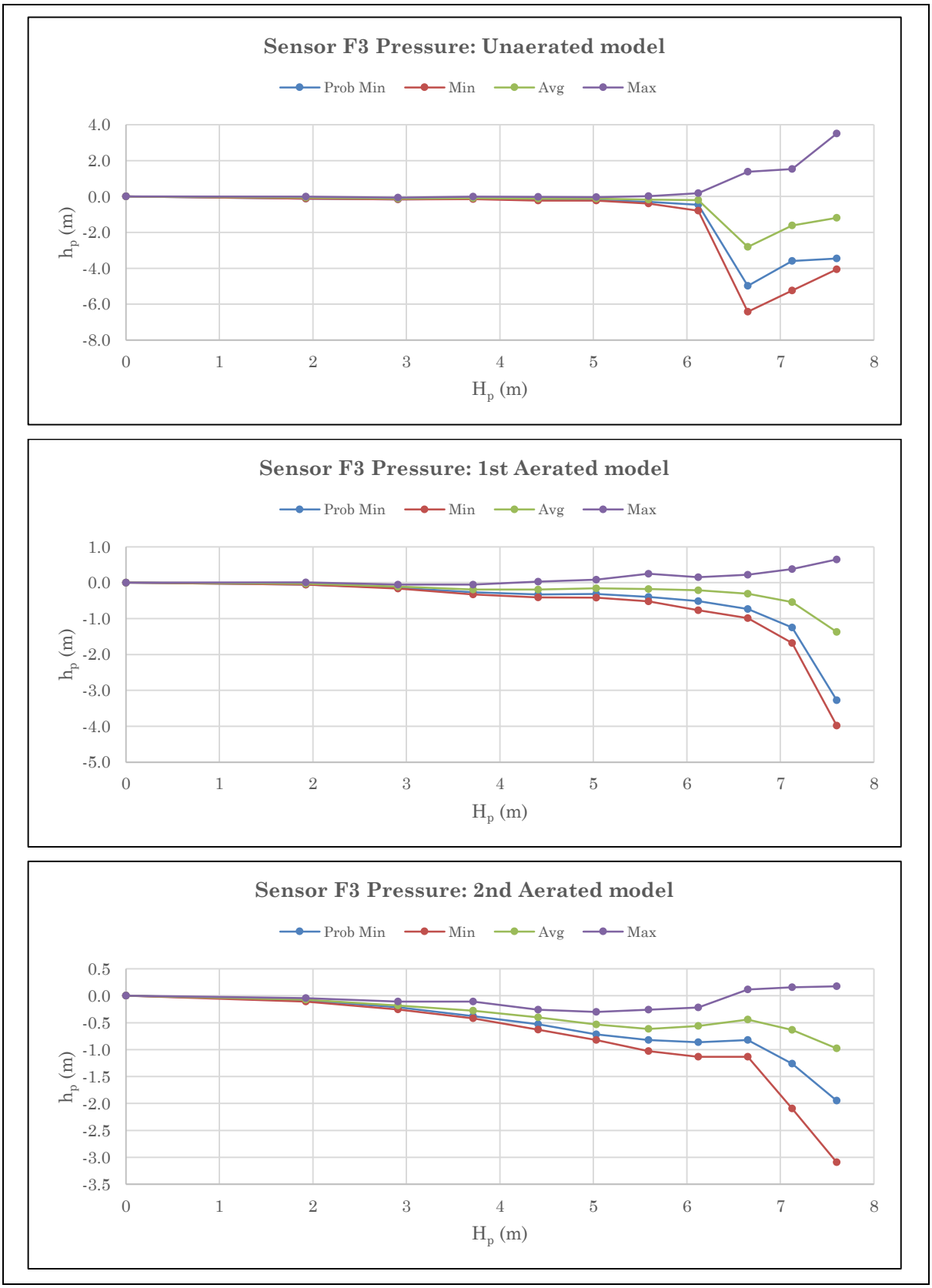

Figure H-24: Prototype pressure data for sensor F3

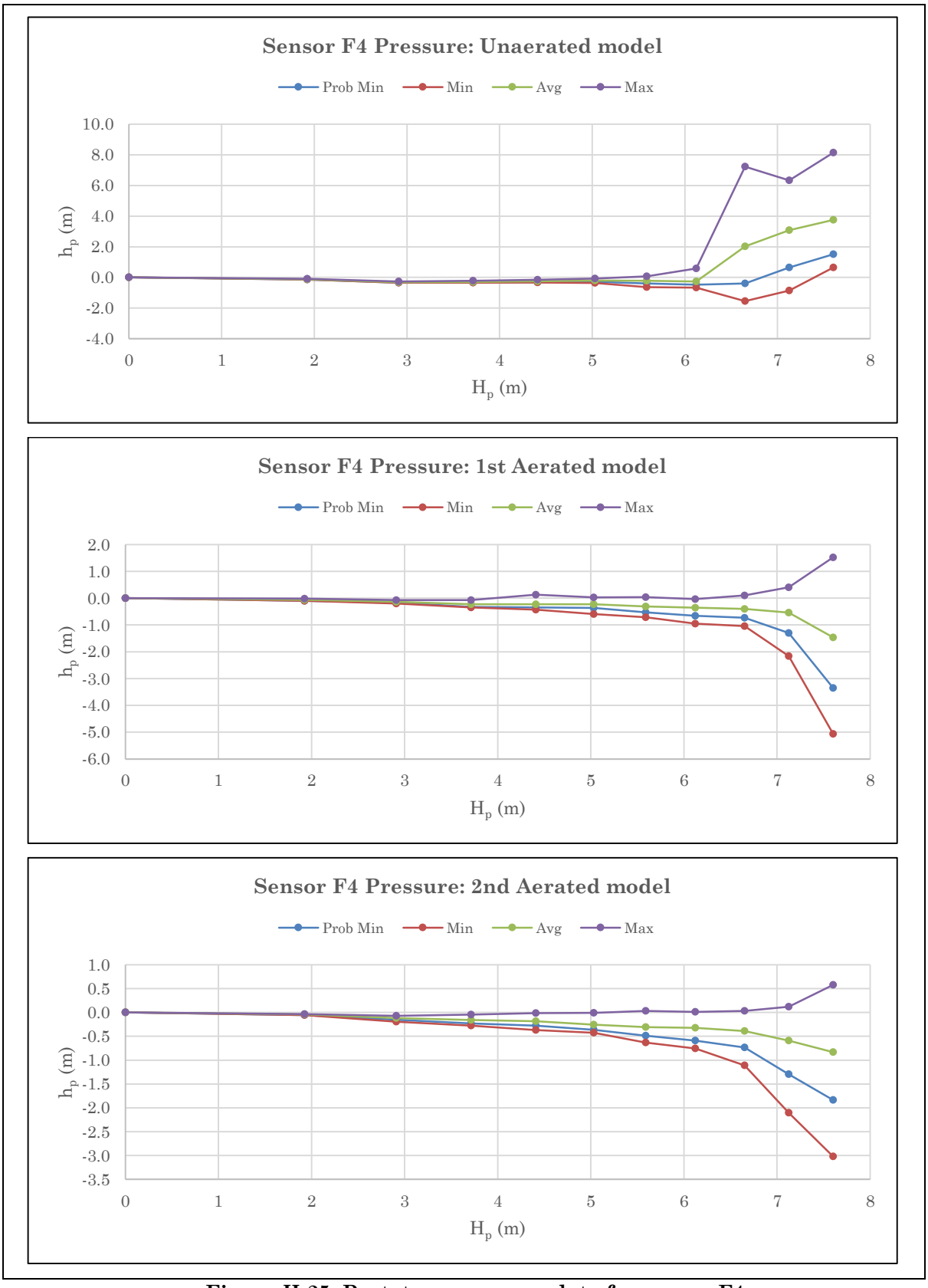

Figure H-25: Prototype pressure data for sensor F4

APPENDIX I
AIR CONCENTRATION DATA

All air concentration data are contained herein as graphs. These graphs are sorted by the relevant test. For the full test schedule, see Appendix G. For complete results in table format, please contact the author through the University of Stellenbosch's Civil Engineering Department.

All values on the x-axis denote time in seconds, and values on the y-axis denote the air concentration in percentage.

I.1. Unaerated Model

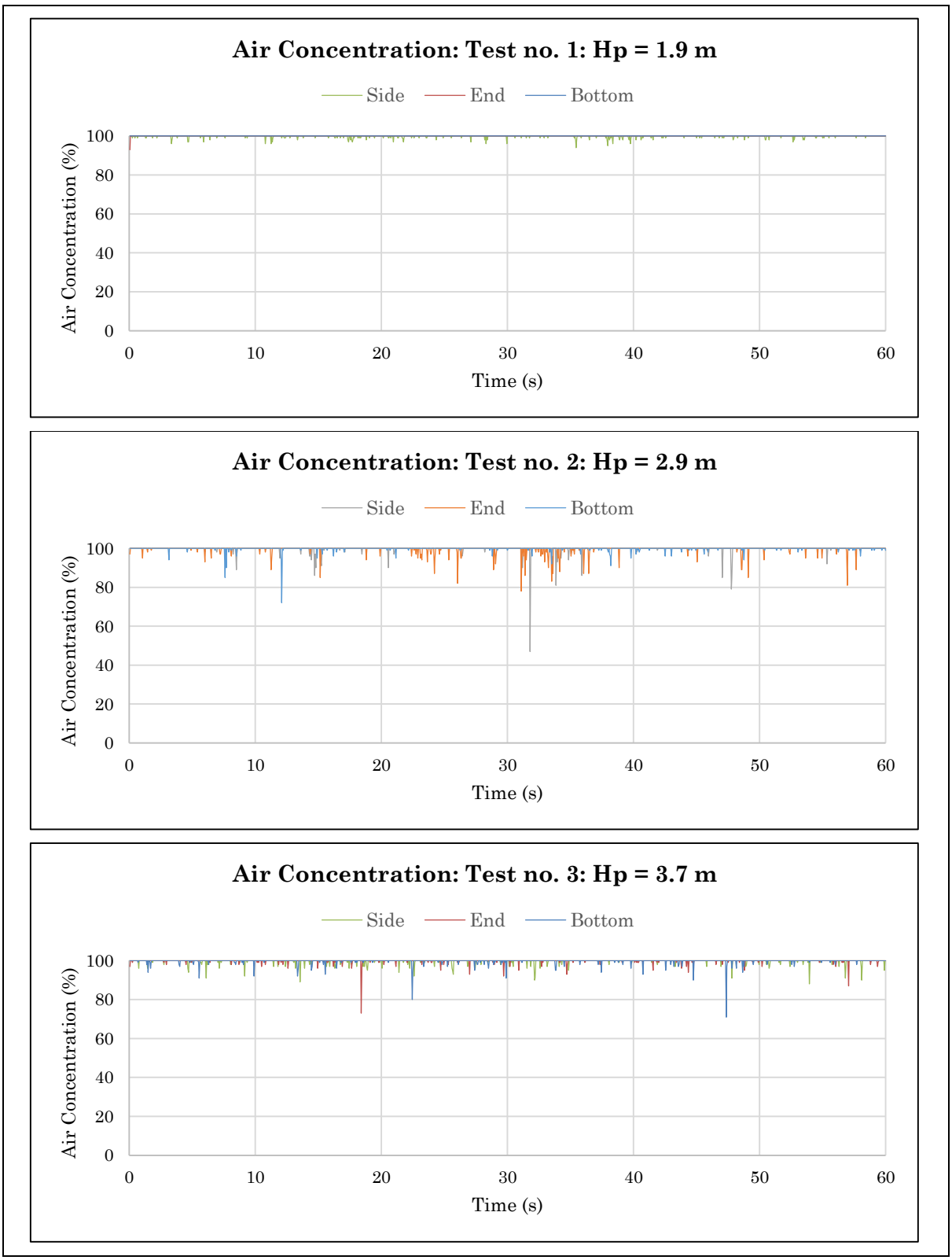

Figure I-1: Air concentration data for tests no. 1 to 3

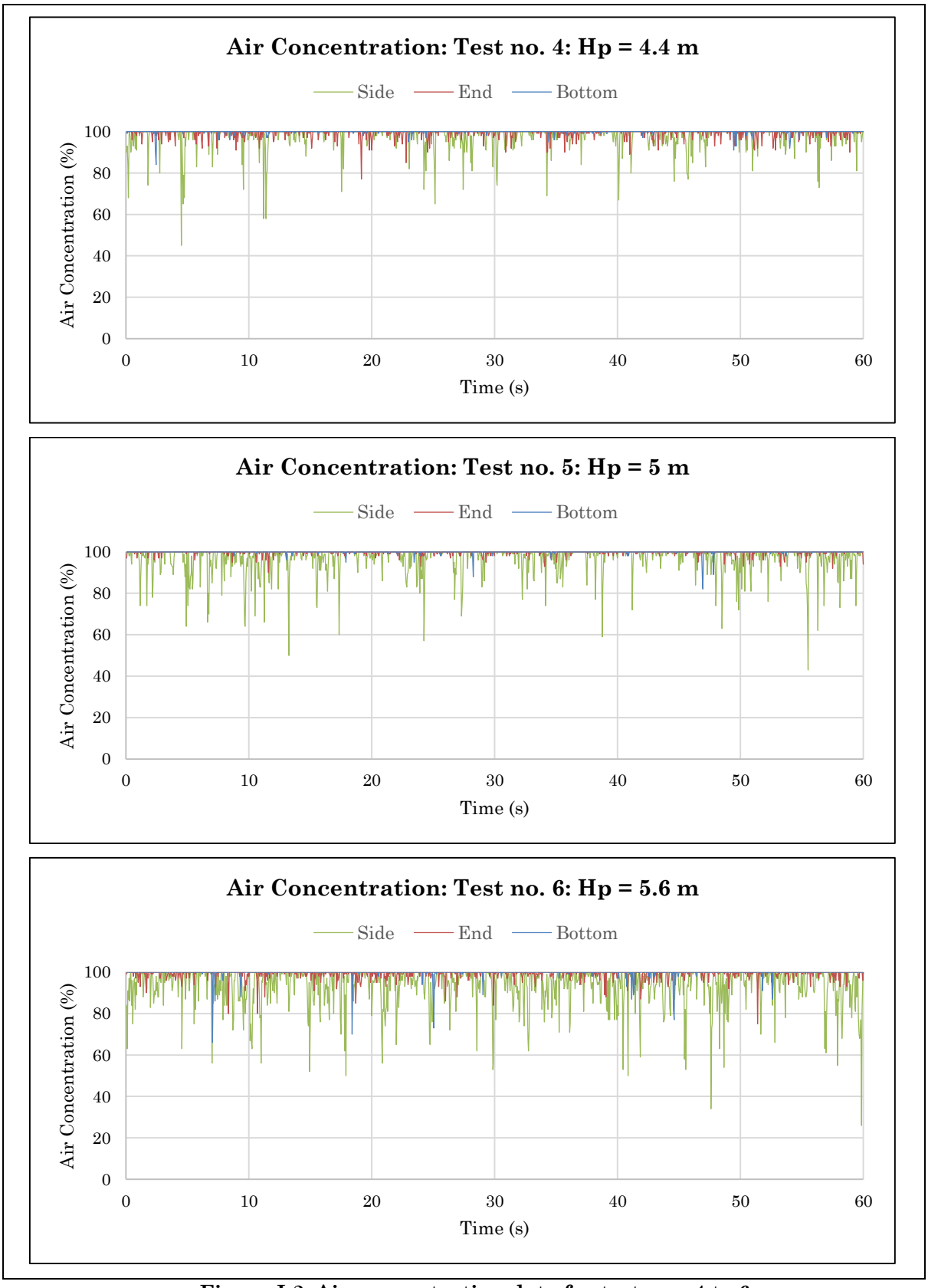

Figure I-2: Air concentration data for tests no. 4 to 6

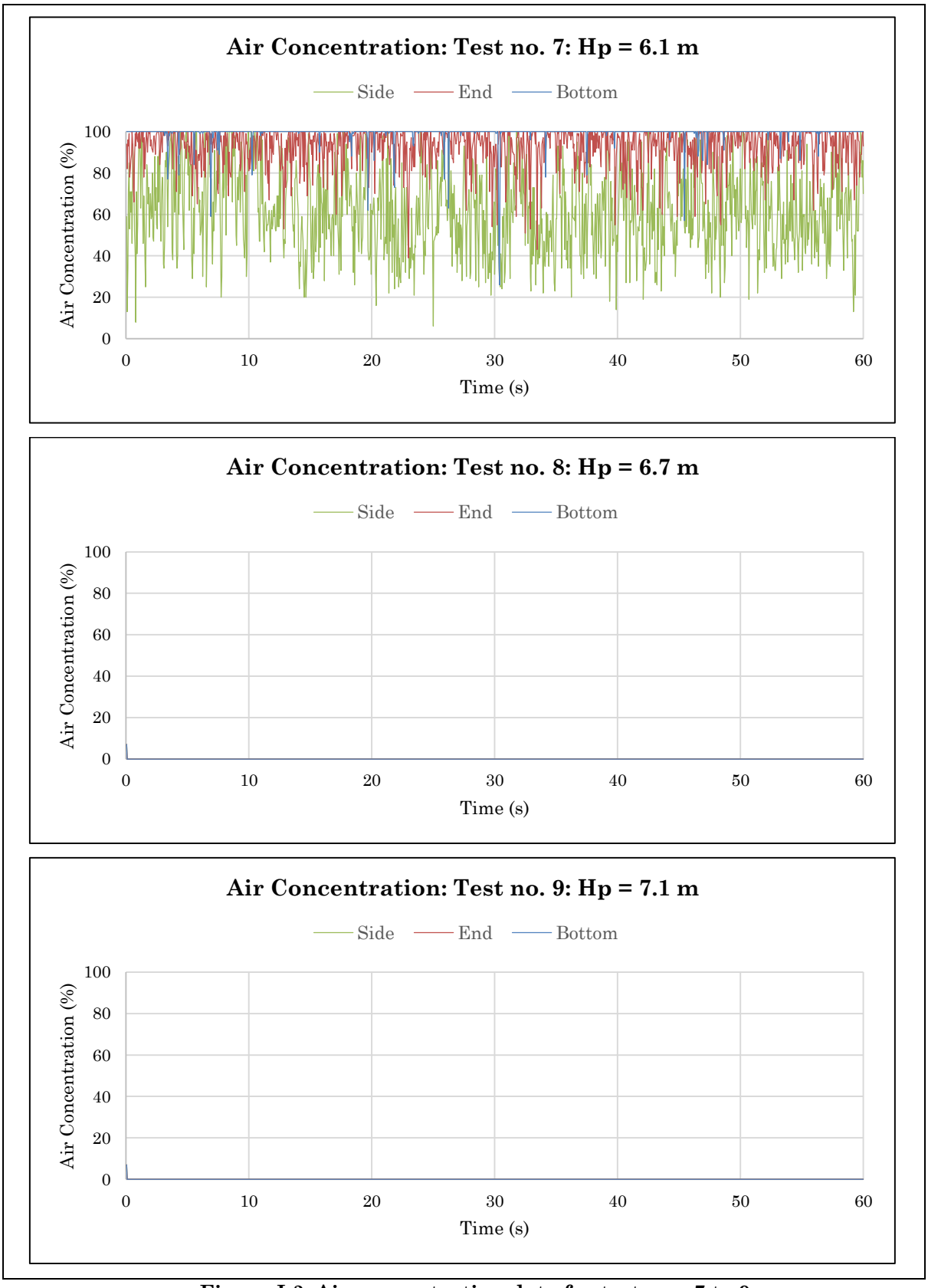

Figure I-3: Air concentration data for tests no. 7 to 9

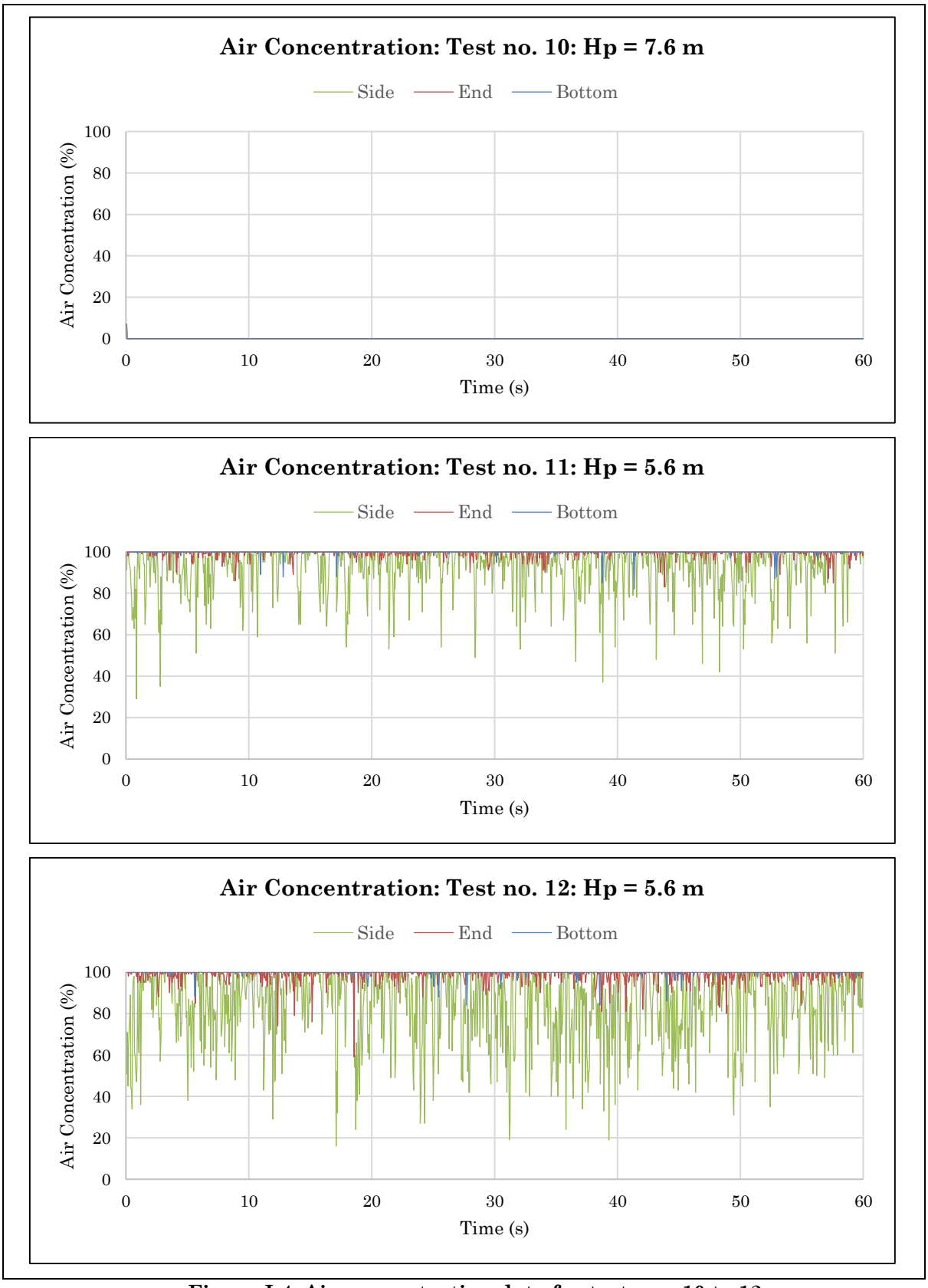

Figure I-4: Air concentration data for tests no. 10 to 12

I.2. 1st Aerated Model

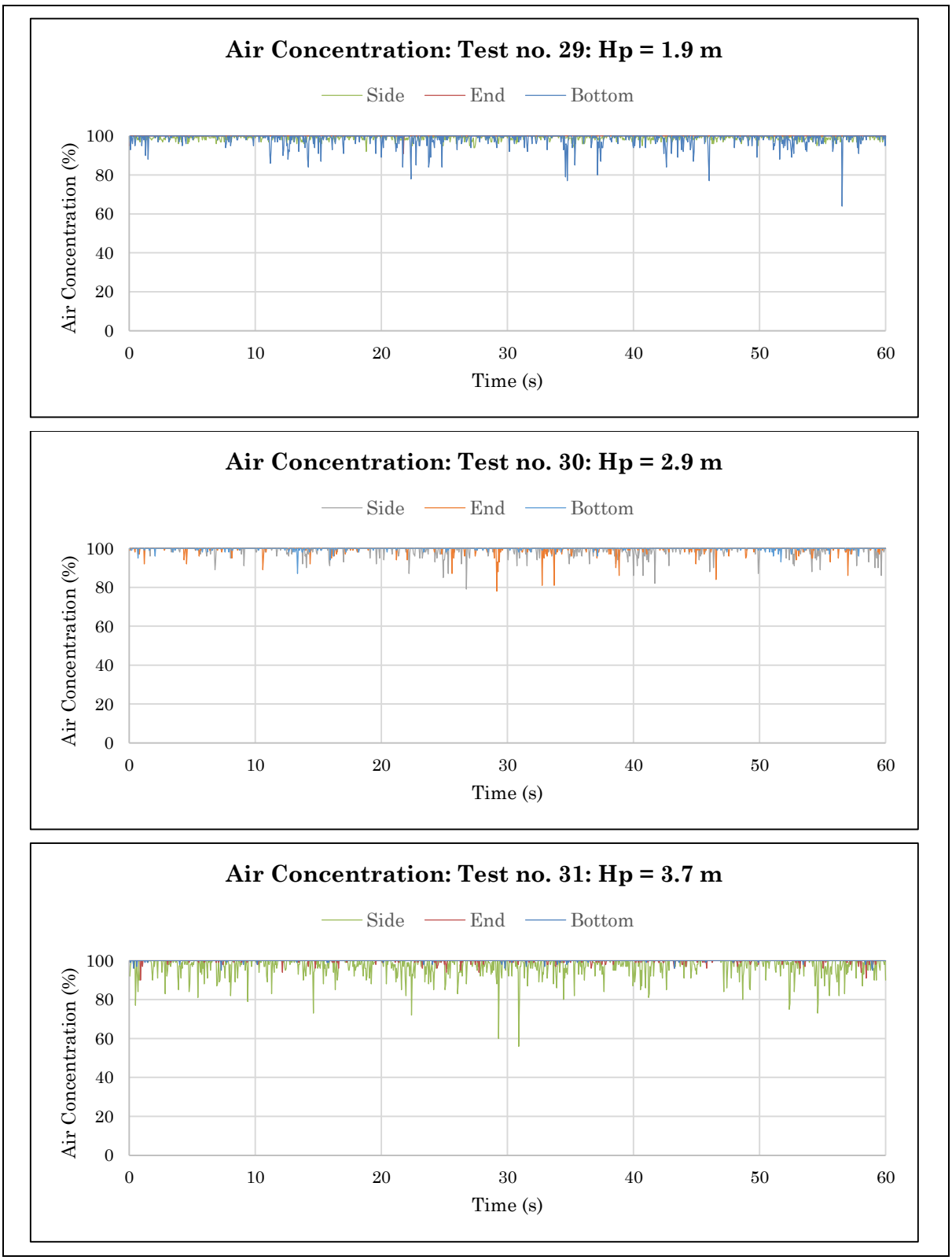

Figure I-5: Air concentration data for tests no. 29 to 31

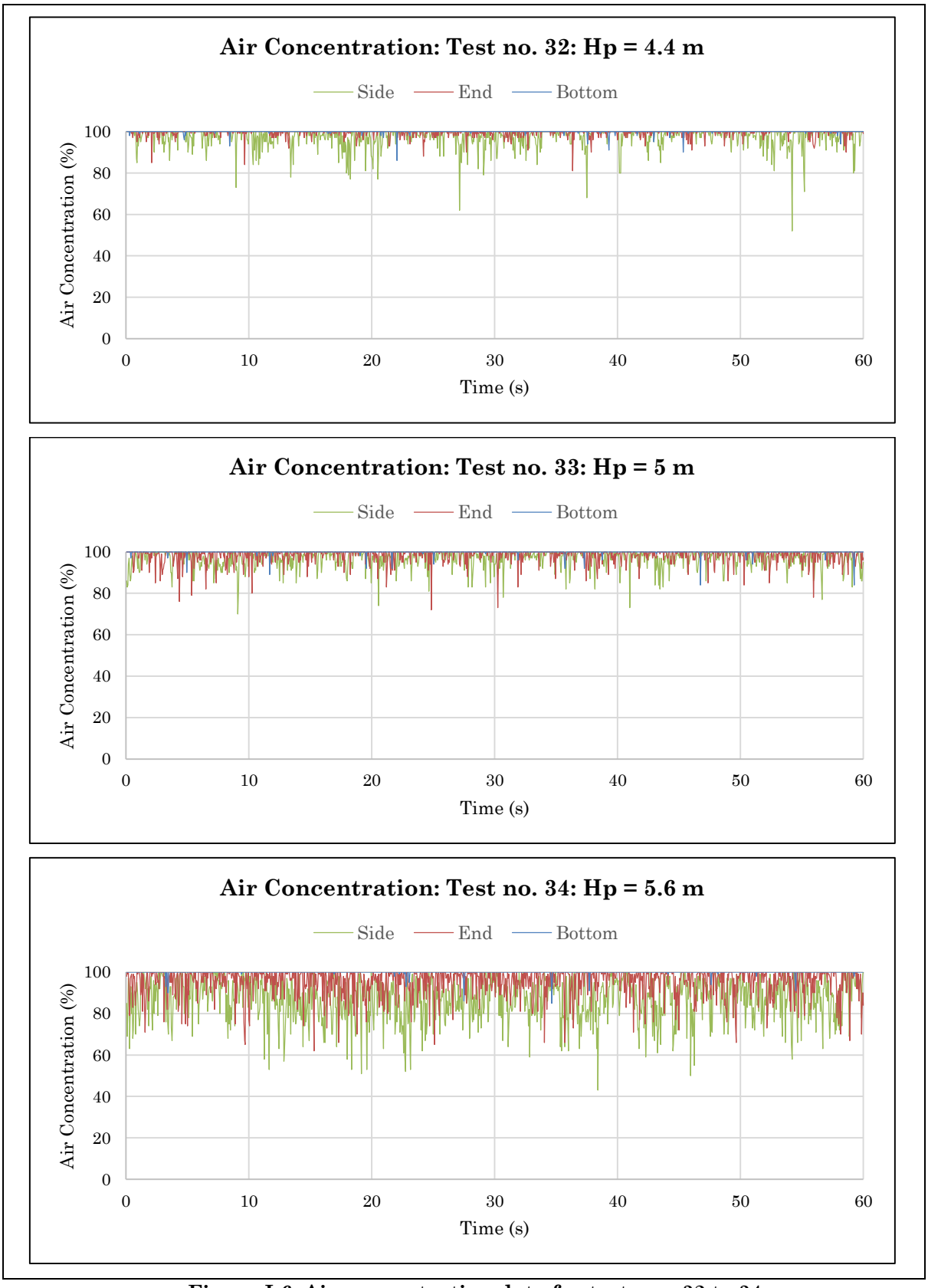

Figure I-6: Air concentration data for tests no. 32 to 34

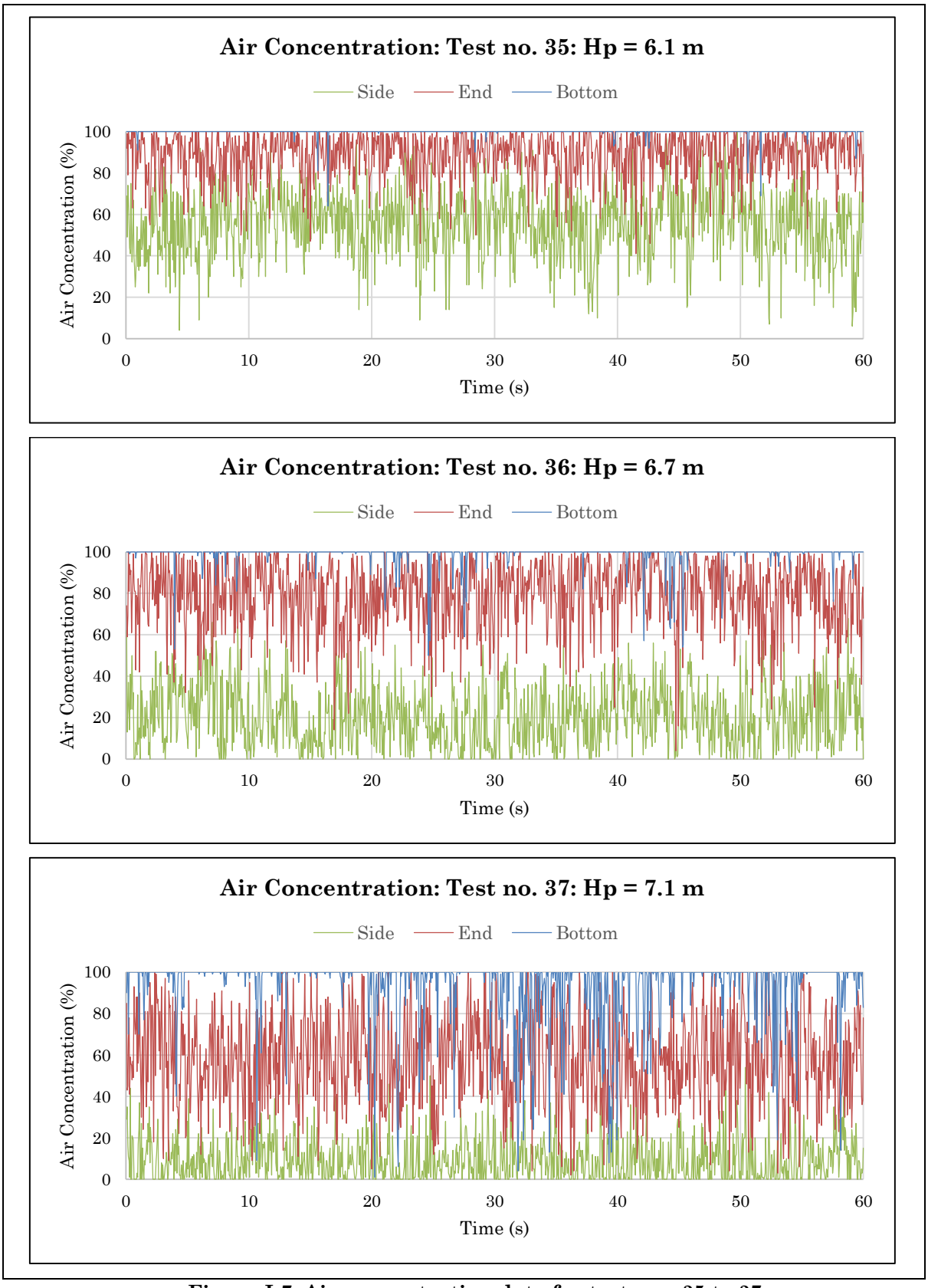

Figure I-7: Air concentration data for tests no. 35 to 37

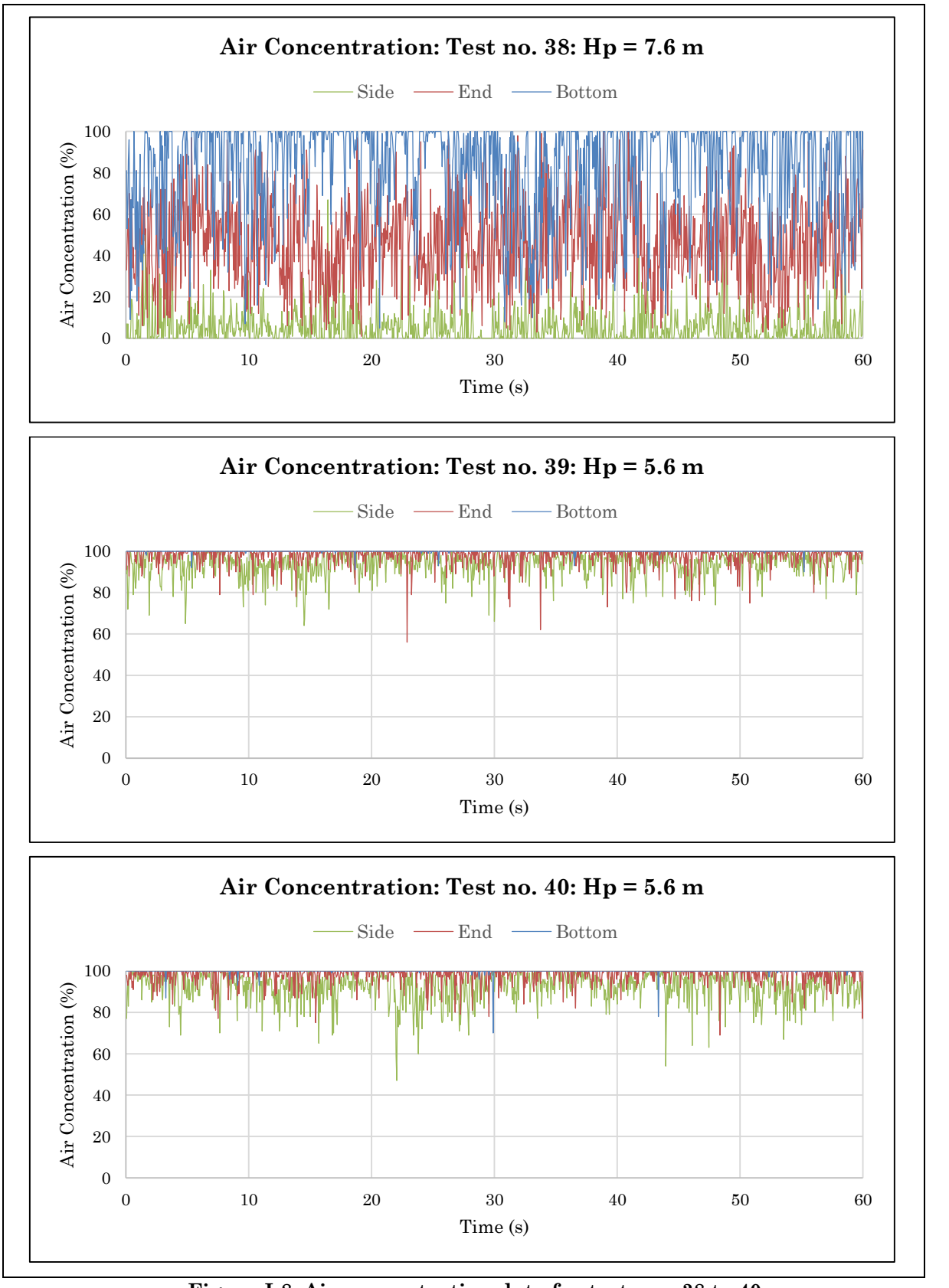

Figure I-8: Air concentration data for tests no. 38 to 40

I.3. 2nd Aerated Model

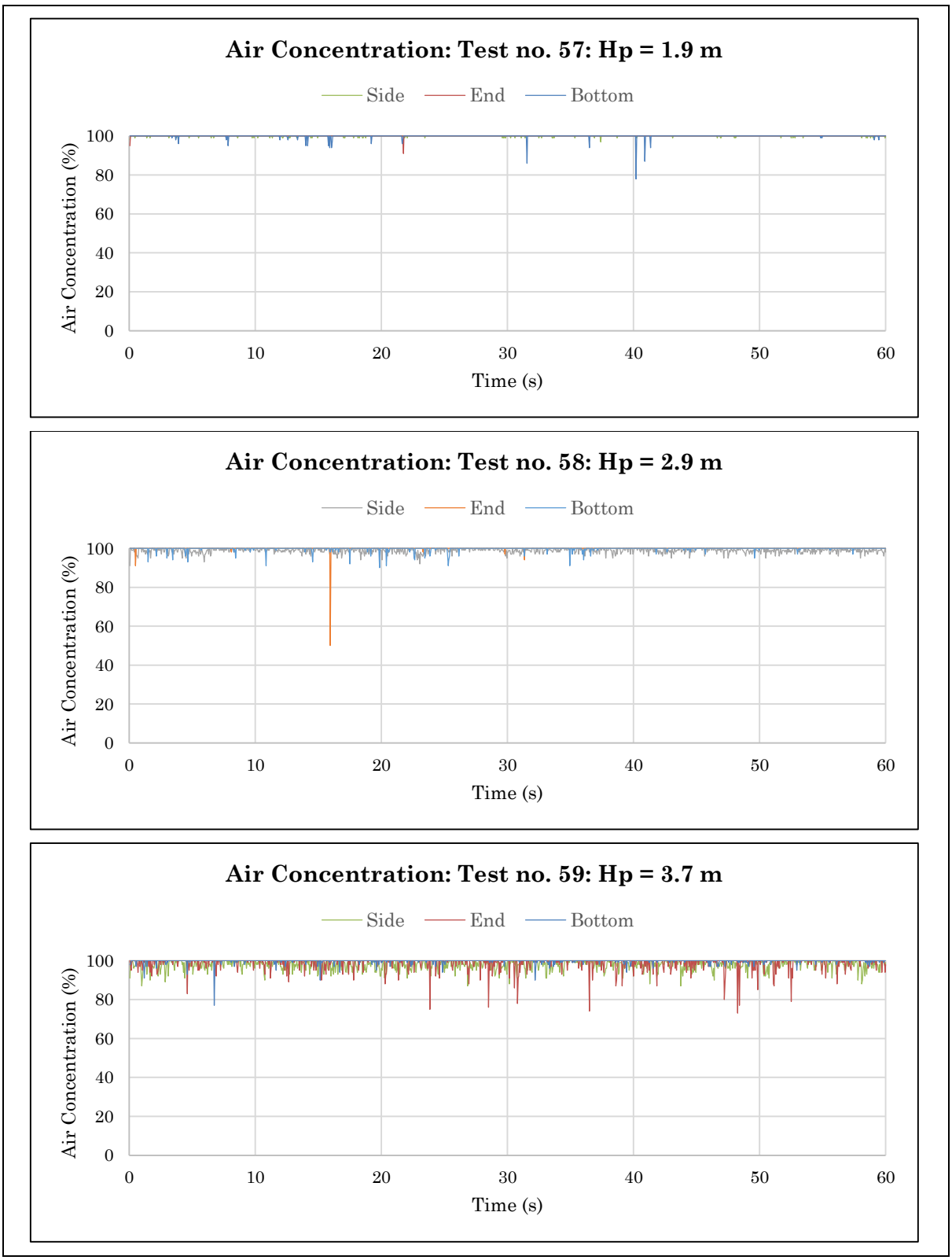

Figure I-9: Air concentration data for tests no. 57 to 59

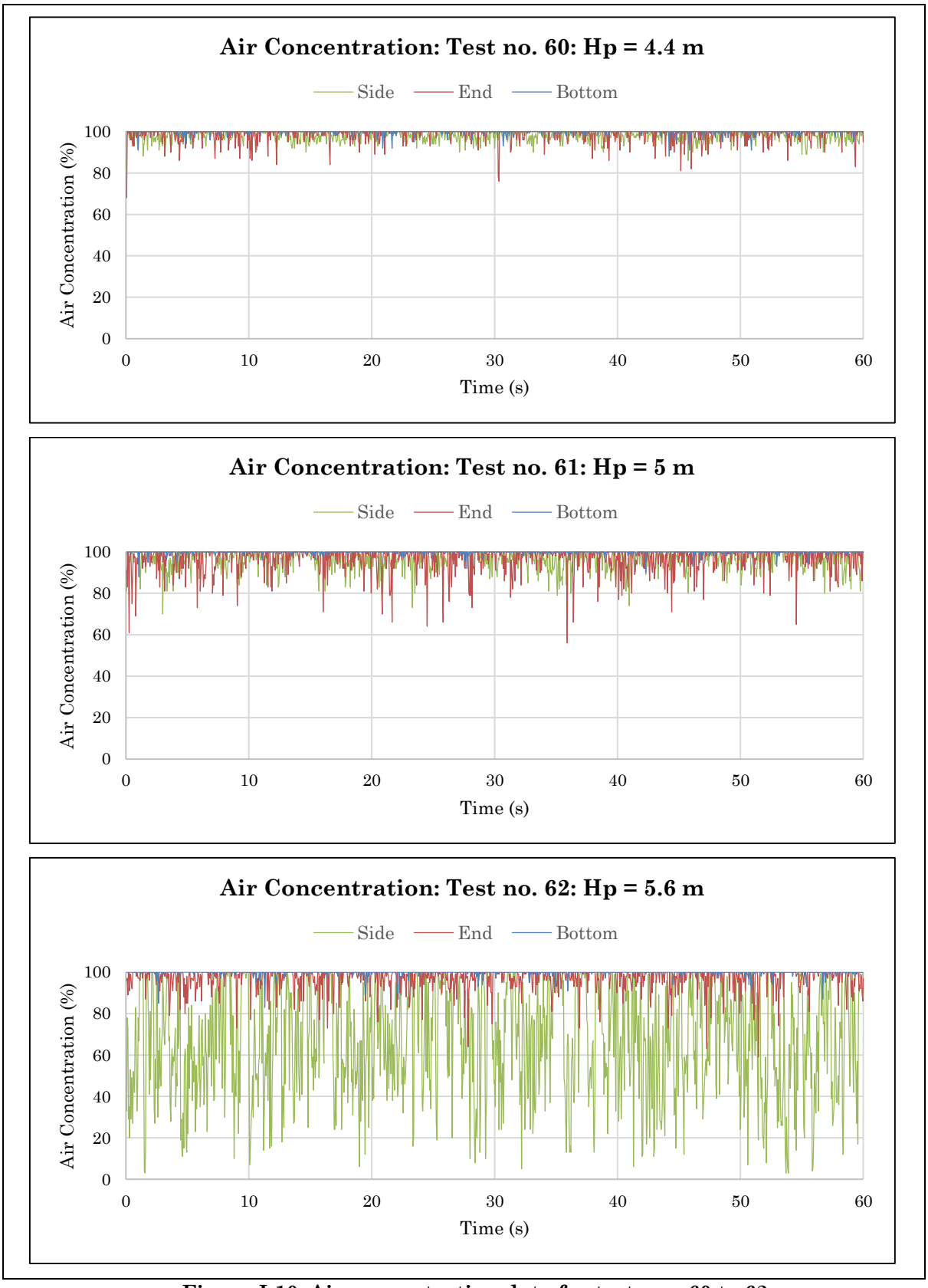

Figure I-10: Air concentration data for tests no. 60 to 62

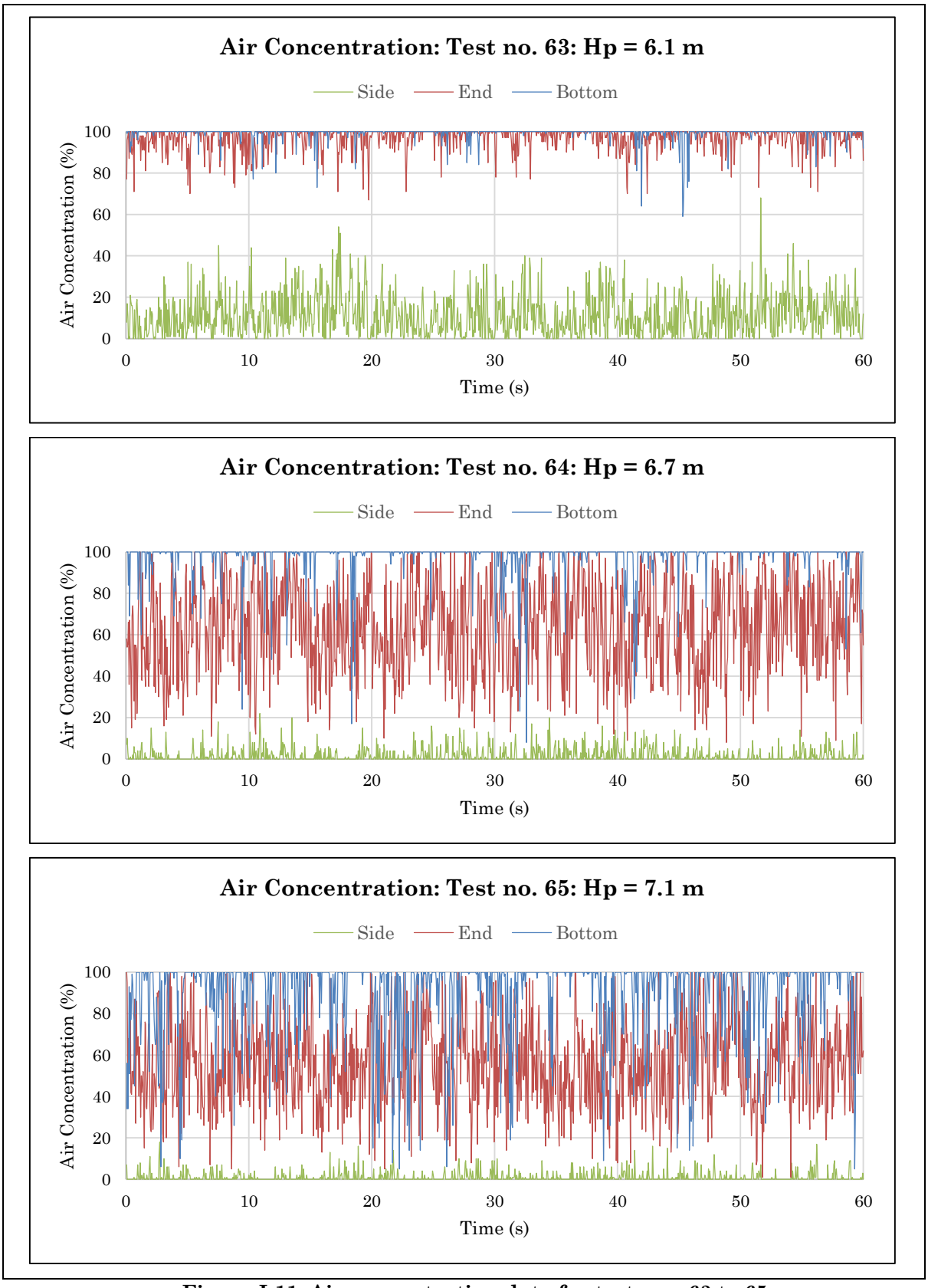

Figure I-11: Air concentration data for tests no. 63 to 65

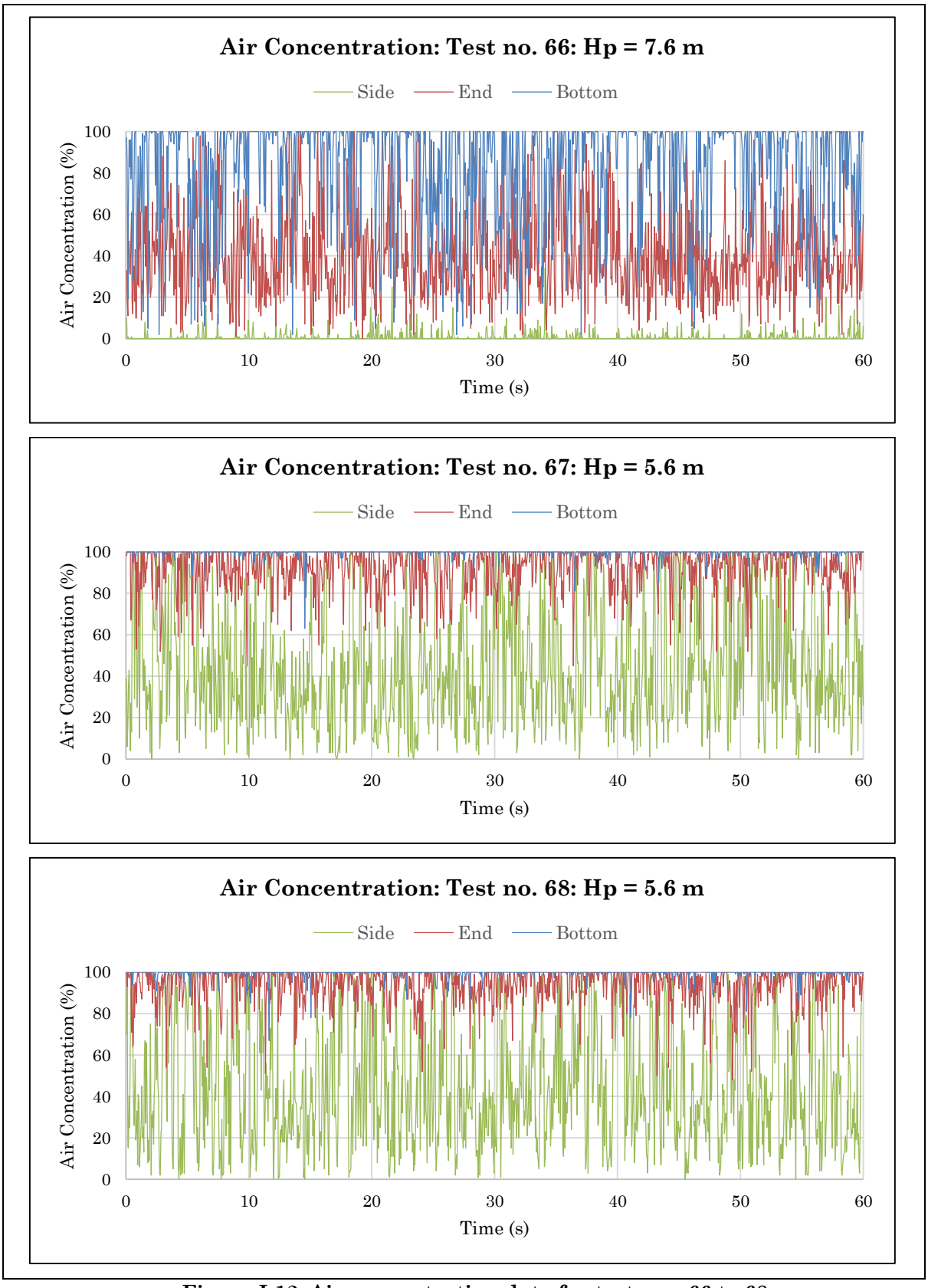

Figure I-12: Air concentration data for tests no. 66 to 68

APPENDIX J
AIR VELOCITY DATA

The air velocity results are contained within Table J-1 and Table J-2. The data from these tables are shown in Figure J-1 and Figure J-2 respectively.

Table J-1: Air velocity data – 1st aerated model

		Model Velocity (m/s)									
q_p (m²/s)		5	10	15	20	25	30	35	40	45	50
Q_m (l/s)		67.1	134.2	201.2	268.3	335.4	402.5	469.6	536.7	603.7	670.8
Time (s)	5	0.66	1.17	1.00	1.07	1.26	1.07	0.95	0.91	1.08	0.74
	10	0.63	1.01	0.77	1.10	1.14	1.07	0.95	0.81	0.88	0.82
	15	0.53	1.03	0.92	1.04	1.26	1.08	0.89	0.85	0.86	0.74
	20	0.57	0.93	0.95	1.00	1.31	1.03	0.97	0.89	0.80	0.69
	25	0.49	0.91	0.89	1.00	1.34	1.03	1.03	0.99	0.78	0.70
	30	0.61	1.01	0.89	0.92	1.03	1.16	1.07	0.93	0.73	0.88
	35	0.60	0.89	0.77	0.89	0.90	1.03	0.92	0.79	1.04	0.90
	40	0.55	0.93	0.71	0.91	0.92	1.12	0.97	0.93	0.98	0.81
	45	0.55	0.87	0.73	0.91	1.08	1.00	1.16	0.89	0.73	0.73
	50	0.56	0.83	0.85	0.89	1.22	1.10	0.99	0.81	0.98	0.77
	55	0.50	0.89	0.97	0.91	1.14	1.14	0.94	0.87	0.69	0.78
	60	0.58	0.81	0.94	0.83	1.04	1.08	0.99	0.89	0.88	0.90
	65	0.60	0.83	0.89	0.86	1.14	0.99	0.92	0.89	0.80	0.73
	70	0.57	0.77	0.73	0.85	0.97	1.10	1.00	0.93	1.00	0.67
	75	0.45	0.69	0.75	0.89	0.94	1.08	0.99	0.85	0.78	0.84
	80	0.46	0.87	0.89	0.89	1.12	1.07	1.00	0.81	0.70	0.69
	85	0.46	0.95	1.00	0.83	1.10	0.99	0.94	0.99	0.90	0.82
	90	0.50	0.83	1.08	0.89	1.08	1.08	1.03	0.85	0.80	0.98
	95	0.44	0.93	0.77	0.90	1.00	0.94	1.13	0.95	0.77	0.77
	100	0.53	1.03	0.73	0.85	1.00	1.10	1.09	0.89	0.77	0.73
	105	0.53	1.05	0.85	0.90	1.18	1.10	1.05	1.03	0.80	0.73
	110	0.55	1.13	0.87	0.92	1.18	1.10	1.11	0.99	0.74	0.82
	115	0.53	1.05	0.89	0.92	1.24	0.92	1.13	0.99	0.78	0.82
	120	0.49	1.03	0.75	0.99	1.07	1.23	1.07	0.94	0.80	0.80

Table J-2: Air velocity data – 2nd aerated model

		Model Velocity (m/s)									
q_p (m²/s)		5	10	15	20	25	30	35	40	45	50
Q_m (l/s)		67.1	134.2	201.2	268.3	335.4	402.5	469.6	536.7	603.7	670.8
Time (s)	5	0.66	1.65	1.74	1.89	2.09	2.08	2.04	1.71	1.14	1.08
	10	0.69	1.57	1.57	1.86	2.24	1.88	2.10	1.81	1.07	1.00
	15	0.69	1.75	1.68	1.81	2.27	2.14	2.01	1.65	1.10	1.16
	20	0.69	1.55	1.49	1.85	2.20	2.00	1.99	1.81	1.23	1.13
	25	0.67	1.48	1.77	1.69	1.78	1.82	2.07	1.89	1.17	1.10
	30	0.69	1.44	1.70	1.81	2.12	1.72	2.17	1.89	1.25	1.18
	35	0.57	1.69	1.71	1.82	2.11	2.11	2.15	1.98	1.19	1.00
	40	0.59	1.61	1.68	1.88	1.96	2.29	2.11	1.78	1.13	1.20
	45	0.63	1.54	1.68	1.85	1.98	2.16	2.01	1.74	1.23	1.12
	50	0.55	1.64	1.58	1.77	2.19	2.04	2.13	1.82	1.07	1.22
	55	0.57	1.67	1.62	1.95	1.94	1.72	1.99	1.75	1.07	1.08
	60	0.53	1.65	1.63	1.91	1.96	2.16	2.03	1.78	0.99	1.20
	65	0.63	1.55	1.49	2.07	1.93	1.92	2.04	1.73	1.07	1.14
	70	0.67	1.53	1.65	2.01	2.23	1.88	2.02	1.56	1.10	1.31
	75	0.53	1.61	1.69	1.88	2.23	1.92	2.17	1.79	1.05	1.20
	80	0.61	1.60	1.75	1.85	2.23	1.93	1.97	1.76	1.21	1.36
	85	0.60	1.42	1.52	1.93	2.19	2.15	2.04	1.75	1.17	1.01
	90	0.60	1.55	1.60	1.77	1.98	2.05	1.99	1.87	1.29	1.23
	95	0.60	1.49	1.69	1.69	2.11	1.90	1.98	1.88	1.23	1.14
	100	0.61	1.46	1.74	1.83	2.25	2.10	1.98	1.82	1.10	1.22
	105	0.55	1.66	1.75	1.85	2.05	2.12	1.87	1.89	1.12	1.32
	110	0.60	1.64	1.76	1.69	2.15	2.14	1.93	1.79	1.12	1.30
	115	0.61	1.54	1.79	1.59	1.97	2.09	1.88	1.83	1.11	1.12
	120	0.64	1.67	1.63	1.89	2.10	2.13	1.89	1.61	1.09	1.13

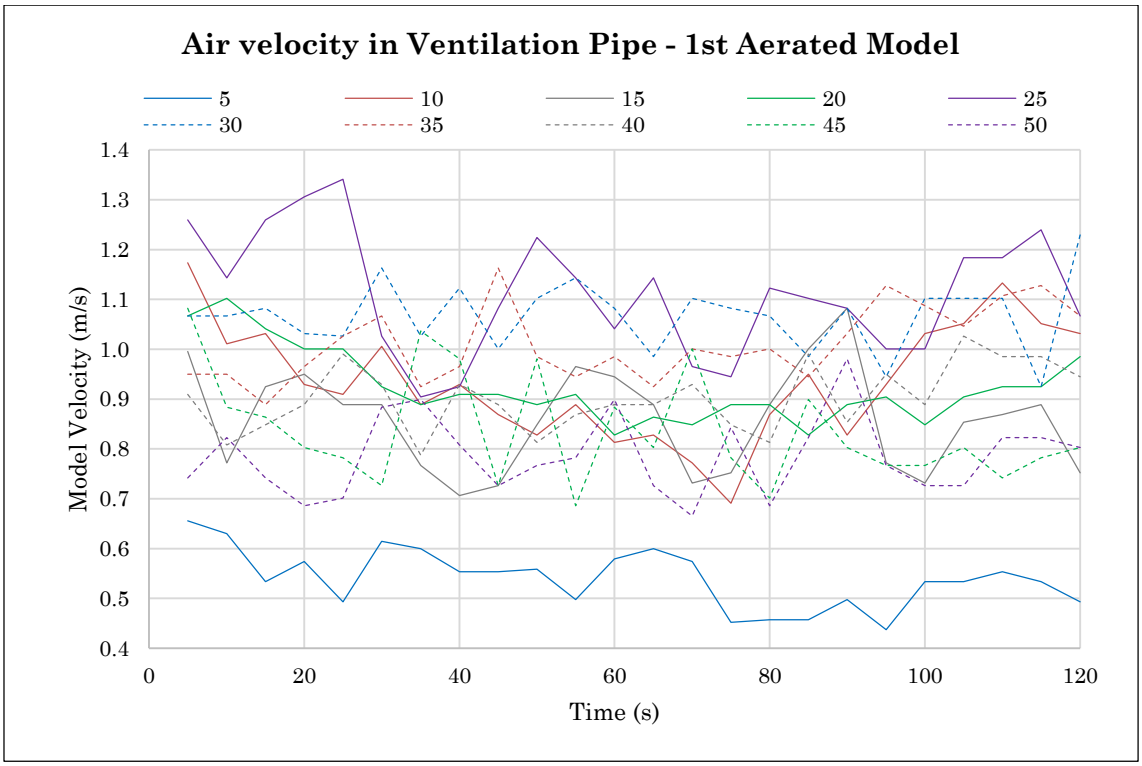

Figure J-1: Air velocity data graph – 1st aerated model

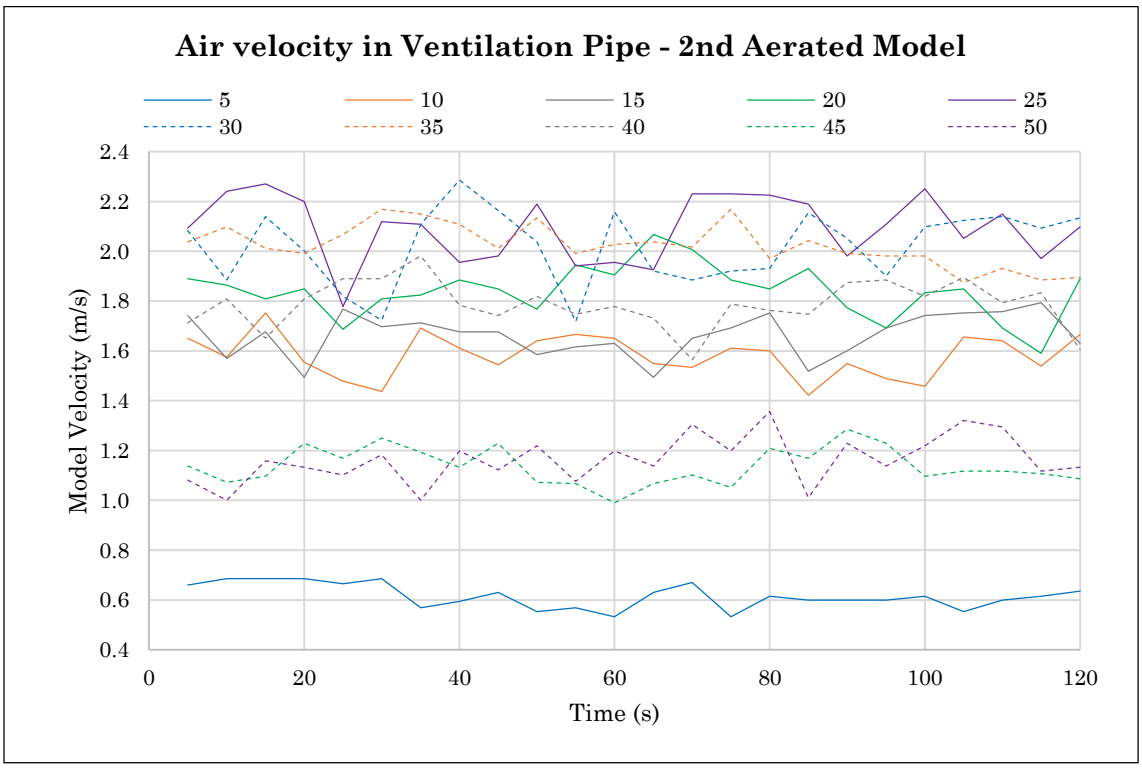

Figure J-2: Air velocity data graph – 2nd aerated model

APPENDIX K
PHOTOGRAPHS OF MODEL TESTS

All photographs of model tests are contained in this appendix. During the model tests, photographs were only taken during the 1st, 3rd, and 5th rounds of testing, as the 2nd, 4th and 6th rounds were repetitions of the prior rounds to measure the pressure on the side and side bottom faces of the splitter.

K.1. 1st Round – Unaerated Model

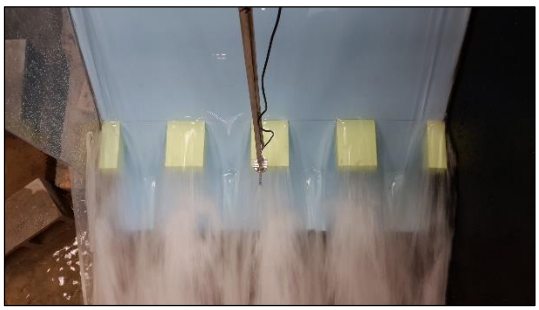

Top View

Side View

Figure K-1: Test 1 – Unaerated, q_p = 5 m²/s

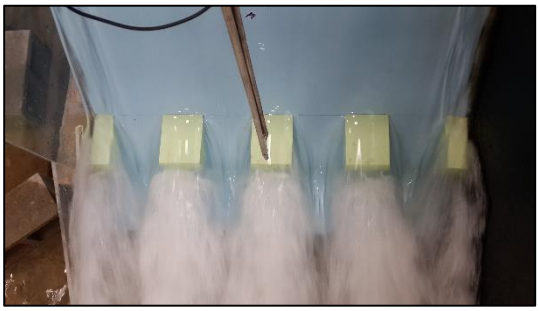

Top View

Side View

Figure K-2: Test 2 – Unaerated, q_p = 10 m²/s

Top View

Side View

Figure K-3: Test 3 – Unaerated, q_p = 15 m²/s

Top View

Side View

Figure K-4: Test 4 – Unaerated, q_p = 20 m²/s

Top View

Side View

Figure K-5: Test 5 – Unaerated, q_p = 25 m²/s

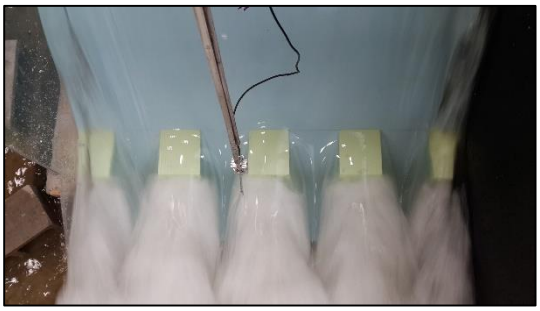

Top View

Side View

Figure K-6: Test 6 – Unaerated, q_p = 30 m²/s

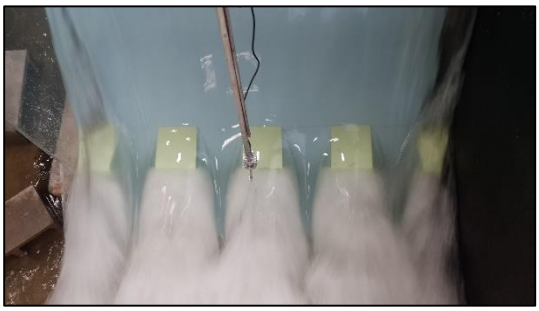

Top View

Side View

Figure K-7: Test 7 – Unaerated, q_p = 35 m²/s

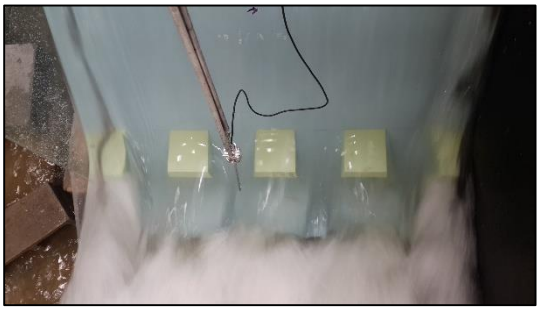

Top View

Side View

Figure K-8: Test 8 – Unaerated, q_p = 40 m²/s

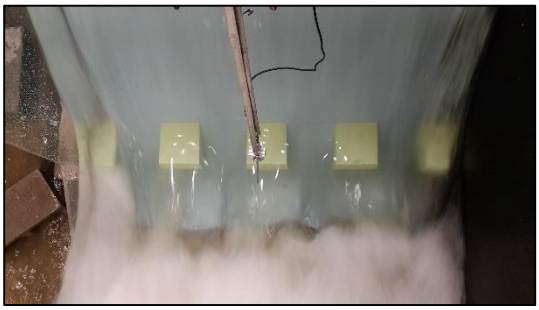

Top View

Side View

Figure K-9: Test 9 – Unaerated, q_p = 45 m²/s

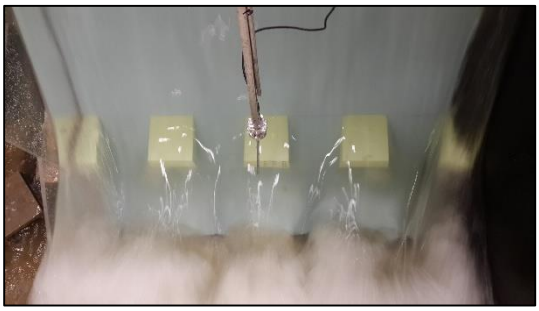

Top View

Side View

Figure K-10: Test 10 – Unaerated, q_p = 50 m²/s

K.2. 3rd Round – 1st Aerated Model

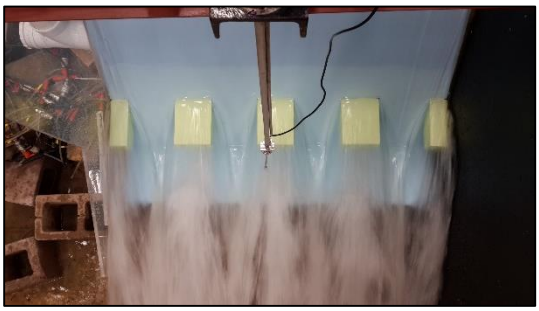

Top View

Side View

Figure K-11: Test 29 – 1st Aerated, q_p = 5 m²/s

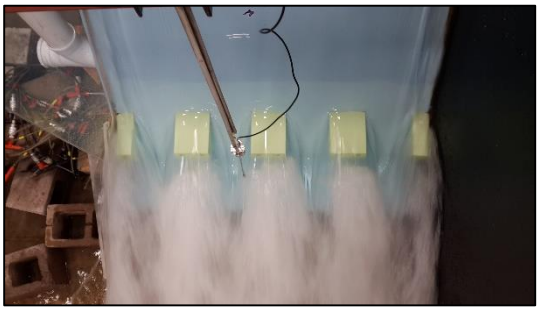

Top View

Side View

Figure K-12: Test 30 – 1st Aerated, q_p = 10 m²/s

Top View

Side View

Figure K-13: Test 31 – 1st Aerated, q_p = 15 m²/s

Top View

Side View

Figure K-14: Test 32 – 1st Aerated, q_p = 20 m²/s

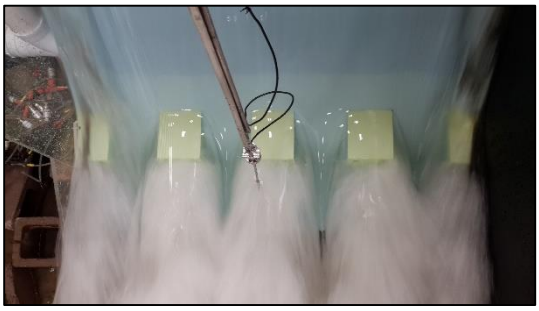

Top View

Side View

Figure K-15: Test 33 – 1st Aerated, q_p = 25 m²/s

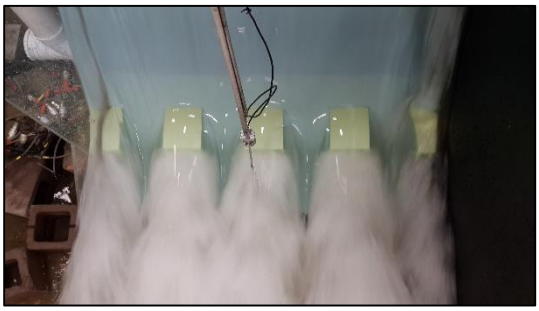

Top View

Side View

Figure K-16: Test 34 – 1st Aerated, q_p = 30 m²/s

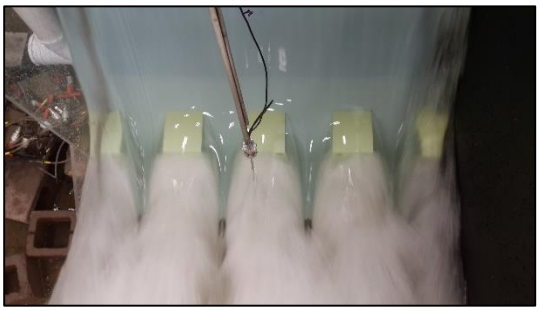

Top View

Side View

Figure K-17: Test 35 – 1st Aerated, q_p = 35 m²/s

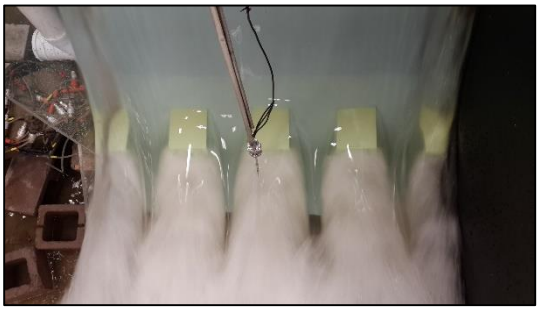

Top View

Side View

Figure K-18: Test 36 – 1st Aerated, q_p = 40 m²/s

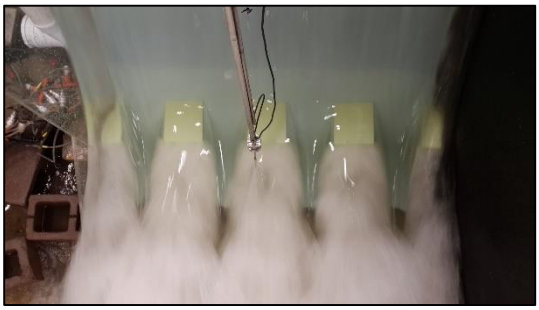

Top View

Side View

Figure K-19: Test 37 – 1st Aerated, q_p = 45 m²/s

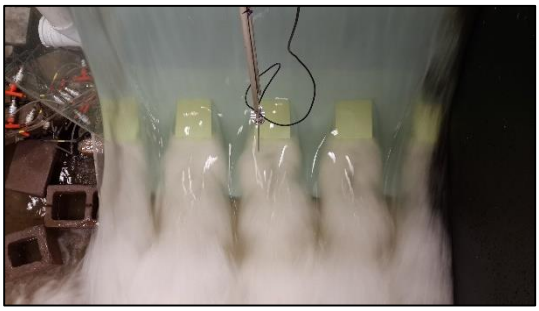

Top View

Side View

Figure K-20: Test 38 – 1st Aerated, q_p = 50 m²/s

K.3. 5th Round – 2nd Aerated Model

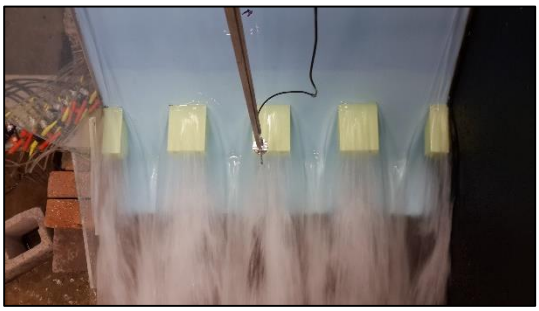

Top View

Side View

Figure K-21: Test 57 – 2nd Aerated, q_p = 5 m²/s

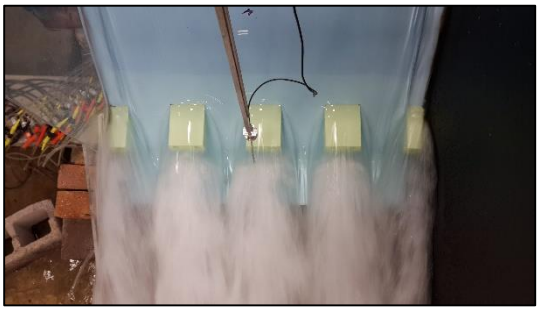

Top View

Side View

Figure K-22: Test 58 – 2nd Aerated, q_p = 10 m²/s

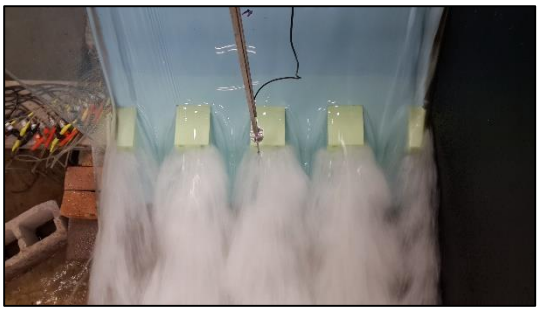

Top View

Side View

Figure K-23: Test 59 – 2nd Aerated, q_p = 15 m²/s

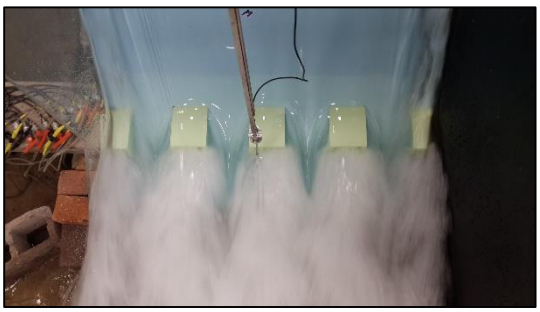

Top View

Side View

Figure K-24: Test 60 – 2nd Aerated, q_p = 20 m²/s

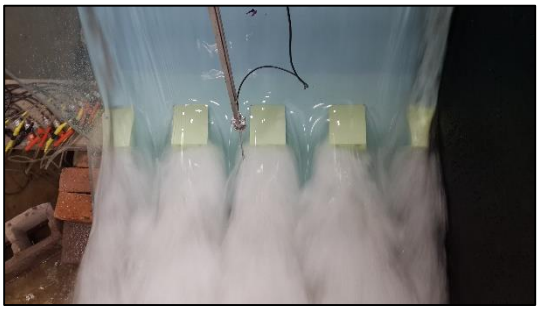

Top View

Side View

Figure K-25: Test 61 – 2nd Aerated, q_p = 25 m²/s

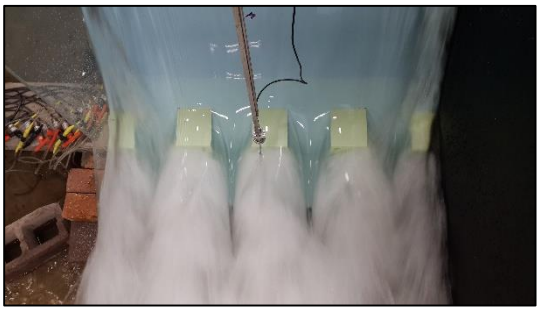

Top View

Side View

Figure K-26: Test 62 – 2nd Aerated, q_p = 30 m²/s

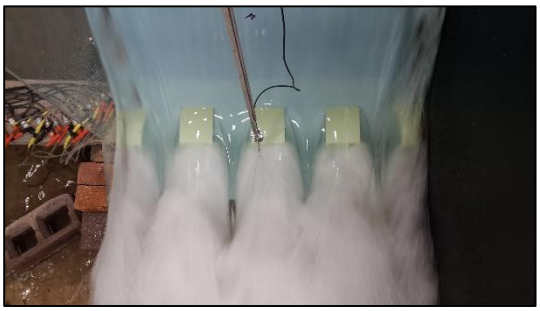

Top View

Side View

Figure K-27: Test 63 – 2nd Aerated, q_p = 35 m²/s

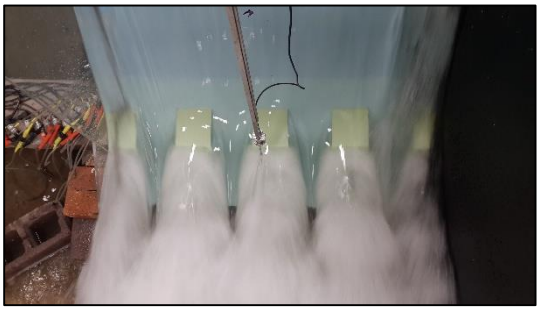

Top View

Side View

Figure K-28: Test 64 – 2nd Aerated, q_p = 40 m²/s

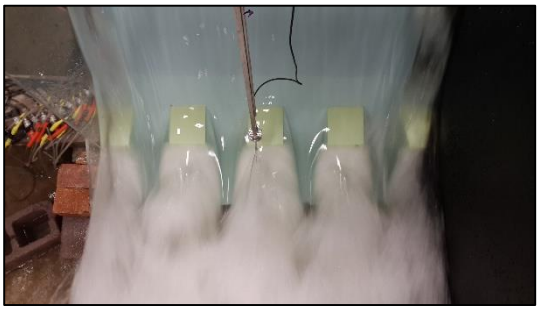

Top View

Side View

Figure K-29: Test 65 – 2nd Aerated, q_p = 45 m²/s

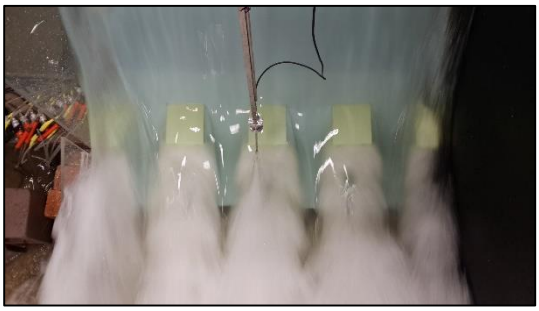

Top View

Side View

Figure K-30: Test 66 – 2nd Aerated, q_p = 50 m²/s